



I.R.Iran

ISSN:2423-5547
e-ISSN:2423-7469



Journal of Renewable Energy and Environment

Volume 9, Number 3, Summer 2022



Materials and Energy
Research Center



Iranian Association of
Chemical Engineers

Journal of Renewable Energy and Environment

DIRECTOR-IN-CHARGE

A. R. Khavandi

Iran university Science and Technology, Tehran, Iran

EDITOR- IN- CHIEF

M. Pazouki

Materials and Energy Research Center, Karaj, Iran

EDITORIAL BOARD

M. Ameri, Shahid Beheshti University, Tehran, Iran

S. S. Chandel, Shoolini University, Solan, India

J. Chaouki, Polytechnique Montréal, Montreal, Canada

H. Ghadadian, Materials and Energy Research Center, Karaj, Iran

B. Ghobadian, Tarbiat Modares University, Tehran, Iran

W.K.H. Hogland, Linnaeus University, Kalmar, Sweden

S. M. Hosseinalipoor, Iran University of Science & Technology, Tehran, Iran

H. A. Kazem, Sohar University, Sohar, Sultanate of Oman

K. Kaygusuz, Karadeniz Technical University, Trabzon, Turkey

A. Mostafaeipour, Yazd University, Yazd, Iran

G. Najafi, Tarbiat Modares University, Tehran, Iran

M. Omidkhab, Tarbiat Modarres University, Tehran, Iran

M. H. Panjeshahi, Tehran University, Tehran, Iran

M. Pazouki, Materials and Energy Research Center, Karaj, Iran

R. Roshandel, Sharif University of Technology, Tehran, Iran

M. B. Shafii, Sharif University of Technology, Tehran, Iran

J. Shayegan, Sharif University of Technology, Tehran, Iran

T. Yusaf, Federation University Australia, Ballarat, Australia

S. A. H. Zamzamin, Materials and Energy Research Center, Karaj, Iran

EDITORIAL ADVISORY BOARD

N. Azbar, Ege University, Izmir, Turkey

M. E. H. Assad, Engineering, University of Sharjah, Sharjah, UAE

A. Maheri, King's College, University of Aberdeen, Aberdeen, UK

M. Mohanraj, Hindusthan College of Engineering and Technology, Coimbatore, India

A. Sedaghat, Australian College of Kuwait, Kuwait

JOURNAL STAFF

M. Fouladian

LANGUAGE EDITOR

S. Saberi

PAGE MAKER

F. Hajizadeh

EXECUTIVE TEAM

V. H. Bazzaz, E. Pouladi, R. Chaluei

DISCLAIMER

The publication of articles in *Journal of Renewable Energy and Environment* does not imply that the editorial board, reviewers, or the publisher accept, approve, or endorse the data and conclusions of authors.

Journal of Renewable Energy and Environment (ISSN: 2423-5547) (e-ISSN: 2423-7469)

Website: www.jree.ir, E-mail: jree@merc.ac.ir

Tel: (+9826)36280040-49 (Ext. 381), Fax: (+9826)36201888

Materials and Energy Research Center (MERC); Iranian Association of Chemical Engineers (IACChE)

CONTENTS

Babak Keyvani Bahador Fani Hamed Karimi Majid Moazzami Ghazanfar Shahgholian	Improved Droop Control Method for Reactive Power Sharing in Autonomous Microgrids	1-9
Rahul Dogra Sanjay Kumar Nikita Gupta	Application of Artificial Neural Network to Solar Potential Estimation in Hilly Region of India	10-16
Davar Reza khani Abdol Hamid Jafari Mohammad Ali Hajabassi	Modified Concrete for Impeding Chloride Diffusion from Sea Water in the Marine Environment	17-31
Shokoofeh Bagheri Hassan Moradi CheshmehBeigi	DC Microgrid Voltage Stability through Inertia Enhancement Using a Bidirectional DC-DC Converter	32-44
Ashkan Zolriasatein Zahra RajabiMashhadi Majid Rezaei Abadchi Nastaran Riahi Noori Siamak Abyazi	A New Approach Based on RTV/SiO ₂ Nano Coating for Tackling Environmental Pollution on Electrical Energy Transmission and Distributions	45-51
Mirmahdi Seyedrahimi-Niaraq Tohid Nouri	Investigating the Economic Effects and the Roadmap of Developing Geothermal Systems to Generate Electricity	52-64
Mehran Gheyrati Asadollah Akram Hassan Ghasemi-Mobtaker	Optimum Orientation of the Multi-Span Greenhouse for Maximum Capture of Solar Energy in Central Region of Iran	65-74
Mohammad Hosseinpour Hassan Ali Ozgoli Seyed Alireza Haji Seyed Mirza Hosseini Amir Hooman Hemmasi Ramin Mehdipour	Energy Analysis of Utilizing Biomass Gasification to Partially Substitution Fossil Fuels in an IBG-GT-ST-Kalina Cycle	75-86
Amrollah Dehghani Sanij Taghi Torabi Abbas Khamseh Alireza Boshehri	The Influence of Research and Development Activities and NanoFab Centers on Product Development in Nanotechnology: Focusing on Solar Thermal Energy and Photovoltaic Technology	87-100
Shafini Mohd Shafie Zakirah Othman A. Harits Nu'man Nik Nurul Anis Nik Yusuf	Multi-Criteria Analysis of Biogas Feed Fuel Cell-Based Electricity Generation: Economic and Environmental Factors	101-104

AIMS AND SCOPE

Journal of Renewable Energy and Environment (JREE) publishes original papers, review articles, short communications and technical notes in the field of science and technology of renewable energies and environmental-related issues including:

- Generation
- Storage
- Conversion
- Distribution
- Management (economics, policies and planning)
- Environmental Sustainability

INSTRUCTIONS FOR AUTHORS

Submission of manuscript represents that it had neither been published nor submitted for publication elsewhere and is result of research carried out by author(s). Only the extended and upgraded articles presented in a conference and/or appeared in a symposium proceedings could be evaluated for publication.

Authors are required to include a list describing all the symbols and abbreviations in the paper. Use of the international system of measurement units is mandatory.

- On-line submission of manuscripts results in faster publication process and is recommended. Instructions are given in the JREE web sites: www.jree.ir
- References should be numbered in brackets and appear in sequence through the text. List of references should be given at the end of the paper. All journal articles listed in the References section must follow with article doi.
- Figure captions are to be indicated under the illustrations. They should sufficiently explain the figures.
- Illustrations should appear in their appropriate places in the text.
- Tables and diagrams should be submitted in a form suitable for reproduction.
- Photographs should be of high quality saved as jpg files.
- Tables' illustrations, figures and diagrams will be normally printed in single column width (8 cm). Exceptionally large ones may be printed across two columns (17 cm).



Research Article

Improved Droop Control Method for Reactive Power Sharing in Autonomous Microgrids

Babak Keyvani^a, Bahador Fani^{b,c}, Hamed Karimi^{b,c}, Majid Moazzami^{b,c}, Ghazanfar Shahgholian^{b,c*}

^a Department of Electrical Engineering, Boroujen Branch, Islamic Azad University, Boroujen, Iran.

^b Smart Microgrid Research Center, Najafabad Branch, Islamic Azad University, Najafabad, Iran.

^c Department of Electrical Engineering, Najafabad Branch, Islamic Azad University, Najafabad, Iran.

PAPER INFO

Paper history:

Received: 01 September 2021

Revised in revised form: 18 December 2021

Scientific Accepted: 07 December 2021

Published: 23 February 2022

Keywords:

Autonomous Microgrids,
Droop Control,
Power Sharing,
Stability,
Control System

ABSTRACT

Conventional droop control method has been widely adopted for power sharing between Distributed Generators (DGs) in microgrids. However, the mismatched feeder impedance of the Voltage-Sourced Inverters (VSI) may generate reactive power sharing error during islanding operation of a microgrid. In this paper, an improved droop control method is suggested to improve the reactive power sharing accuracy. In the proposed method, the slope correction of the droop characteristics is performed in such a way that the reactive power sharing error is reduced. In this method, the errors of reactive power sharing are detected by applying a clear signal to the microgrids and, then, by adding a new term to the P- ω and correcting the slope of Q-E, the reactive power sharing is done. In this way, the proposed method can successfully improve the reactive power sharing accuracy even at different X/R ratios. Another feature of this method is its high operation speed compared to the other methods of droop feature correction. The simulation results for a prototype microgrid point to the efficiency and flexibility of the proposed method.

<https://doi.org/10.30501/jree.2021.298138.1235>

1. INTRODUCTION

With the technological development of the world and the expansion of industries, demand for electric power has been continuously increasing over the last years [1-5]. Therefore, widespread use of renewable energy sources plays an important role in the modern electrical system [6-9].

Microgrid (MG) is an important and necessary part of the development of smart grids [10-12]. MGs are becoming more and more interesting due to their ability to reduce environmental impact of electric supply, reduce investment in plant, equipment, and cost, increase energy efficiency and stability as well as ride-through capability provided by energy storage, and alleviate the consequences of sudden grid outages [13, 14]. From the perspective of customers, a microgrid is a grid system that supplies reliable and high-quality electric power autonomously [15, 16]. The most relevant challenges concerning microgrid protection and control include modeling, bidirectional power flows, uncertainty, stability issues, and low inertia [17, 18].

In summary, the reasons for the popularity of microgrids include (a) the ability to combine a variety of energy generation methods and (b) uninterrupted power supply in areas with unreliable centralized power grids [19, 20]. So far,

various studies have been done on the microgrid in terms of classifications, control, optimization, policy, and stability [21, 22].

A microgrid can operate in grid connected or standalone (islanded) modes [23-26]. It enjoys the capability of operating in islanded mode and in an autonomous fashion [27, 28]. Separation of microgrids from the distribution network brings about a significant change in the performance and control objectives of distributed sources within the microgrid [29, 30].

The control in the micro-grid system makes it difficult to coordinate various micro-power types to establish stable frequency and voltage [31-33]. The microgrid control objectives include [34, 35]: (a) reactive and active power can be independently controlled; (b) voltage sag and system imbalances can be corrected; and (c) the microgrid can meet the requirements of the grid's load dynamics. Microgrid control methods and parameters to be controlled are listed in Table 1 for the two MG operating modes.

Proper harmony among various generation sources should be made to prevent any interference. To achieve the control objectives, there are two methods of centralized and local strategies for microgrid in the autonomous mode [36]. Table 2 briefly describes the advantages and disadvantages of these two methods [37, 38].

The sharing of reactive power in an autonomous microgrid is affected by the asymmetry of local loads and the impedance

*Corresponding Author's Email: shahgholian@iaun.ac.ir (Gh. Shahgholian)

URL: https://www.jree.ir/article_145339.html

Please cite this article as: Keyvani, B., Fani, B., Karimi, H., Moazzami, M. and Shahgholian, Gh., "Improved droop control method for reactive power sharing in autonomous microgrids", *Journal of Renewable Energy and Environment (JREE)*, Vol. 9, No. 3, (2022), 1-9. (<https://doi.org/10.30501/jree.2021.298138.1235>).



mismatch, which is a challenge [39, 40]. Several methods have been proposed for the reactive power sharing in autonomous MGs in various pieces of literature [41, 42].

Droop control in stand-alone microgrids is an important method for sharing demand power between generators [43, 44]. However, the analysis of the method indicates the poor

performance of this control method in reactive power sharing [45, 46].

An analytical method for an island microgrid was presented to evaluate the full control method in [47]; in order to evaluate the performance of the controller, three types of load were examined.

Table 1. Control methods for inverter-based MG

Operation mode	The parameters must be controlled		Control method
	Active and reactive power	Voltage and frequency	
Grid-connected mode	×	-	Constant current control PQ control
Islanded mode	×	×	P-f control Q-V control

Table 2. Control methods in mg based on structure

Control structure	Characteristic	Advantage	Disadvantage
Centralized	It has a main controller and determines what other controllers located in each inverter should do.	Performs quite well.	Relying on the proper performance of the main controller. Requiring active communication network.
Decentralized	Several inverters work together to establish the voltage, frequency, and network, which is done only on the basis of local measurements by each inverter.	Reliable MG performance does not depend on any one unit. No need for high-speed communications. Local information only.	Possibility of slowing down the transient response of inverters after a disturbance. Dependence of the ability to divide loads for inverters on feeder impedances and control parameters.

Also, the simulation results demonstrated that the error intensity and the duration of how the microgrid reaches the fast frequency convergence and the fast performance of the protection system could improve the stability of the system.

An auxiliary controller was proposed in [48] to reduce the fluctuations due to increase in overlap by analyzing the microgrid eigenvalue which does not require network impedance monitoring to adjust the controller. It was also shown that increasing the reactive power drop causes the generated reactive power to be less affected by active charge changes.

In the islanded operation mode, the conventional method for proper load sharing between sources and regulation of the voltage and frequency in the local strategy is to employ the Q-E and P- ω droop characteristics [49, 50]. In this approach, the active power is controlled using the frequency which results in proper real power sharing among DGs, while utilization of conventional droop voltage characteristic does not result in ideal reactive power sharing among DGs because the voltage is a local quantity [51]. Considering the intrinsic relation between the DG terminal voltage and its reactive power generation, it can be easily concluded that changing the Q-E curve specifications, which is the slope or y-intercept, can have a direct impact on the reactive power generation of the DGs and, consequently, power sharing among them [52]. The approach of virtual impedance control is capable of concurrently reviewing the power control instability and power sharing. Given that adding or removing any DG in each point of the microgrid, namely plug-and-play, changes the configuration of the microgrids, without knowing this microgrid configuration in real time, virtual impedance control may not operate well or properly.

In [53], a strategy was provided to correct the Q-E characteristic to improve the ideal reactive power in a microgrid with three micro-sources with local controls. In this

approach, the micro-sources work with the conventional curves of Q-E and P- ω in normal conditions and at fixed time intervals, the reactive power sharing error decreases by adjusting the y-intercept of the Q-E characteristic.

Various strategies have been proposed in the literature to address the inaccurate reactive power sharing problem in islanded microgrids. Virtual impedance-based methods were proposed in [54, 55] to enhance the reactive power sharing. This methods focus on reducing the feeder impedance difference of DGs. The virtual impedance is usually considered inductive to increase the X/R ratio of the feeder impedance and, consequently, to reduce the coupling between active and reactive power controls. In [56, 57], a virtual impedance technique was proposed to solve the sharing error caused by mismatched feeder impedances; the main idea was to reduce the difference in the output impedance of DG units. Despite the good performance of these methods, the controller requires a communication structure to obtain instantaneous information about the MG to adopt the desired virtual impedance. In [58, 59], control strategies based on adaptive virtual impedance control were proposed. In [59], an adaptive virtual impedance control scheme was proposed for overcoming the unbalanced and harmonic power sharing in islanded microgrids. In [58], an adaptive complex virtual impedance method was proposed for ideal reactive power sharing in the islanded microgrids. In [54], an improved droop control method was applied for power decoupling and accurate reactive power sharing. The method functions based on virtual power source and composite virtual negative impedance for low-voltage microgrids. In [60], an adaptive voltage droop control method was proposed to improve the reactive power sharing. This method uses two terms to be added to the conventional reactive power droop curve: the first is added to correct the voltage drop across the transmission lines; the second is used to make the system

stable under heavy loading conditions. However, this method needs detailed information of the network in advancing the operation.

In this paper, a method for modifying the Q-V characteristic was proposed to achieve the ideal reactive power sharing in microgrids with local control-based micro-sources. In this method, all micro sources operate with the conventional Q-E and P- ω characteristics. At certain times, the Q-E droop curves are adjusted by modifying the characteristic slope so that the reactive power sharing error can be reduced. The proposed method first determines the reactive power sharing errors by injecting small active-reactive power deviations. Then, accurate reactive power sharing is achieved by adding a new term in the P- ω characteristic and modifying the slope of the Q-E droop curve. By using the proposed scheme, the reactive power sharing error is significantly reduced. After correction, the proposed droop controller is automatically switched to the conventional droop controller.

The remainder of the paper is organized as follows:

In the second section, the conventional control method for the microgrid is mentioned. In the third part, the process of correcting the characteristic is stated. In the fourth part, the simulation results for a microgrid with three scattered

production units and two linear loads are given. Finally, the conclusion of the article is given in the fifth part.

2. CONVENTIONAL DROOP CONTROL METHOD ANALYSIS

A common method in the case of universal microgrid applications is droop control [61]. For low-voltage microgrids, typical droop control is unusual, as the line impedance between the distributed generation units is usually strong enough to connect the active and reactive DG power [62, 63]. The performance of conventional droop control needs to be improved because the assumption of a droop curve in a part of the operating area of capacitive connection inverters is not valid [64].

Figure 1 shows the general diagram of an island microgrid in which a power line (indicated by solid line) is required to trade electrical power, while trade control and status information are shown with a communication line (indicated by dashed line) [65, 66]. Figure 2 shows the equivalent circuit of one DG unit which is connected with an interface filter to the common bus of an AC microgrid. V_T and V_P are the voltage of the ends of the filter capacitor and the common bus voltage, respectively. Line resistance is ignored. Reactance between the inverter and the common bus is denoted by X_i .

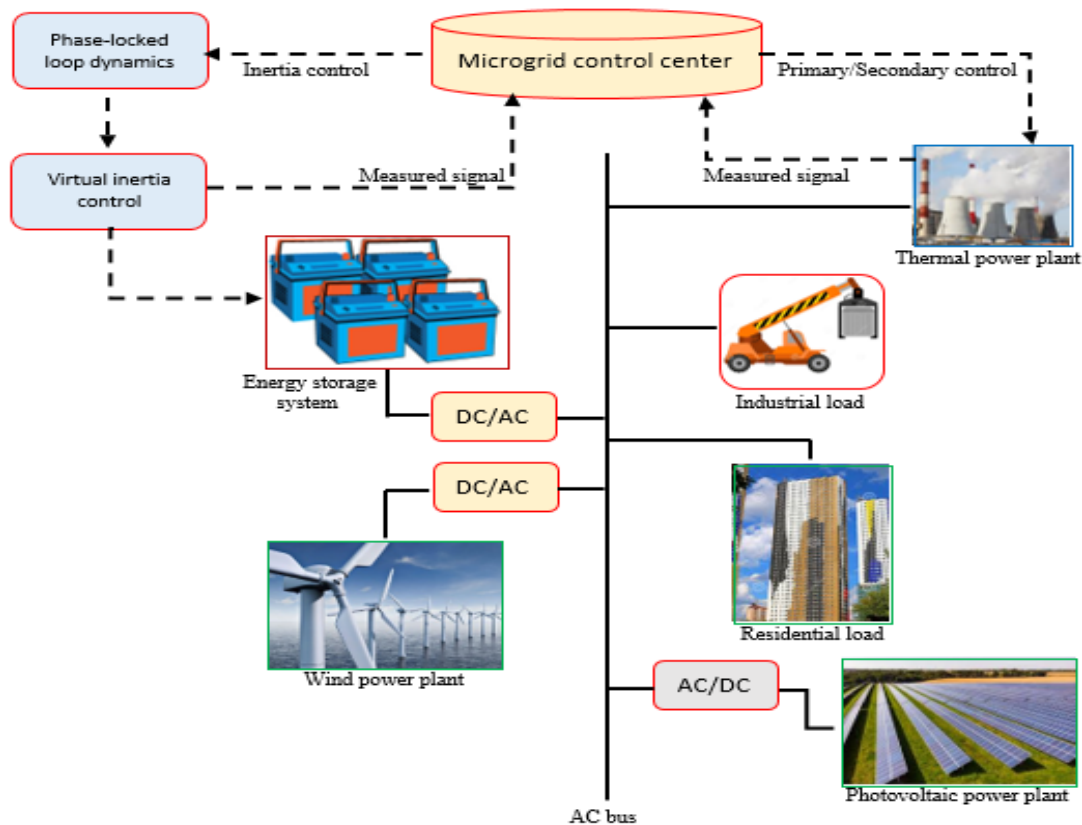


Figure 1. Illustration of the AC microgrid configuration [66]

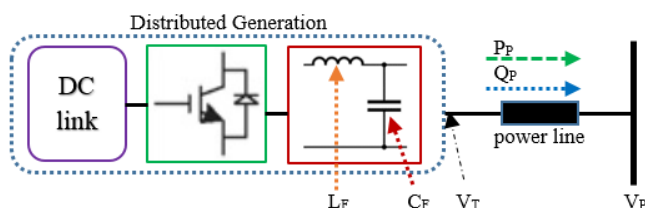


Figure 2. The equivalent circuit of a DG unit connected to a common bus

Based on the equivalent circuit of a DG unit connected to a common bus, the active and reactive output powers of each DG unit are extracted as follows:

$$P_i = \frac{V_T V_P}{X_i} \sin \delta_i \quad (1)$$

$$Q_i = \frac{V_T V_P \cos \delta_i - V_P}{X_i} \quad (2)$$

Neglecting the line resistance and assuming $\cos \delta_i \approx 1$, the active power is proportional to δ_i (or its derivative ω) and, consequently, changing the voltage phase angle of DGs impacts their output active power. According to (2), the output reactive power of a DG unit can be controlled by voltage magnitude of V_T [67]. Therefore, the frequency and voltage droop characteristics are extracted as follows:

$$\omega = \omega_0 - n_p \cdot P \quad (3)$$

$$E = E_0 - n_q \cdot Q \quad (4)$$

where ω_0 and E_0 are no load frequency and voltage, respectively, and n_p and n_q are frequency and voltage droop coefficients, respectively.

It is assumed that DG i^{th} and DG j^{th} are operating in a parallel way with the same nominal capacity and droop characteristic slope. It should be considered that the phase angle changes of δ_i are very small. Increasing the inductance of the network and the slope of the voltage droop characteristic are the two main approaches to improving the reactive power sharing error. Increase in the impedance is usually done by virtual impedance control, which requires the control with a higher bandwidth for the inverter [68]. It should be noted that increasing the droop slope may increase the reactive power sharing error; however, this slope increase generates other issues like V_P reduction or the required reactive power changes (due to voltage changes). Therefore, it can be said that increasing the slope is not a good option to improve the reactive power sharing error.

3. CHARACTERISTIC CORRECTION PROCESS

Reactive power sharing error is caused by various factors in the microgrid. Most reactive power sharing error correction strategies are based on complex circuit models and settings. Therefore, in this section, a correction method is proposed to eliminate the temporary reactive power sharing error without the need for microgrid configuration. Given the frequency is a global parameter throughout the network, any quantity placed on a characteristic with frequency leads to the ideal sharing of that quantity. Therefore, the strategy used to modify the Q-E characteristic is based on the same property. Before starting the process, the production of all micro sources is considered to be approximately the same as the active power P_0 . Also, the production of reactive power by each micro-source in ideal sharing conditions is equal to Q_0 .

As the feature correction process starts in all the micro-sources, the active power in the droop characteristic of P- ω is replaced with a linear combination of P and Q as in the following to have a new power-frequency characteristic:

$$\omega = \omega_0 - n_p \cdot (a \cdot P + b \cdot Q) \quad (5)$$

In these conditions, the Q-E curve remains with the same conditions as that before the compensation.

$$E = E_0 - n_q \cdot Q \quad (6)$$

In this process, the slope of n_q in the above relation is corrected to reach the reactive power sharing.

By keeping the values of a and b fixed in all the micro-sources, $aP + bQ$ will have the same values, as the value of $aP + bQ$ is associated with a feature with one frequency. The goal is to return the value of P to P_0 at the end of the process and the value of Q to Q_0 in all micro-sources. Assuming that the network impedance is mainly inductive, the reactive power is mainly dependent on the voltage and it is determined by the Q-E characteristic. Therefore, the main goal of the characteristic modification process is to modify the slope of Relation (6) so that the reactive power generation of the micropower reaches Q_0 . However, Q_0 is a function of the reactive power of the load and the grid, which is an unknown value. If the slope correction of the Q-E characteristic in all micro sources takes place in such a way that the active power returns to P_0 and since $aP + bQ$ are the same in all micro-sources, it can be concluded that Q has the same value in all micro sources and it points to the ideal sharing of reactive power. At the end of the character correction process, $aP + bQ$ is replaced again with the normal character P- ω . The overall process is shown in Figure 3.

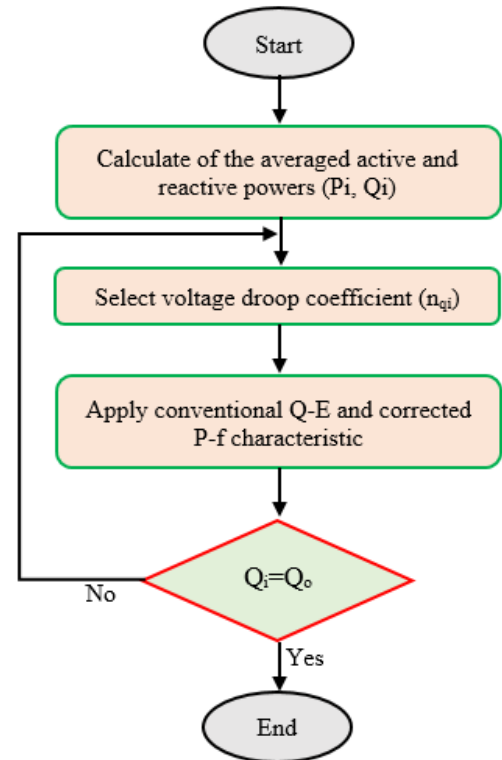


Figure 3. Flowchart of the proposed method

Figure 4 shows the process of the given character correction to synchronize reactive power. As shown in this figure, the character correction process is determined by starting signal activation. The timer block measures the process duration. At the beginning of the process, the sampling and holding block samples and stores the initial amount of active power equal to P_0 to be used during the process.

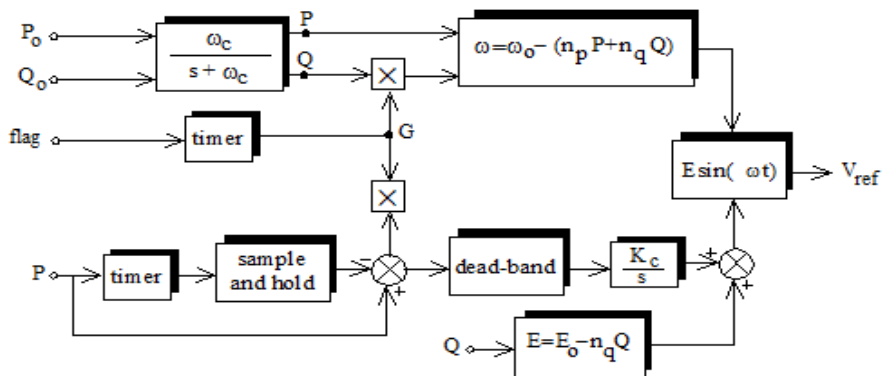


Figure 4. Reactive power synchronizing correction plan

4. SIMULATION RESULTS AND DISCUSSION

In order to evaluate the operational accuracy of the algorithm for correcting the Q-E feature and power ideal sharing between the microgrid sources, the sample microgrid composed of some DGs and loads in Figure 5 is used. Each DG system includes a power supply and an inverter interfaced with the network. In the operation connected to the network, the active and reactive reference power is normally supplied through the main network and the approach of normal droop control can be applied to follow the power. Therefore dividing the power in the network connected mode does not make any problems for the network [69, 70]. When the microgrid is operating autonomously, all the required load of the microgrid should be properly shared through DG units.

The rated rms voltage (L-L) for microgrid 208 V (60 Hz). The active and reactive loads are 3525 W and 1425 Var, respectively.

The filter parameters in the interface inverter include $R_F = 0.2 \Omega$, $L_F = 5 \text{ mH}$, and $C_F = 40 \mu\text{F}$. Sampling-switching frequency is $9 \text{ KHz} \sim 4.5 \text{ KHz}$. Droop coefficients are $n_p = 0.00125$ and $n_q = 0.00143$. Integration dead-band, Integral gain K_c , and LPF time constant are 6 W, 0.0286, and 0.0158 sec, respectively.

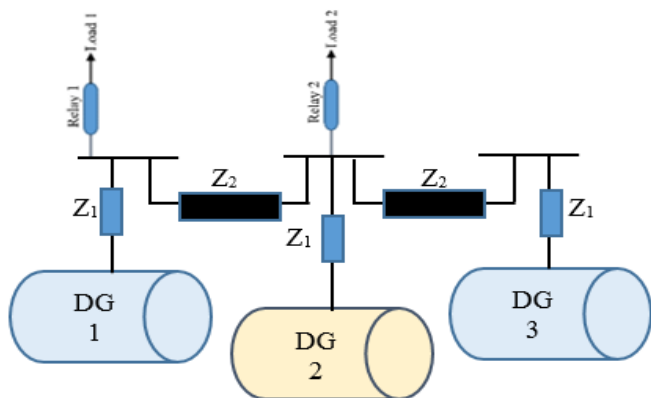


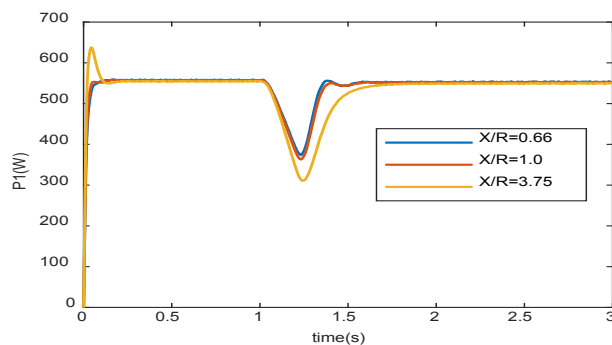
Figure 5. The microgrid consists of three DG units and two linear loadfor simulation

The simulation is done in 3 seconds and the feature correction process is applied on the network in 1-2 seconds to share the reactive power. The simulation results are compared with those in [71] to demonstrate the effect of the proposed method on the power sharing improvement.

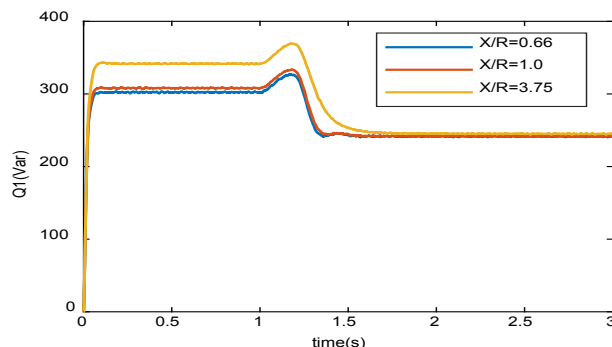
To evaluate the robustness of the proposed method to network changes, the microgrid shown in Figure 5 is simulated with three different X/R ratios of low X/R = 0.66,

medium X/R = 1, and high X/R = 3.75. Here, power sharing scheme between loads 1 and 2 as well as the microgrid behavior under this condition are analyzed. Figures 6, 7, and 8 show the active and reactive power drawn from the DG1 to DG3, respectively. The results show that the proposed scheme can proportionally share both active and reactive power in the microgrid at different X/R ratios.

According to the conditions mentioned for the microgrid in Figure 5, the output impedance of each DG unit is the most important factor in determining the reactive power drawn from that DG. Therefore, since DG1 has the smallest output impedance with respect to other DGs, it has the lowest voltage drop at the output and, consequently, DG1 provides the largest part of the microgrid reactive power, as shown in Figures 6(b), 7(b), and 8(b). As seen, the use of conventional droop characteristics before $t = 1 \text{ s}$ leads to a large difference between the reactive powers of the DGs. After starting the process of correcting the droop characteristics, the reactive power sharing error decreases rapidly in less than 0.5 seconds. In other words, all three DGs produce reactive power equal to 243 Var.

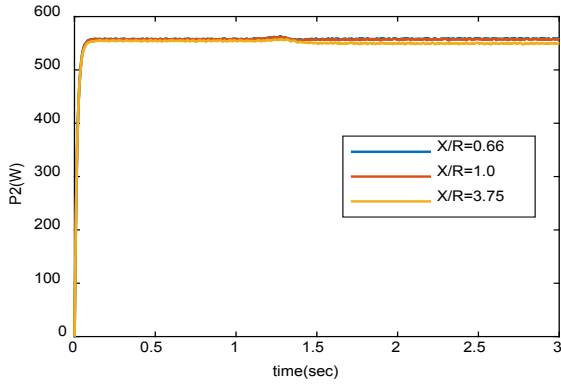


(a) Output active power

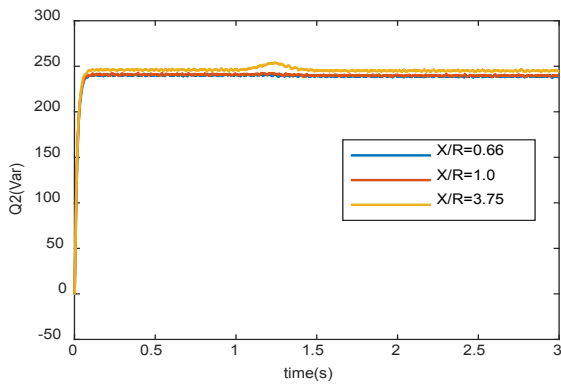


(b) Output reactive power

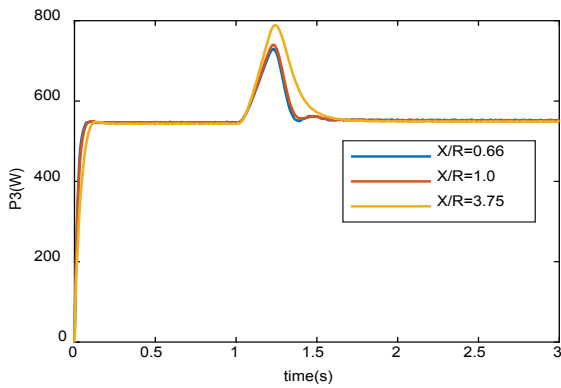
Figure 6. Output power of the DG1 before, after, and during the reference feature correction process



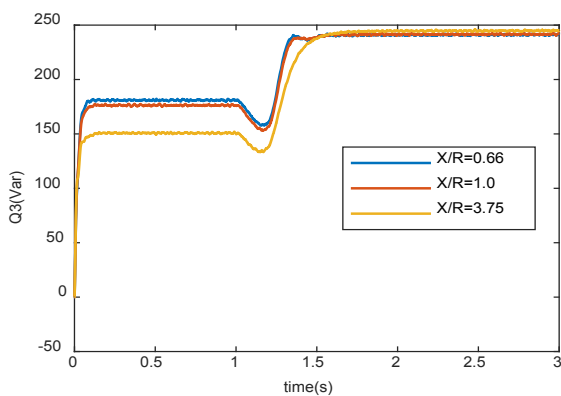
(a) Output active power



(b) Output reactive power

Figure 7. Output power of the DG2 before, after, and during the reference feature correction process

(a) Output active power

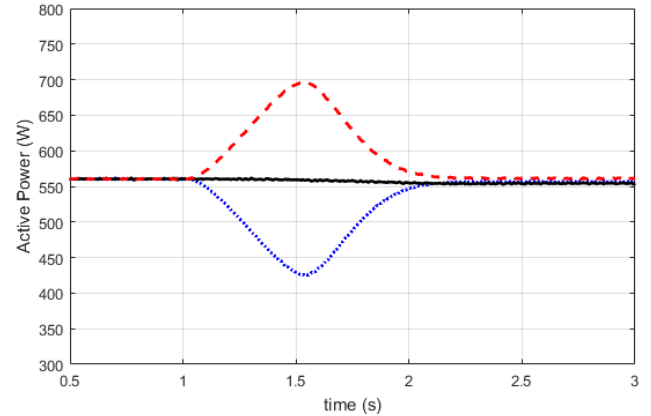
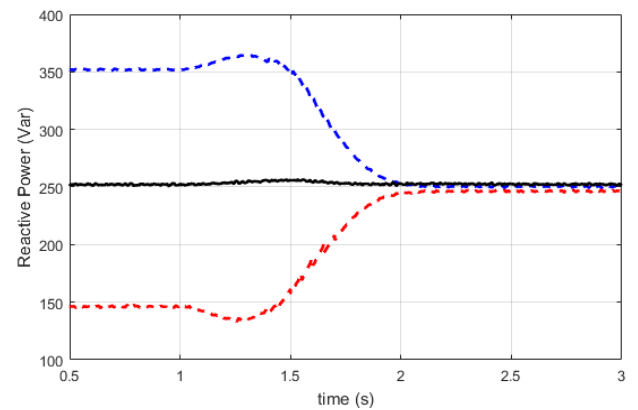


(b) Output reactive power

Figure 8. Output power of the DG3 before, after, and during the reference feature correction process

s. In other words, the active power is ideally shared using the conventional droop characteristics even though the feeder impedances of DGs vary.

The performance of the method presented in [70] can be compared with that of the proposed method using the simulation shown in Figures 9 and 10. As seen, the proposed method is much faster and experiences fewer oscillations to achieve the proper reactive power sharing. Also, according to output power dynamics of the proposed method (see Figures 6, 7, and 8), the overall time to reach the desired conditions is shorter than virtual impedance method.

**Figure 9.** Output active power of the microgrids before, after, and during the reference feature correction process**Figure 10.** Output reactive power of the microgrids before, after, and during the reference feature correction process

5. CONCLUSIONS

The purpose of this paper was to improve the reactive power sharing error for microgrids with different X/R ratios and any type of topology. In this strategy, first, DGs are controlled using the conventional droop method. Then, at a certain time, the droop characteristics were compensated with a special structure. After the correction of the reactive power sharing error, the proposed droop controller returned to the conventional droop characteristic. To evaluate the method dynamics, simulation results were presented for different system conditions and it was shown that the proposed method was not sensitive to network structure and X/R ratio. The simulation results also showed that this method led to the appropriate reactive power sharing and the reactive power sharing error was minimized. Therefore, the proposed method was resilient with respect to the network changes and X/R ratio changes. The authors' focus for future work is to provide a plan for load sharing in the event of fault.

As illustrated in Figures 6(a), 7(a), and 8(a), the output active powers of DG units are equal prior to the moment $t = 1$

6. ACKNOWLEDGEMENT

The authors thank the editor, the editor of the journal, the executive agents of the journal, and the judges for their suggestions to improve the quality of the article.

REFERENCES

- Rahmani, M., Faghihi, F., Moradi-Cheshmeh-Beigi, H. and Hosseini, S., "Frequency control of islanded microgrids based on fuzzy cooperative and influence of STATCOM on frequency of microgrids", *Journal of Renewable Energy and Environment (JREE)*, Vol. 5, (2018), 27-33. (<http://dx.doi.org/10.30501/jree.2018.94119>).
- Mahdavian, M. and Behzadfar, N., "A review of wind energy conversion system and application of various induction generators", *Journal of Novel Researches on Electrical Power*, Vol. 8, (2020), 55-66. (<http://jeps.iaud.ac.ir/article-1-255-fa.html>).
- Ahmadpour, A., Seyed Shenava, S., Dejamkhooy, A. and Mokaramian, E., "Electromagnetic force analysis of transformer on the ferroresonance due to consecutive 3-phase short-circuit faults using finite element method (FEM)", *Journal of Intelligent Procedures in Electrical Technology*, Vol. 11, (2020), 47-60. (<https://dori.net/dor/20.1001.1.23223871.1399.11.41.4.3>).
- Jafari, A. and Shahgholian, Gh., "Analysis and simulation of a sliding mode controller for mechanical part of a doubly-fed induction generator based wind turbine", *IET Generation, Transmission and Distribution*, Vol. 11, (2017), 2677-2688. (<http://dx.doi.org/10.1049/iet-gtd.2016.1969>).
- Samadinasab, S., Namdari, F. and Bakhshipoor, M., "A novel approach for earthing system design using finite element method", *Journal of Intelligent Procedures in Electrical Technology*, Vol. 8, (2017), 54-63. (<https://dori.net/dor/20.1001.1.23223871.1396.8.29.6.0>).
- Shahgholian, Gh., "An overview of hydroelectric power plant: Operation, modeling, and control", *Journal of Renewable Energy and Environment (JREE)*, Vol. 7, (2020), 14-28. (<http://dx.doi.org/10.30501/JREE.2020.221567.1087>).
- Amooshahi, H., Hooshmand, R.A., Khodabakhshian, A. and Moazzami, M., "A new load-shedding approach for microgrids in the presence of wind turbines", *Electric Power Components and Systems*, Vol. 1, (2016), 726-736. (<http://dx.doi.org/10.1080/15325008.2015.1131761>).
- Hosseini, E. and Shahgholian, Gh., "Partial- or full-power production in WECS: A survey of control and structural strategies", *European Power Electronics and Drives*, Vol. 27, (2017), 125-142. (<http://dx.doi.org/10.1080/09398368.2017.1413161>).
- Hosseini, E. and Shahgholian, Gh., "Output power levelling for DFIG wind turbine system using intelligent pitch angle control", *Automatika*, Vol. 58, (2017), 363-374. (<http://dx.doi.org/10.1080/00051144.2018.1455017>).
- Mohammadjafari, M., Ebrahimi, R. and Parvin Darabad, V., "Optimal economic operation and battery sizing for microgrid energy management systems considering demand response", *International Journal of Smart Electrical Engineering*, Vol. 8, (2019), 129-136. (<https://dori.net/dor/20.1001.1.22519246.2019.08.04.1.2>).
- Tayebi, A., Sharifi, R., Salemi, A. and Faghihi, F., "Investigating the effect of different penetration of renewable energy resources on islanded microgrid frequency control using a robust method", *Signal Processing and Renewable Energy*, Vol. 5, (2021), 15-34. (http://spre.azad.ac.ir/article_678747.html).
- Dong, R., Liu, S., Liang, G., An, X. and Xu, Y., "Output control method of microgrid VSI control network based on dynamic matrix control algorithm", *IEEE Access*, Vol. 7, (2019), 158459-158480. (<http://dx.doi.org/10.1109/ACCESS.2019.2949909>).
- Golpîra, H. and Bevrani, H., "Microgrids impact on power system frequency response", *Energy Procedia*, Vol. 156, (2019), 417-424. (<http://dx.doi.org/10.1016/j.egypro.2018.11.097>).
- Qi, Y., Lin, P., Wang, Y. and Tang, Y., "Two-dimensional impedance-shaping control with enhanced harmonic power sharing for inverter-based microgrids", *IEEE Transactions on Power Electronics*, Vol. 34, (2019), 11407-11418. (<http://dx.doi.org/10.1109/TPEL.2019.2898670>).
- Abbaspour, E., Fani, B. and Heydariyan-Forushani, E., "A bi-level multi agent based protection scheme for distribution networks with distributed generation", *International Journal of Electrical Power and Energy Systems*, Vol. 112, (2019), 209-220. (<http://dx.doi.org/10.1016/j.ijepes.2019.05.001>).
- Kumar, J., Agarwal, A. and Agarwal, V., "A review on overall control of DC microgrids", *Journal of Energy Storage*, Vol. 21, (2019), 113-138. (<http://dx.doi.org/10.1016/j.est.2018.11.013>).
- Bagheri, S. and Moradi Cheshmeh Beigi, H., "DC microgrid voltage stability through inertia enhancement using a bidirectional dc-dc converter", *Proceedings of the IEEE/IWEC*, Shahrood, Iran, Vol. 1, (2021), 1-5. (<http://dx.doi.org/10.1109/IWEC52400.2021.9467032>).
- Rahbarimaghham, H., "Optimal control of micro-grid (MG) to improve voltage profile including combined heat and power system", *Journal of Intelligent Procedures in Electrical Technology*, Vol. 9, (2019), 43-50. (<https://dori.net/dor/20.1001.1.23223871.1397.9.36.5.0>).
- Olivares, D.E., Mehrizi-Sani, A., Etemadi, A.H., Cañizares, C.A., Iravani, R., Kazerani, M., Hajimiragha, A.H., Gomis-Bellmunt, O., Saeedifard, M., Palma-Behnke, R., Jiménez-Estévez, G.A. and Hatziargyriou, N.D., "Trends in microgrid control", *IEEE Transactions on Smart Grid*, Vol. 5, (2014), 1905-1919. (<http://dx.doi.org/10.1109/TSG.2013.2295514>).
- Zandi, F., Fani, B. and Golsorkhi, A., "A visually-driven nonlinear droop control for inverter dominated islanded microgrids", *Electrical Engineering*, Vol. 102, (2020), 1207-1222. (<http://dx.doi.org/10.1007/s00202-020-00942-7>).
- Zamanian, S., Sadi, S., Ghaffarpour, R. and Mahdavian, A., "Inverter-based microgrid dynamic stability analysis considering inventory of dynamic and static load models", *Journal of Intelligent Procedures in Electrical Technology*, Vol. 11, (2021), 91-109. (<https://dori.net/dor/20.1001.1.23223871.1399.11.44.6.1>).
- Eberlein, S. and Rudion, K., "Small-signal stability modelling, sensitivity analysis and optimization of droop controlled inverters in LV microgrids", *International Journal of Electrical Power and Energy Systems*, Vol. 125, (2021), 106404. (<http://dx.doi.org/10.1016/j.ijepes.2020.106404>).
- Hsu, C.T., Cheng, T.J., Huang, H.M., Lee, Y.D., Chang, Y.R. and Jiang, J.L., "Over frequency control of photovoltaic inverters in an island microgrid", *Microelectronics Reliability*, Vol. 92, (2019), 42-54. (<http://dx.doi.org/10.1016/j.microrel.2018.11.011>).
- Karimi, H., Shahgholian, Gh., Fani, B., Sadeghkhan, I. and Moazzami, M., "A protection strategy for inverter interfaced islanded microgrids with looped configuration", *Electrical Engineering*, Vol. 101, (2019), 1059-1073. (<http://dx.doi.org/10.1007/s00202-019-00841-6>).
- Lo, K.Y. and Chen, Y.M., "Design of a seamless grid-connected inverter for microgrid applications", *IEEE Transactions on Smart Grid*, Vol. 11, (2020), 194-202. (<http://dx.doi.org/10.1109/TSG.2019.2919905>).
- Rezkallah, M., Singh, S., Singh, B., Chandra, A., Ibrahim, H. and Ghandour, M., "Implementation of two-level coordinated control for seamless transfer in standalone microgrid", *IEEE Transactions on Industry Applications*, Vol. 57, (2021), 1057-1068. (<http://dx.doi.org/10.1109/TIA.2020.3037269>).
- Saim, A., Mellah, R., Houari, A., Machmoum, M. and Djeriou, A., "Adaptive resonant based multi-loop control strategy for parallel distributed generation units in standalone microgrid application", *Electric Power Systems Research*, Vol. 143, (2017), 262-271. (<http://dx.doi.org/10.1016/j.epsr.2016.10.010>).
- Agrawal, R., Changan, D.D. and Bodhe, A., "Small signal stability analysis of stand-alone microgrid with composite load", *Journal of Electrical Systems and Information Technology*, Vol. 7, (2020), 12. (<http://dx.doi.org/10.1186/s43067-020-00020-9>).
- Kaur, A., Kaushal, J. and Basak, P., "A review on microgrid central controller", *Renewable and Sustainable Energy Reviews*, Vol. 55, (2016), 338-345. (<http://dx.doi.org/10.1016/j.rser.2015.10.141>).
- Gorji, S., Zamanian, S. and Moazzami, M., "Techno-economic and environmental base approach for optimal energy management of microgrids using crow search algorithm", *Journal of Intelligent Procedures in Electrical Technology*, Vol. 11, (2020), 49-68. (<https://dori.net/dor/20.1001.1.23223871.1399.11.43.4.7>).
- Xu, Z., Yang, P., Zheng, C., Zhang, Y., Peng, J. and Zeng, Z., "Analysis on the organization and development of multi-microgrids", *Renewable and Sustainable Energy Reviews*, Vol. 81, (2018), 2204-2216. (<http://dx.doi.org/10.1016/j.rser.2017.06.032>).
- Li, Y., Meng, K., Dong, Z.Y. and Zhang, W., "Sliding framework for inverter-based microgrid control", *IEEE Transactions on Power Systems*, Vol. 35, (2020), 1657-1660. (<http://dx.doi.org/10.1109/TPWRS.2020.2965762>).

33. Silva, G.F., Donaire, A., Seron, M.M., McFadyen, A. and Ford, J., "String stability in microgrids using frequency controlled inverter chains", *IEEE Control Systems Letters*, Vol. 6, (2022), 1484-1489. (<http://dx.doi.org/10.1109/LCSYS.2021.3114143>).
34. Shahedi, R., Sabahi, K., Tayana, M. and Hajizadeh, A., "Self-tuning fuzzy PID controller for load frequency control in ac micro-grid with considering of input delay", *Journal of Intelligent Procedures in Electrical Technology*, Vol. 9, (2019), 19-26. (<https://dori.net/dor/20.1001.1.23223871.1397.9.35.3.6>).
35. Fayazi, H., Moazzami, M., Fani, B. and Shahgholian, Gh., "A first swing stability improvement approach in microgrids with synchronous distributed generators", *International Transactions on Electrical Energy Systems*, Vol. 31, (2021), e12816. (<http://dx.doi.org/10.1002/2050-7038.12816>).
36. Bidram, A. and Davoudi, A., "Hierarchical structure of microgrids control system", *IEEE Transactions on Smart Grid*, Vol. 3, (2012), 1963-1976. (<http://dx.doi.org/10.1109/TSG.2012.2197425>).
37. Saleh, M., Esa, Y. and Mohamed, A.A., "Communication-based control for dc microgrids", *IEEE Transactions on Smart Grid*, Vol. 10, (2019), 2180-2195. (<http://dx.doi.org/10.1109/TSG.2018.2791361>).
38. Li, L., Sun, Y., Liu, Z., Hou, X., Shi, G. and Su, M., "A decentralized control with unique equilibrium point for cascaded-type microgrid", *IEEE Transactions on Sustainable Energy*, Vol. 10, (2019), 324-326. (<http://dx.doi.org/10.1109/TSTE.2018.2871641>).
39. Hoang, T.V. and Lee, H.H., "Distributed control scheme for accurate reactive power sharing with enhanced voltage quality for islanded microgrids", *Journal of Power Electronics*, Vol. 20, (2020), 601-613. (<http://dx.doi.org/10.1007/s43236-020-00047-1>).
40. Qi, Y., Fang, J. and Tang, Y., "Utilizing the dead-time effect to achieve decentralized reactive power sharing in islanded ac microgrids", *IEEE Journal of Emerging and Selected Topics in Power Electronics*, Vol. 8, (2020), 2350-2361. (<http://dx.doi.org/10.1109/JESTPE.2019.2904077>).
41. Schiffer, J., Seel, T., Raisch, J. and Sezi, T., "Voltage stability and reactive power sharing in inverter-based microgrids with consensus-based distributed voltage control", *IEEE Transactions on Control Systems Technology*, Vol. 24, (2016), 96-109. (<http://dx.doi.org/10.1109/TCST.2015.2420622>).
42. Chen, F., Chen, M., Li, Q., Meng, K., Guerrero, J.M. and Abbott, D., "Multiagent-based reactive power sharing and control model for islanded microgrids", *IEEE Transactions on Sustainable Energy*, Vol. 7, (2016), 1232-1244. (<http://dx.doi.org/10.1109/TSTE.2016.2539213>).
43. Paspatis, A.G., Konstantopoulos, G.C. and Dedeoglu, S., "Control design and small-signal stability analysis of inverter-based microgrids with inherent current limitation under extreme load conditions", *Electric Power Systems Research*, Vol. 193, (2021), 106929. (<http://dx.doi.org/10.1016/j.epr.2020.106929>).
44. Moon, H., Kim, Y. and Moon, S., "Frequency-based decentralized conservation voltage reduction incorporated into voltage-current droop control for an inverter-based islanded microgrid", *IEEE Access*, Vol. 7, (2019), 140542-140552. (<http://dx.doi.org/10.1109/ACCESS.2019.2943538>).
45. Fani, B., Zandi, F. and Karami-Horestani, A., "An enhanced decentralized reactive power sharing strategy for inverter-based microgrid", *International Journal of Electrical Power and Energy Systems*, Vol. 98, (2018), 531-542. (<http://dx.doi.org/10.1016/j.ijepes.2017.12.023>).
46. Raju, E.S.N. and Jain, T., "A two-level hierarchical controller to enhance stability and dynamic performance of islanded inverter-based microgrids with static and dynamic loads", *IEEE Transactions on Industrial Informatics*, Vol. 15, (2019), 2786-2797. (<http://dx.doi.org/10.1109/TII.2018.2869983>).
47. Khaledian, A. and Golkar, M.A., "Analysis of droop control method in an autonomous microgrid", *Journal of Applied Research and Technology*, Vol. 15, (2017), 371-377. (<http://dx.doi.org/10.1016/j.jart.2017.03.004>).
48. Khaledian, A. and Golkar, M.A., "A new power sharing control method for an autonomous microgrid with regard to the system stability", *Automatika*, Vol. 59, (2018), 87-93. (<http://dx.doi.org/10.1080/00051144.2018.1501462>).
49. Lai, J., Lu, X., Li, X. and Tang, R., "Distributed multiagent-oriented average control for voltage restoration and reactive power sharing of autonomous microgrids", *IEEE Access*, Vol. 6, (2018), 25551-25561. (<http://dx.doi.org/10.1109/ACCESS.2018.2829881>).
50. Han, H., Liu, Y., Sun, Y., Su, M. and Guerrero, J.M., "An improved droop control strategy for reactive power sharing in islanded microgrid", *IEEE Transactions on Power Electronics*, Vol. 30, (2015), 3133-3141. (<https://doi.org/10.1109/TPEL.2014.2332181>).
51. Yu, H., Qian, A. and Wang, S., "Analysis and optimization of droop controller for microgrid system based on small-signal dynamic mode", *IEEE Transactions on Smart Grid*, Vol. 7, (2016), 695-705. (<http://dx.doi.org/10.1109/TSG.2015.2501316>).
52. Agundis-Tinajero, G., Segundo-Ramírez, J., Visairo-Cruz, N., Savaghebi, M., Guerrero, J.M. and Barocio, E., "Power flow modeling of islanded AC microgrids with hierarchical control", *International Journal of Electrical Power and Energy Systems*, Vol. 105, (2019), 28-36. (<https://doi.org/10.1016/j.ijepes.2018.08.002>).
53. Guerrero, J.M., Vicuna, L.G., Matas, J., Castilla, M. and Miret, J., "Output impedance design of parallel-connected ups inverters with wireless load sharing control", *IEEE Transactions on Industrial Electron.*, Vol. 52, (2005), 1126-1135. (<https://doi.org/10.1109/TIE.2005.851634>).
54. Dou, C., Zhang, Z., Yue, D. and Song, M., "Improved droop control based on virtual impedance and virtual power source in low-voltage microgrid", *IET Generation, Transmission and Distribution*, Vol. 11, (2017), 1046-1054. (<http://dx.doi.org/10.1049/iet-gtd.2016.1492>).
55. Zhu, Y., Zhuo, F., Wang, F., Liu, B., Gou, R. and Zhao, Y., "A virtual impedance optimization method for reactive power sharing in networked microgrid", *IEEE Transactions on Power Electronics*, Vol. 31, (2016), 2890-2904. (<http://dx.doi.org/10.1109/TPEL.2015.2450360>).
56. Yao, W., Chen, M., Matas, J., Guerrero, J.M. and Qian, Z.M., "Design and analysis of the droop control method for parallel inverters considering the impact of the complex impedance on the power sharing", *IEEE Transactions on Industrial Electronic*, Vol. 58, (2011), 576-588. (<http://doi.org/10.1109/TIE.2010.2046001>).
57. Zhong, Q., "Robust droop controller for accurate proportional load sharing among inverters operated in parallel", *IEEE Transactions on Industrial Electronics*, Vol. 60, (2013), 1281-1290. (<http://dx.doi.org/10.1109/TIE.2011.2146221>).
58. Zandi, F., Fani, B., Sadeghkhani, I. and Orakzadeh, A., "Adaptive complex virtual impedance control scheme for accurate reactive power sharing of inverter interfaced autonomous microgrids", *IET Generation, Transmission and Distribution*, Vol. 12, (2018), 6021-6032. (<http://dx.doi.org/10.1049/iet-gtd.2018.5123>).
59. Liu, B., Liu, Z., Liu, J., An, R., Zheng, H. and Shi, Y., "An adaptive virtual impedance control scheme based on small-ac-signal injection for unbalanced and harmonic power sharing in islanded microgrids", *IEEE Transactions on Power Electronics*, Vol. 34, (2019), 12333-12355. (<http://dx.doi.org/10.1109/TPEL.2019.2905588>).
60. Rokrok, E. and Golshan, M., "Adaptive voltage droop scheme for voltage source converters in an islanded multibusmicrogrid", *IET Generation, Transmission and Distribution*, Vol. 4, (2010), 562-578. (<http://dx.doi.org/10.1049/iet-gtd.2009.0146>).
61. Cao, W., Su, H., Cao, J., Sun, J. and Yang, D., "Improved droop control method in microgrid and its small signal stability analysis", *Proceedings of the IEEE/ICRERA*, Milwaukee, WI, Vol. 1, (2014), 197-202. (<http://dx.doi.org/10.1109/ICRERA.2014.7016556>).
62. Gayatri, M.T.L., Parimi, A.M. and Kumar, A.V.P., "A review of reactive power compensation techniques in microgrids", *Renewable and Sustainable Energy Reviews*, Vol. 81, (2018), 1030-1036. (<http://dx.doi.org/10.1016/j.rser.2017.08.006>).
63. Tayab, U.B., Roslan, M.A.B. and Hwai, L.J., Kashif, M., "A review of droop control techniques for microgrid", *Renewable and Sustainable Energy Reviews*, Vol. 76, (2017), 717-727. (<http://dx.doi.org/10.1016/j.rser.2017.03.028>).
64. Deng, W., Dai, N., Lao, K.W. and Guerrero, J.M., "A virtual-impedance droop control for accurate active power control and reactive power sharing using capacitive-coupling inverters", *IEEE Transactions on Industry Applications*, Vol. 56, (2020), 6722-6733. (<http://dx.doi.org/10.1109/TIA.2020.3012934>).
65. Kerdphol, T., Rahman, F.S., Watanabe, M. and Mitani, Y., "Robust virtual inertia control of a low inertia microgrid considering frequency measurement effects", *IEEE Access*, Vol. 7, (2019), 57550-57560. (<https://doi.org/10.1109/ACCESS.2019.2913042>).
66. Shahgholian, Gh., "A brief review on microgrids: Operation, applications, modeling, and control", *International Transactions on Electrical Energy Systems*, Vol. 31, (2021), e12885. (<https://doi.org/10.1002/2050-7038.12885>).

67. Arefifar, S., ABde-Rady, Y. and Mohamed, I., "Probabilistic optimal reactive power planning in distribution systems with renewable resources in grid-connected and islanded modes", *IEEE Transactions on Industrial Electronics*, Vol. 61, (2014), 5830-5839. (<https://doi.org/10.1109/TIE.2014.2308144>).
68. Mohamed, Y. and El-Saadany, E.F., "Adaptive decentralized droop controller to preserve power sharing stability of paralleled inverters in distributed generation microgrids", *IEEE Transactions on Power Electronics*, Vol. 23, (2008), 2806-2816. (<http://dx.doi.org/10.1109/TPEL.2008.2005100>).
69. Li, Y. and Nan-Kao, C., "An accurate power control strategy for power-electronics-interfaced distributed generation units operating in a low-voltage multi bus microgrid", *IEEE Transactions on Power Electronics*, Vol. 24, (2009), 2977-2988. (<https://doi.org/10.1109/TPEL.2009.2022828>).
70. Tummuru, N.R., Mishra, M.K. and Srinivas, S., "An improved current controller for grid connected voltage source converter in microgrid applications", *IEEE Transactions on Sustainable Energy*, Vol. 6, (2015), 595-605. (<http://doi.org/10.1109/TSTE.2015.2399496>).
71. Mahood, H., Michaleson, D. and Jiang, J., "Accurate reactive power sharing in an islanded microgrid using adaptive virtual impedances", *IEEE Transactions on Power Electronics*, Vol. 30, (2015), 1606-1617. (<http://dx.doi.org/10.1109/TPEL.2014.2314721>).



Research Article

Application of Artificial Neural Network to Solar Potential Estimation in Hilly Region of India

Rahul Dogra ^a, Sanjay Kumar ^b, Nikita Gupta ^{b*}

^a School of Computing and Electrical Engineering (SCEE), Indian Institute of Technology Mandi (IIT Mandi), Mandi, India.

^b Department of Electrical Engineering, University Institute of Technology, Himachal Pradesh University (HPU), Shimla, India.

PAPER INFO

Paper history:

Received: 22 October 2021

Revised in revised form: 29 December 2021

Scientific Accepted: 05 January 2022

Published: 10 May 2022

Keywords:

Artificial Neural Networks (ANN),
Global Sun Radiation,
Solar,
Mean Absolute Percentage Error (MAPE)

ABSTRACT

The use of these conventional resources causes continuous depletion of fossil fuels and increased greenhouse effect. Solar power is the major renewable resource used for power generation across the globe. Solar energy activities depend on the available potential of any geographical location. Therefore, prior to the installation of solar technologies for these activities, estimation of solar potential is very important due to costly technologies. Data of solar potential is not present at every location in Himachal Pradesh (H. P.) due to the high cost of measurement instruments. The objective of this study includes the solar potential estimation for 12 cities of the H. P. The present study could be divided into two parts. Initially, Artificial Neural Networks (ANNs) are utilized to estimate global sun radiation utilizing meteorological and geographical data from 23 places. The ANN model with seven input parameters including latitude, longitude, altitude, air temperature, humidity, pressure, and wind speed were used to estimate the solar irradiation. Statistical indicators including Mean Absolute Percentage Error (MAPE) were used for the performance evaluation of these ANNs. The minimum MAPE value was obtained to be 2.39 % with Multi-Layer Perception (MLP) architecture 7-11-1. For the 12 districts of the H. P., the acquired network 7-11-1 was utilized to estimate Global Solar Radiation (GSR). The output of ANN model was implemented in Geographic Information System (GIS) environment to obtain the solar potential map for each month. The available map of the present study may be helpful for solar application in each district.

<https://doi.org/10.30501/jree.2022.307064.1267>

1. INTRODUCTION

In recent years, the application of solar technologies has become more popular for sustainable development as they are environmental-friendly or inexpensive [1]. The usage of these traditional resources will not be able to close the gap between supply and demand. Solar offers a wide range of applications including power plants, water heating, water treatment, irrigation pumps, and more [2, 3]. India's solar energy potential is estimated to be at 750 GW. The Indian government plans to install 100 GW of solar electricity by 2022, out of a total capacity of 750 GW [4]. To attain this target, state-wise solar purchase obligations are given by Ministry of New and Renewable Energy (MNRE) in India. In this context, Himachal Pradesh (H. P.) state has given 776 MW generations through solar power. Therefore, it is mandatory by the government to have energy mix through renewable energy sources. The government of H. P. is looking for solar applications in each state. Solar applications, on the other hand, required data such as the state's daily or monthly average GSR [5]. Due to the high expense of radiation

measuring tools, routine measurements of global sun radiation are not practicable for each potential state site. The high cost of these instruments motivated the researchers to find other alternative techniques like empirical relation, Artificial Intelligence (AI), etc. Studies [6-8] used sunshine duration parameter to predict GSR using the following equation.

$$\frac{H}{H_0} = a + b \left(\frac{S}{S_0} \right) \quad (1)$$

where H and H_0 are monthly average daily GSR and extraterrestrial radiation, respectively. S represents monthly average daily hours of bright sunshine; S_0 is the monthly average day length; a and b are the coefficients of correlation of regression. To determine solar radiation in any similar region, the main theoretical relation can be considered [9]. Different researchers have proposed empirical models to estimate the solar radiation [7, 10].

Besharat et al. [11] reviewed 78 empirical models in their study. The authors made a case study for Yazd, Iran to estimate GSR by selecting several models from each group and found that sunshine-based model composed of exponential relation had the best performance among other models. The main disadvantage of these models required the values of empirical coefficients. All these empirical

*Corresponding Author's Email: guptanikita08@gmail.com (N. Gupta)

URL: https://www.jree.ir/article_149613.html



coefficients have been location dependent [11]. Therefore, the coefficients of one location are not accurate for another location for GSR estimation until both locations do not have similar meteorological characteristics. Different locations have different geographical and metrological parameters that affect the GSR.

In order to deal with complexity and empirical model disadvantages, researchers used Artificial Intelligence (AI) techniques to estimate GSRs for the desired location. Among empirical and AI methods [12], ANN is the most popular machine learning systems due to its capability to handle complexity and nonlinearity of the system [13]. Many researchers have also reported in the literature that ANN models have better accuracy than empirical models [10, 14].

Various parameters including temperature, relative humidity, precipitation, clearness index, wind speed, latitude, sunshine duration, evaporation, etc. are used as input for estimation of GSR.

Almaraashi [15] estimated daily global sun radiation in 7 Saudi Arabian regions using several feature selection algorithms such as the Monte Carlo Uninformative Variable Elimination algorithm (MCUVE), Relief F algorithm, random-frog algorithm, and Laplacian Score algorithm (LS), and NN predictor. Then, 31 input parameters were used for the study and out of these parameters, the most important parameters were selected using feature selection algorithms. After that, the NN predictor was employed to calculate GSR in various Saudi Arabian locations.

Jovic et al. [16] used four-parameter Dry-Bulb Temperature (DBT), Wet-Bulb Temperature (WBT), Mean Sea Level (MSL), and Relative Humidity (RH) to estimate the GSR. The Adaptive Neuro-Fuzzy Inference System (ANFIS) was applied to find the most influential parameters responsible for GSR prediction. Among these parameters, the DBT and RH were found the most influential to estimate GSR. The minimum Root Mean Square Error (RMSE) for the DBT and RH was found to be 3.25 and 3.92, respectively.

Xue [17] used Genetic Algorithm (GA) and Particle Swarm Optimization (PSO) to increase the performance of Back Propagation Neural Network (BPNN) model for GSR estimation in Beijing. The input parameters used for ANN were sunshine duration, mean temperature, month of the year, rainfall, relative humidity, wind speed, and daily global GSR and daily diffuse radiation as output. The results depicted that the BPNN optimized by PSO had RMSE 0.78 and BPNN optimized by GA model had RMSE value 0.867. Therefore, the BPNN optimized by PSO achieved better performance accuracy to estimate GSR.

Premalatha et al. [18] trained the neural network using parameters like minimum, maximum, and difference of temperatures (T_{\min} , T_{\max} , ΔT); sunshine and theoretical sunshine hours (S , S_0) and extraterrestrial radiation (H_0). Total 32 numbers of input parameters combinations were employed to estimate the monthly mean daily GSR. Authors also concluded that two or three variables were sufficient to predict GSR. The combination of ΔT , H_0 and ΔT , S_0 , H_0 parameters was found to be most influenced combination for GSR estimation. The minimum MAPE obtained for the ΔT , H_0 combination was 2.61 %.

Kumar et al. [8] used rainfall and humidity quantity, temperature, sunshine hours, and barometric pressure as input parameters to estimate GSR. Different combinations of the input parameters and hidden layer neurons effect were analyzed by developing three ANN models. According to the

authors, the model using all of the meteorological input factors has the best accuracy. The authors' research has been expanded in order to identify the most important parameter for calculating solar radiation. An ANN's synaptic weights were analyzed at the synapse level using the connection weight approach, which revealed that temperature and humidity, followed by pressure, were the most acceptable parameters. With these three inputs, the ANN found a minimum MAPE of 12.15 percent.

Satellite-based data have been used to assess the Global Horizontal Insolation (GHI) of Himachal Pradesh [19]. Yadav et al. (2014) [20] used ANN-based model for solar radiation estimation. Authors also find the most suitable parameters for solar radiation estimation using Waikato Environment for Knowledge Analysis. Authors further extended the study and found the solar potential for Himachal region [21].

Adaptive Neuro Fuzzy Inference System (ANFIS) was utilized by [22] to estimate the GSR of Tamil Nadu (India). To estimate the monthly worldwide GSR (kWh/m^2) in Tamil Nadu, the model used the following input parameters: ambient temperature ($^{\circ}\text{C}$), atmospheric pressure (kPa), relative humidity (%), and wind speed (m/s). There were 372 samples in all that were used for both training and testing. A total of 204 data samples were used for training, with the remaining 168 data samples for testing. The coefficients of determination (R^2), RMSE, and Mean Bias Error (MBE) were determined as -1.031 , 0.0078 , and 0.9898 , respectively. The obtained results were compared with those of other model available in the literature for other regions and they exhibited better accuracy. From the literature, it can be inferred that ANN can be used for the solar potential estimation. However, the solar mapping for Indian Context is very limited. In the present study, the solar radiation has been estimated using ANN and solar maps have been generated for Western region of Himalaya. The developed ANN model can also use solar radiation estimation for different regions. The generated potential maps can be used for site selection of solar plants along with other solar applications in the present region. Therefore, the objectives of the present study include: a) investigating the solar potential for Western Himalayan region of India, especially H. P., where state government has mandated 776 MW generations through solar power, b) developing the ANN models using different combinations of geographical and metrological parameters; and c) developing a solar map from the estimated GSR for H. P.

2. METHODOLOGY

The following steps are carried out to investigate the solar potential in H. P.:

2.1. Data collection

The location and atmosphere parameters included longitude (Long), latitude (Lat), altitude (H), humidity (RH), pressure (P), wind speed (WS), and air temperature (T) [8-27] to estimate the GSR in H. P. The meteorological parameters namely pressure (kPa), wind speed (m/sec.), humidity (%), and temperature ($^{\circ}\text{C}$) were taken from NASA [23]. Solar radiation handbook data was used to compile average daily monthly GSR ($\text{kWh/m}^2/\text{day}$) data for 23 cities. The monthly average data were taken for the period of 1986 to 2000 [17]. The data on the city, Hamirpur, was obtained from the Centre for Energy situated at institute, National Institute of

Technology, NIT in Hamirpur, H. P., India. The geographical parameters include the latitude, altitude, and longitude of these 23 cities given in references.

2.2. ANN-based methodology for GSR estimation

A neural network is a network of a large number of neurons called processing unit, which maps the input and output data. Neural networks have an ability to generalize, which eases the complex and nonlinear problems. The most commonly used neural network in engineering areas is feed forward trained by the Back-Propagation (BP) having neurons as the major processor. These are divided into three levels: input, output, and hidden layers, with no feedback connections in any of them [24]. All layers are made up of neurons and all neurons are linked together by synaptic weights [25]. Moreover, the number of neurons in hidden layers may be changed through trial and error [26, 27]. Gradient descent and gradient descent with a momentum convergence rate are examples of back-propagation techniques that are overly slow. As a result, the Levenberg–Marquardt (LM) method was utilized to train the neural network in this study, which has a fast convergence rate [28, 29]. The fundamental neural network architecture is shown in Figure 1.

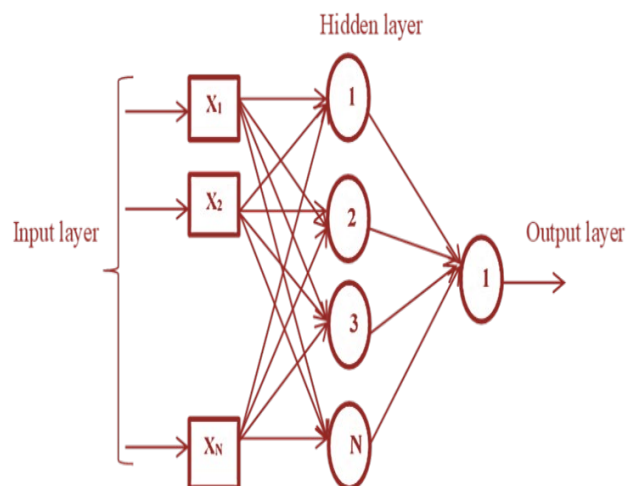


Figure 1. Basic architecture of the ANN

The steps taken in this study are illustrated in Figure 2. The input and output parameters were defined first in order to create the ANN model. For the 23 cities in India, seven characteristics were used as inputs, as explained in data collection. Several MLP designs were trained and evaluated in order to develop an ANN model in this work. The feed forward neural network was trained using the LM algorithm. Data were allocated at random to train the network. 70 % of the data were used for training, 15 % for testing, and the remaining 15 % for validation.

The number of neurons in the hidden layer is updated and the network is trained numerous times to refine the results obtained. The 7 inputs, 1 hidden layer, and 1 output layer lead to statistical error of MAPE using various experiments. MAPE's mathematical equations are as follows:

$$\text{MAPE} = \left(\frac{1}{n} \sum_{j=1}^n \left| \frac{\text{SR}_{j(\text{estimated})} - \text{SR}_{j(\text{actual})}}{\text{SR}_{j(\text{actual})}} \right| \right) \times 100 \quad (2)$$

For estimating GSR, the lowest MAPE value and the correlation coefficient value were evaluated. The model with the lowest MAPE value was also used to calculate GSR for 12

districts in H. P., India. The estimated worldwide solar radiation was mapped using the ARCGIS software.

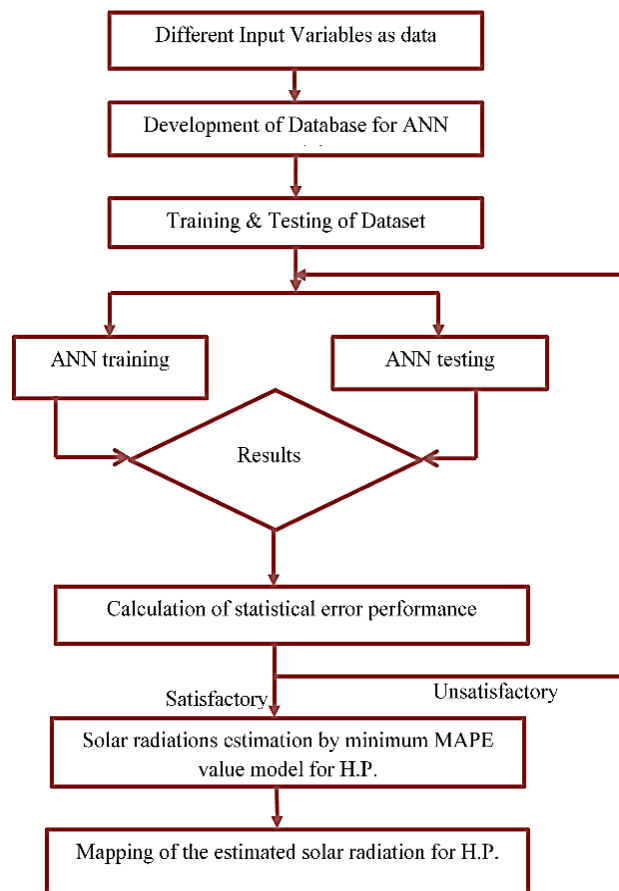


Figure 2. Flow diagram showing different steps to determine the ranking of parameters

Finally, the estimated GSR using the best proposed model by ANN for H. P. was used for mapping solar energy in the GIS environment.

3. RESULTS AND DISCUSSION

3.1. GSR estimation using ANN for 23 cities in India

This study used data from 23 cities in various climate zones to develop an ANN model for global sun radiations. The output of the same is estimated using BPLM technique for ANN. Neurons of the hidden layer of ANN are modified and multiple trainings are executed for achieving an optimum solution. Table 1 shows the training and testing data accuracies of ANN architectures.

Table 1 demonstrates that the estimated and observed values of GSR have the best agreement with an error value of less than 5 %. The network architecture consisting of 7-11-1 neurons in the input, hidden, and output layers, respectively, obtained a minimal MAPE value of 2.39 percent, as shown in Table 1. Figure 3 shows the optimal architectural neural network model given by ANN.

Figure 4 shows the regression plot for ANN architecture 7-11-1 that determines the relationship between output corresponding to the target values for training and that for testing. Scale of 0 to 1 is used to measure the value of R, and the values 0.998 and 0.912 are obtained in the training and testing periods, respectively. The obtained results show the optimal network architecture for calculating GSR with 7-11-1.

Table 1. Training and testing data accuracies of ANN architecture

ANN architecture (No. of neurons)	Correlation coefficient		MAPE	RMSE
	Training	Testing		
7-5-1	0.853	0.770	5.210	1.446
7-6-1	0.958	0.732	2.562	0.731
7-7-1	0.906	0.868	4.792	0.968
7-8-1	0.838	0.808	5.856	1.7834
7-9-1	0.866	0.834	5.291	1.494
7-10-1	0.971	0.921	3.427	0.853
7-11-1	0.998	0.912	2.369	0.719
7-12-1	0.920	0.815	3.768	0.891
7-13-1	0.889	0.835	4.363	0.913
7-14-1	0.880	0.783	5.140	1.038
7-15-1	0.807	0.754	5.879	1.898

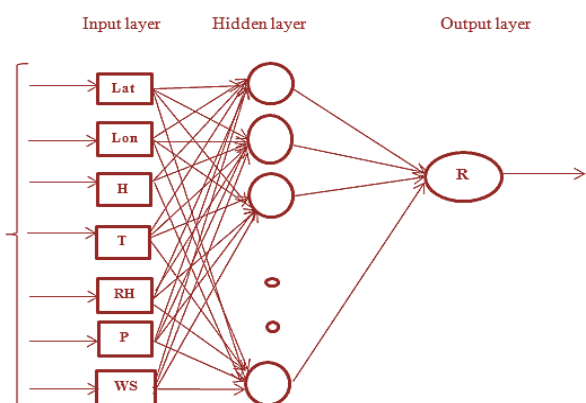


Figure 3. The best proposed ANN model for the GSR estimation in the present study

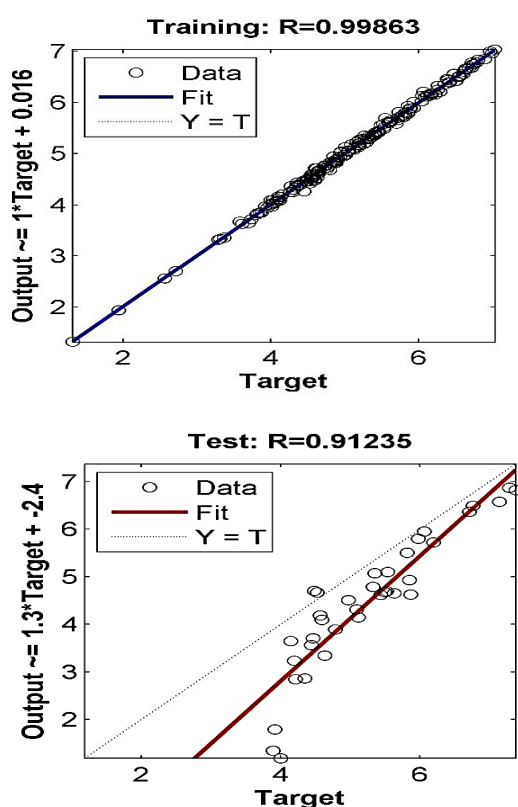


Figure 4. Regression plot for the best ANN architecture 7-11-1

Figure 5 shows the convergence plot for 7-11-1. The convergence plot signifies that as the mean square error increases, epochs continue decreasing. The convergence plot depicts that testing and validation have similar characteristics. The best performance of the convergence plot takes place at Iteration 58 (epoch).

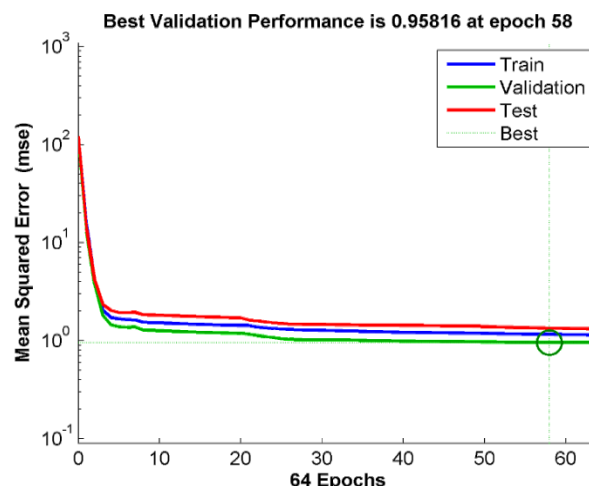


Figure 5. Convergence of neural network 7-11-1

3.2. GSR estimation using ANN for 12 cities in Himachal Pradesh (H. P.)

ANN architecture 7-11-1 with the least MAPE of 2.39 % is utilized in the study to estimate the global sun radiation of H. P. The input parameters taken from NASA include location and atmosphere, i.e., altitude, longitude, and latitude; temperature pressure, humidity, and speed of wind. These parameters are further used to estimate the GSR.

Figures 6 and 7 show the estimated GSRs for H. P. over a twelve-month period. According to the findings, H. P.'s solar potential ranges from 3.7 to 5.8 kWh/m². The solar potential of the district Lahaul Spiti was found to be the lowest. Among all the districts in H. P., Kangra has the highest solar potential. The field measurement data for GSR were obtained from the Centre for Energy and Environment, National Institute of Technology, Hamirpur, H. P., India for the validation of the suggested model.

3.3. GSR mapping

The feasibility of solar power plant needs proper site selection. For feasibility analysis, the creation of solar map is an essential part. Therefore, the estimated values of GSRs were depicted in monthly maps. The solar radiation availability for each district was distributed in three classes: (i) Low (below 4.0 kWh/m²), (ii) medium (4.0 to 6.0 kWh/m²), and (iii) high (above 6.0 kWh/m²). The monthly solar energy availability digital maps with provincial boundaries are depicted in Figures 6 and 7. From Figures 6 and 7, it can be concluded that there is seasonal variation of

solar potential in each district and the solar potential for the beginning of the months of years has low solar radiation. The Kangra and Una districts have medium solar potential during January. In February, Chamba has medium solar potential. The average value of global solar irradiation in H. P. ranges between 1.9 kWh/m² and 6.9 kWh/m². In April and May, each district exhibits good solar potential. From Figures 6 and 7, It is clear that the districts Una, Hamirpur, Kanga, and Chamba receive good GSR throughout the year and can be used for solar application.

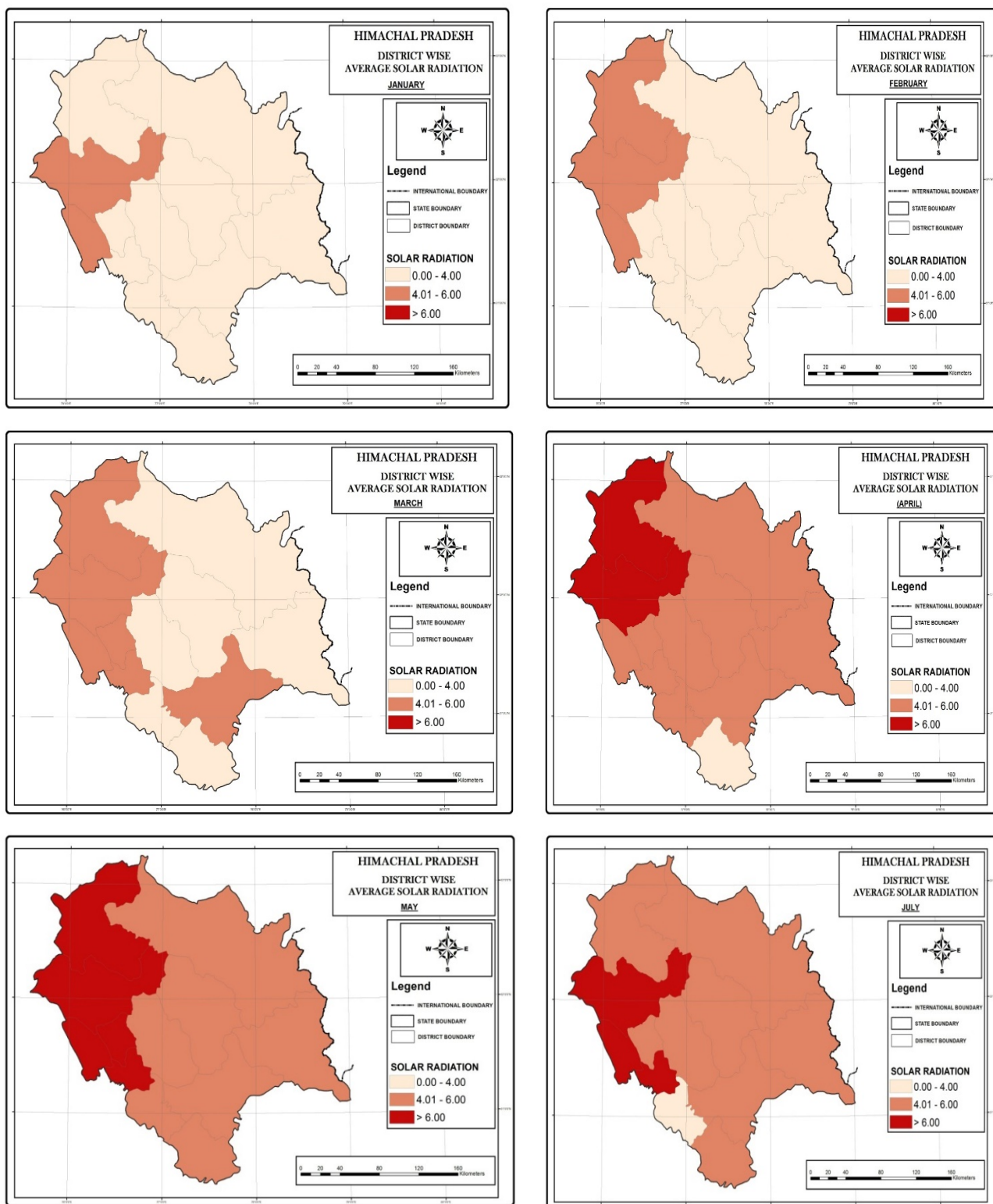


Figure 6. The solar energy maps for months of January to July in H. P.

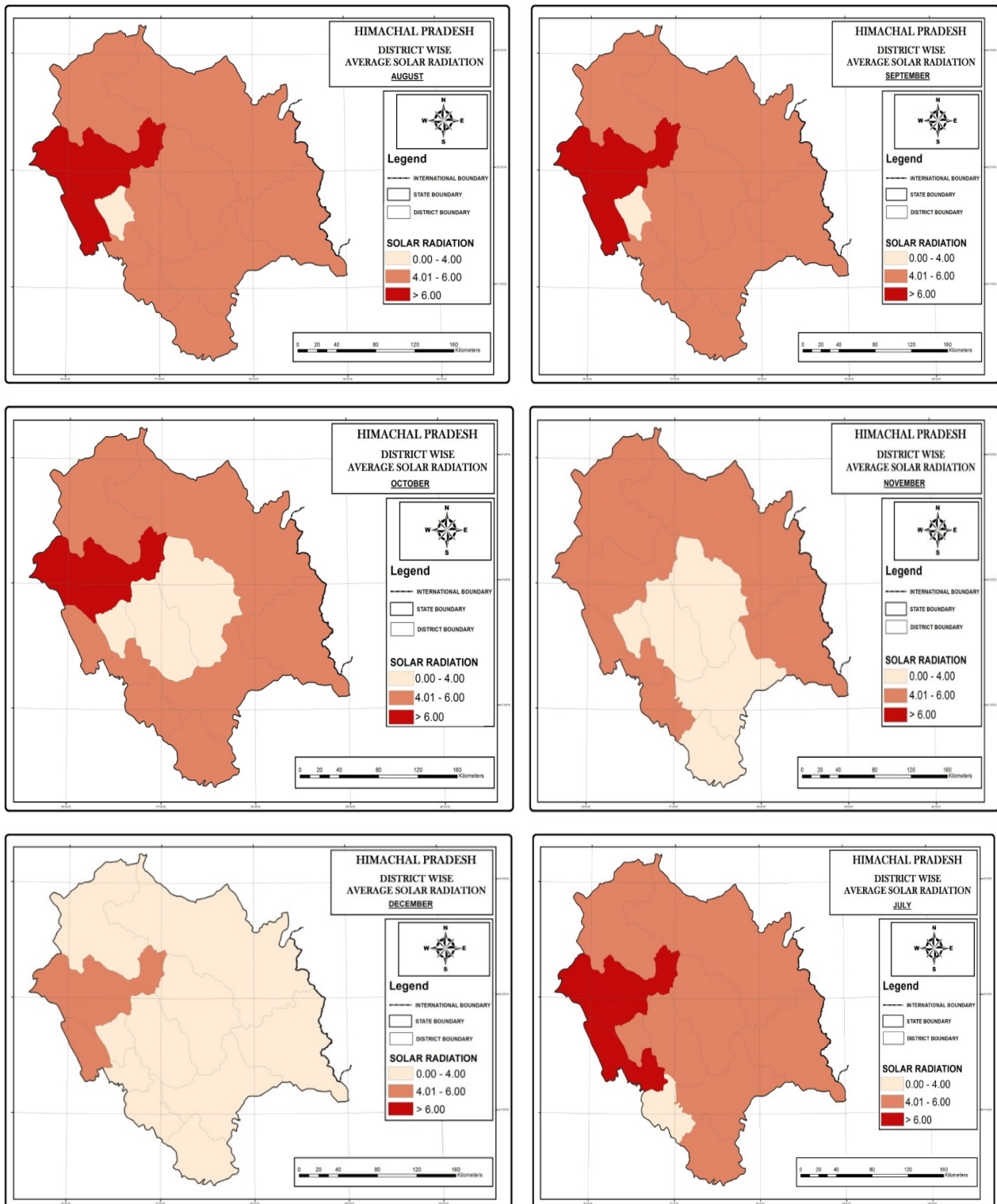


Figure 7. The solar energy maps for months of August to December in H. P.

4. CONCLUSIONS

In the presented work, ANN model was developed to estimate the GSR of different geographical and climatic zones of 23 cities in India. The statistical errors were used for the performance of the model. MAPE and R-values were obtained by different ANN models. The statistical performance error evaluation of accuracy demonstrates that the neural network consisting of 7-11-1 MLP architecture has a minimum MAPE value of 2.369. The neural network model with the architecture 7-11-1 was used to estimate the GSR of Western Himalaya region in Himachal Pradesh. The obtained results

show that the ANN model developed in this study are very helpful to find the solar potential where measuring instruments are not installed. The solar potential estimated by ANN model for 12 districts of H. P. state was used to create a solar map of twelve districts of H. P. The obtained solar maps in this study are used for site selection of solar plant in future work.

5. ACKNOWLEDGEMENT

This research was conducted in collaboration with the Faculty of Himachal Pradesh University.

NOMENCLATURE

MAPE	Mean Absolute Percentage Error
MLP	Multi-Layer Perception
GSR	Global Solar Radiation
GIS	Geographic Information System
ANN	Artificial Neural Networks
H	monthly average daily GSR (W/m^2)
H_0	extraterrestrial radiation (W/m^2)
S	monthly average daily hours of sunshine
S_0	monthly average day length
a, b	coefficients of correlation of regression
Long	Longitude ($^\circ$)
Lat	Latitude ($^\circ$)
RH	Humidity (%)
P	Pressure (kPa)
WS	Wind Speed (m/sec.)
T	Air Temperature ($^\circ C$)
BP	Back-Propagation
LM	Levenberg–Marquardt
RMSE	Root Mean Square Error

REFERENCES

- Masson, V., Bonhomme, M., Salagnac, J.L., Briottet, X. and Lemonsu, A., "Solar panels reduce both global warming and urban heat island", *Frontiers in Environmental Science*, Vol. 2, (2014), 14. (<https://doi.org/10.3389/fenvs.2014.00014>).
- Yang, W., Zhou, X. and Xue, F., "Impacts of large scale and high voltage level photovoltaic penetration on the security and stability of power system", *Proceedings of 2010 Asia-Pacific Power and Energy Engineering Conference*, IEEE, 1-5. (<https://doi.org/10.1109/APPEEC.2010.5448930>).
- Lahimer, A.A., Alghoul, M.A., Yousif, F., Razykov, T.M., Amin, N. and Sopian, K., "Research and development aspects on decentralized electrification options for rural household", *Renewable and Sustainable Energy Reviews*, Vol. 24, (2013), 314-324. (<https://doi.org/10.1016/j.rser.2013.03.057>).
- Byrne, J., Taminiau, J., Kurdgelashvili, L. and Kim, K.N., "A review of the solar city concept and methods to assess rooftop solar electric potential, with an illustrative application to the city of Seoul", *Renewable and Sustainable Energy Reviews*, Vol. 41, (2015), 830-844. (<https://doi.org/10.1016/j.rser.2014.08.023>).
- Sharma, V., Sharma, S., Verma, O.P., Bhardwaj, B., Sharma, T.K. and Pachauri, N., "Prediction and optimization of abrasive wear loss of ultrahigh strength martensitic steel using response surface methodology, Harris Hawk and artificial neural network", *International Journal of System Assurance Engineering and Management*, (2021), 1-17. (<https://doi.org/10.1007/s13198-021-01160-5>).
- Chen, J.L., He, L., Yang, H., Ma, M., Chen, Q., Wu, S.J. and Xiao, Z.L., "Empirical models for estimating monthly GSR: A most comprehensive review and comparative case study in China", *Renewable and Sustainable Energy Reviews*, Vol. 108, (2019), 91-111. (<https://doi.org/10.1016/j.rser.2019.03.033>).
- Antonopoulos, V.Z., Papamichail, D.M., Aschonitis, V.G. and Antonopoulos, A.V., "Solar radiation estimation methods using ANN and empirical models", *Computers and Electronics in Agriculture*, Vol. 160, (2019), 160-167. (<https://doi.org/10.1016/j.compag.2019.03.022>).
- Kumar, S. and Tarlochan, K., "Development of ANN based model for solar potential assessment using various meteorological parameters", *Energy Procedia*, Vol. 90, (2016), 587-592. (<https://doi.org/10.1016/j.egypro.2016.11.227>).
- Duffie, J.A., Beckman, W.A., and Blair, N., Solar engineering of thermal processes, photovoltaics and wind, John Wiley & Sons, (2020). (https://books.google.co.in/books?id=4vXPDwAAQBAJ&dq=Duffie+J.+A.+Beckman.+W.+A.+%26+Blair.+N.+%20%282020%29.+Solar+engineering+of+thermal+processes,+photovoltaics+and+wind.+John+Wiley+%26+Sons.&lr=&source=gb_s_navlinks_s).
- Zhang, J., Zhao, L., Deng, S., Xu, W. and Zhang, Y., "A critical review of the models used to estimate solar radiation", *Renewable and Sustainable Energy Reviews*, Vol. 70, (2017), 314-329. (<https://doi.org/10.1016/j.rser.2016.11.124>).
- Besharat, F., Dehghan, A.A. and Faghih, A.R., "Empirical models for estimating GSR: A review and case study", *Renewable and Sustainable Energy Reviews*, Vol. 21, (2013), 798-821. (<https://doi.org/10.1016/j.rser.2012.12.043>).
- Shavandi, H. and Ramyani, S.S., "A linear genetic programming approach for the prediction of solar global radiation", *Neural Computing and Applications*, Vol. 23, No. 3, (2013), 1197-1204. (<https://doi.org/10.1007/s00521-012-1039-6>).
- Gairaa, K., Khellaf, A., Messlem, Y. and Chellali, F., "Estimation of the daily GSR based on Box–Jenkins and ANN models: A combined approach", *Renewable and Sustainable Energy Reviews*, Vol. 57, (2016), 238-249. (<https://doi.org/10.1016/j.rser.2015.12.111>).
- Irvin, J.D. and Wilamowski, B.M., Intelligent systems: The industrial electronics handbook, CRC Press, (2018), 1-12. (<https://doi.org/10.1201/9781315218427>).
- Almaraashi, M., "Investigating the impact of feature selection on the prediction of solar radiation in different locations in Saudi Arabia", *Applied Soft Computing*, Vol. 66, (2018), 250-263. (<https://doi.org/10.1016/j.asoc.2018.02.029>).
- Jović, S., Aničić, O., Marsenić, M. and Nedić, B., "Solar radiation analyzing by neuro-fuzzy approach", *Energy and Buildings*, Vol. 129, (2016), 261-263. (<https://doi.org/10.1016/j.enbuild.2016.08.020>).
- Xue, X., "Prediction of daily diffuse solar radiation using artificial neural networks", *International Journal of Hydrogen Energy*, Vol. 42, No. 47, (2017), 28214-28221. (<https://doi.org/10.1016/j.ijhydene.2017.09.150>).
- Premalatha, M. and Naveen, C., "Analysis of different combinations of meteorological parameters in predicting the horizontal GSR with ANN approach: A case study", *Renewable and Sustainable Energy Reviews*, Vol. 91, (2018), 248-258. (<https://doi.org/10.1016/j.rser.2018.03.096>).
- Ramachandra, T.V., Krishnadas, G. and Jain, R., "Solar potential in the Himalayan landscape", *International Scholarly Research Notices*, (2012). (<https://doi.org/10.5402/2012/203149>).
- Yadav, A.K., Malik, H. and Chandel, S.S., "Selection of most relevant input parameters using WEKA for artificial neural network based solar radiation prediction models", *Renewable and Sustainable Energy Reviews*, Vol. 31, (2014), 509-519. (<https://doi.org/10.1016/j.rser.2013.12.008>).
- Yadav, A.K., Malik, H. and Chandel, S.S., "Application of rapid miner in ANN based prediction of solar radiation for assessment of solar energy resource potential of 76 sites in Northwestern India", *Renewable and Sustainable Energy Reviews*, Vol. 52, (2015), 1093-1106. (<https://doi.org/10.1016/j.rser.2015.07.156>).
- Sumithira, T.R. and Kumar, A.N., "Prediction of monthly GSR using adaptive neuro fuzzy inference system (ANFIS) technique over the State of Tamilnadu (India): A comparative study", *Applied Solar Energy*, Vol. 48, No. 2, (2012), 140-145. (<https://doi.org/10.3103/S0003701X1202020X>).
- NASA, (2019). (<https://power.larc.nasa.gov/data-access-viewer/>).
- Wu, C.L., Chau, K.W. and Li, Y.S., "Methods to improve neural network performance in daily flows prediction", *Journal of Hydrology*, Vol. 372, (2009), 80-93. (<https://doi.org/10.1016/j.jhydrol.2009.03.038>).
- Reddy, K.S. and Ranjan, M., "Solar resource estimation using artificial neural networks and comparison with other correlation models", *Energy Conservation & Management*, Vol. 44, (2003), 2519-2530. ([https://doi.org/10.1016/S0196-8904\(03\)00009-8](https://doi.org/10.1016/S0196-8904(03)00009-8)).
- Arora, M.K. and Mathur, S., "Multi-source classification using Artificial Neural Network in a rugged terrain", *Geocarto International*, Vol. 16, (2001), 37-44. (<https://doi.org/10.1080/10106040108542202>).
- Wasserman, P., Advanced methods in neural computing, Van Nostrand Reinhold, New York, (1993). (<https://dl.acm.org/doi/abs/10.5555/562821>).
- Hagan, M.T. and Menhaj, M., "Training feed forward networks with the Marquardt algorithm", *IEEE Transactions on Neural Networks and Learning Systems*, Vol. 5, (1994), 989-993. (<https://doi.org/10.1109/72.329697>).
- Hagan, M.T., Demuth, H.B. and Beale, M.H., Neural network design, PWS Publishing, Boston, MA (1996). (<https://dl.acm.org/doi/10.5555/249049>).



Research Article

Modified Concrete for Impeding Chloride Diffusion from Sea Water in the Marine Environment

Davar Rezakhani ^a, Abdol Hamid Jafari ^{a*}, Mohammad Ali Hajabassi ^b

^a Department of Materials Science and Technology, Shahid Bahonar University, Kerman, Kerman, Iran.

^b Department of Mechanical Engineering, Shahid Bahonar University, Kerman, Kerman, Iran.

PAPER INFO

Paper history:

Received: 11 July 2021

Revised in revised form: 17 January 2022

Scientific Accepted: 25 September 2021

Published: 11 May 2022

Keywords:

Chloride,
Diffusion,
Graphene Oxide,
Marine Environment,
Ground Granulated Blast Furnace Slag

ABSTRACT

The application of nanomaterials to concrete is an innovative approach to enhance mechanical properties and durability performances. In this work, the addition of a combination of Graphene Oxide Nano-Platelets (GONP) and Ground Granulated Blast Furnace Slag (GGBFS) was studied as admixture in concrete. Tests on mechanical and chloride permeation properties were conducted. The results showed that the mix with 0.05 % GONP and the mix with 30 % GGBFS obtained better mechanical strength than the rest of the mixes. The highest electrical resistivity was achieved for the 90-day cured sample with 50 % GGBFS in CONP-free concrete and the 0.01 % GONP in GGBFS-free concrete, which was found to be the most effective in increasing concrete resistance to chloride permeation. The mix with 0.1 w % GONP and 50 w % GGBFS exhibited considerable performance even with other mechanical and durability performances. The addition of 0.1 % graphene oxide and 50 % granular slag increased the compressive strength of the concrete sample by 19.9 % during 28 days and 17.6 % during 90 days compared to the conventional concrete sample. Concrete with a combination of 0.1 % graphene oxide and 50 % granular slag experienced an increase in flexural strength by 15 % during 28 days and 13.6 % during 90 days. A significant reduction in electrical conductivity from 4012C to 1200C was observed for 90-day cured samples containing 0.1 wt % GO and 50 wt % GGBFS compared to the conventional sample. Response Surface Method (RSM) applied to the test data presented an optimized concrete mix containing 0.08 w % GONP and 50 w % GGBFS, the outcome of which was in close agreement with the experimental results.

<https://doi.org/10.30501/jree.2022.293613.1227>

1. INTRODUCTION

Concrete remains the most widely used industrial material and new-found modifiers help improve its durability, mechanical properties, and specifically corrosion resistance [1, 2]. An important issue about marine structures is chloride permeation causing rapid rebar corrosion and interference in protection systems including cathodic protection so much so that it has been reported to be the main problem in concrete structures worldwide [3-8]. Even inland, temperature, and humidity fluctuations causing cyclic expansion-contraction and hydration-dehydration could cause the initiation and propagation of cracks in concrete, instigating rebar corrosion and concrete spalling with the subsequent loss of load-bearing capacity. In a chloride-containing environment, its permeation from solution-filled pores, chlorine contaminated cement, or diffusion along paths in the matrix of the concrete may exacerbate the rate of deterioration manifold. Total amount of chloride in concrete consists of bound and free chlorides and the latter is responsible for breaking the passive layer on the

bars [9, 10]. In effect, the level of chloride bound to concrete could directly affect corrosion as these immobile ions diminish the overall diffusion rate and accumulation of Cl^- at the rebar-concrete interface [11, 12]. The rate of chlorine ion permeation depends on the materials used and the production parameters such as water-to-cement ratio, additives, and degree of hydration [13].

The application of nanomaterials to concrete is an innovative approach to enhancing its mechanical and durability properties. Nanomaterials in concrete have many advantages including the enhancement of mechanical strength and filling of the voids at a nano level. Concrete has pores on both nano (10^{-9} m) and micro (10^{-6} m) scales. Compaction of concrete reduces the amount of porosity. However, small cavities remain in the concrete composite. The strength of concrete depends on the formation of calcium hydrate silicate products (C-S-H), and the products are pore-dependent at nano and micro levels. Filling of these pores with inert or reactive materials can increase the strength and durability properties, reduce crack formation, and so on. Upon applying pozzolanic materials to concrete, it can only fill small cavities. Therefore, nanometer pores can be filled using these nanomaterials [14, 15]. Nanoparticles react with calcium

*Corresponding Author's Email: jafham2020@gmail.com (A.H. Jafari)

URL: https://www.jree.ir/article_149660.html



hydroxide ($\text{Ca}(\text{OH})_2$) and CSH gels in the pores. This measure creates a denser structure and fills pores on the cement [15]. Many researchers have studied the mechanical and durability properties of concrete with nano admixtures and as usual, it exhibits better results than conventional cement composites [16, 17]. A large number of researchers have demonstrated the incorporation of nanomaterials. In recent years, carbon nanomaterials such as Carbon Nanotubes (CNTs), Carbon Nanofibers (CNFs), and Graphene Oxide (GO) have attracted the attention of many concrete researchers due to their unique mechanical, thermal, chemical, and electrical properties [18-20]. However, the application of materials such as carbon nanotube is difficult due to their poor dispersibility. GO sheets with oxygenated functions are more accessible to cement particles, thus allowing nano sheets to act as cores for cement phases and increase the reaction of cement with water [21]. Graphene oxide nano plates have been studied because of their hydrophobic effect at low concentrations [22-26]. Graphene oxide contains functional oxygen groups in its layered structure that increase the inter-planar space causing easier thinning out in aqueous environments. It has been reported that admixing of GO nano plates to cement expedites its hydration process and increases the total hydration products [26]. This has been attributed to its high surface energy that facilitates the absorption of hydration products that acts as nucleation sites for hydration reaction [25]. Yang et al. reported that with the addition of 0.1 wt % GO, cement hydration increased by 10.4 % on Day 28 [27]. Graphene oxide nano particle effect on cement hydration could change the intra-structural porosity with a subsequent increase in cement strength and toughness. Wang et al. maintained that the microstructure of the GO-reinforced cement matrix had a massive crystal structure covering, implying that leaching of Calcium Hydroxide (CH) during the hydration stages was enhanced on Day 28 (curing age) [28]. Addition of GO to cement-based composites has an adverse effect on performance due to its large area that tends to absorb more water molecules for wetting and its large high-capacity lateral size due to the clustering of GO nanoplates [29, 30]. Regardless of the disadvantages mentioned above, combining a small amount of GO at about 1 % by weight of cement improves the compressive strength by 63 % [31]. Lu et al. confirmed that the addition of only 0.05 wt % nano-sized graphene oxide caused 10.4 % and 12.6 % improvements in compressive and flexural strengths after 28 days. Other researchers claimed the improvement rates of 78.6 %, 60.7 %, and 38.9 % in tensile, flexural, and compressive strengths, respectively, by 0.03 % GO addition [32, 33]. Gang Xu et al. reported a 29 % increase in the compressive strength of cement pastes after 28-day curing by admixing 0.02 wt % GO [26]. Hue peng et al. pointed to a 21.86 % increase in flexural strength and overall toughness by admixing 0.03 wt % GO with the cement [25]. The addition of 0.05 % GO was reported to enhance the compressive strength by 15-33 % and flexural strength by 41-58 % [17, 34]. Shang et al. stated that the compressive strength with the inclusion of 0.04 % GO to the cement paste was enhanced by 15.1 % compared to the plain cement paste [35]. The compressive and tensile strengths increased by over 40 % with the inclusion of 0.03 % GO by weight of cement to OPC (Ordinary Portland Cement) paste on Day 28 at the curing age [36]. In the research done by Lee et al., cementitious composites replaced with conventional cement additives, such as Fly Ash (FA), Silica Fume (SF), Nano-Silica (NS), and Ground Granulated Blast-furnace Slag

(GGBS) and graphene oxide were studied for comparison. The cementitious composites replaced with GO had compressive strength of 10.6–41.5 % higher than that of the plain mixture and also, higher than that obtained with other cement additives. In this study, the pore structure analysis revealed that the majority of pores had micro pores with diameters not exceeding 2.5 nm which improved their strength [37]. Kudźma et al. studied the effect of graphene oxide with low oxygen content on Portland cement based composites. In this study, the amounts of GO investigated were 0.02 %, 0.04 %, and 0.06 % by weight of cement, while for mortars, an extra composition with 0.1 % was also prepared. According to the results, the fluidity of cement paste and mortar increased and the hydration process was slightly retarded with the addition of GO. However, improvements in compressive and flexural strength were established in the mortars containing GO. The maximum effects (~ 22 % and ~ 6 %, respectively) were obtained with the addition of 0.06 % GO [38].

Hassani et al. used a dose of 0.1 to 2 % GO and observed that high bond strength was created due to the nuclearization of C-S-H by GO shells. As demonstrated by the results, there was an increase in the amount of C-S-H gel which helps reduce the permeability of concrete and increase the durability of concrete structures [39]. Gong et al. studied the effect of GO admixture on cement paste with an optimal dose of GO 0.03 % by weight of cement and found that due to the reduction of the cavity structure, the mechanical strength increased by more than 40 % compared to the conventional matrix [36]. They observed changes in efficiency, heat of hydration, and cavity structures. Analysis of pore structure indicated that the total porosity and capillary pores were reduced by 13.5 % and 27.7 % and gel pores increased. According to the results of this study, more C-S-H products are produced, leading to a reduction in capillary pores and an increase in gel pores. Wang et al. used 0.02, 0.04, 0.06 and 0.08 % Graphene oxides. At 0.08 % dosage, the flexural strength and compressive strength were at maximum, i.e., increased by 27 % and 16.4 %, respectively. They observed that at low amounts of graphene oxide, hydration products bound to each other and remained in specific locations, and when the dose increased, the hydration product would tend to form clusters such as structure to prevent the propagation of small cracks [40]. Kai Guo et al. investigated the impact of GO on chloride penetration resistance of concrete and demonstrated that the addition of 0.06 wt % GO nano plates was enough to achieve the highest chloride penetration resistance [23]. Therefore, previous studies have shown that the chances of improving the mechanical properties, permeability, and durability of cement when using graphene oxide are higher. The required dose of GO is lower than other nanomaterials to obtain the same effect [41, 42].

Other nano-sized additives such as Ground Granulated Blast furnace Slag-GGBFS are mainly used to reduce free chloride by binding it to concrete [43-48]. GGBFS is a by-product of iron production in the blast furnaces where slag is water or steam quenched and ground to a fine mesh powder [49]. Researchers report the beneficial effect of GGBFS on compressive strength while adversely affecting the hydration rate, thus prolonging the time to attain maximum mechanical strength [50-52]. Chen et al. reported the effect of around 45 wt % GGBFS on reducing the chloride penetration [53]. Samad et al. found that GGBS concrete gained much more strength than the Portland cement concrete until 56 curing

days [54]. Khatib and Hibbert et al. reported a significant flexural strength increase with up to 60 wt % GGBFS admixture; however, additional increases would adversely affect it [55]. Dejian Shen et al. investigated the residual tensile stress and the cracking potential of concrete and reported improvements to both parameters with up to 50 wt % GGBFS addition [56]. The beneficial effect of GGBFS was reported upon affecting the pore size, hence curtailing permeability [52]. Güneysi et al. observed that only minute amounts typically less than 1000 Coulombs of charged chloride ion would be detected during the RCPT test when 20-50 wt % GGBFS was added to concrete. Others reported a 29 % reduction in passing electrical charge by adding up to 50 wt % GGBFS [57]. The diffusion coefficient of chloride in concrete also decreased with the addition of GGBFS [58, 59]. It has been observed that GGBFS can be effectively used to reduce the pore sizes and cumulative pore volume considerably, leading to more durable and impermeable concrete. According to the studies of Hwang and Lin, GGBFS has the potential to replace cement in high percentages because of its in-built cementitious property. The continued use of slag cement in the construction industry requires a consideration of the effect of electrochemically reducing pore solution on depassivation of steel reinforcement in cement system. Studies revealed that the inhibition of corrosion in slag concrete resulting from its low electrical conductivity caused a refined pore structure [48]. Nowadays, due to different environmental conditions, structures do not work as expected. Damage in the form of structural cracks due to stresses as well as scaling and shrinkage due to loss of fine aggregates and high wear, leakage, etc. lead to failure of concrete structures, and the use of ordinary concrete leads to premature destruction of structures. Therefore, the use of high-strength modified concrete as a building material in marine structures can be useful. The advantage of using such high performance concretes can reduce the cost of materials by reducing the thickness of the structure, increasing the mechanical, physical, and corrosion properties or saving the required materials. The use of GO in concrete is progressing due to its exceptional properties. Interest in GO has increased in various fields around the world because GO is more inexpensive than multi-walled CNTs, single-walled CNTs, and CNFs (which are 250, 1280, and 218 times more expensive than GO per 100 g, respectively) [60]. Therefore, GO became the best candidate for this research. This investigation was carried out to develop a nano-reinforced concrete composite in addition to GONP and GGBFS with varying percentages by weight of cement. No study has been reported on GO and GGBFS inclusion in concrete composites with regard to compressive strength, flexural strength, chloride permeation, and the cost analysis to get a clear picture whether this investigation is helpful for practical application in the construction industry. The present study focuses on the use of GONP-GGBFS as a nano-filler to develop a concrete for industrial applications in marine environment. The present research examines the effect of GONP and GGBFS addition on mechanical and permeability properties of concrete structures in marine environment. The optimized pozzolanic composition is achieved through the RSM optimization method to test this approach to designing a chlorine-resistant concrete for marine environments. The following are the specific objectives and scope of the present study:

- To study properties of concrete with the inclusion of GONP and GGBFS, thereby obtaining the mechanical performance of nano-modified concrete designed for industrial applications in marine environment;
- To determine the durability performance of nano-modified GONP-GGBFS based concrete mixes;
- To study the microstructural behavior of selected GONP-GGBFS-based concrete mixes through SEM and XRD analyses.

2. EXPERIMENTAL

2.1. Materials

Type-II Portland cement with the chemical composition of Table 1 and the mechanical properties of the cement mortar in Table 2, measured per ASTM C109, was used. The sand and gravel gradation per ASTM C136 and ASTM C117 is shown in Tables 3 and 4. The GGBFS was procured from local sources with Blaine fineness of $3500 \text{ cm}^2\text{g}^{-1}$. The CaO/SiO₂ ratio was 1.4 based on the semi quantitative XRD (Figure 1) and XRF analysis (Table 5) corresponding to ASTM E1621-13. The water-to-cement ratio (W/C) was kept at 0.4. The FE-SEM microstructure images of nanoplatelets are shown in Figure 2, according to which the particle length varies from 2 μm to 15 μm and the average thickness is 7.7 nm. The FE-SEM images show the morphology of graphene oxide nano-sheets to be wrinkled thin lamellar layers interlinked to form a three-dimensional porous structure [21, 61, 62]. According to previous studies [22, 63-66], the inter-planar distance in the crystalline GO structure could be calculated from XRD pattern using Bragg's law: $\lambda = 2d \sin(\theta)$, where λ is the X-ray beam wavelength (in this case, $\lambda = 1.54 \text{ \AA}$), d the distance between adjacent layers, θ the diffraction angle. According to XRD analysis in Figures 3 and 4, $d = \lambda / 2 \sin(\theta) = 1.54 \text{ \AA} / 2 \sin(\theta)$ which would come to 6.8 \AA for the initial sharp peak. The elemental analysis and physical properties of the GO are shown in Tables 6 and 7.

Table 1. The chemical analysis and hydration times of type-II cement according to ASTM C114 and ASTM C191

Constituent	%
SiO ₂	21
Al ₂ O ₃	4.5
Fe ₂ O ₃	4
CaO	65.6
MgO	2.3
NaO	0.25
KO	0.41
Alkaline equivalent	0.52
SO ₃	1.2
Cl	0.02
Insoluble residue	0.2
3CaO.SiO ₂	66.9
2CaO.SiO ₂	9.8
3CaO.Al ₂ O ₃	6.2
4CaO.Al ₂ O ₃ .Fe ₂ O ₃	12.2
Initial hydration time (min)	104
Final hydration time (min)	225

Table 2. Compressive strength of portland type-II cements mortar according to ASTM C109

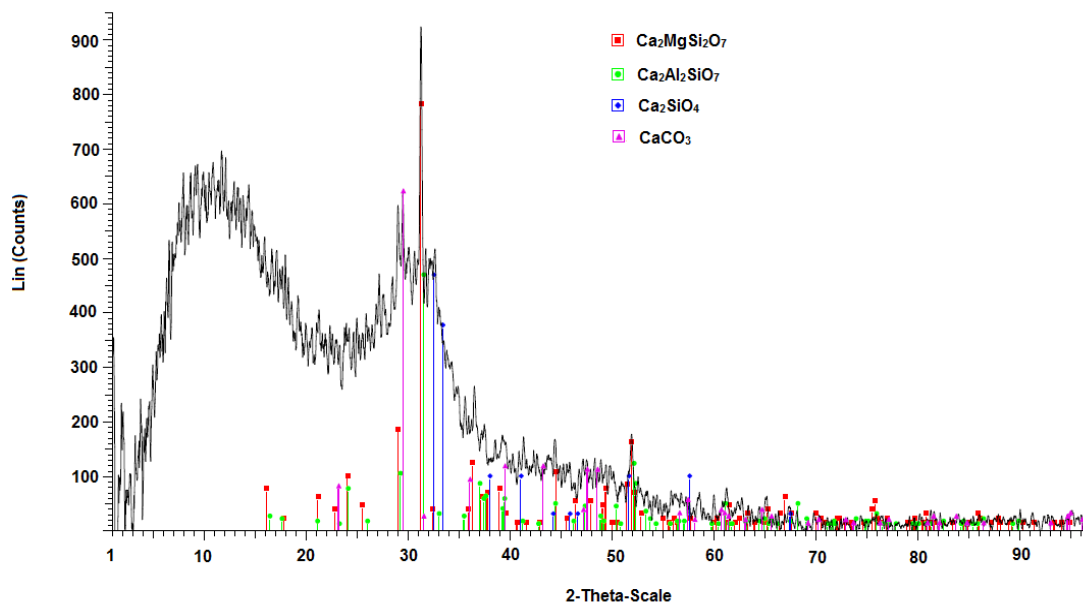
Age (days)	Compressive strength (N.mm ⁻²)
3	20.60
7	23.40
28	25.86
90	31.03

Table 3. Gradation of sand per ASTM C106 and ASTM C117

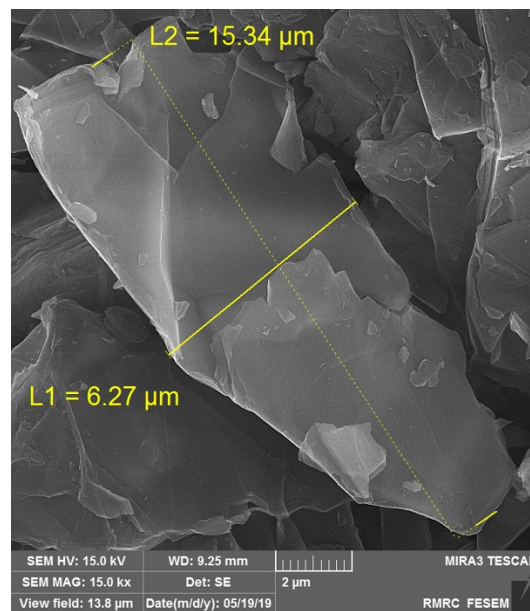
Square mesh size (mm)	Sieve number	Cumulative percentage of remained sand on the sieve (%)
9.500	3.8	0.0
4.750	4.0	9.6
2.360	8.0	35.3
1.180	16.0	58.0
0.600	30.0	75.0
0.300	50.0	84.9
0.150	100.0	95.1
0.075	200.0	97.7

Table 4. Gradation of gravel per ASTM C106 and ASTM C117

Square mesh size (mm)	Sieve number	Cumulative percentage of remained oval gravel on the sieve (%)	Cumulative percentage of remained pea gravel on the sieve (%)
50.00	2	0.0	0.0
37.50	1.5	0.0	0.0
25.00	1	0.0	0.0
19.00	3.4	5.3	0.0
12.50	1.2	65.7	31.3
9.50	3.8	93.6	62.8
4.75	4	99.9	99.6
2.36	8	99.9	99.9

**Figure 1.** XRD analysis of GGBFS**Table 5.** XRF and XRD chemical analysis results of GGBFS

Constituent	wt %
Na ₂ O	0.55
P ₂ O ₅	0.06
CaO	43.64
SrO	0.18
MgO	6.17
S	1.25
TiO ₂	1.81
BaO	0.32
Al ₂ O ₃	9.16
Cl	0.02
MnO	1.96
L.O.I	1.50
SiO ₂	31.10
K ₂ O	1.11
Fe ₂ O ₃	1.17
TOTAL SUM	100.00



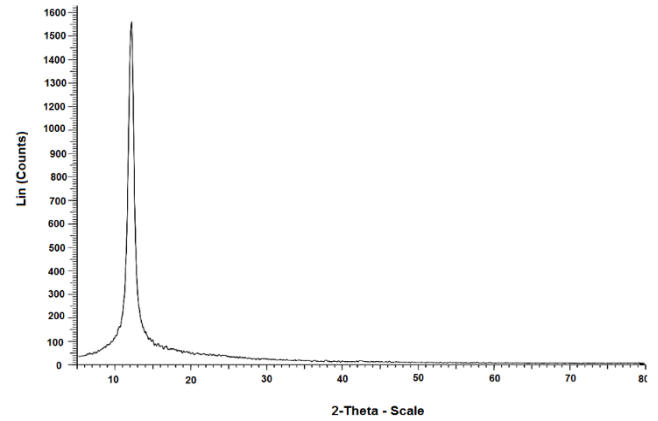
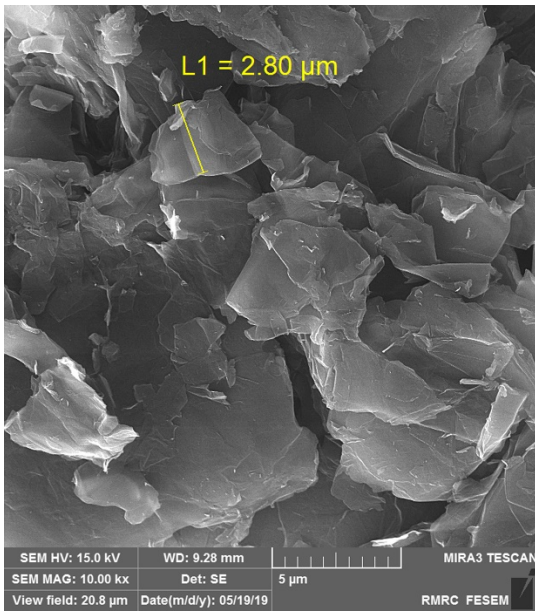


Figure 3. XRD analysis of dry GO before dispersion in water

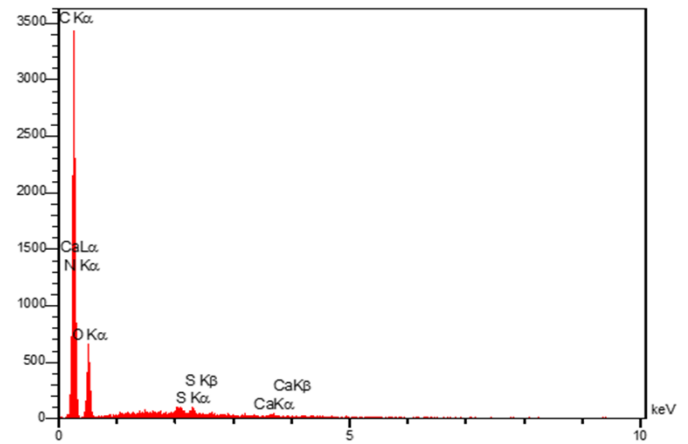
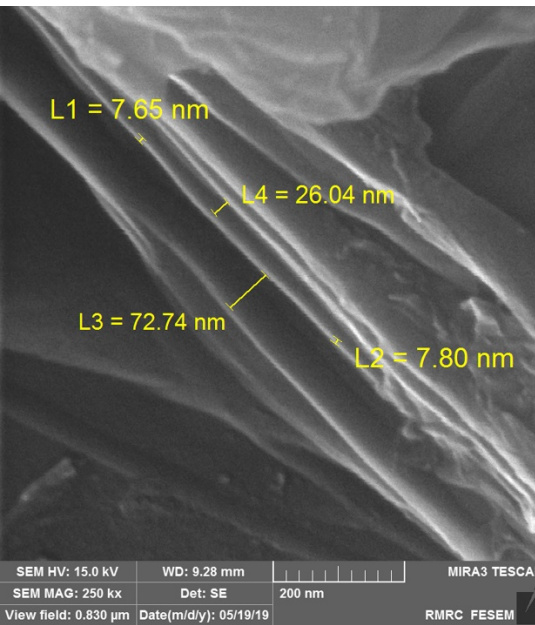


Figure 4. EDS area elemental analysis of GONP

Table 6. Elemental EDS analysis of graphene oxide nanoparticles

Element	C	N	O	S	Ca
%	70.87	0.88	27.81	0.28	0.16

Table 7. Physical properties of commercially procured GONP

Purity (%)	Size (μm)	Platelet thickness(nm)	No. of layers	Original packaged form
> 99	2-16	7.5-8.5	5-8	Black powder



Figure 2. FE-SEM image of GO nanolayers with an average thickness of about 7.7 nm

2.2. Mortar mixing and curing procedure

Concrete mixes with compositions shown in Table 8 containing 30, 40, and 50 wt % of GGBFS and 0.01, 0.05, and 0.1 wt % of GONP were prepared. The GO solution for each mixing design was prepared according to the following:

1. For 0.01 wt % GO mix; 0.85 g of GO powder was added to 170 g water and 42.5 g polycarboxylate as a super plasticizer;
2. For 0.05 wt % GO mix; the total needed amount of GO powder (4.25 g) was divided into two equal parts and each was added to 508gr water and 21.25 g polycarboxylate,
3. For 0.1 wt % GO mix; the total amount of GO powder (8.5 g) was divided into three equal parts and each was added to 691.3 g water and 14.16 g polycarboxylate.

The weight percentage of GO was kept at 0.4 % in all solutions so as to homogenize them. The total dispersion is

achieved through sonication using a 300W and 20 kHz frequency transducer for 30 minutes. The graphene oxide solution and cement and aggregates mortar were mixed in a shear mixer for 3 minutes followed by 30 seconds on a shaker. The W/C ratio was kept constant by adding just the difference between the total water required and the water used to make

the GO solution. ASTM C192M-16 standard was followed to make samples, which were kept in the molds in laboratory conditions for 24 hours and then, cured for 28 and 90 days at 25 °C and relative humidity of > 95 % in a water bath containing Lime. Polycarboxylate was used as a Super Plasticizer and 0.5 % by weight of cement in all samples.

Table 8. Quantity of materials used in m³ of concrete samples

MIX	GGBFS (wt %)	GO (wt %)	GGBFS (kg/ m ³)	GO (kg/m ³)	OPC (kg/m ³)	Water (kg/m ³)	Fine aggregate (kg/m ³)	Coarse aggregate (kg/m ³)	SP (kg/m ³)
C	0.00	0.00	0.0	0.0000	425	170	1005.5	676.5	0.0425
G1	0.00	0.01	0.0	0.0425	425	170	1005.5	676.5	0.0425
G2	0.00	0.05	0.0	0.2125	425	170	1005.5	676.5	0.0425
G3	0.00	0.10	0.0	0.4250	425	170	1005.5	676.5	0.0425
S1	30	0.00	127.5	0.0000	297.5	170	1005.5	676.5	0.0425
S2	40	0.00	170.0	0.0000	255	170	1005.5	676.5	0.0425
S3	50	0.00	212.5	0.0000	212.5	170	1005.5	676.5	0.0425
SG1	30	0.01	127.5	0.0425	297.5	170	1005.5	676.5	0.0425
SG2	30	0.05	127.5	0.2125	297.5	170	1005.5	676.5	0.0425
SG3	30	0.10	127.5	0.4250	297.5	170	1005.5	676.5	0.0425
SG4	40	0.01	170.0	0.0425	255	170	1005.5	676.5	0.0425
SG5	40	0.05	170.0	0.2125	255	170	1005.5	676.5	0.0425
SG6	40	0.10	170.0	0.4250	255	170	1005.5	676.5	0.0425
SG7	50	0.01	212.5	0.0425	212.5	170	1005.5	676.5	0.0425
SG8	50	0.05	212.5	0.2125	212.5	170	1005.5	676.5	0.0425
SG9	50	0.10	212.5	0.4250	212.5	170	1005.5	676.5	0.0425

◆ OPC - Ordinary Portland Cement, GO – Graphene Oxide, GGBFS – Ground Granulated Blast Furnace Slag, SP – (Carboxylate based) Super Plasticizer

3. METHOD

3.1. Mechanical tests

ASTM C39M-18 and C78M-18 standard tests were followed for examining the compression and flexural strength of concrete specimens.

3.2. Resistance to chlorine permeation test (RCPT)

Chloride permeability resistance was evaluated per ASTM C1202 accelerated test on cylindrical samples with 10 cm diameter and 5 cm length made specifically for the test. An electrical current passed through the concrete sample under a constant 60 V DC potential difference for six hours on the one side and was measured on the other side. One end was immersed in 3 % sodium chloride solution and the other in a 0.3 M solution of sodium hydroxide [67]. The total coulombs of electricity passed, becoming proportional to the electrical resistance of the specimen which inversely relates to chloride ion penetrating the sample. Therefore, the lower the electric current, the higher the resistance to chloride ingress.

3.3. Electrical resistivity of concrete

Wenner's four-point line array test is a well-established technique for measuring the resistivity of soil and semiconducting materials. For determining the resistivity of concrete, this test is applied with modifications based on AASTHO TP 95-11 standard. In a more common form, four equally spaced electrodes are arranged linearly to measure the electrical resistivity. The two outer electrodes apply an AC current to the concrete surface, while the electrical potential is measured between the inner probes. The electrodes in a four-probe square array are arranged in a square position at 50 to 100 mm spacing [68, 69].

3.4. Response surface optimization and statistical analysis

The selection of the optimal concrete composition in terms of the highest electrical resistance and mechanical properties was done by Response Surface Method (RSM). The experimental data were the required input for the Design-Expert software version 7.0.1.0 and a Central Composite Face centered Design (CCFD) comprising technique was employed. The variables considered in the optimization were the weight percentages of graphene oxide and granulated blast furnace slag, whereas the response variables were the compressive strength, flexural strength, RCPT data, and electrical resistance. The software assigns the required number of experiments based on the number of variables (Percentages of GGBFS and GO) and responses measured (RCPT, Electrical resistance, compressive strength, and Flexural strength) which comes to 10 runs (Table 9). The experimental data were fitted to a polynomial model of quadratic equations and the optimization software performed an analysis for determining the best combination of maximum mechanical properties and electrical resistivity and the lowest RCPT possible. For each response, a function that related it to the two variables of weight percentages of graphene oxide and ground granulated slag was determined (Table 10). Finally, a goal function was determined that gave the general desirability of the combined four different responses.

4. RESULTS AND DISCUSSION

4.1. Mechanical properties

Figures 5 and 6 show the results of mechanical tests for samples following 28 and 90 curing days demonstrating the marginal enhancement of mechanical properties, mainly in G1, G2, S1, SG1, and SG3 mixes.

Table 9. The designed experimental runs as fed to the software modified for higher accuracy

Run No.	A (GGBFS) (wt %)/100	B(GO) (wt %)/100	Compressive strength (R1)	Flexural strength (R2)	RCPT (R3)	Electrical resistivity (R4)
1	0	0.0000	28.4	2.2	7008.46	14
2	0.40	0.0000	33	2.4	4352.14	38.1
3	0.50	0.0000	34.1	2.3	3788.19	49
4	0.30	0.0005	32.4	2.9	7702.52	36.6
5	0.30	0.0010	35.1	2.9	4250.64	28.9
6	0.40	0.0005	33.7	2.6	3766.93	36.3
7	0.40	0.0010	33.8	2.5	2428.01	36.8
8	0.50	0.0005	34.4	2.5	3460.95	45.6
9	0.50	0.0010	33.4	2.6	2058.18	40.8
10	0	0.0010	32.9	2.8	5862.41	12.4

Table 10. The models selected for each response (variables are A: GGBFS wt % and B: GO wt %)

Response	Model	Final equations for each response	R ²
Compressive strength (R1)	Quadratic	$R1 = +28.22493 + 16.35659 * A + 4444.14506 * B - 10071.42857 * A * B - 9.50178 * A^2 + 4.33096E+005 * B^2$	0.9273
Flexural strength (R2)	Quadratic	$R2 = +2.21221 + 1.89760 * A + 1164.36197 * B - 785.71429 * A * B - 3.52313 * A^2 + 5.69751E+005 * B^2$	0.8515
RCPT (R3)	Quadratic	$R3 = +7096.35542 + 528.13747 * A + 3.71687E+006 * B - 1.39000E+006 * A * B - 16135.60973 * A^2 - 4.88790E+009 * B^2$	0.8388
Electrical resistivity (R4)	Quadratic	$R4 = +13.91885 + 64.69156 * A + 5545.50359 * B - 9214.28571 * A * B + 2.73428 * A^2 - 6.72432E+006 * B^2$	0.9755

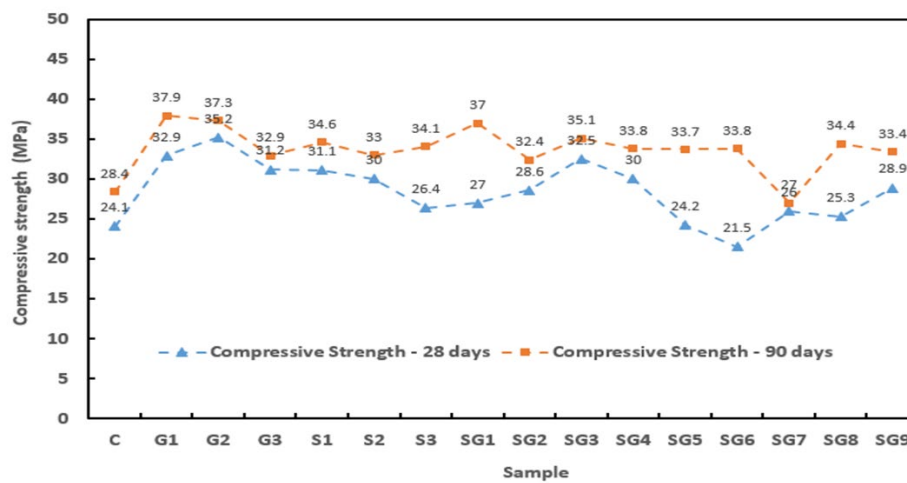


Figure 5. Compressive strength of concrete samples on 28 and 90 days (curing time)

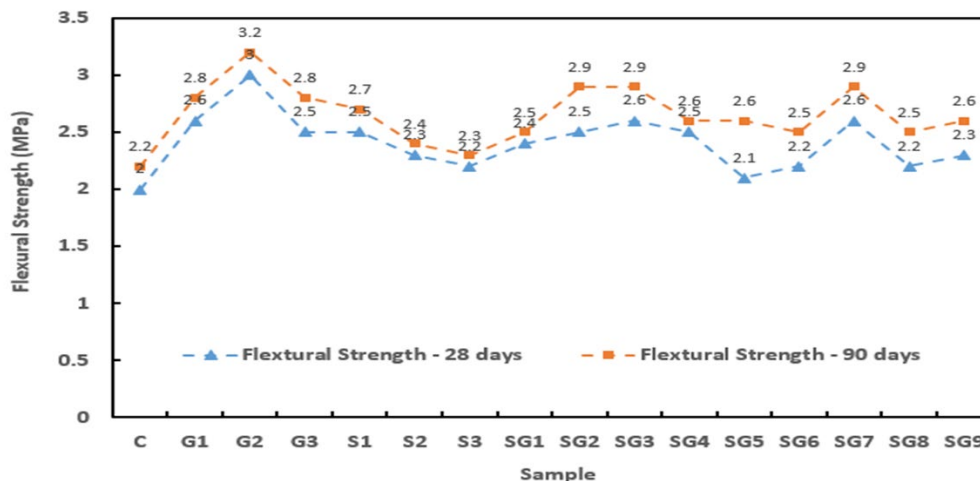


Figure 6. Flexural strength of concrete samples on 28 and 90 days (curing time)

These results show that the addition of 30 wt % GGBFS in GO-free concrete samples resulted in 21.8 % and 29.0 % increases in compressive strength at curing time 28-days and 90-days, respectively. Literature reports indicate that increasing the GGBFS content delays the curing time of concrete to reach maximum strength [56-59, 70, 71]. This is because of the slow calcium hydroxide-dependent pozzolanic reaction of GGBFS (Eq.1):



As the Portland cement gradually hardens by forming phases such as allite and billet, calcium hydroxide is released, which leaches out and deteriorates concrete. When GGBFS is added to the cement mixture, the hydrated calcium silicate is formed instead by the direct interaction of calcium hydroxide and GGBFS [71]. This is a good adhesive and results in improved mechanical properties.

Figure 7 shows the effect of GONP and GGBFS individually on compressive strength. While additions below 30 wt % GGBFS to GONP-free concrete have good effect on mechanical properties (Figure 7b), any addition above that is not beneficial either and may lower the compressive strength. For example, a 17.8 % reduction in compressive strength on Day 28 (curing time) was observed by increasing GGBFS from 30 wt % to 50 wt %. in GONP-free samples. However, in this study, some cases even after admixes of up to 40 wt % did not exhibit significant reductions in compressive strength compared to the 30 wt % case. For instance, following 28 days curing of 0.01 wt % GONP-40 wt % GGBFS concrete mixes (SG4), the compressive strength increased by

approximately 11 % compared to 0.01 wt % GONP-30 wt % GGBFS (SG1); however, for most mixtures containing GGBFS and GONP, admixing only 30 wt % GGBFS with varying amounts of GONP was enough for achieving high levels of compressive strength. This is true for 28- and 90-day cured samples (SG3) and 90-day cured (SG1) samples; this finding is in good agreement with the published literature [54, 72]. A reduction by nearly 11.7 % of compressive strength after 28 days of curing is reported when 50 wt % GGBFS is added [54], although the 0.05 wt % GONP-50 wt % GGBFS samples (SG8) cured for 90 days exhibited a 6 % increase in the compressive strength as compared to 0.05 wt % GONP-30 wt % GGBFS (SG2). In the GONP and GGBFS mixes, the effect of GONP addition on mechanical properties exhibited an uncertain trend. For example, in 30 wt % GGBFS samples, the addition between 0.01 and 0.1 % GONP improved the 28-day compressive and flexural strength by 20.37 % and 8.33 %, respectively; however, the GONP addition to 40 % GGBFS samples lowered compressive strength.

Overall, based on the reports by other researchers, it can be concluded that the discrepancies in the mechanical strength observed at shorter curing times do not warrant changing the limit for the best weight percentage of GGBFS [54, 73]. Therefore, if only mechanical strength is aimed at, a 30 wt % GGBFS addition is enough to get the desired increase in compressive strength. In the GGBFS-free samples, the addition of 0.05 wt % of GONP resulted in 30-40 % improvement in compressive strength after 28 and 90 curing days; however, this declines when over 0.05 % GONP is used (Figure 7a).

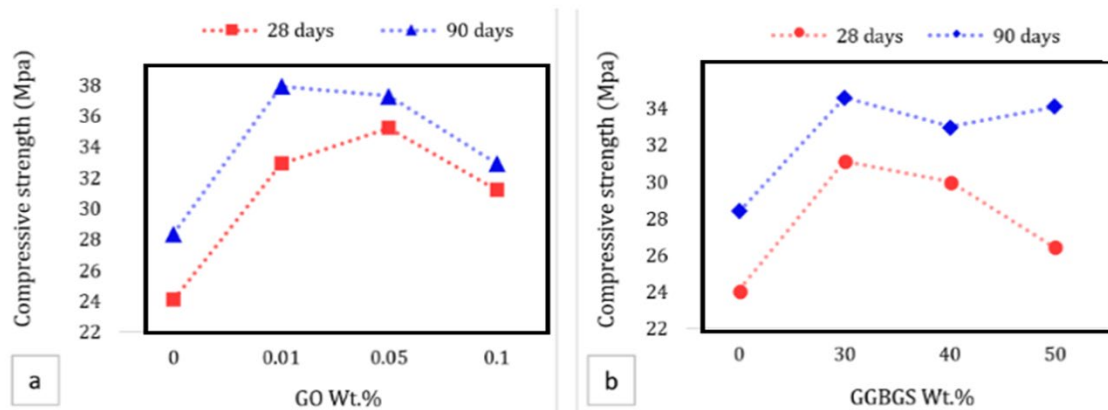


Figure 7. The effect of (a) GONP and (b) GGBFS individually on compressive strength



Figure 8. The compressive strength of 40 wt % GGBFS-containing samples with different GO additions

Figure 8 shows the changes in compressive strength upon increasing GONP content in 28- and 90-day cured samples

(S2), (SG4), (SG5), and (SG6). Overall, higher graphene oxide content leads to a delay in gaining strength. An increase

in the compressive strength of the GONP-containing concretes with curing time was reported and in the present work, the highest mechanical strengths were obtained for the G1, G2, and SG1 samples following 90 curing days (Table 11).

MPa) and 31 % (37.3 MPa) improvements, respectively. The strength-giving property of graphene oxide depends to a large extent on the quality of its production, its purity, and its proper dispersion in the concrete mix, which has given rise to the scatter seen in the results seen in some studies [22].

Table 11. The highest mechanical results for different mixes on 90 days (curing time)

Sample code	Compressive strength (MPa)	Flexural strength (MPa)	Improvement (%)
G1	37.9	2.8	33.4
G2	37.3	3.2	31.3
SG1	37.0	2.5	30.2

GONP’s impact is more pronounced in GGBFS free samples [74]. Increases of 15-48 % in compressive strength have been reported for 0.05 wt % graphene oxide addition [17, 33, 36]. Mao Li et al. observed a 16 % decrease in compressive strength when 0.05 % GO was added in the presence of 25 % GGBFS [75]. In the current study, the maximum compressive strength was measured for the 28- and 90-day cured samples with 0.05 % GO, showing 46 % (35.2

4.2. Wenner test and RCPT results

Free chloride is known for fast diffusion into concrete, but GGBFS in concrete may reduce this using the chloride binding capacity of concrete [76-79]. Figures 9 and 10 show Wenner test and RCPT results for 28- and 90-day cured samples, respectively.

Figure 9 shows the Wenner test results from SG9 samples (0.1 wt % GONP and 50 wt % GGBFS), exhibiting high surface electrical resistivity and the least electrical charge conduction (1200 to 2058 C), a sign of high resistance to chloride ingress. The observation that the addition of GGBFS in 28- and 90-day cured samples significantly decreases the charge conducted in RCPT tests points to the increased resistance against chloride penetration.

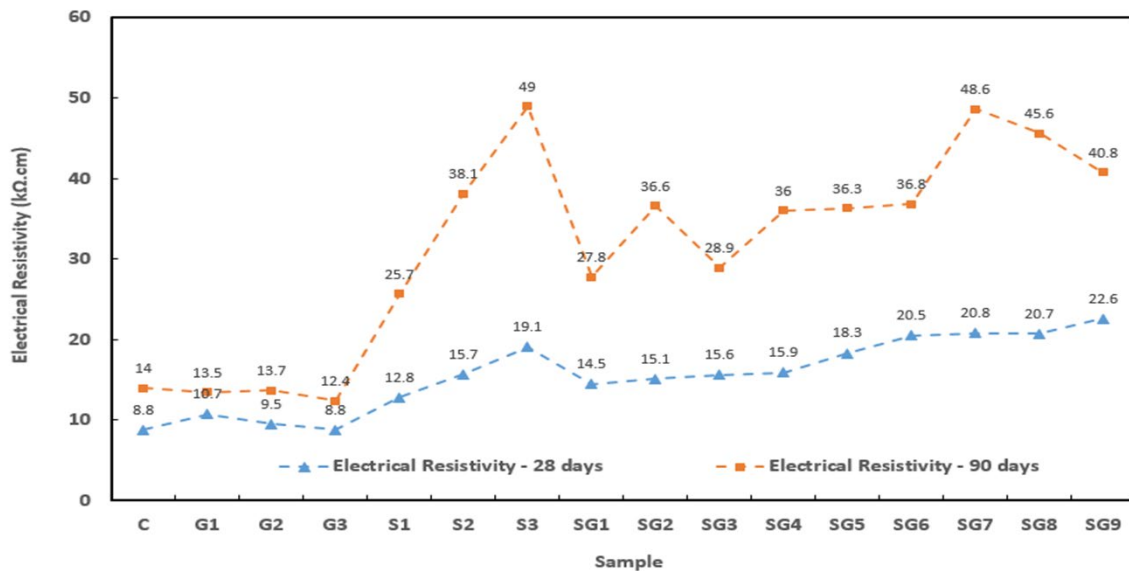


Figure 9. The Wenner test results of 28- and 90-day cured concrete samples

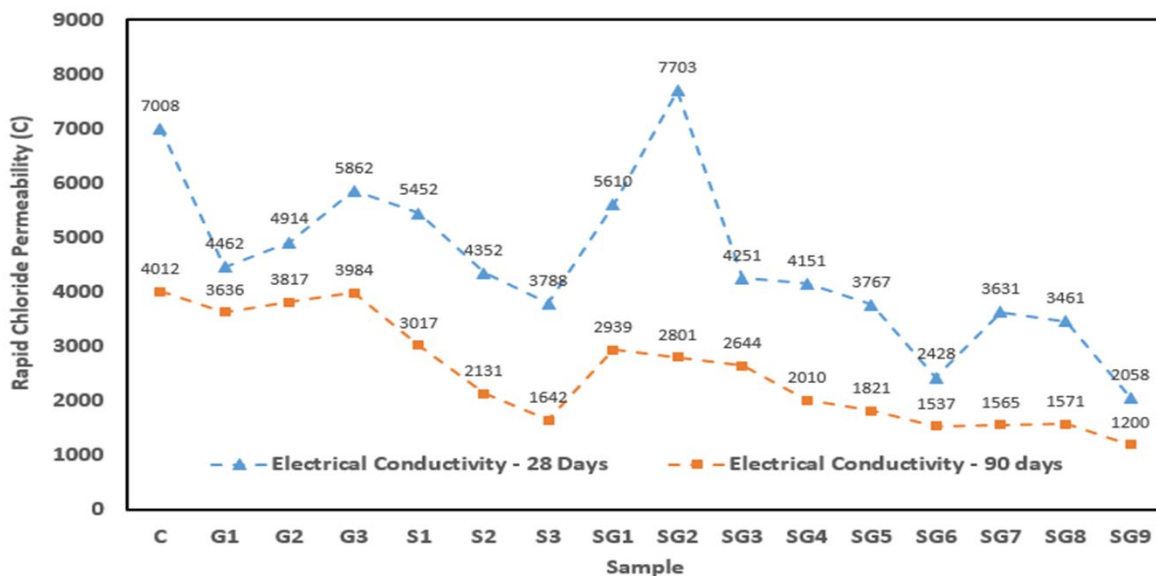


Figure 10. The RCPT test results of 28- and 90-day cured concrete samples

The ASTM 1202-12 Standard [67] designates such charge conduction as low chloride permeability (Table 12). Maochieh et al. reported conducted currents following 91 days of curing for 40 wt % and 60 wt % GGBFS concretes as 1394 C and 1883 C, respectively, while other published papers exhibited conduction in the region of 1659.6 C [58, 59].

Table 12. Chloride ion penetrability based on charge passed according to ASTM 1202-12 Standard [67]

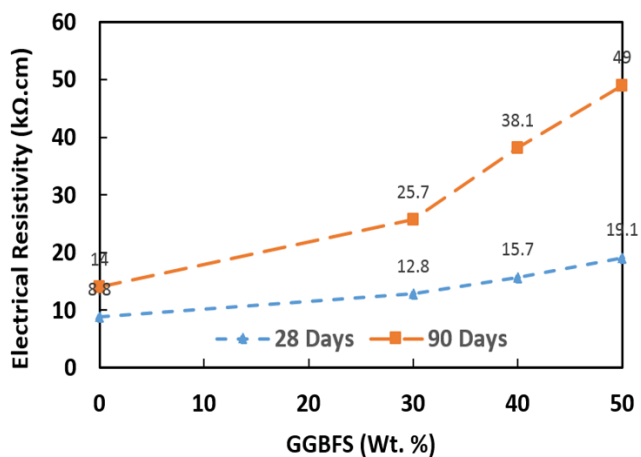
The charge passed (C)	Chloride ion permeability
>4000	High
2000-4000	Moderate
1000-2000	Low
100-1000	Very low
<100	Negligible

Electrical charge transfer during the RCPT test significantly declines in the concrete containing higher GGBFS content, confirming the positive role of GGBFS in decreasing the chloride permeability and movement by immobilizing the free chloride. In our study, the 28-day 30 wt % GGBFS concrete passed nearly 5452 C and after 90 days, it conducted 3017 C which is desirable in terms of chloride permeability. In the current study, the addition of GONP to ordinary concrete increased the conductivity and decreased electrical resistance, although for G1 (0.01 wt % GONP), a reduction of nearly 9.3 % in electrical conductivity was observed. The highest electrical resistivity was achieved (49 kΩ.cm) for 90-day cured samples with 50 % GGBFS. Maochieh reports the electrical resistivity of the 90-day cured 60 wt % GGBFS

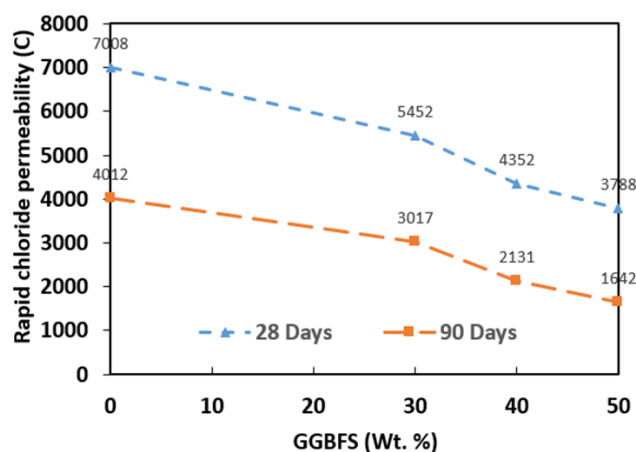
concretes as 34.8 kΩ.cm [80]. Overall, GONP in GGBFS free concrete did not have a positive effect on chloride permeability. According to results from Figures 9 and 10, the lowest charge was passed when concretes contained GGBFS and GONP. For example, the addition of 0.1 wt % GONP with 50 wt % GGBFS reduced the passing charge from 1642 C to 1200 C. A significant reduction in electrical conductivity from 4012 C to 1200 C was observed for 90-day cured samples containing 0.1 wt % GO-50 wt % GGBFS (SG9) compared to the control sample. Based on these results, the addition of 0.1 wt % GO and 50 wt % GGBFS could effectively reduce the passing current in the conductivity test and enhance the resistance of concrete to chloride penetration. Figure 11 shows the effect of GONP and GGBFS individually on Wenner test and RCPT.

Addition of GONP to conventional concrete increased the conductivity and decreased electrical resistance, although for G1 (0.01 wt % GONP), a reduction of nearly 9.3 % in electrical conductivity was observed. The highest electrical resistivity was achieved (49 kΩ.cm) for 90-day cured samples with 50 % GGBFS and 0.1 % GONP to be highly effective in increasing concrete resistance to chloride penetration.

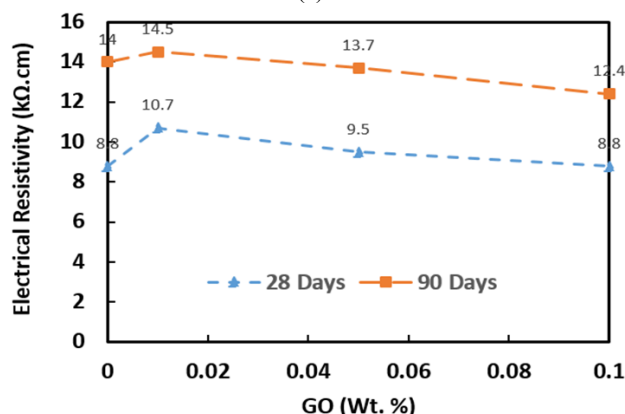
The values of electrical conductivity for admixture were obtained by other researchers in the same condition are shown in Table 13 [23, 35-48], proving that the chloride ion penetrability value for 90-day cured samples containing 0.1 wt % GO-50 wt % GGBFS (SG9) is low and this mix has good resistance to chlorine ion permeability compared to other admixtures.



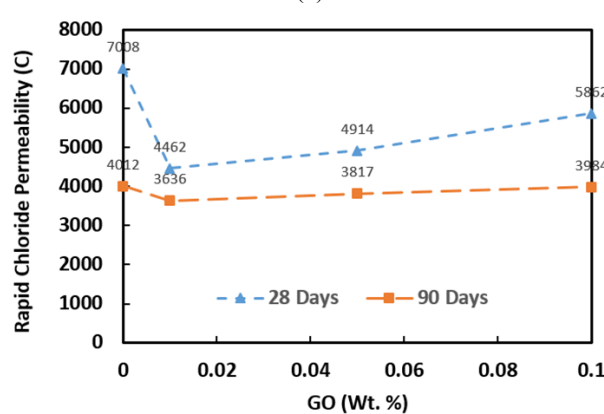
(a)



(b)



(c)



(d)

Figure 11. The effect of (a,b) GGBFS and (c,d) GONP individually on electrical resistance and electrical conductivity

Table 13. The charge passed values for admixtures obtained from some other studies and this research

Mix	The charge passed (C)	Reference
5 wt % Silica Fume	850	[72]
30 wt % Fly Ash	2000	[81]
50 wt % Fly Ash	2550	[81]
30 wt % GGBFS	1750	[81]
40 wt % GGBFS	1394	[72]
40 wt % GGBFS	6300	[82]
50 wt % GGBFS	1340	[81]
50 wt % GGBFS	1600	[72]
60 wt % GGBFS	1883	[72]
60 wt % GGBFS	3000	[82]
0.03 wt %GO	1630	[83]
0.06 wt %GO	1530	[83]
0.09 wt %GO	1560	[83]
0.1 wt % GO-50 wt % GGBFS	1200	This paper

4.3. Cost analysis

The cost of casting the mixed designed was analyzed, as reported in Tables 14 and 15. The cost of concrete composites was evaluated using the commercialized market prices of the materials. The economic Index for strength (compressive strength/cost per m³) was observed to have the maximum value at the mix G1 (with 0.01 % GO inclusion) compared to the rest of the mixes and the economic index for electrical conductivity (electrical conductivity/cost per m³) shows that the mix SG9 is a better mix than the rest in terms of chlorine ion permeability and economy. Table 15 shows that the cost of materials for making SG9 sample is 24.5 % higher than that of conventional concrete; however, considering economic

index for electrical conductivity, use of this mix is cost-effective. According to this table, the value of this index for SG9 decreased by more than 4 times compared to that for the conventional concrete.

Table 14. Cost of materials

Materials	Cost (USD/kg)
OPC	0.1
GO	16.32
GGBFS	0.15
Water	0.0007
Fine aggregate	0.02
Coarse aggregate	0.013
SP	1.6

◆ OPC - Ordinary Portland Cement, GO – Graphene Oxide, GGBFS – Ground Granulated Blast Furnace Slag, SP – (Carboxylate based) Super Plasticizer

4.4. Optimization results

The levels of the priority given to the responses were RCPT (high), Electrical resistance (high), compressive strength (moderate), and Flexural strength (low). By feeding the experimental data from the mechanical, RCPT, and the Wener tests to the response surface method software, the relation between each response and GONP and GGBFS alterations was modeled, as shown in Figure 12. Optimization results helped predict that 0.08 wt % GO and 50 wt % GGBFS and 90-day curing led to the most desirable mechanical and physical properties with a remarkable improvement in chlorine ingress resistance. This was shown to be in good agreement with the actual results from real-world experiments. The desirability level of this composition based on the criteria specified for the software was calculated as 0.831 (Figure 13).

Table 15. Cost analysis of different mixes per m³ of concrete

Mix	Cost (USD)								Properties		Economic index	
	GGBFS	GO	OPC	Water	FA	CA	SP	Total cost	CS	EC	EI ₁	EI ₂
C	0	0	42.5	0.119	20.11	8.794	0.068	71.591	28.4	4012	0.397	56.040
G1	0	0.694	42.5	0.119	20.11	8.794	0.068	72.285	37.9	3636	0.524	50.300
G2	0	3.468	42.5	0.119	20.11	8.794	0.068	75.059	37.3	3817	0.497	50.853
G3	0	6.936	42.5	0.119	20.11	8.794	0.068	78.527	32.9	3984	0.418	50.733
S1	19.125	0	29.75	0.119	20.11	8.794	0.068	77.966	34.6	3017	0.444	38.696
S2	25.5	0	25.5	0.119	20.11	8.794	0.068	80.091	33	2131	0.412	26.607
S3	31.875	0	21.25	0.119	20.11	8.794	0.068	82.216	34.1	1642	0.415	19.971
SG1	19.125	0.694	29.75	0.119	20.11	8.794	0.068	78.6601	37	2939	0.470	37.363
SG2	19.125	3.468	29.75	0.119	20.11	8.794	0.068	81.434	32.4	2801	0.398	34.395
SG3	19.125	6.936	29.75	0.119	20.11	8.794	0.068	84.902	35.1	2644	0.413	31.142
SG4	25.5	0.694	25.5	0.119	20.11	8.794	0.068	80.785	33.8	2010	0.418	24.881
SG5	25.5	3.468	25.5	0.119	20.11	8.794	0.068	83.559	33.7	1821	0.403	21.793
SG6	25.5	6.936	25.5	0.119	20.11	8.794	0.068	87.027	33.8	1537	0.388	17.661
SG7	31.875	0.694	21.25	0.119	20.11	8.794	0.068	82.910	27	1565	0.325	18.876
SG8	31.875	3.468	21.25	0.119	20.11	8.794	0.068	85.684	34.4	1571	0.401	18.335
SG9	31.875	6.936	21.25	0.119	20.11	8.794	0.068	89.152	33.4	1200	0.375	13.460

◆ OPC - Ordinary Portland Cement, GO – Graphene Oxide, GGBFS – Ground Granulated Blast Furnace Slag, FA - Fine Aggregate, CA - Coarse Aggregate, SP – (Carboxylate based) Super Plasticizer, CS – Compressive Strength, EC – Electrical Conductivity, EI₁- The economic Index for Strength, EI₂ - The economic Index for electrical conductivity

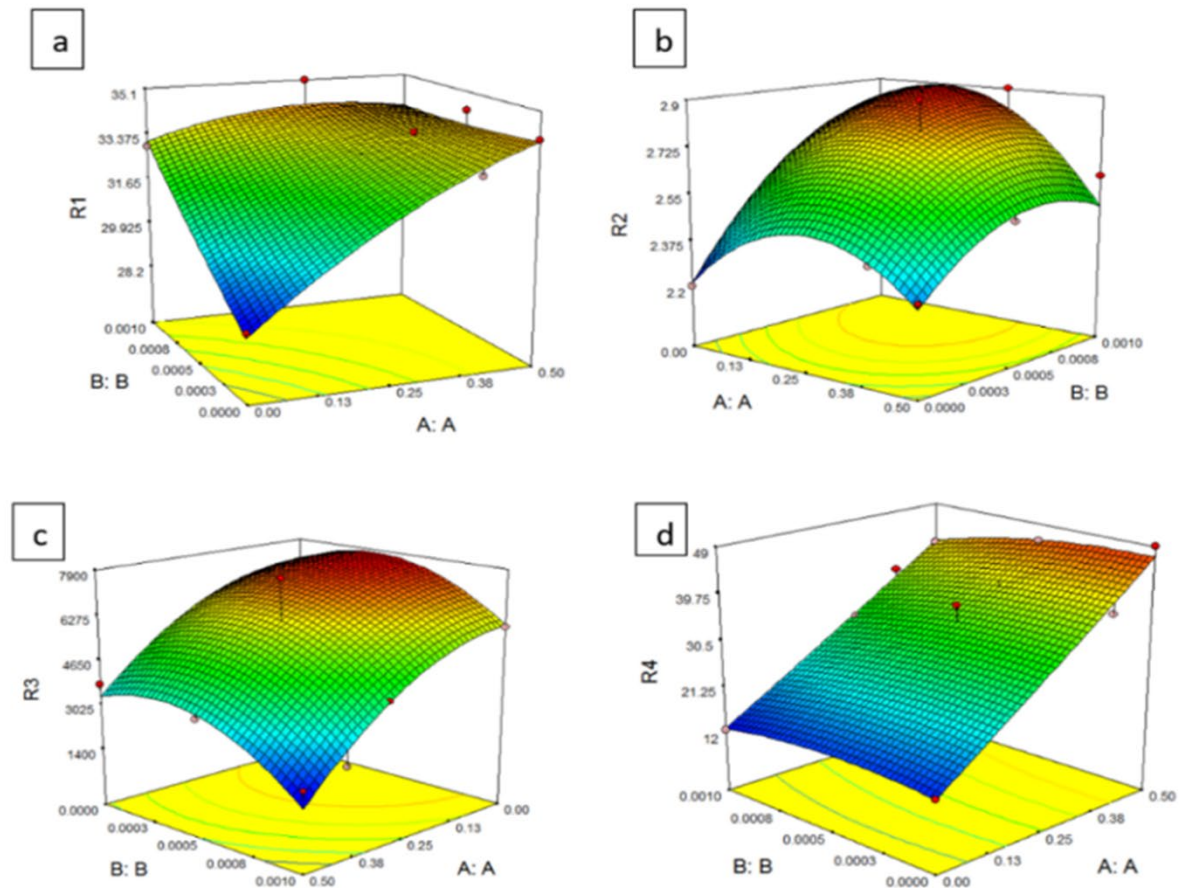


Figure 12. The effect of GO and GGBFS variation on (a) compressive strength, (b) flexural strength, (c) RCPT results, and (d) surface electrical resistivity

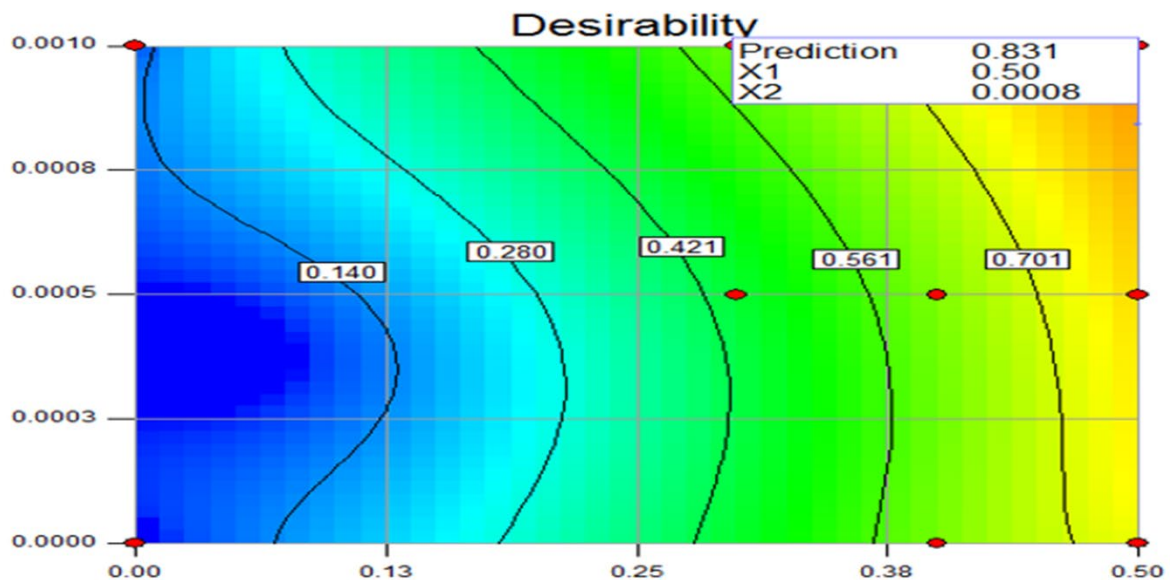


Figure 13. Desirability contour of different compositions and the selected final mixture

5. CONCLUSIONS

- The addition of slag up to 30 % by weight was effective in improving the compressive and flexural strength of graphene oxide-free specimens; however, addition of more than 30 % by weight could even reduce the compressive and flexural strength of concrete specimens. Therefore, the addition of 30 wt % GGBFS to concrete after 90 days resulted in the highest mechanical properties; however, to improve the resistance against chloride penetration, this should be increased to 50 wt %, thus forfeiting some mechanical strength.
- Prolonging the curing duration in concrete samples with GONP and GGBFS is essential to achieving higher levels of mechanical properties.

- GGBFS had a more pronounced role than GONP in developing the concrete resistance against chloride penetration.
- In the GGBFS-free samples, addition of 0.05 wt % of GONP yielded the improvement of compressive and flexural strength after 28 and 90 curing days; however, this strength declined when using over 0.05 % GONP.
- In the GGBFS-free samples, addition of 0.01 wt % of GONP was enough to achieve the highest chloride penetration resistance.
- Combined GONP and GGBFS additions enhanced the resistance to chloride permeation.
- The addition of 0.1 % graphene oxide and 50 % granular slag increased the compressive strength of concrete sample by 19.9% during 28 days and 17.6% during 90 days compared to the conventional concrete sample.
- Concrete with a combination of 0.1 % graphene oxide and 50 % granular slag caused an increase in flexural strength by 15 % during 28 days of curing and by 13.6 % during 90 days of curing.
- A high reduction in electrical conductivity from 4012 C to 1200 C was observed for 90-day cured samples containing 0.1 wt % GO and 50 wt % GGBFS compared to the conventional sample.
- In the GONP-free samples, the addition of 50 wt % GGBFS exhibited the highest surface electrical resistivity and the least electrical charge conduction, which is a sign of high resistance to chloride ingress.
- Based on experimental data, 0.1 wt % GONP and 50 wt % GGBFS admixtures in concrete were of optimal mixing in terms of chlorine ion penetration and corrosion resistance.
- From the cost analysis and the economic index calculated, the economic Index for Strength (compressive strength/cost per m³) was observed to have maximum value at mix G1 (with 0.01 % GO inclusion) compared to the rest of the mixes and the economic Index for electrical conductivity (electrical conductivity/cost per m³) showed that mix SG9 was the optimum mix.

Based on experimental data and optimization as well as statistical analysis, a concrete mix containing 0.08 wt % GONP and 50 wt % GGBFS combined high mechanical properties and excellent resistance against chloride ions permeation.

6. ACKNOWLEDGEMENT

The authors appreciatively acknowledge the Research Council of Shahid Bahonar University.

REFERENCES

1. Li, W., Dong, W., Tam, V.W.Y. and Yu, T., "Durability deterioration of concrete under marine environment from material to structure: A critical review", *Journal of Building Engineering*, Vol. 35, (2021), 1-17. (<https://doi.org/10.1016/j.jobe.2020.102074>).
2. James, A., Bazarchi, E., Chiniforush, A., Aghdam, P., Hosseini, M.R., Akbarnezhad, A., Martek, I. and Ghodoosi, F., "Rebar corrosion detection, protection and rehabilitation of reinforced concrete structures in coastal environments: A review", *Construction and Building Materials*, Vol. 224, (2019), 1026-1039. (<https://doi.org/10.1016/j.conbuildmat.2019.07.250>).
3. Fan, J., Zhu, H., Shi, J., Li, Z. and Yang, S., "Influence of slag content on the bond strength, chloride penetration resistance, and interface phase evolution of concrete repaired with alkali activated slag/fly ash", *Construction and Building Materials*, Vol. 263, (2020), 1-9. (<https://doi.org/10.1016/j.conbuildmat.2020.120639>).
4. Ramezani-pour, A.A., Ghoreishian, S., Ahmadi, B., Balapour, M. and Ramezani-pour, A.M., "Modeling of chloride ions penetration in cracked concrete structures exposed to marine environments", *Structural Concrete*, Vol. 19, (2018), 1460-1471. (<https://doi.org/10.1002/suco.201700285>).
5. Goyal, A., Olorunnipa, E.K., Sadeghi Pouya, H., Ganjian, E. and Olubanwo, A.O., "Potential and current distribution across different layers of reinforcement in reinforced concrete cathodic protection system- A numerical study", *Construction and Building Materials*, Vol. 262, (2020), 1-10. (<https://doi.org/10.1016/j.conbuildmat.2020.120580>).
6. Bahekar, P.V. and Gadve, S.S., "Impressed current cathodic protection of rebar in concrete using carbon FRP laminate", *Construction and Building Materials*, Vol. 156, (2017), 242-251. (<https://doi.org/10.1016/j.conbuildmat.2017.08.145>).
7. Du, F., Jin, Z., She, W., Xiong, C., Feng, G. and Fan, J., "Chloride ions migration and induced reinforcement corrosion in concrete with cracks: A comparative study of current acceleration and natural marine exposure", *Construction and Building Materials*, Vol. 263, (2020), 1-11. (<https://doi.org/10.1016/j.conbuildmat.2020.120099>).
8. Rodrigues, R., Gaboreau, S., Gance, J., Ignatiadis, I. and Betelu, S., "Reinforced concrete structures: A review of corrosion mechanisms and advances in electrical methods for corrosion monitoring", *Construction and Building Materials*, Vol. 269, (2021), 1-36. (<https://doi.org/10.1016/j.conbuildmat.2020.121240>).
9. Tuutti, K., Corrosion of steel in concrete: Cement-och betonginst, (1982). (<https://lucris.lub.lu.se/ws/files/4709458/3173290.pdf>).
10. Zhang, D. and Shao, Y., "Enhancing chloride corrosion resistance of precast reinforced concrete by carbonation curing", *ACI Materials Journal*, Vol. 116, (2019), 3-12. (<https://doi.org/10.14359/51714461>).
11. Tang, L. and Nilsson, L., "Service life prediction for concrete structures under seawater by a numerical approach", *The Durability of Building Materials and Components*, Vol. 7, (1996), 97-106. (https://jglobal.jst.go.jp/en/detail?JGLOBAL_ID=200902187425051487).
12. Jung, M.S., Kim, K.B., Lee, S.A. and Ann, K.Y., "Risk of chloride-induced corrosion of steel in SF concrete exposed to a chloride-bearing environment", *Construction and Building Materials*, Vol. 166, (2018), 413-422. (<https://doi.org/10.1016/j.conbuildmat.2018.01.168>).
13. Stanish, K., Hooton, R.D. and Thomas, M.D., "Testing the chloride penetration resistance of concrete: A literature review", *The United States Federal Highway Administration*, (2001). (https://www.researchgate.net/publication/237321599_Testing_the_Chloride_Penetration_Resistance_of_Concrete_A_Literature_Review).
14. Daniyal, M., Azam, A. and Akhtar, S., "Application of nanomaterials in civil engineering", *Nanomaterials and Their Applications*, Springer, Singapore, (2018), 169-189. (https://doi.org/10.1007/978-981-10-6214-8_6).
15. Sobolev, K. and Gutiérrez, M.F., "How nanotechnology can change the concrete world", *American Ceramic Society Bulletin*, Vol. 84, (2005), 113-116. (<https://doi.org/10.1002/9780470588260.ch17>).
16. Chuah, S., Pan, Z., Sanjayan, J.G., Wang, C.M. and Duan, W.H., "Nano reinforced cement and concrete composites and new perspective from graphene oxide", *Construction and Building Materials*, (2014). (<https://doi.org/10.1016/j.conbuildmat.2014.09.040>).
17. Pan, Z., He, L., Qiu, L., Korayem, A.H., Li, G. and Zhu, J.W., "Mechanical properties and microstructure of a graphene oxide-cement composite", *Cement and Concrete Composites*, Vol. 58, (2015), 140-147. (<https://doi.org/10.1016/j.cemconcomp.2015.02.001>).
18. Wang, Y., Iqbal, Z. and Mitra, S., "Rapidly functionalized, water-dispersed carbon nanotubes at high concentration", *Journal of the American Chemical Society*, Vol. 128 (2006), 95-99. (<https://doi.org/10.1021/ja053003q>).
19. Liu, C., Huang, X., Wu, Y., Deng, X., Liu, J., Zheng, Z. and Hui, D., "Review on the research progress of cement-based and geopolymer materials modified by graphene and graphene oxide", *Nanotechnology Reviews*, Vol. 9, (2020), 155-169. (<https://doi.org/10.1515/ntrev-2020-0014>).
20. Anwar, A., Mohammed, B.S., Abdul Wahab, M. and Liew, M.S., "Enhanced properties of cementitious composite tailored with graphene oxide nanomaterial- A Review", *Developments in the Built*

- Environment*, (2019), 1-43. (<https://doi.org/10.1016/j.dibe.2019.100002>).
21. Mohammed, A., Sanjayan, J.G., Duan, W. and Nazari, A., "Incorporating graphene oxide in cement composites: A study of transport properties", *Construction and Building Materials*, Vol. 84, (2015), 341-347. (<https://doi.org/10.1016/j.conbuildmat.2015.01.083>).
 22. Somasri, M. and Kumar, N.B., "Graphene oxide as nano material in high strength self-compacting concrete", *Materials Today Proceedings*, Vol. 43, (2021), 2280-2289. (<https://doi.org/10.1016/j.matpr.2020.12.1085>).
 23. Guo, K., Miao, H., Liu, L., Zhou, J. and Liu, M., "Effect of graphene oxide on chloride penetration resistance of recycled concrete", *Nanotechnology Reviews*, Vol. 8, (2018), 681-689. (<https://doi.org/10.1515/ntrev-2019-0059>).
 24. Birenboim, M., Nadvir, R., Alatawna, A., Buzaglo, M., Schahar, G. and Lee, J., "Reinforcement and workability aspects of graphene-oxide-reinforced cement nanocomposites", *Composites Part B: Engineering*, Vol. 161, (2019), 68-76. (<https://doi.org/10.1016/j.compositesb.2018.10.030>).
 25. Peng, H., Ge, Y., Cai, C., Zhang, Y. and Liu, Z., "Mechanical properties and microstructure of graphene oxide cement-based composites", *Construction and Building Materials*, Vol. 194, (2019), 102-109. (<https://doi.org/10.1016/j.conbuildmat.2018.10.234>).
 26. Xu, G., Du, S., He, J. and Shi, X., "The role of admixed graphene oxide in a cement hydration system", *Carbon*, Vol. 148, (2019), 141-150. (<https://doi.org/10.1016/j.carbon.2019.03.072>).
 27. Yang, H., Monasterio, M., Cui, H. and Han, N., "Experimental study of the effects of graphene oxide on microstructure and properties of cement paste composite" *Composites Part A: Applied Science and Manufacturing*, Vol. 102, (2017), 263-272. (<https://doi.org/10.1016/j.compositesa.2017.07.022>).
 28. Wang, Q., Wang, J., Lu, C.-X., Liu, B.-W., Zhang, K. and Li, C.-Z., "Influence of graphene oxide additions on the microstructure and mechanical strength of cement", *New Carbon Materials*, Vol. 30, (2015), 349-356. ([https://doi.org/10.1016/S1872-5805\(15\)60194-9](https://doi.org/10.1016/S1872-5805(15)60194-9)).
 29. Li, X., Lu, Z., Chuah, S., Li, W., Liu, Y., Duan, W.H. and Li, Z., "Effects of graphene oxide aggregates on hydration degree, sorptivity, and tensile splitting strength of cement paste", *Composites Part A: Applied Science and Manufacturing*, Vol. 100 (2017), 1-8. (<https://doi.org/10.1016/j.compositesa.2017.05.002>).
 30. Dikin, D.A., Stankovich, S., Zimney, E.J., Piner, R.D., Dommett, G.H.B., Evmenenko, G., Nguyen, S.T. and Ruoff, R.S., "Preparation and characterization of graphene oxide paper", *Nature*, Vol. 448, (2007), 457-460. (<https://doi.org/10.1038/nature06016>).
 31. Li, X., Korayem, A.H., Li, C., Liu, Y., He, H., Sanjayan, J.G. and Duan, W.H., "Incorporation of graphene oxide and silica fume into cement paste: A study of dispersion and compressive strength", *Construction and Building Materials*, Vol. 123, (2016), 327-335. (<https://doi.org/10.1016/j.conbuildmat.2016.07.022>).
 32. Lu, L. and Ouyang, D., "Properties of cement mortar and ultra-high-strength concrete incorporating graphene oxide nanosheets", *Nanomaterials*, Vol. 7, (2017), 187. (<https://doi.org/10.3390/nano7070187>).
 33. Lv, S., Ma, Y., Qiu, C., Sun, T., Liu, J. and Zhou, Q., "Effect of graphene oxide nanosheets of microstructure and mechanical properties of cement composites", *Construction and Building Materials*, Vol. 49, (2013), 121-127. (<https://doi.org/10.1016/j.conbuildmat.2013.08.022>).
 34. Li, G.Y., Wang, P.M. and Zhao, X., "Mechanical behavior and microstructure of cement composites incorporating surface-treated multi-walled carbon nanotubes", *Carbon*, Vol. 43, (2005), 1239-1245. (<https://doi.org/10.1016/J.CARBON.2004.12.017>).
 35. Shang, Y., Zhang, D., Yang, C. and Liu, Y., "Effect of graphene oxide on the rheological properties of cement pastes", *Construction and Building Materials*, Vol. 96, (2015), 20-28. (<https://doi.org/10.1016/j.conbuildmat.2015.07.181>).
 36. Gong, K., Pan, Z., Korayem, A.H., Qiu, L., Li, D., Collins, F., Wang, C.M. and Duan, W.H., "Reinforcing effects of graphene oxide on portland cement paste", *Journal of Materials in Civil Engineering*, Vol. 27, (2015), A4014010. ([https://doi.org/10.1061/\(ASCE\)MT.1943-5533.0001125](https://doi.org/10.1061/(ASCE)MT.1943-5533.0001125)).
 37. Lee, S., Jeong, H., Kim, D. and Won, J., "Graphene oxide as an additive to enhance the strength of cementitious composites", *Composite Structures*, (2020), 1-27. (<https://doi.org/10.1016/j.compstruc.2020.112154>).
 38. Kudźma, A., Škamat, J., Stonys, R., Krasnikovs, A., Kuznetsov, D., Girskas, G. and Antonovič, A., "Study on the effect of graphene oxide with low oxygen content on Portland cement based composites", *Materials*, Vol. 12, (2019), 1-17. (<https://doi.org/10.3390/ma12050802>).
 39. Hassani, A., Fakhim, B., Rashidi, A. and Ghoddousi, P., "The influence of graphene oxide on mechanical properties and durability increase of concrete pavement", *International Journal of Transportation Engineering (IJTE)*, Vol. 2, (2014), 119-130. (http://www.ijte.ir/article_7874_1114.html).
 40. Wang, L., Zhang, S., Zheng, D., Yang, H., Cui, H., Tang, W. and Li, D., "Effect of graphene oxide (GO) on the morphology and microstructure of cement hydration products", *Nanomaterials*, Vol. 7, (2017), 1-10. (<https://doi.org/10.3390/nano7120429>).
 41. Li, W., Li, X., Chen, S.J., Long, G., Liu, Y.M. and Duan, W.H., "Effects of nanoalumina and graphene oxide on early-age hydration and mechanical properties of cement paste", *Journal of Materials in Civil Engineering*, Vol. 29, (2017), 1-9. ([https://doi.org/10.1061/\(ASCE\)MT.1943-5533.0001926](https://doi.org/10.1061/(ASCE)MT.1943-5533.0001926)).
 42. Silvestre, J., Silvestre, N. and De Brito, J., "Review on concrete nanotechnology", *European Journal of Environmental and Civil Engineering*, Vol. 20, (2016), 455-485. (<https://doi.org/10.1080/19648189.2015.1042070>).
 43. Bondar, D., Nanukuttan, S.V., Soutsos, M.N., Basheer, P.M. and Provis, J.L., "Suitability of alkali-activated GGBS/fly ash concrete for chloride environments", *ACI Special Publications: American Concrete Institute*, Vol. 35, (2017), 1-14. (https://www.researchgate.net/publication/317950089_Suitability_of_alkali_activated_ggbsfly_ash_concrete_for_chloride_environments).
 44. Du, H., Gao, H.J. and Dai S., "Improvement in concrete resistance against water and chloride ingress by adding graphene nanoplatelet", *Cement and Concrete Research*, Vol. 83, (2016), 114-123. (<https://doi.org/10.1016/j.cemconres.2016.02.005>).
 45. Xu, Y. and Fan, Y., "Effect of on graphene oxide the concrete resistance to chloride ion permeability", *IOP Conference Series: Materials Science and Engineering: IOP Publishing: IOP Publishing*, (2018), 032020. (<https://doi.org/10.1088/1757-899X/394/3/032020>).
 46. Karri, S.K., Rao, G.R. and Raju, P.M., "Strength and durability studies on GGBS concrete", *SSRG International Journal of Civil Engineering (SSRG-IJCE)*, Vol. 2, (2015), 34-41. (<https://doi.org/10.14445/23488352/IJCE-V2I10P106>).
 47. Dalla, P.T., Tragazikis, I.K., Exarchos, D.A., Dassios, K.G., Barkoula, N.M. and Matikas, T.E., "Effect of carbon nanotubes on chloride penetration in cement mortars", *Applied Sciences*, Vol. 9, (2019), 1032. (<https://doi.org/10.3390/app9051032>).
 48. Song, H. and Saraswathy, V., "Studies on the corrosion resistance of reinforced steel in concrete with ground granulated blast-furnace slag-An overview", *Journal of Hazardous Materials*, Vol. 138, (2006), 226-233. (<https://doi.org/10.1016/j.jhazmat.2006.07.022>).
 49. Richardson, D.N., "Strength and durability characteristics of a 70 % ground granulated blast furnace slag (GGBFS) concrete mix", (2006). (https://scholarsmine.mst.edu/cgi/viewcontent.cgi?article=1042&context=civarc_enveng_facwork).
 50. Kumar, V.P., Gunasekaran, K. and Shyamala, T., "Characterization study on coconut shell concrete with partial replacement of cement by GGBS", *Journal of Building Engineering*, (2019), 100830. (<https://doi.org/10.1016/j.jobbe.2019.100830>).
 51. Woo, H.M., Kim, C.-Y. and Yeon, J.H., "The heat of hydration and mechanical properties of mass concrete with high-volume GGBFS replacements", *Journal of Thermal Analysis and Calorimetry*, Vol. 132, (2018), 599-609. (<https://doi.org/10.1007/s10973-017-6914-z>).
 52. Özbay, E., Erdemir, M. and Durmuş, H.İ., "Utilization and efficiency of ground granulated blast furnace slag on concrete properties—A review", *Construction and Building Materials*, Vol. 105, (2016), 423-434. (<https://doi.org/10.1016/j.conbuildmat.2015.12.153>).
 53. Chen, H.-J., Huangm S.-S., Tang, C.-W., Malek, M.A. and Ean, L.-W., "Effect of curing environments on strength, porosity, and chloride ingress resistance of blast furnace slag cement concretes a construction site study", *Construction and Building Materials*, Vol. 35, (2012), 1063-1070. (<https://doi.org/10.1016/j.conbuildmat.2012.06.052>).
 54. Samad, S., Shah, A. and Limbachiya, M.C., "Strength development characteristics of concrete produced with blended cement using ground granulated blast furnace slag (GGBS) under various curing conditions", *Sādhanā*, Vol. 42, (2017), 1203-1213. (<https://doi.org/10.1007/s12046-017-0667-z>).

55. Khatib, J. and Hibbert, J., "Selected engineering properties of concrete incorporating slag and metakaolin", *Construction and Building Materials*, Vol. 19, (2005), 460-472. (<https://doi.org/10.1016/j.conbuildmat.2004.07.017>).
56. Shen, D., Jiao, Y., Kang, J., Feng, Z. and Shen, Y., "Influence of ground granulated blast furnace slag on the early-age cracking potential of internally cured high-performance concrete", *Construction and Building Materials*, Vol. 233, (2020), 117083. (<https://doi.org/10.1016/j.conbuildmat.2019.117083>).
57. Güneş, E. and Gesoğlu, M., "A study on durability properties of high-performance concretes incorporating high replacement levels of slag", *Materials and Structures*, Vol. 41, (2008), 479-493. (<https://doi.org/10.1617/s11527-007-9260-y>).
58. Park, J.-H. and Lee, H.-S., "Effect of curing condition on the chloride ion diffusion coefficient in concrete with GGBFS", *Journal of the Korea Institute of Building Construction*, Vol. 19, (2019), 421-429. (<https://doi.org/10.3390/ma12193233>).
59. Yoon, Y.-S., Cho, S.-J. and Kwon, S.-J., "Prediction equation for chloride diffusion in concrete containing GGBFS based on 2-Year cured results", *Journal of the Korea Institute for structural maintenance and inspection*, Vol. 23, (2019), 1-9. (<https://doi.org/10.11112/jksmi.2019.23.2.1>).
60. Sharma, S. and Kothiyal, N.C., "Comparative effects of pristine and ball-milled graphene oxide on physico-chemical characteristics of cement mortar nanocomposites", *Construction and Building Materials*, Vol. 115, (2016), 256-268. (<https://doi.org/10.1016/j.conbuildmat.2016.04.019>).
61. Mahendran, R., Sridharan, D., Santhakumar, K., Selvakumar, T., Rajasekar, P. and Jang, J.-H., "Graphene oxide reinforced polycarbonate nanocomposite films with antibacterial properties", *Indian Journal of Materials Science*, (2016), 1-10. (<https://doi.org/10.1155/2016/4169409>).
62. Eigler, S. and Hirsch, A., "Chemistry with graphene and graphene oxide—challenges for synthetic chemists", *Angewandte Chemie International Edition*, Vol. 53, (2014), 7720-7738. (<https://doi.org/10.1002/anie.201402780>).
63. Babak, F., Abolfazl, H., Alimorad, R. and Parviz, G., "Preparation and mechanical properties of graphene oxide: Cement nanocomposites", *The Scientific World Journal*, (2014), 1-11. (<https://doi.org/10.1155/2014/276323>).
64. Guerrero-Contreras, J. and Caballero-Briones, F., "Graphene oxide powders with different oxidation degrees, prepared by synthesis variations of the Hummers method", *Materials Chemistry and Physics*, Vol. 153, (2015), 209-220. (<https://doi.org/10.1016/j.matchemphys.2015.01.005>).
65. Male, U., Srinivasan, P. and Singu, B.S., "Incorporation of polyaniline nanofibres on graphene oxide by interfacial polymerization pathway for supercapacitor", *International Nano Letters*, Vol. 5, (2015), 231-240. (<https://doi.org/10.1007/s40089-015-0160-90>).
66. Hemidouche, S., Boudriche, L., Boudjemaa, A. and Hamoudi, S., "Removal of lead (II) and cadmium (II) cations from water using surface-modified graphene", *The Canadian Journal of Chemical Engineering*, Vol. 95, (2017), 508-515. (<https://doi.org/10.1002/cjce.22693>).
67. ASTM C1202, Standard test method for electrical indication of concrete's ability to resist chloride ion penetration, Annual Book of ASTM Standards, (2012). (<https://www.astm.org/Standards/C1202>).
68. Lataste, J., Sirieix, C., Breyse, D. and Frappa, M., "Electrical resistivity measurement applied to cracking assessment on reinforced concrete structures in civil engineering", *NDT & E International*, Vol. 36, (2003), 383-394. ([https://doi.org/10.1016/S0963-8695\(03\)00013-6](https://doi.org/10.1016/S0963-8695(03)00013-6)).
69. Azarsa, P. and Gupta, R., "Electrical resistivity of concrete for durability evaluation: A review", *Advances in Materials Science and Engineering*, (2017), 1-9. (<https://doi.org/10.1155/2017/8453095>).
70. Yang, H.-M., Kwon, S.-J., Myung, N.V., Singh, J.K., Lee, H.-S. and Mandal, S., "Evaluation of strength development in concrete with ground granulated blast furnace slag using apparent activation energy", *Materials*, Vol. 13, (2020), 442. (<https://doi.org/10.3390/ma13020442>).
71. Oner, A. and Akyuz, S., "An experimental study on optimum usage of GGBS for the compressive strength of concrete", *Cement and Concrete Composites*, Vol. 29, (2007), 505-514. (<https://doi.org/10.1016/j.cemconcomp.2007.01.001>).
72. Zhao, H., Sun, W., Wu, X. and Gao, B., "The properties of the self-compacting concrete with fly ash and ground granulated blast furnace slag mineral admixtures", *Journal of Cleaner Production*, Vol. 95, (2015), 66-74. (<https://doi.org/10.1016/j.jclepro.2015.02.050>).
73. Muhmood, L., Vitta, S. and Venkateswaran, D., "Cementitious and pozzolanic behavior of electric arc furnace steel slags", *Cement and Concrete Research*, Vol. 39, (2009), 102-109. (<https://doi.org/10.1016/j.cemconres.2008.11.002>).
74. Li, X., Liu, Y.M., Li, W.G., Li, C.Y., Sanjayan, J.G. and Duan, W.H., "Effects of graphene oxide agglomerates on workability, hydration, microstructure, and compressive strength of cement paste", *Construction and Building Materials*, Vol. 145, (2017), 402-410. (<https://doi.org/10.1016/j.conbuildmat.2017.04.058>).
75. Li, M. and Kim, J.-M., "Strength properties and microstructure of steel slag-based hardened cementitious composite with graphene oxide", *MATEC Web of Conferences: EDP Sciences*, (2017), 03012. (<https://doi.org/10.1051/mateconf/201713803012>).
76. Yu, L., Jiang, L., Chu, H., Guo, M., Zhu, Z. and Dong, H., "Effect of electrochemical chloride removal and ground granulated blast furnace slag on the chloride binding of cement paste subjected to NaCl and Na₂SO₄ attack", *Construction and Building Materials*, Vol. 220, (2019), 538-546. (<https://doi.org/10.1016/j.conbuildmat.2019.06.033>).
77. Dhir, R., El-Mohr, M. and Dyer, T., "Chloride binding in GGBS concrete", *Cement and Concrete Research*, Vol. 26, (1996), 1767-1773. ([https://doi.org/10.1016/S0008-8846\(96\)00180-9](https://doi.org/10.1016/S0008-8846(96)00180-9)).
78. Luo, R., Cai, Y., Wang, C. and Huang, X., "Study of chloride binding and diffusion in GGBS concrete", *Cement and Concrete Research*, Vol. 33, (2003), 1-7. ([https://doi.org/10.1016/S0008-8846\(02\)00712-3](https://doi.org/10.1016/S0008-8846(02)00712-3)).
79. Khan, M. and Kayali, O., "Chloride binding ability and the onset corrosion threat on alkali-activated GGBFS and binary blend pastes", *European Journal of Environmental and Civil Engineering*, Vol. 22, (2018), 1023-1039. (<https://doi.org/10.1080/19648189.2016.1230522>).
80. Chi, M.C., Chi, J.H. and Wu, C.H., "Effect of GGBFS on compressive strength and durability of concrete", *Advanced Materials Research: Trans. Tech. Publ.*, Vol. 1145, (2018), 22-26. (<https://doi.org/10.4028/www.scientific.net/AMR.1145.22>).
81. Jang, S., Karthick, S. and Kwon, S., "Investigation on durability performance in early aged high-performance concrete containing GGBFS and FA", *Advances in Materials Science and Engineering*, (2017), 1-11. (<https://doi.org/10.1155/2017/3214696>).
82. Cheng, A., "Influence of GGBS on durability and corrosion behavior of reinforced concrete", *Materials Chemistry and Physics*, Vol. 93, (2005), 404-411. (<https://doi.org/10.1016/j.matchemphys.2005.03.043>).
83. Guo, K., Miao, H., Liu, L., Zhou, J. and Liu, M., "Effect of graphene oxide on chloride penetration resistance of recycled concrete", *Nanotechnology Reviews*, Vol. 8, (2019), 681-689. (<https://doi.org/10.1515/ntrev-2019-0059>).



Research Article

DC Microgrid Voltage Stability through Inertia Enhancement Using a Bidirectional DC-DC Converter

Shokoofeh Bagheri ^a, Hassan Moradi CheshmehBeigi ^{a,b*}

^a Department of Electrical Engineering, Faculty of Engineering, Razi University, P. O. Box: 67144-14971, Kermanshah, Iran.

^b Industrial Intelligent Systems Research Center (IISRC), Razi University, Kermanshah, Iran.

PAPER INFO

Paper history:

Received: 01 October 2021

Revised in revised form: 27 December 2021

Scientific Accepted: 12 December 2021

Published: 28 May 2022

Keywords:

Renewable Energy Source (RES),
DC Microgrid (DCMG),
Cascaded Buck-Boost Converter (CBBC),
Virtual Inertia,
Virtual DC Machine (VDCM),
DC Bus

ABSTRACT

Today, the presence of energy storage systems along with the alternative nature of renewable energy sources has become undeniable and one of these types of systems is battery energy storage systems. The most important factor in studying the stability of DC microgrids (DCMGs) is the stabilization of the DC bus voltage when an error occurs on its reference value. Therefore, batteries along with power electronic converters play an important role in maintaining DCMG stability. In this paper, the use of Cascaded Buck-Boost Converter (CBBC) can be considered as a suitable alternative to bidirectional buck-boost converter due to such advantages as high power density, 98 % efficiency, and higher operating temperature in battery. The control strategy is applied in the microgrid implemented in the converter system set with storage, and Virtual DC Machine (VDCM) is based on charging and discharging battery through CBBC. In the studied control method, the theoretical properties of the DC machine, which is responsible for amplifying the virtual inertia in the system, are directed to the CBBC for correct switching. VDCM can be changed from motoring to generating mode or vice versa, regardless of mechanical machinery. Therefore, the proposed control system is simulated in an islanded DCMG in Matlab/Simulink and the stability of the studied system is analyzed according to the small-signal model of the proposed control and converter units. According to the simulation results and small-signal model analysis, the stability of the proposed idea under different scenarios is confirmed.

<https://doi.org/10.30501/jree.2021.298032.1233>

1. INTRODUCTION

The development of industry in the 21st century compared to the 18th century has caused many gaps in electricity consumption to the extent that this has led to global energy supply problems. Given the declining trend in fossil fuel resources, now is the time to take fundamental steps to address this major challenge. Also, due to the difficult conditions for the transportation of conventional energy resources to remote areas that do not have access to the route of large power plants and their electricity must be provided autonomously [1]; today, the share of power generation for these areas is associated with the high penetration of Renewable Energy Sources (RESs) [2]. However, on the other hand, all RESs have unique performance characteristics and to integrate them simultaneously, it is necessary to create a suitable method for the optimal use of these resources in the system. For example, one of these features is the random and alternating nature of renewable energy output, which will have a significant impact on system power quality, voltage, and frequency. Therefore, to solve this problem, energy

storage technology was provided in the system [3]. In fact, energy storage points to a significant improvement in the efficiency, stability, and resilience of the power grid [4]. On the other hand, due to the remoteness of some areas from the utility grid and the location of sources that have units with DC output including photovoltaic (PV) systems, Fuel Cell (FC), Energy Storage System (ESS), and DC loads, and this has led to the wider applicability of DC microgrids (DCMGs) [5]. The most important factor studied to analyze the stability of DCMGs is to adjust the DC bus voltage to its reference value. Factors that cause instability when faults occur in DCMGs are fluctuations in the output power of RESs and frequent switching of AC or DC loads with different power consumption. Therefore, to improve the quality of DCMG performance, the implementation of virtual inertia control technique through battery energy storage system and Power Electronic Converters (PECs) has been proposed. Virtual inertia mimicry that results from simulation of the mechanical inertia properties of a rotating machine, i.e., synchronous generators (SGs) in the power grid, is essential to describing the dynamic behavior and stability of the grid [6]. The first concept is the proposed control technique of virtual synchronous generators [7, 8]. In [9], virtual inertia was developed according to the dynamic behavior of the battery based on the second-order SG model with the MULTIPLE signal

*Corresponding Author's Email: ha.moradi@razi.ac.ir (H. Moradi CheshmehBeigi)

URL: https://www.jree.ir/article_150510.html



classification (MUSIC) algorithm technique. To mimic virtual inertia in low-voltage islanded DCMGs, the coordinated control based on bus signaling was investigated in [10]. The authors in [11] proposed adaptive virtual inertia control based on the variable droop coefficient. In this method, by changing the DC bus voltage, the droop characteristic actually changes, that is, the voltage change rate is defined as a variable of the droop coefficient function. Continuous virtual inertia with predictive control, improved active damping compensation, and the use of additional ESSs in [12-14] were studied to maintain DC bus voltage stability and reduce the effect of constant power load. Negative damping of the DC converter immediately creates a positive feedback that causes instability in the DC link voltage; thus, a virtual inertia technique is proposed by forming a negative feedback loop to improve the damping performance and stability of the DC voltage in [15]. In order to create DCMG stability, damping amplification was proposed by implementing the frequency-dependent virtual impedance method when using RESs in [16]. In [17-19], the transient response process of the power system was enhanced with the help of virtual inertia control and virtual capacitor, but the stability analysis of controlling the increase in damping of DC link voltage fluctuations and inertia was omitted. In [20], the aim was to implement an inertia and damping control strategy based on charging and discharging capacitors using ESS. This technique was used to control the output parameters of DCMG converters. Other implemented virtual inertia simulation methods included droop + low pass filter control and power management technique based on charging and discharging the battery energy storage system based on DCMG power flow in [21, 22]. Despite the implementation of all the introduced control techniques, the introduction of a Virtual DC Machine (VDCM) scheme for virtual inertia simulation has recently been welcomed [23] and the aim of this paper is to improve the VDCM design using accurate real DC machine equations. Using the mechanical equations governing the rotor of a real DC machine, the inertia properties can be applied to a bidirectional DC-DC converter. In order to maintain stability and control DC bus voltage disturbances, the connection between the ESS converter and the bus is designed to be flexible. On the other hand, choosing the Cascaded Buck-Boost Converter (CBBC) can be very effective in the performance of the VDCM unit. The proposed converter is considered due to the ability to reverse the working direction and transfer enough power when needed for different modes of operation [24, 25]. The objectives of the article are:

- The problem of inertia deficiency can be solved with the presence of battery by presenting virtual inertia emulation based on real DC machine equations and CBBC;
- Flexible exchange of VDCM power flow on initial transient response and fault moments in DCMG;
- Optimal battery performance using correct CBBC switching for charging and discharging mode;
- Reducing DC bus voltage drop significantly compared to conventional scheme;
- Checking the performance of the CBBC as an interface between battery and DCMG;
- Evaluation of system stability using the small-signal model of the proposed VDCM control scheme and CBBC;

- Simulation of the proposed scheme in an islanded DCMG (see Figure 1(a)) under different scenarios and comparison with the typical scheme;

This article is organized as follows: The structure of an islanded DCMG is introduced in Section 2. The concept of virtual inertia, VDCM modeling, and control strategy are presented in Section 3. Section 4 examines the VDCM stability analysis with small-signal modeling. Finally, the validation of the simulation results and the final conclusion are presented in Sections 5 and 6, respectively.

2. PROPOSED STRUCTURE OF THE STUDIED DCMG

The structure of the DCMG studied including Wind Turbine (WT), PV module, FC stack, battery, and local AC and DC loads is shown in Figure 1(a), 1(b). Each unit is connected to the DC bus in parallel via PECs. However, it is difficult to maintain the bus voltage due to the different nature of the mentioned units under momentary changes in sources and loads. DCMG can be described in three parts: 1) RESs production unit: WT based on the Permanent Magnet Synchronous Generator (PMSG) and the PV that are connected to the bus via a DC-DC boost converter. However, to rectify the output current of the WT, the Gritz 3-phase diode bridge is used before the boost converter; 2) Backup unit: The FC connected to the boost converter and the lead-acid battery connected to the bidirectional CBBC are used to ensure power balance and continuity in microgrid stability; 3) Load unit: The AC and DC loads are connected to the DCMG via a Voltage Source Inverter (VSI) and buck converter, respectively. Since the main focus of this paper is on the concept of inertia amplification via VDCM in DCMG, the modeling and design of other component controllers in this paper has been omitted.

3. DETAILED DESCRIPTION OF THE PROPOSED CONTROLLER STRUCTURE

3.1. Principle of virtual inertia

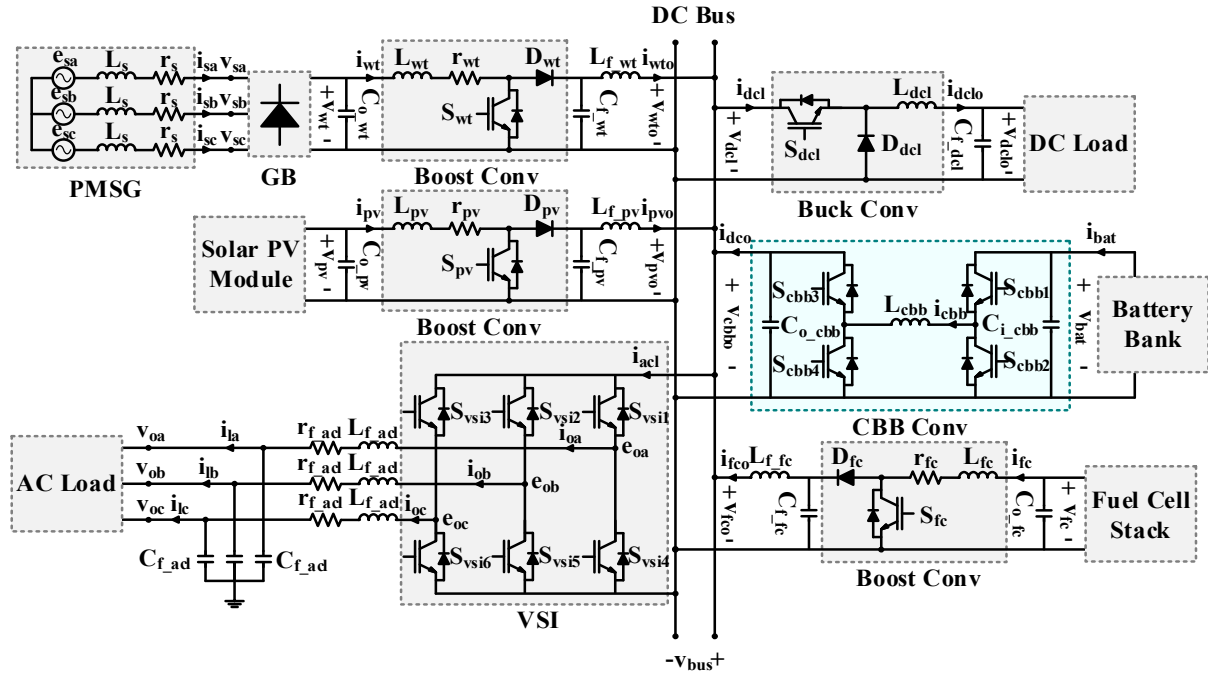
SGs are usually power generators in conventional power grids. SGs are rotary machines that, due to their high inertia, prevent changes in grid frequency when a sudden error occurs. The concept of inertia means the inherent resistance to changing the angular velocity of a rotating object. On the other hand, although power generation with the help of RESs has significant advantages today, the use of this type of generators causes problems such as reducing inertia in the grid. Now, in order to improve the performance of the grid or microgrid, the virtual inertia emulation technique can be used in the system. The use of PECs along with the implementation of its proper control technique to perform the correct switching operation is one of the new methods that has recently been considered to emulate virtual inertia in the system, whose coordination between these processes proves the stability of the grid.

3.2. VDCM modeling

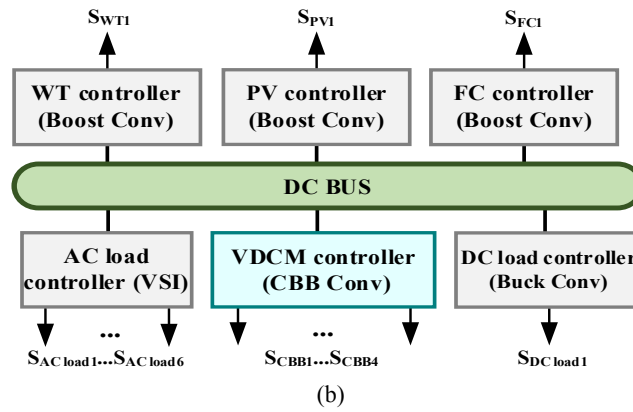
The battery with a single-phase converter connected to it and the implemented control system form the VDCM set, which will first introduce the CBBC converter in Figure 2(a). The use of 4 active switches in this converter caused the power transfer between two DC sources in two different directions. According to the figure, the proposed converter has 4

operating modes: charge, transfer, discharge, and idle. Under these conditions, the DC bus voltage can be adjusted to its reference value by the appropriate delivery d to the active switches. Therefore, using this converter to change the performance of the virtual machine in different operating modes of motoring, generating, and standby in the field of

storage is a good option that motors operation to support the required power load using the battery power supply, the generating operation is to store additional DCMG power in the battery and standby operation occurs when there is a power balance between supply and demand in microgrid.

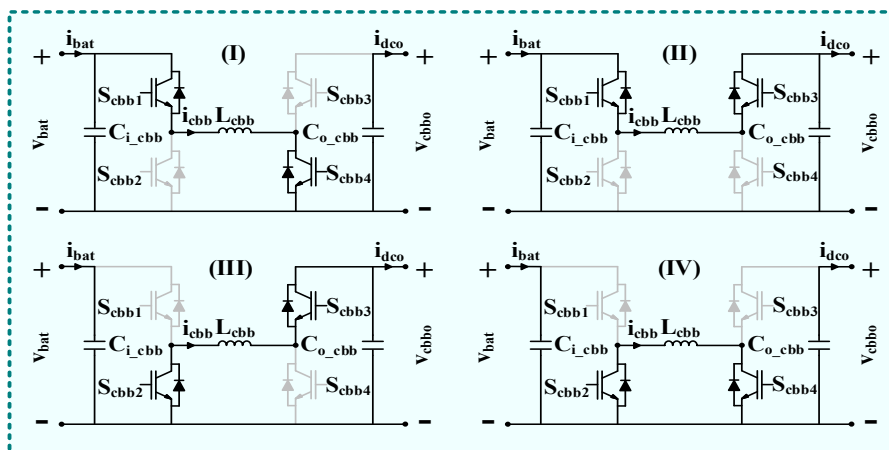


(a)



(b)

Figure 1. (a) Structure of the islanded DCMG; (b) Typical scheme of the DCMG controller



(a)

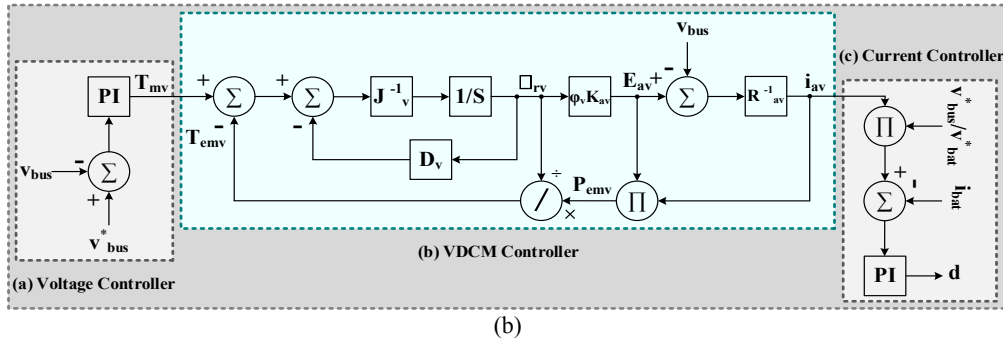


Figure 2. (a) Operating modes of the proposed converter (CBBC), (b) Controller of the virtual inertia part

3.3. Control strategy

One of the important purposes of inserting an output capacitor in a VDCM system is to improve the DC bus voltage transient in the event of a DCMG fault. By storing electrical energy (equivalent to inertia) in the output capacitor, active power support is provided to the system. In this way, Relations 1 and 2 can be considered equivalent to each other:

$$W_r = \frac{1}{2} J_v \omega_{rv}^2 \quad (1)$$

$$W_e = \frac{1}{2} C_{dc} v_{dc}^2 \quad (2)$$

According to Figure 2(b) the implemented control strategy based on a separately excited DC machine, which is in fact the control of bus voltage, is equivalent to controlling the speed of DC machine [26]. The virtual inertia control unit consists of 3 main blocks, i.e., DC bus voltage controllers, VDCM, current regulation and PWM modulation. In the bus voltage control

unit, first, using the PI controller, based on the amount of difference between the bus voltage reference and its measured value at any moment, T_{mv} is obtained. This value is then entered into the VDCM controller unit and based on Equations 3-5, I_{av} is determined. In the next block, the purpose is to determine the appropriate d for the correct switching CBBC for the PWM block. In this section, I_{av} is multiplied by the conversion constant $\frac{V_{bus}^*}{V_{bat}^*}$ to get the I_{bat}^* . The value obtained is compared with the measured value. Finally, upon entering the PI controller, the converter is required in the operating mode.

$$T_{emv} - T_{mv} = J_v \frac{d\omega_{rv}}{dt} + D_v \omega_{rv} \quad (3)$$

$$P_{emv} = E_{av} I_{av}, T_{emv} = \frac{P_{emv}}{\omega_{rv}} \rightarrow P_{emv} = T_{emv} \omega_{rv} \quad (4)$$

$$V_{bus} - E_{av} = R_{av} I_{av} \quad (5)$$

Table 1. DCMG system parameters

VDCM system parameters				Other parameters			
Parameter	Value	Parameter	Value	Parameter	Value	Parameter	Value
V_{bat}^*	96 V	$\phi_v K_{av}$	9.45015	V_{bus}	400 V	P_{DCMG}^*	18 KW
P_{VDCM}^*	4 KW	C_{i_cbb}	1 mF	Switches type	IGBT/Diode	P_{PMSG}^*	5 KW
R_{av}	1 Ω	C_{o_cbb}	2 mF	K_{VC}^P	50	P_{PV}^*	5 KW
J_v	0.001	L_{cbb}	50 μ H	K_{VC}^I	1.5	P_{FC}^*	4 KW
D_v	0.5	SoC	80 %	K_{CC}^P	65	$P_{AC\ load}^*$	7 KW
L_v	0.5 mH	f_s	5 KHz	K_{CC}^I	8	$P_{DC\ load}^*$	4 KW

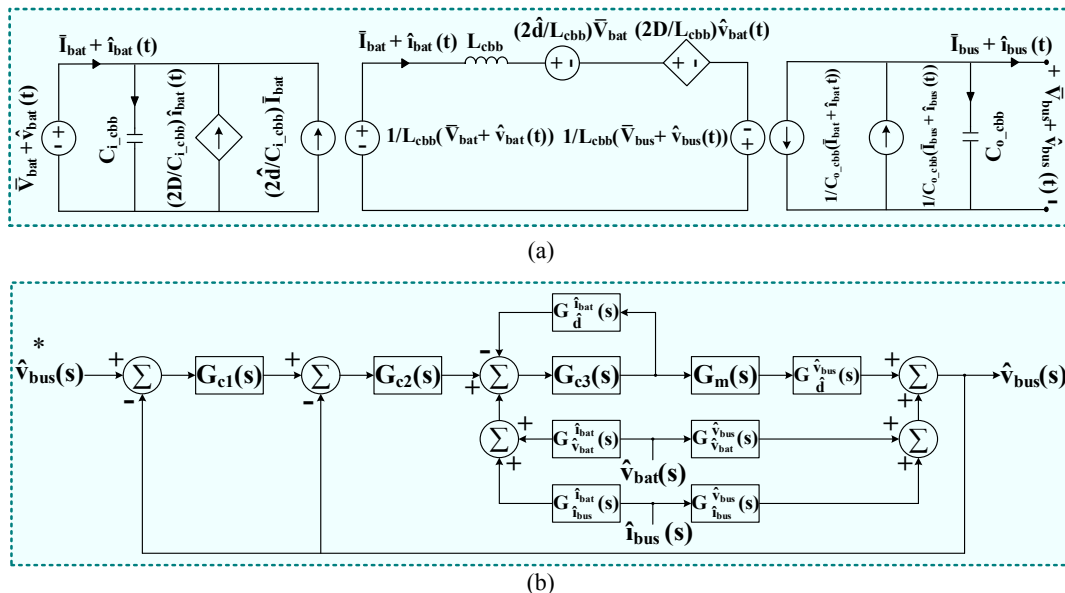


Figure 3. Small-signal model of the VDCM: (a) Small-signal model of the CBBC, (b) Block diagram model of the control VDCM system

4. STABILITY ANALYSIS OF THE VDCM SYSTEM

To evaluate the stability of VDCM implemented in DCMG in small disturbances, first, the CBBC small-signal model in Figures 3(a), 3(b) and the control system applied to it by system linearization are analyzed [27].

In this section, Equations 6 and 7 are first obtained using Figure 3(a) and relations KVL and KCL applied to the CBBC.

$$\frac{(1-C_{o_cbb})}{C_{o_cbb}} [\bar{I}_{bus} + \hat{i}_{bus}(t)] - \frac{1}{sC_{o_cbb}L_{cbb}} [\bar{V}_{bat} + \hat{v}_{bat}(t)] + \frac{2\bar{d}}{sC_{o_cbb}L_{cbb}^2} \bar{V}_{bat} + \frac{2D}{sC_{o_cbb}L_{cbb}^2} \hat{v}_{bat}(t) - \frac{1+(sC_{o_cbb}L_{cbb})^2}{sC_{o_cbb}L_{cbb}^2} [\bar{V}_{bus} + \hat{v}_{bus}(t)] = 0 \quad (6)$$

$$-\frac{1}{L_{cbb}} [\bar{V}_{bat} + \hat{v}_{bat}(t)] + \frac{1+(sC_{o_cbb}L_{cbb})^2}{sC_{o_cbb}L_{cbb}^2} [\bar{I}_{bat} + \hat{i}_{bat}(t)] + \frac{2\bar{d}}{L_{cbb}} \bar{V}_{bat} + \frac{2D}{L_{cbb}} \hat{v}_{bat}(t) - \frac{(1-C_{o_cbb})}{sC_{o_cbb}L_{cbb}} [\bar{I}_{bus} + \hat{i}_{bus}(t)] = 0 \quad (7)$$

According to Figure 2(b) in the small-signal model, Relationships 8-12 are calculated:

$$\Delta V \left(K_{VC}^P + \frac{K_{VC}^I}{s} \right) = T_{mv} \quad (8)$$

$$T_{mv} - T_{emv} = \Delta T_v \quad (9)$$

$$(\Delta T_v - D_v \omega_{rv}) \frac{1}{sJ_v} = \omega_{rv} \quad (10)$$

$$\omega_{rv} \varphi_v K_{av} = E_{av} \quad (11)$$

$$E_{av} \left(\frac{sJ_v R_{av} + D_v R_{av} + (\varphi_v K_{av})^2}{\varphi_v K_{av} R_{av}} \right) = \Delta V \left(\frac{sK_{VC}^P + K_{VC}^I}{s} \right) \quad (12)$$

and....:

$$G_{vv}(s) = \frac{\hat{v}_{bus}}{\hat{v}_{bat}} = \frac{2D-1}{1+(sC_{o_cbb}L_{cbb})^2} \quad (13)$$

$$G_{vd}(s) = \frac{\hat{v}_{bus}}{\bar{d}} = \frac{2\bar{V}_{bat}}{1+(sC_{o_cbb}L_{cbb})^2} \quad (14)$$

$$Z(s) = \frac{\hat{v}_{bus}}{\hat{i}_{bus}} = \frac{s(1-C_{o_cbb})L_{cbb}^2}{1+(sC_{o_cbb}L_{cbb})^2} \quad (15)$$

$$G_{iv}(s) = \frac{\hat{i}_{bat}}{\hat{v}_{bat}} = -\frac{sC_{o_cbb}^2(2D-1)}{1+(sC_{o_cbb}L_{cbb})^2} \quad (16)$$

$$G_{ii}(s) = \frac{\hat{i}_{bat}}{\hat{i}_{bus}} = \frac{(1-C_{o_cbb})}{1+(sC_{o_cbb}L_{cbb})^2} \quad (17)$$

$$G_{id}(s) = \frac{\hat{i}_{bat}}{\bar{d}} = -\frac{2sC_{o_cbb}^2\bar{V}_{bat}}{1+(sC_{o_cbb}L_{cbb})^2} \quad (18)$$

$$G_{c1}(s) = \frac{E_{av}}{\Delta V} = \frac{\varphi_v K_{av} R_{av} (sK_{VC}^P + K_{VC}^I)}{s^2 J_v R_{av} + s D_v R_{av} + s (\varphi_v K_{av})^2} \quad (19)$$

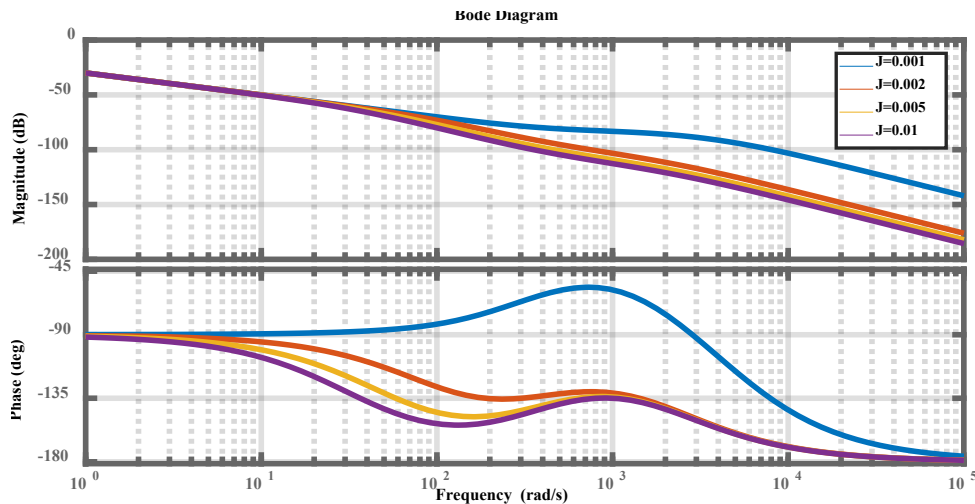
$$G_{c2}(s) = \frac{I_{bat}^*}{E_{av} - V_{bus}} = \frac{V_{bus}^*}{R_{av} V_{bat}^*} \quad (20)$$

$$G_{c3}(s) = \frac{d}{\Delta I_{bat}} = \frac{sK_{CC}^P + K_{CC}^I}{s} \quad (21)$$

Therefore, $G_m(s) = 1$ and using Equations 13-21, we reach Equation 22:

$$G_{vo}(s) = \frac{G_{c1}(s)G_{c2}(s)G_{c3}(s)G_m(s)G_{vd}(s)}{1+G_{c3}(s)G_{id}(s)+G_{c2}(s)G_{c3}(s)G_m(s)G_{vd}(s)} \quad (22)$$

It should be noted that the stability of other DCMG components at the outset has been demonstrated in previous papers; thus, this paper applies the stability analysis to the proposed VDCM unit and the analysis of the other units is omitted. In the following, according to the explanations given, it is clear that by emulation of virtual inertia through the proposed strategy, the VDCM unit is stable and, along with other components, leads to DCMG stability. Bode, Open Loop Step Response, and Root Locus diagrams are shown separately in Figure 4(a)-4(c), respectively. According to the obtained figures, the effect of J_v and D_v control parameters on VDCM performance can be observed. The value of $J_v = 0.001$ is assumed according to the Bode diagram (Figure 4(a)), but selecting other values for J_v can mimic the high inertia in the system, which causes the DC bus voltage to return to its reference value over a longer period of time when power imbalance occurs in the DCMG. Also, by selecting $D_v = 0.5$ according to the response to the unit step input (Figure 4(b)), the appropriate response of this parameter to disturbances in the system can be seen because considering higher values for this parameter, the system performance is very slow. Also, the system poles are located to the left of the imaginary axis according to the Root Locus diagram (Figure 4(c)). Thus, we conclude that the proposed VDCM can be used as a suitable option to support DCMG in the event of an error.



(a)

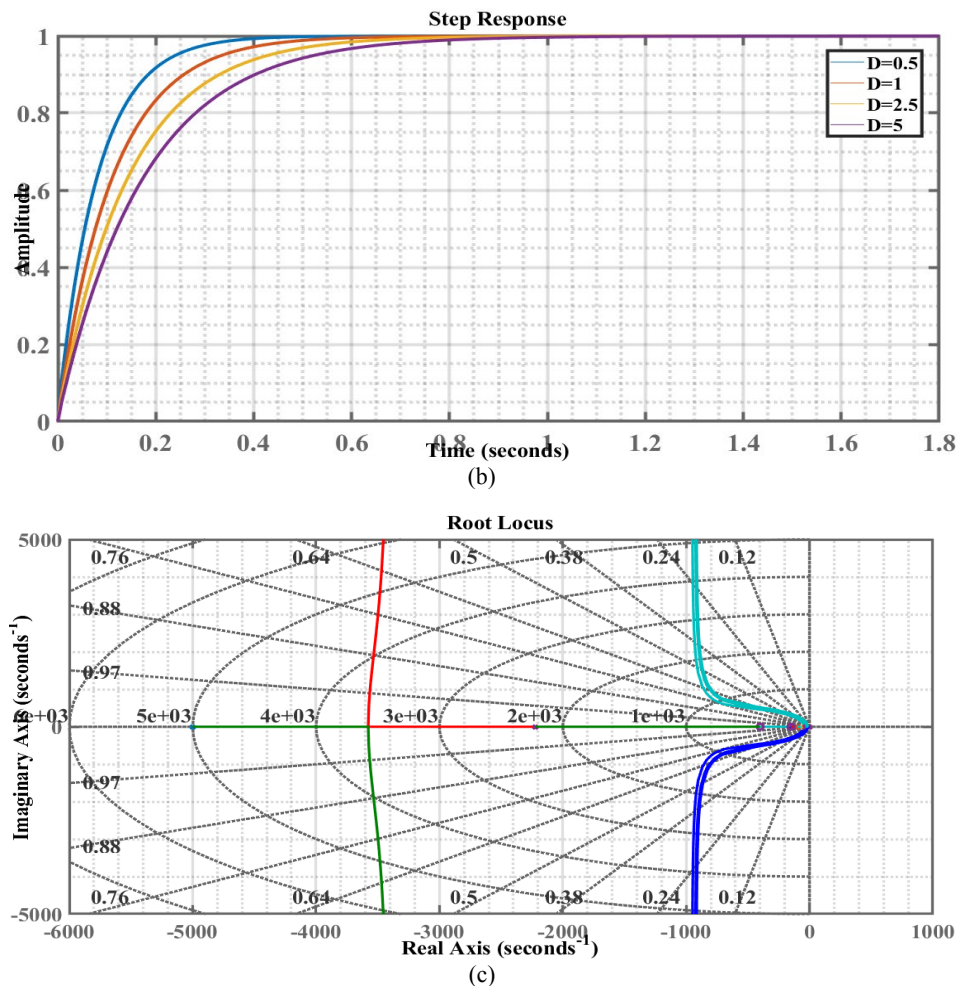


Figure 4. Stability analysis diagrams of the control system: (a) Bode diagram, (b) Open Loop Step Response diagram, (c) Root Locus diagram

5. SIMULATION RESULTS UNDER DIFFERENT SCENARIOS

Validation and confirmation of the studied DCMG (as shown in Figure 1) has been analyzed according to the proposed control strategy under four scenarios in different operating conditions in Matlab/Simulink environment:

5.1. Virtual inertia control analysis in a system under random load fluctuation

Scenario 1: Evaluate the performance of VDCM in three operating modes: generating, standby and motoring

Figure 5(a) shows the amount of power of the microgrid components, i.e., generating units, VDCM, and energy consumed by the load. In this scenario, the output power of WT, PV, and FC is constant. However, the load increases by amount of 3 KW at 0.6 s and 1.2 s per step such that at the moments between 1.2 s to 1.8 s, microgrid in the amount of 17 KW provides power consumption and at 1.8 s and 2.4 s, as the load added in each step decreases and the load returns to its nominal value. Therefore, the output power of the battery at each stage is proportional to the power required by the microgrid. The proposed control system prevents battery overcurrent at load change moments compared to a conventional VDCM such that in the following, in the load increase and decrease scenario, different parameters of VDCM and DC bus in different functions are discussed, as shown in Figures 5(b), 5(c), and 5(d).

As the load increases, the VDCM performance is shown in Figure 5 from the beginning of the simulation time to 1.8 s. According to Figures 5(a)-5(d), by simulating virtual inertia, it is possible to see the improvement of microgrid performance in simultaneous supply of AC and DC loads. Figure 5(a)-5(d) shows the set of microgrid power and VDCM in microgrid power supply, battery output current, DC link side current, and DC bus voltage, respectively. According to Figures 5(b) and 5(c), which show changes in battery output current and DC link current, VDCM initially generates a mode at 0.6 s in the standby mode and changes to the motoring mode at 1.2 s. As explained in the previous sections, VDCM operation is like a real DC machine. In this way, when the first load is added, i.e., at a moment of 0.6 s, the output currents of the battery and the DC link quickly change from the generating mode to the standby mode. Therefore, according to Figure 5(d), virtual inertia simulation using the proposed scheme compared to VDCM control based on the bidirectional buck-boost converter, the DC bus voltage waveform is placed with much less fluctuation on its reference value. At 1.2 s, when the output current of the battery as well as the current of the DC link change due to the increase in load, the VDCM switches from the standby mode to the motoring mode, which again leads to a slight drop in the DC bus voltage. As shown in Figures 5(b) and 5(c), VDCM provides the required microgrid power.

According to the figure, the microgrid is located at load reduction moments 1.8 s and 2.4 s at which according to the figures, the three motoring, standby, and generating operations occur at the moments before 1.8 s and 2.4 s, respectively. At

1.8 s and 2.4 s, the load is reduced by 3 KW at each stage. The DC bus voltage increases rapidly and by simulating virtual inertia, the bus overvoltage is reduced. Meanwhile, the output currents of the battery and the DC link are also negative due to

the change in load and VDCM is switched from the motoring mode to standby and, then, to the generating mode. As a result, VDCM performance is significantly improved.

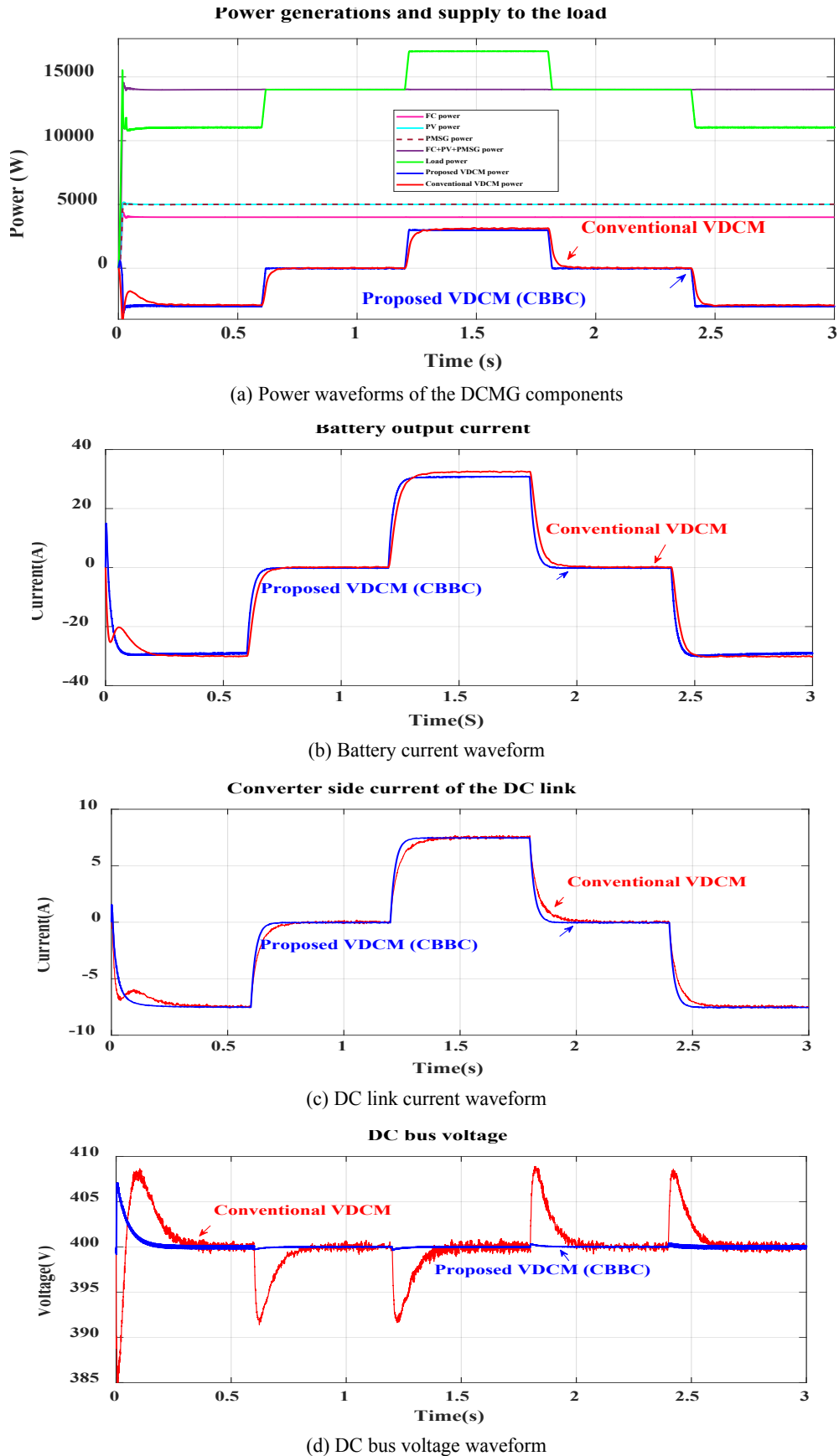
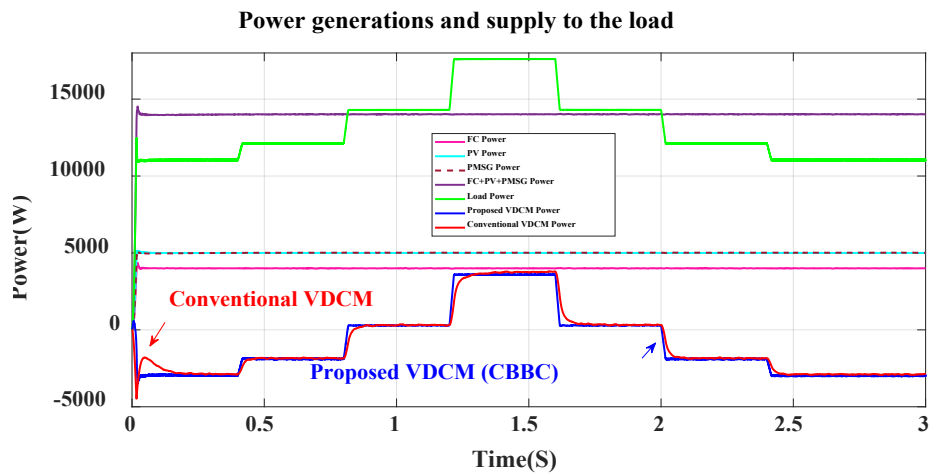


Figure 5. The simulation results of the DCMG components power output under constant sources and variable load conditions with 3 KW power in each step, according to the proposed VDCM performance and comparison with the conventional scheme

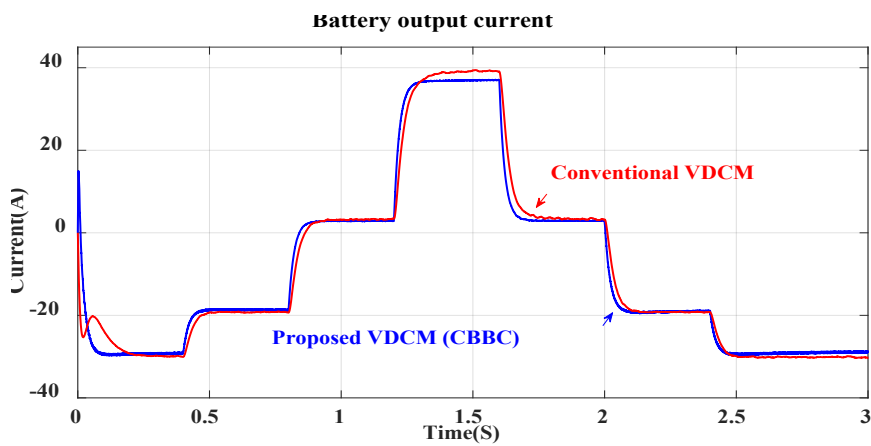
Scenario 2: Investigation of VDCM performance under load fluctuation changes with increase in 10, 20, and 30 % of rated load

In Scenario 1 in the previous section, the performance of VDCM in different operating modes was examined. Based on the results obtained from the simulation, it is determined that the proposed method has significantly improved the DC bus voltage compared to the conventional VDCM scheme. In addition to improving the bus voltage drop, DCMG's initial transient mode is also completely enhanced. Now, in this section, the tested scenario is related to the entry of random load fluctuations at the moments of 0.4 s, 0.8 s, and 1.2 s. According to Figure 6(a), the load at 0.4 s at 10 % of the nominal load (11 KW + 1.1 KW), 0.8 s at 20 % of the rated

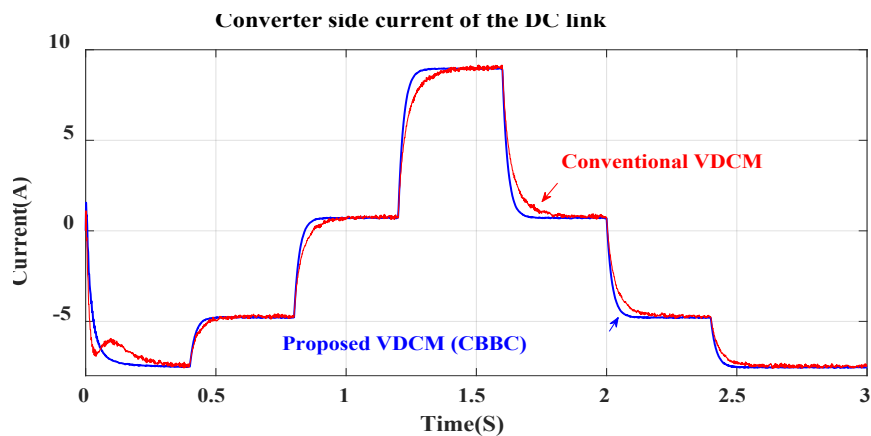
load (11 KW + 2.2 KW), and 1.2 s at 30 % of the nominal load (11 KW + 3.3 KW) has been added. Therefore, the microgrid provides a load of 17.6 KW at its maximum capacity at 1.2 s to 1.6 s. In this scenario, VDCM is in two modes of generating and motoring operation. According to Figure 6(b), depending on the needs of the microgrid, the battery is charged at some point (battery output current: negative) and at other times in the discharge mode (battery output current: positive). Also, changes in DC link current can be seen in Figure 6(c). It can be said that the DC link current is in different operating modes (negative or positive) due to the entry and exit random loads to DCMG. On the other hand, the improvement of DC bus voltage changes can also be seen in Figure 6(d).



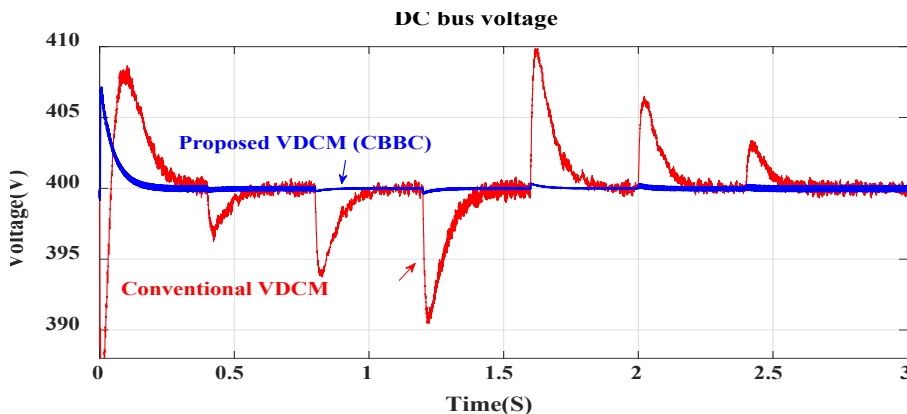
(a) Power waveforms of the DCMG components



(b) Battery current waveform



(c) DC link current waveform



(d) DC bus voltage waveform

Figure 6. The simulation results of the DCMG components power output under constant sources and load fluctuation conditions by increasing 10, 20, and 30 % of nominal load in each step according to the proposed VDCM performance and comparison with the conventional scheme

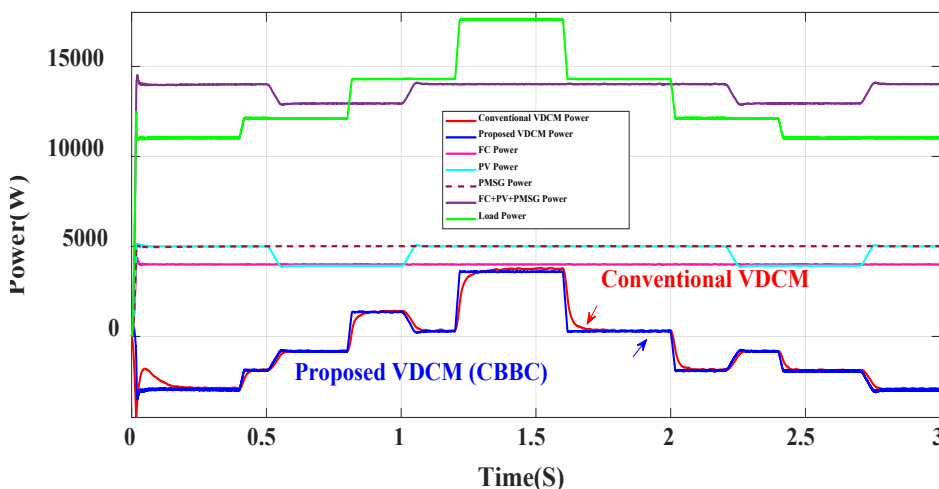
5.2. Virtual inertia control analysis in a system under the sudden change in generated power and random load fluctuation

Scenario 1: Investigation of VDCM performance under PV rated power changes with random load fluctuations

In this scenario, in addition to the changes in random load fluctuations at 0.4 s, 0.8 s, and 1.2 s, the output power of the PV array according to Figure 7(a) is also equal to 20 % in

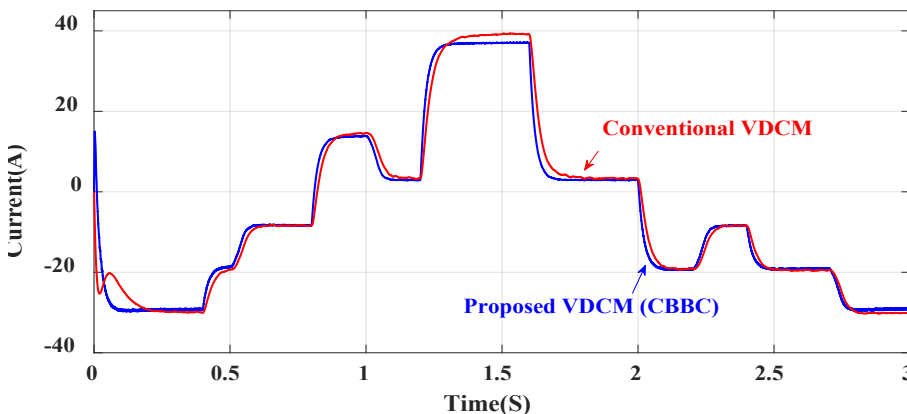
each step at 0.5 s to 1 s and 2.2 s to 2.7 s decreases. In other words, the power of the microgrid PV array decreases by 1 KW at each time interval and returns to its initial state. Charging and discharging the battery energy storage system can be seen in Figure 7(b) in the conventional scheme compared to the proposed technique. In Figure 7(c), the DC link current changes according to load fluctuations and PV output power. The proposed scheme supports the waves and overvoltages generated as well as transient states and keeps the bus steady for as fewer changes as possible (Figure 7(d)).

Power generations and supply to the load

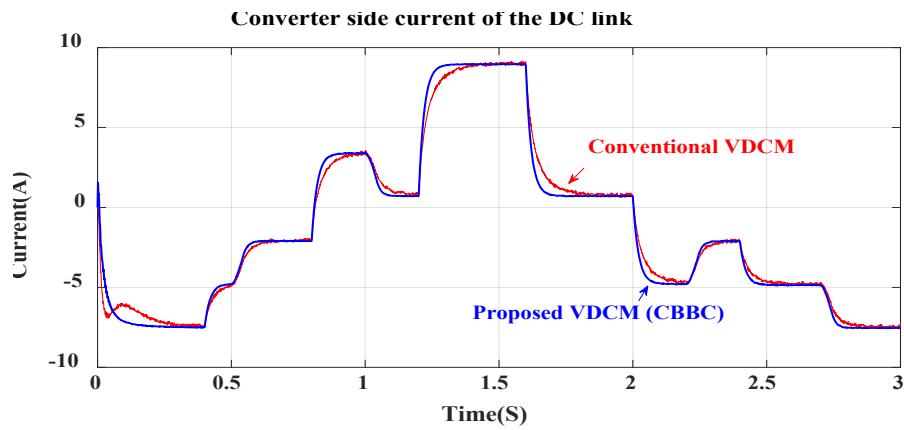


(a) Power waveforms of the DCMG components

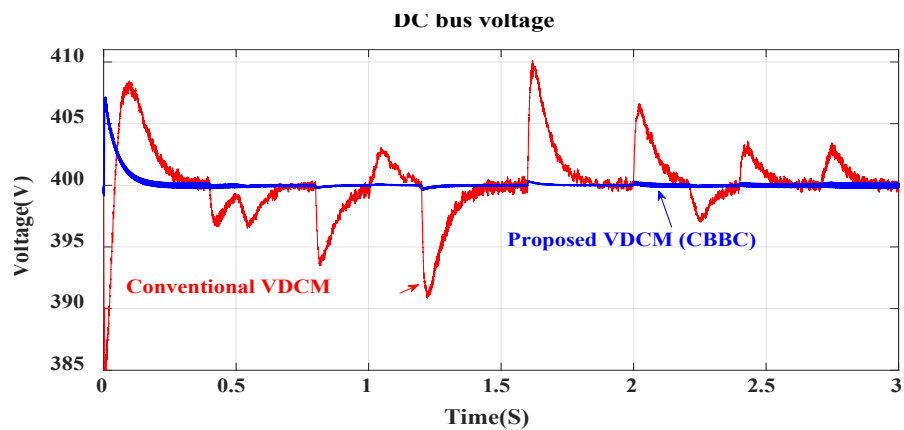
Battery output current



(b) Battery current waveform



(c) DC link current waveform



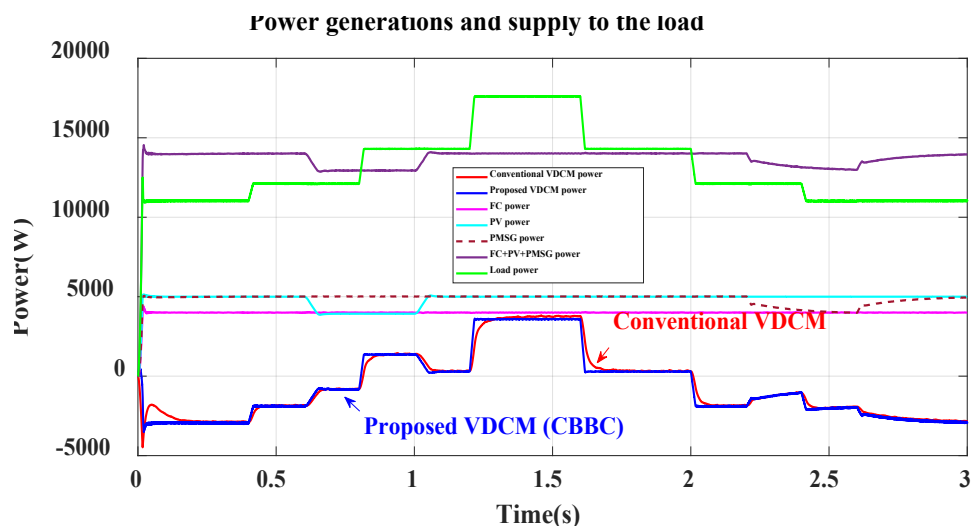
(d) DC bus voltage waveform

Figure 7. The simulation results of the DCMG components power output under 20 % PV source changes in two stages and load fluctuations conditions with increasing 10, 20, and 30 % nominal load in each stage according to the proposed VDCM performance and comparison with the conventional scheme

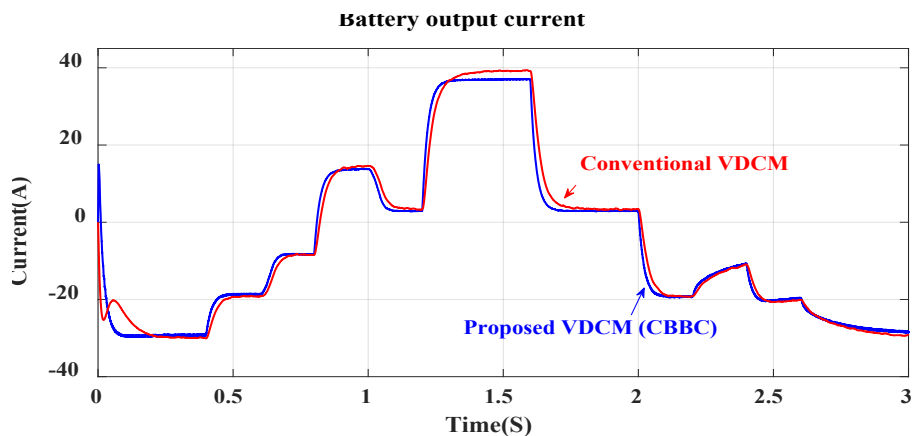
Scenario 2: Investigation of VDCM performance under rated power changes of PV and PMSG with random load fluctuations

In this scenario, as in the previous scenario, in addition to the changes in random load fluctuations at moments 0.4 s, 0.8 s, and 1.2 s, the output power of the PV arrays and PMSG according to Figure 8(a) as much as 20 % in each step at moments 0.6 s to 1 s and 2.2 s to 2.6 s decreases. In other words, the power of the PV array of the microgrid is reduced by 1 KW in the period of 0.6 s to 1 s and returns to its initial

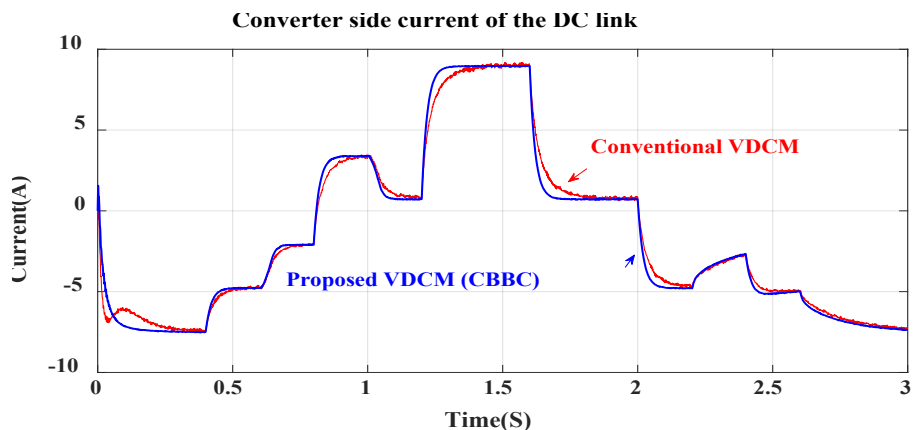
state, and the output power of PMSG decreases by 1 KW in the period of 2.2 s to 2.6 s and returns to the initial state. The transient states of DC bus voltage fluctuations in the conventional VDCM scheme are quite obvious during the changes made in Figure 8(d). However, the proposed scheme supports the waves and overvoltages generated as well as transient states and keeps the bus steady in as little change as possible, and as in Figures 8(b) and 8(c) which represent current waveforms, VDCM proposed is providing the required DCMG power.



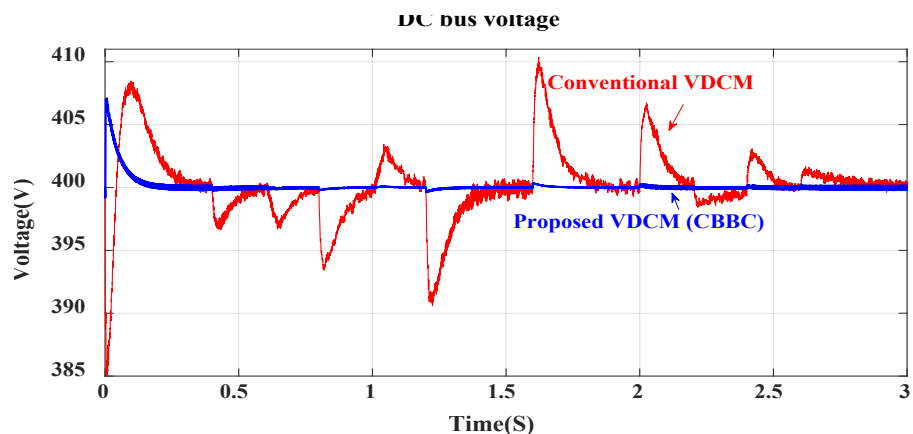
(a) Power waveforms of the DCMG components



(b) Battery current waveform



(c) DC link current waveform



(d) DC bus voltage waveform

Figure 8. The simulation results of the DCMG components under changes of 20 % PV source, 20 % PMSG source, and load fluctuations conditions with increasing 10, 20, and 30 % nominal load in each step according to the proposed VDCM performance and comparison with the conventional scheme

In this section, according to the simulation results obtained during 4 different test scenarios, as can be seen, the performance of the VDCM unit in DCMG is similar in all scenarios. That is, when the consumer unit demand exceeds the output capacity of RESs and FC units, the VDCM unit provides the power required by the consumer and its output specifications are in the motoring mode (discharging). On the other hand, when the consumer demand is less than the production capacity of the microgrid, the output specifications of the VDCM unit are in generating mode (charging) and the extra microgrid power is stored in this unit. Therefore, in the proposed scheme, in order to meet the needs of the consumer

during changes, the DC bus voltage is kept constant at its reference value.

6. CONCLUSIONS

Power fluctuations and DC bus voltage drops in DCMGs have become undeniable due to the presence of RESs. Therefore, the trend to use RESs at high power levels along with the implementation of DCMGs was also welcomed. In order to solve this problem, in this paper, a control strategy called VDCM was designed through a proposed converter that enhanced the inertia of the microgrid. DCMG simulations were performed under different scenarios. According to the

simulation results, the virtual inertia control technique implemented on CBBC improved the voltage stability of the 400 V bus and suppressed fluctuations during sudden changes in sources and load consumption. The effects of J_v and D_v were also investigated using the small-signal model CBBC and control system. Therefore, the VDCM controller for the desired converter had a suitable dynamic characteristic. Finally, it can be said that with a suitable VDCM switch between different motoring and generating modes, the performance of the microgrid has a significant advantage.

7. ACKNOWLEDGEMENT

The authors thank all the personnel of the 7th Iran Wind Energy Conference (IWEC2021) who published this paper at the conference.

NOMENCLATURE

d	Duty cycle (s)
W_r	Kinetic energy stored in the VDCM (j)
W_e	Electrical energy stored in the output capacitor (j)
ω_{rv}	Virtual rotor speed (rad/s)
J_v	Virtual inertia (kg.m ²)
D_v	Virtual damping
R_{av}	Virtual armature resistance (Ω)
L_v	Virtual inductance (H)
T_{emv}	Virtual electromagnetic torque (N.m)
T_{mv}	Virtual mechanical torque (N.m)
P_{emv}	Virtual electromagnetic power (W)
E_{av}	Inductive armature voltage (V)
V_{bat}^*	Battery voltage reference (V)
V_{bus}^*	DC bus voltage reference (V)
I_{bat}^*	Battery current reference (A)
I_{av}	Virtual armature current (A)
C_{dc}	Output capacitor DC link (F)
P_{DCMG}^*	DC microgrid power reference (W)
P_{VDCM}^*	Virtual DC machine power reference (W)
P_{PMSG}^*	Wind turbine power reference (W)
P_{emv}	Virtual electromagnetic power (W)
E_{av}	Inductive armature voltage (V)
V_{bat}^*	Battery voltage reference (V)
V_{bus}^*	DC bus voltage reference (V)
I_{bat}^*	Battery current reference (I)
I_{av}	Virtual armature current (A)
C_{dc}	Output capacitor DC link (F)
P_{DCMG}^*	DC microgrid power reference (W)
P_{VDCM}^*	Virtual DC machine power reference (W)
P_{PMSG}^*	Wind turbine power reference (W)
P_{emv}	Virtual electromagnetic power (W)

REFERENCES

- Chauhan, A. and Saini, R., "A review on Integrated Renewable Energy System based power generation for stand-alone applications: Configurations, storage options, sizing methodologies and control", *Renewable and Sustainable Energy Reviews*, Vol. 38, (2014), 99-120. (<https://doi.org/10.1016/j.rser.2014.05.079>).
- Ertugrul, N. and Abbott, D., "DC is the Future [Point of view]", *Proceedings of the IEEE*, Vol. 108, No. 5, (2020), 615-624. (<https://doi.org/10.1109/JPROC.2020.2982707>).
- Sun, Y., Zhao, Z., Yang, M., Jia, D., Pei, W. and Xu, B., "Overview of energy storage in renewable energy power fluctuation mitigation", *CSEE Journal of Power and Energy Systems*, Vol. 6, No. 1, (2019), 160-173. (<https://doi.org/10.17775/CSEEJPES.2019.01950>).
- Byrne, R.H., Nguyen, T.A., Copp, D.A., Chalamala, B.R. and Gyuk, I., "Energy management and optimization methods for grid energy storage systems", *IEEE Access*, Vol. 6, (2017), 13231-13260. (<https://doi.org/10.1109/ACCESS.2017.2741578>).
- Dragicevic, T., Vasquez, J.C., Guerrero, J.M. and Skrlec, D., "Advanced LVDC electrical power architectures and microgrids: A step toward a new generation of power distribution networks", *IEEE Electrification Magazine*, Vol. 2, No. 1, (2014), 54-65. (<https://doi.org/10.1109/MELE.2013.2297033>).
- Hammad, E., Farraj, A. and Kundur, D., "On effective virtual inertia of storage-based distributed control for transient stability", *IEEE Transactions on Smart Grid*, Vol. 10, No. 1, (2017), 327-336. (<https://doi.org/10.1109/TSG.2017.2738633>).
- Zhu, X., Xie, Z., Jing, S. and Ren, H., "Distributed virtual inertia control and stability analysis of dc microgrid", *IET Generation, Transmission & Distribution*, Vol. 12, No. 14, (2018), 3477-3486. (<https://doi.org/10.1049/iet-gtd.2017.1520>).
- Tamrakar, U., Shrestha, D., Maharjan, M., Bhattarai, B.P., Hansen, T.M. and Tonkoski, R., "Virtual inertia: Current trends and future directions", *Applied Sciences*, Vol. 7, No. 7, (2017), 654. (<https://doi.org/10.3390/app7070654>).
- Golpîra, H., Atarodi, A., Amini, S., Messina, A.R., Francois, B. and Bevrani, H., "Optimal energy storage system-based virtual inertia placement: A frequency stability point of view", *IEEE Transactions on Power Systems*, Vol. 35, No. 6, (2020), 4824-4835. (<https://doi.org/10.1109/TPWRS.2020.3000324>).
- Wu, D., Tang, F., Dragicevic, T., Guerrero, J.M. and Vasquez, J.C., "Coordinated control based on bus-signaling and virtual inertia for islanded DC microgrids", *IEEE Transactions on Smart Grid*, Vol. 6, No. 6, (2015), 2627-2638. (<https://doi.org/10.1109/TSG.2014.2387357>).
- Yan, X., Congcong, B. and Yuan, F. editors, "Virtual inertia control strategy at energy-storage terminal in DC microgrid", *2017 IEEE Conference on Energy Internet and Energy System Integration (EI2)*, (2017), 1-5. (<https://doi.org/10.1109/EI2.2017.8245653>).
- Yi, Z., Zhao, X., Shi, D., Duan, J., Xiang, Y. and Wang, Z., "Accurate power sharing and synthetic inertia control for dc building microgrids with guaranteed performance", *IEEE Access*, Vol. 7, (2019), 63698-63708. (<https://doi.org/10.1109/ACCESS.2019.2915046>).
- Li, Y., He, L., Liu, F., Li, C., Cao, Y. and Shahidehpour, M., "Flexible voltage control strategy considering distributed energy storages for DC distribution network", *IEEE Transactions on Smart Grid*, Vol. 10, No. 1, (2017), 163-172. (<https://doi.org/10.1109/TSG.2017.2734166>).
- Zhi, N., Ding, K., Du, L. and Zhang, H., "An SOC-based virtual DC machine control for distributed storage systems in DC microgrids", *IEEE Transactions on Energy Conversion*, Vol. 35, No. 3, (2020), 1411-1420. (<https://doi.org/10.1109/TEC.2020.2975033>).
- Yang, Y., Li, C., Xu, J., Blaabjerg, F. and Dragičević, T., "Virtual inertia control strategy for improving damping performance of DC microgrid with negative feedback effect", *IEEE Journal of Emerging and Selected Topics in Power Electronics*, Vol. 9, No. 2, (2020), 1241-1257. (<https://doi.org/10.1109/JESTPE.2020.2998812>).
- Guo, L., Zhang, S., Li, X., Li, Y.W., Wang, C. and Feng, Y., "Stability analysis and damping enhancement based on frequency-dependent virtual impedance for DC microgrids", *IEEE Journal of Emerging and Selected Topics in Power Electronics*, Vol. 5, No. 1, (2016), 338-350. (<https://doi.org/10.1109/JESTPE.2016.2598821>).
- Li, C., Li, Y., Cao, Y., Zhu, H., Rehtanz, C. and Häger, U., "Virtual synchronous generator control for damping DC-side resonance of VSC-MTDC system", *IEEE Journal of Emerging and Selected Topics in Power Electronics*, Vol. 6, No. 3, (2018), 1054-1064. (<https://doi.org/10.1109/JESTPE.2018.2827361>).
- Rouzbehi, K., Candela, J.I., Gharehpetian, G.B., Harnefors, L., Luna, A. and Rodriguez, P., "Multiterminal DC grids: Operating analogies to AC power systems", *Renewable and Sustainable Energy Reviews*, Vol. 70, (2017), 886-895. (<https://doi.org/10.1016/j.rser.2016.11.270>).
- Hirase, Y., Sugimoto, K., Sakimoto, K. and Ise, T., "Analysis of resonance in microgrids and effects of system frequency stabilization using a virtual synchronous generator", *IEEE Journal of Emerging and Selected Topics in Power Electronics*, Vol. 4, No. 4, (2016), 1287-1298. (<https://doi.org/10.1109/JESTPE.2016.2581818>).
- Zhu, X., Meng, F., Xie, Z. and Yue, Y., "An inertia and damping control method of DC-DC converter in DC microgrids", *IEEE Transactions on Energy Conversion*, Vol. 35, No. 2, (2019), 799-807. (<https://doi.org/10.1109/TEC.2019.2952717>).
- Lin, G., Zuo, W., Li, Y., Liu, J., Wang, S. and Wang, P., "Comparative analysis on the stability mechanism of droop control and VID control in DC microgrid", *Chinese Journal of Electrical Engineering*, Vol. 7, No. 1, (2021), 37-46. (<https://doi.org/10.23919/CJEE.2021.000003>).

22. dos Santos Neto, P.J., dos Santos Barros, T.A., Silveira, J.P.C., Ruppert Filho, E., Vasquez, J.C. and Guerrero, J.M., "Power management strategy based on virtual inertia for DC microgrids", *IEEE Transactions on Power Electronics*, Vol. 35, No. 11, (2020), 12472-12485. (<https://doi.org/10.1109/TPEL.2020.2986283>).
23. Samanta, S., Mishra, J.P. and Roy, B.K., "Virtual DC machine: An inertia emulation and control technique for a bidirectional DC–DC converter in a DC microgrid", *IET Electric Power Applications*, Vol. 12, No. 6, (2018), 874-884. (<https://doi.org/10.1049/iet-epa.2017.0770>).
24. Chen, X., Pise, A.A. and Batarseh, I., "Magnetics-based efficiency optimization for low power cascaded-buck-boost converter", *IEEE Transactions on Circuits and Systems I: Regular Papers*, Vol. 67, No. 12, (2020), 5611-5623. (<https://doi.org/10.1109/TCSI.2020.2994940>).
25. Wang, Z., Chen, B., Zhu, L., Zheng, Y., Guo, J., Chen, D., Ho, M. and Leung, K.N., "A 3.3-MHz fast-response load-dependent-on/off-time buck-boost DC-DC converter with low-noise hybrid full-wave current sensor", *Microelectronics Journal*, Vol. 74, (2018), 1-12. (<https://doi.org/10.1016/j.mejo.2018.01.010>).
26. Samanta, S., Mishra, J.P. and Roy, B.K., "Virtual DC machine: An inertia emulation and control technique for a bidirectional DC–DC converter in a DC microgrid", *IET Electric Power Applications*, Vol. 12, No. 6, (2018), 874-884. (<http://doi.org/10.1049/iet-epa.2017.0770>).
27. Erickson, R.W. and Maksimović, D., *Fundamentals of power electronics*, Springer Science & Business Media, New York, (2007). (<https://doi.org/10.1007/b100747>).



Research Article

A New Approach Based on RTV/SiO₂ Nano Coating for Tackling Environmental Pollution on Electrical Energy Transmission and Distributions

Ashkan Zolriasatein^{a*}, Zahra RajabiMashhadi^a, Majid Rezaei Abadchi^a, Nastaran Riahi Noori^a, Siamak Abyazi^b

^a Department of Non-Metallic Materials Research, Niroo Research Institute (NRI), P. O. Box: 14665517, Tehran, Tehran, Iran.

^b Department of High Voltage Studies Research, Niroo Research Institute (NRI), P. O. Box: 14665517, Tehran, Tehran, Iran.

PAPER INFO

Paper history:

Received: 14 August 2021

Revised in revised form: 05 January 2022

Scientific Accepted: 18 January 2022

Published: 29 May 2022

Keywords:

Silicon Rubber Nanocomposite,

Salt Fog Test,

Hydrophobicity,

Leakage Current,

Breakdown Voltage

ABSTRACT

The crisis of contamination that leads to the accumulation of dust particles on insulation equipment and electrical insulators has disrupted the electricity grid. Electric discharge on infected insulators in wet conditions is a serious threat to the reliability of the grid, which can lead to grid failure and blackout. In this regard, the importance of hydrophobic and dustproof coatings in the electricity industry has increased in recent years. In this paper, silica nanoparticles in the silicon rubber matrix were used to coat ceramic insulators to decrease the environmental impact of dust and moisture on the insulator's coatings. One of the essential properties of these coatings is their hydrophobicity to prevent possible problems in power transmission. With this regard, nanocomposites were applied to 70 kN insulators and the tests were designed according to the available standards. The performance of these nanocoatings was evaluated by the implementation of electrical, salt fog, and hydrophobicity tests. Finally, the nanocomposite sample containing 3 wt % silica was recognized as the best one.

<https://doi.org/10.30501/jree.2022.299858.1244>

1. INTRODUCTION

The pollution issue is one of the most significant problems in the transmission and distribution of electrical lines. Electric discharge on infected insulators in wet conditions is a serious threat to the reliability of the grid, which can lead to grid failure and blackout [1]. One of the newest solutions is to use nanocoatings on the porcelain insulator surface. Hydrophobic nanocoatings change the surface chemistry and contact angle to protect the substrate against environmental contamination, sunlight damage, temperature changes, and rainfall. Application of these nano coatings can be helpful and effective in removing one of the significant weaknesses of ceramic insulators that perform poorly in the presence of contamination and moisture. If the insulator surface was hydrophobic or superhydrophobic by using nanocomposites, it would prevent the occurrence of dry sparks on the insulator surface due to contamination [2]. The classification of commonly used coatings on ceramic insulators is shown in Figure 1. Nanocoatings are divided into three general categories:

- 1- Silicone rubber coatings vulcanized at room temperature (RTV) modified by nanoparticles with thicknesses of several hundred microns;

- 2- Nano ceramic thin film coatings with heat treatment (these coatings are generally nanometer thick);
- 3- Polymeric-ceramic thin film nanocoatings without heat treatment.

The best performance can be expected from silicone-based coatings vulcanized at room temperature modified by nanoparticles with thicknesses of several hundred microns (Category 1).

One of the most critical components of reliability in power lines is selecting suitable high voltage insulators. Electrical insulators are the essential parts of distribution systems. Insulators must have high voltage breakdown, high resistance to water absorption, and low Dielectric Loss Factor. Therefore, identifying and investigating the destructive factors of insulators and the methods to deal with them can significantly enhance the power distribution.

Ceramic and glass insulators are the most economical insulators widely used throughout the world for power transmission and distribution. There have been many reports of inefficiencies of these types of insulators, such as problems with an electrical discharge in ceramic and glass insulators in humid and polluted areas. As a result of electric discharge, power lines may be cut off for a while, and irreparable damage occurs in hospitals, mechanized factories, and various industrial centers. Because of this phenomenon, a conductive layer is created on the insulators' surface due to the presence of dust and moisture, thereby leaking the flow and reducing

*Corresponding Author's Email: azolriasatein@nri.ac.ir (A. Zolriasatein)
URL: https://www.jree.ir/article_150570.html



the breakdown voltage [3, 4]. Different methods have been proposed to solve these problems, including cleaning and rinsing with water, changing the chemistry of the using materials in the insulator, such as using polymer-concrete composites and applying self-cleaning coatings on the insulator surface. By altering the surface chemistry and increasing contact angle, the surface is protected against environmental contamination, sunlight damage, temperature changes, and rainfall [2-5]. Hydrophobic nano-coatings are the most cost-effective, environmentally friendly, self-cleaning, UV-resistant, anti-dandruff and dust-proof. Thus, utilization of these nano-coatings to remove one of the significant weaknesses of ceramic insulators, which is the formation of a conductive layer in the presence of contamination and moisture, can be very useful. In addition, coated insulators require less washing, which is also economically and valuable [6].

This paper investigated the application of RTV hydrophobic nano coatings reinforced with nano-silica particles on 70 KN ceramic insulators. The electrical and hydrophobic properties of these coated insulators were examined through different tests such as dry and wet leakage current, breakdown voltage, salt fog, and the degree of hydrophobicity.

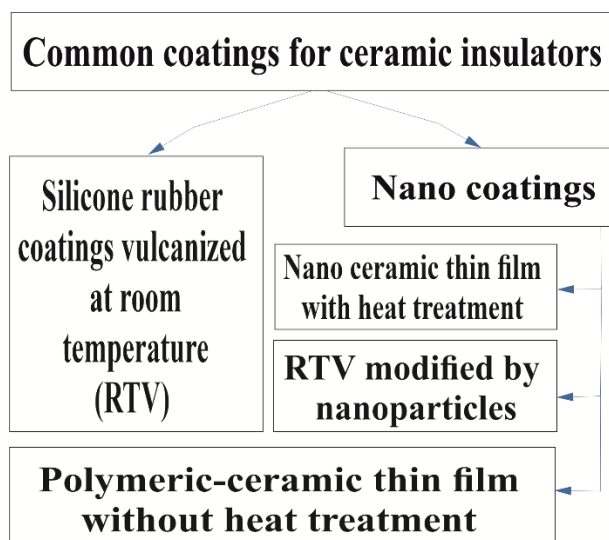


Figure 1. Common coatings used on ceramic insulators

2. EXPERIMENTAL

To investigate the effect of nano-silica on the properties of coated insulators, three samples consisting of different percentages of nano-silica (1, 3, and 5 %) were prepared. A typical coating sample was also prepared with a conventional Canadian RTV CSL product (S0 sample). One non-coated sample was also considered as the control sample (SH sample).

2.1. Ceramic insulator

A 70 kN plate insulator made by the Iran Insulator Company was used to coat and carry out the required tests. These electrical insulators made of clay limit the electric current in a certain direction. The specifications of these insulators are shown in Figure 2 and Table 1.

2.2. Preparing nano coating

Room Temperature Vulcanized Silicone Rubber (RTV1) was obtained from WACKER, USA. (Solid Content = 70 % and

Viscosity 1500 mPa.s at 25 °C by Brookfield method). Nano Silica powder was obtained from FADAK COMPLEX NEW TECHNOLOGIES, Iran. (Grade A1 with Purity of 98 %, particle size: 20 nm, spherical morphology, and Specific Surface Area: 167 m²/g). Toluene, as a solvent, was obtained from Dr. Mojallali, Iran. (Grade Laboratory- Extra pure with Molecular mass: 98.08 g/mol and Specific density: 1.84 g/cm³).

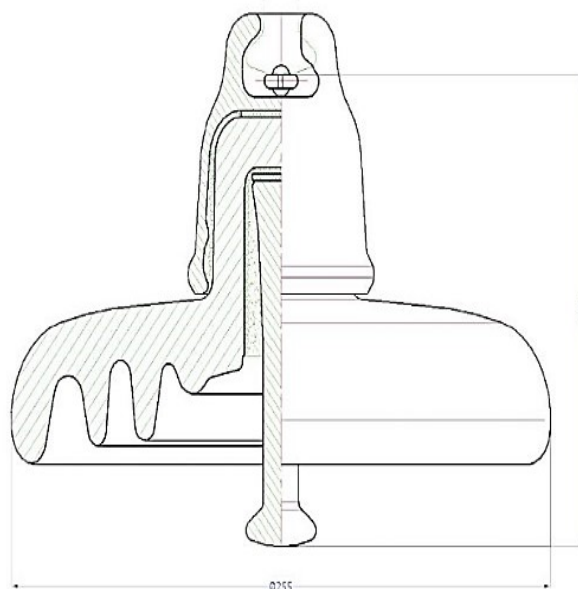


Figure 2. Ceramic insulators used in this research

Table 1. Specifications of used insulators

Properties (unit)	Value
Weight (kg)	4.4
Locking device	R Clip
Ball and socket size (mm)	16
Unit spacing (mm)	146
Porcelain disc diameter (mm)	255
Creepage distance (mm)	295
Electromechanical falling load (kN)	70
Power frequency puncture voltage (kV)	110
Power frequency withstand voltage (kV)	Wet: 40 Dry: 70
50 % Impulse flashover voltage (kV)	Positive: 120 Negative: 125

First, according to the density of composite components, including RTV1 and SiO₂, the density of different composites including 1, 3, and 5 % silica as well as pure RTV1 sample was calculated, according to Eq. 1:

$$\frac{1}{\rho_{com}} = \left(\frac{\%wt}{\rho}\right)_{SiO_2} + \left(\frac{\%wt}{\rho}\right)_{RTV1} \quad (1)$$

Then, the required mass for coating insulators with specific dimensions was calculated (200 gr) and finally, the precise mass of each component was calculated according to the percentage of each component. Toluene was also used as a solvent in the pure and composite samples (30 wt % of RTV1). Subsequently, coatings were prepared as follows:

2.2.1. Pure RTV1

RTV1 and Toluene were thoroughly mixed with a mechanical stirrer for 5 minutes and poured into a particular container for spraying on the insulator.

2.2.2. Nano composite samples

SiO₂ nanoparticles and Toluene were stirred with the magnetic stirrer for 2 minutes. Then, SiO₂ nanoparticles were utterly dispersed in the solvent by an ultrasonic bath for 2 minutes (1 % and 3 % samples) and 4 minutes (5 % samples). Afterward, RTV1 was added to the above solution and mixed with a mechanical stirrer for 1 to 3 minutes until complete homogenization. The chemical composition of the samples is presented in Table 2.

Table 2. The chemical compositions of the samples

Sample No.	RTV1 (wt %)	SiO ₂ (wt %)	Density (g/cm ³)
S0	1	0	1.41
S1	0.99	0.01	1.4166
S3	0.97	0.03	1.4300
S5	0.95	0.05	1.4437

3. METHOD

3.1. Applying nano coating

To apply nanocoating on the ceramic insulators, the gun with a nozzle diameter of 1.8 mm and a windpump were used to spray the coating on the insulator surface. The equipment was used for the coating process, as shown in Figure 3.



Figure 3. a) Gun used for spraying, b) Nozzles with a diameter of 1.8 mm, and c) Equipment needed for insulator coating operations

The coating was sprayed at a distance of 20 cm from the insulator and after seven days, subsequent tests were carried out. According to the product catalog purchased from Wacker Company, RTV1 resin was utterly cured for seven days. One evidence is that it has a hardness above 30 Shore A. All of our examples passed this hardness level. Figure 4 shows the coated samples.

3.2. Performed tests

Electrical tests including wet and dry leakage current, breakdown voltage, salt fog, and hydrophobic class determination were performed to evaluate and compare the composite samples with the control sample.



Figure 4. Insulation prepared from the exterior and interior views

4. RESULTS AND DISCUSSION

4.1. Hydrophobicity

The hydrophobicity class of coatings was investigated by spray method according to IECTS 62073 standard. Equipment used includes a spray bottle, pure water without chemicals such as detergents and solvents, a magnifying device, and a lamp. The sample area should be between 50 and 100 cm and the spraying process should be performed from 25 ± 10 cm and take 20 to 30 seconds. The hydrophobicity class of samples should be determined 10 seconds after the spraying process has finished. Determination of the hydrophobic class with six different modes HC1 to HC6 was performed. HC1 and HC6 were shown to be wholly hydrophobic and hydrophilic, respectively. Results are presented in Table 3. HC stands for "Hydrophobicity Class".

A drop of water tends to wet a surface that is chemically high in surface energy. If the water droplet's adherence to itself is more significant than an outer surface, it is called a hydrophobic surface and in this case, the angle of contact is greater than 90° . If the chemistry of a surface is hydrophobic, the contact angle increases with the surface roughness [6, 7]. In order to determine the class of hydrophobicity by spray to prove to the surface hydrophobicity, the shape of the water droplets from the top view should be circular and the amount of hydrophobicity decreases, as the droplets come out of the circle shape. As shown in Table 3, some droplets on the surface of the control sample SH and the pure sample S0 are oval; however, the number of these oval droplets decreased with increasing silica content in the S1, S3, and S5 samples. By comparing the test results based on existing criteria, the hydrophobicity class of samples SH and S0 was determined to be HC2 equivalent (high and favorable hydrophobicity), whereas for samples containing silica nanoparticles (samples S1, S3, and S5), a hydrophobic class equivalent to HC1 was determined, which is completely hydrophobic. The accepted standard hydrophobicity for this report is HC2 and HC1; thus, these samples are approved.

The result of this test shows hydrophobicity improvement due to the addition of silica nanoparticles to the RTV-SIR. The reason for the hydrophobicity difference between pure RTV and composite with silica is the low gravity between surface and water, as a consequence of low surface energy, which is a property of the hydrophobic surfaces. In addition, on the hydrophobic surfaces, the droplet/coating intersection can be replaced with the droplet/air intersection and it significantly reduces tensile strength. Since the hydrophobic surfaces create an air layer between the drop surface and the solid layer, it is expected that the wet surface area be reduced, which also reduces the tensile force between the drop surface and the hydrophobic surface. In this case, the water droplet automatically moves on the surface of the hydrophobic

surface, while the spontaneous behavior of the water droplet motion on the pure RTV coating is limited [7, 8].

Table 3. Results of hydrophobicity class test

Sample No.	Sample picture	Hydrophobicity class
SH		HC2
S0		HC2
S1		HC1
S3		HC1
S5		HC1

4.2. Electrical test

4.2.1. Dry leakage current

Dry leakage current was measured according to IEC 60060 standard. According to the standard, the laboratory environment was standardized at a temperature of 12.5 °C, 846.1 hPa, and 54.5 % humidity. The sample was installed in an appropriate location for applying voltage. The voltage of 20 kV was applied to the insulator, and the ammeter noted the leakage current after being fixed. As shown in Figure 5, the insulator is observed under test conditions. The rods hung at the bottom of the insulator are the conductor for the power line simulator.

The results of the samples dry leakage current test are listed in Table 4. Figure 6 also shows changes of dry leakage current with an increasing percentage of nano-silica in the coating. According to Table 4, the dry leakage current increased more than the uncoated sample by applying pure RTV to Sample S0 (control sample SH). However, it was expected that dry leakage would not be reduced by applying coatings because the performance of nanocoating on insulators was more significant in salt fog or contaminated tests [8-10].

Table 4. Dry leakage current test results

Sample No.	Dry leakage current (μA)	Improvement (%)
SH	356	-
S0	364	2.25
S1	364	2.25
S3	367	3.09
S5	354	-0.56



Figure 5. Insulator mounted for electrical testing

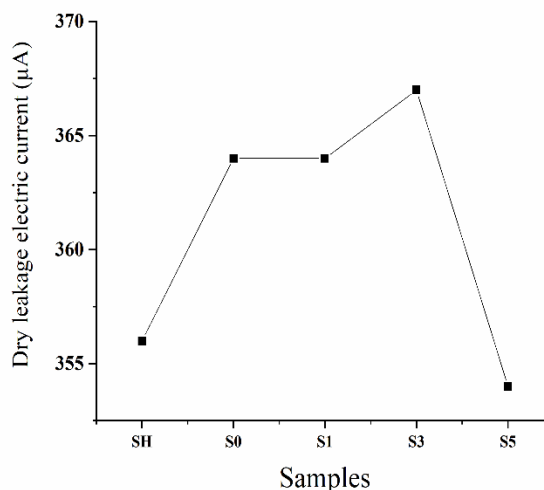


Figure 6. Changes of dry leakage current with an increasing percentage of nano silica in the coating

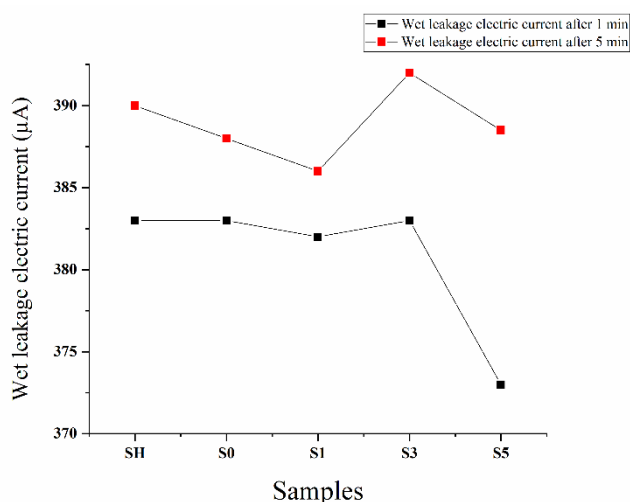
4.2.2. Wet leakage current

This test was performed according to IEC 60071 standard. The wet leakage current test had the exactly dry leakage current test conditions. In this test, water (a combination of distilled water and municipal water) was sprayed with a specific resistance rate of $100 \pm 15 \mu\text{S}/\text{sec}$ and an injection rate of about 1 to 2 mm/min at an oblique angle of 45° . Therefore, water is sprayed to the insulator at an angle of 45° and the voltage of 20 kV is applied for two different durations, 1 and 5 minutes.

The results of the wet leakage current test of the samples are listed in Table 5. Figure 7 also shows changes of wet leakage current with an increasing percentage of nano-silica in the coating. According to the table, the worst case is the S3, with its leakage rate even higher than the control sample (SH) after 5 minutes. S1 sample, which has the lowest wet leakage current and is considered the best, reduced the current leakage rate by 1.02 %. However, the results of all the samples are very close together and precise analysis and comparison are not possible [10-12].

Table 5. Wet leakage current test results

Sample No.	Wet leakage current after 1 min (μA)	Wet leakage current after 5 min (μA)	Improvement after 5 min (%)
SH	383	390	-
S0	383	388	-0.51
S1	382	386	-1.02
S3	383	392	-0.51
S5	373	388.5	0.38

**Figure 7.** Changes of wet leakage current with an increasing percentage of nano silica in the coating

4.2.3. Breakdown voltage

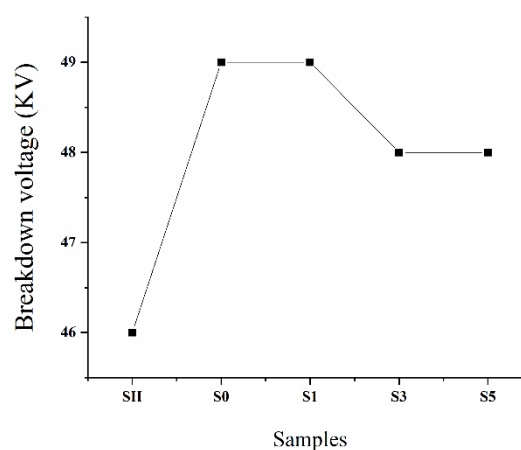
This test was performed according to the IEC60383 standard and evaluated the insulator's performance under contamination conditions. The test conditions were the same as the leakage current tests. However, in this test, the applied voltage to the samples increased after exposure to water until the spark on the insulator surface was observed and its value was recorded at the moment of electrical failure. The breakdown voltage was reported by dividing the recorded voltage by the correction factor according to the ambient conditions. The correction factor for this test was 0.98 % according to environmental conditions. The breakdown voltage test results of the samples are listed in Table 6. Figure 8 also shows the breakdown voltage changes with an increasing percentage of nano-silica in the coating [13-15].

Table 6. Breakdown voltage test results

Sample No.	Breakdown voltage (kV)	Improvement (%)
SH	46	-
S0	49	6.52
S1	49	6.52
S3	48	4.35
S5	48	4.35

According to the standard of acceptance, since the minimum breakdown voltage of 50 kV is accepted, based on the results, none of the coated insulators were accepted. However, the results presented in Table 5 are too close and can be considered as a fall within the error range of the test. Results

also show that application of RTV coating and increase of nanoparticles percentage improved the breakdown voltage. The presence of silica nanoparticles in the composite composition increased the number of crosslinks, reduced the gap between the polymer chains, ultimately improved the hardness of the coatings, and resulted in the presence of samples in power lines under environmental conditions, such as rainfall and lightning. In addition, electrical properties maintain coverage. In the samples with higher nanoparticles percentages, such as S5 (samples with 5 % nanoparticles), there was a probability of optimum dispersion of the filler in the polymeric field [10, 11].

**Figure 8.** Changes of breakdown voltage with an increasing percentage of nano silica in the coating

4.2.4. Salt fog test

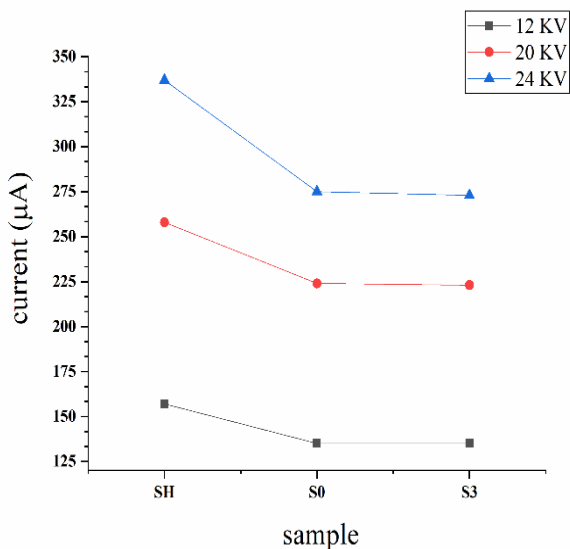
A salt fog test was performed on coated insulators according to IEC 62217 standard. In this test, insulators coated with pure RTV resin and composite containing 3 % silica nanoparticles (S0 and S3 samples) were compared with the control sample (SH). Insulators were immersed in a test chamber containing 800 g of salt in 100 ml of distilled water for 5 h. Then, the leakage current was measured at three voltage levels of 12, 20, and 24 kV. Figure 9 shows the samples in the salt fog chamber.

The results of the salt fog test after five hours are shown in Table 7. Figure 10 also shows the leakage current changes at three voltage levels of 12, 20, and 24 kV. Results show that utilizing silica nanoparticles in the coatings of insulators reduced the leakage current at different voltages [15-17].

**Figure 9.** Samples in the salt fog chamber

Table 7. Results of the salt fog test for five hours

Sample No.	Leakage current (μA)		
	12 kV	20 kV	24 kV
SH	157	258	337
S0	135	224	275
S3	135	223	273

**Figure 10.** Changes of leakage current at 3 voltage levels of 12, 20 and 24 kV

5. CONCLUSIONS

Since the crisis of micro grids in humid areas has caused problems in electricity transmission, the use of these hydrophobic coatings can prevent the contamination of electrical equipment and their disruption.

In the test of hydrophobic class determination of spray-coated insulators, control samples (SH) and pure RTV (S0) of HC2 class and optimum hydrophobicity were evaluated. The samples containing silica nanoparticles were all evaluated with HC1 class and completely hydrophobic.

In electrical tests including dry leakage current, wet leakage current and breakdown voltage, the presence of silica nanoparticles had a normal effect on the electrical properties of the coatings and the reported numbers were very close. However, the improvement of the electrical properties resulted from an increment in the number of crosslinks and the decrement in the gap between the polymer chains by the addition of nanoparticles. It was also shown that these nanocomposite polymer coatings could be used to eliminate the adverse effects of dust and other environmental contaminants instead of removing ceramic insulators.

6. ACKNOWLEDGEMENT

This work was supported by the Niroo Research Institute (NRI) [grant number 237100]. The authors would like to thank their colleagues A. Mehdikhani and M. Maleki in Ceramic and Polymer Laboratory, and also B. Elmdoost, A. Feizinia, and Y. Ghorbani in Wire and Cable Reference Laboratory of Niroo Research Institute, for their technical assistance.

REFERENCES

- Reynders, J.P., Jandrell, I.R. and Reynders, S.M., "Review of aging and recovery of silicone rubber insulation for outdoor use", *IEEE Transactions on Dielectrics and Electrical Insulation*, Vol. 6, No. 5, (1999), 620-631. (<https://doi.org/10.1109/TDEI.1999.9286749>).
- Song, W., Shen, W.-W., Zhang, G.-J., Song, B.-P., Lang, Y., Su, G.-Q., Mu, H.-B. and Deng, J.-B., "Aging characterization of high temperature vulcanized silicone rubber housing material used for outdoor insulation", *IEEE Transactions on Dielectrics and Electrical Insulation*, Vol. 22, No. 2 (2015), 961-969. (<https://doi.org/10.1109/TDEI.2015.7076797>).
- Gorur, R.S., De La O, A., El-Kishky, H., Chowdhary, M., Mukherjee, H., Sundaram, R. and Burnham, J.T., "Sudden flashover of nonceramic insulators in artificial contamination tests", *IEEE Transactions on Dielectrics and Electrical Insulation*, Vol. 4, No. 1, (1997), 79-87. (<https://doi.org/10.1109/94.590870>).
- Zolriasatein, A., Rajabi Mashhadi, Z., Navazani, S., Rezaei Abadchi, M., Riahi Noori, N. and Abdi, N., "Investigation of electrical properties of silica-reinforced RTV nanocomposite coatings", *Journal of Materials Science: Materials in Electronics*, Vol. 32, No. 9, (2021), 12265-12274. (<https://doi.org/10.1007/s10854-021-05855-0>).
- Li, J., Zhao, Y., Hu, J., Shu, L. and Shi, X., "Anti-icing performance of a superhydrophobic PDMS/modified nano-silica hybrid coating for insulators", *Journal of Adhesion Science and Technology*, Vol. 26, No. 4, (2012), 665-679. (<https://doi.org/10.1163/016942411X574826>).
- Syakur, A. and Sutanto, H., "Determination of hydrophobic contact angle of epoxy resin compound silicon rubber and silica", *Proceedings of IOP Conference Series: Materials Science and Engineering*, IOP Publishing, No. 190, (2017), 012025-012032. (<https://doi.org/10.1088/1757-899X/190/1/012025>).
- Guo, K., Du, Y., Wu, Y., Mi, X., Li, X. and Chen, S., "Morphology and FT-IR analysis of anti-pollution flashover coatings with adding nano SiO₂ particles", *Proceedings of IOP Conference Series: Materials Science and Engineering*, IOP Publishing, No. 274, (2017), 012031-012040. (<https://doi.org/10.1088/1757-899X/274/1/012031>).
- Li, J., Wei, Y., Huang, Z., Wang, F., Yan, X. and Wu, Z., "Electrohydrodynamic behavior of water droplets on a horizontal superhydrophobic surface and its self-cleaning application", *Applied Surface Science*, Vol. 403, (2017), 133-140. (<https://doi.org/10.1016/j.apsusc.2017.01.141>).
- Ghosh, D., Bhandari, S., Chaki, T.K. and Khatgir, D., "Development of a high performance high voltage insulator for power transmission lines from blends of polydimethylsiloxane/ethylene vinyl acetate containing nanosilica", *RSC Advances*, Vol. 5, No. 71, (2015), 57608-57618. (<https://doi.org/10.1039/C5RA08277C>).
- Hui, S., Chaki, T.K. and Chattopadhyay, S.J.P.E., "Dielectric properties of EVA/LDPE TPE system: Effect of nanosilica and controlled irradiation", *Polymer Engineering & Science*, Vol. 50, No. 4, (2010), 730-738. (<https://doi.org/10.1002/pen.21577>).
- Zolriasatein, A., Navazani, S., Abadchi, M.R. and Noori, N.R., "Two-component room temperature vulcanized silicone-rubber (RTV2) properties modification: Effect of aluminum three hydrate and nanosilica additions on the microstructure, electrical, and mechanical properties", *Journal of Materials Science: Materials in Electronics*, Vol. 32, No. 7, (2021), 8903-8915. (<https://doi.org/10.1007/s10854-021-05562-w>).
- Taipalus, R., Harmia, T., Zhang, M.Q. and Friedrich, K., "The electrical conductivity of carbon-fibre-reinforced polypropylene/polyaniline complex-blends: Experimental characterisation and modelling", *Composites Science and Technology*, Vol. 61, No. 6, (2001), 801-814. ([https://doi.org/10.1016/S0266-3538\(00\)00183-4](https://doi.org/10.1016/S0266-3538(00)00183-4)).
- Nangir, M., Massoudi, A. and Tayebifard, S.A., "Investigating the effect of ultrasonication time on transition from monolithic porous network to size-tunable monodispersed silica nanosphere in Stöber method", *Advanced Ceramics Progress*, Vol. 4, No. 2, (2018), 37-43. (<https://dx.doi.org/10.30501/acp.2018.91124>).
- Dang, Z.M., Zhang, Y.H. and Tjong, S.C., "Dependence of dielectric behavior on the physical property of fillers in the polymer-matrix composites", *Synthetic Metals*, Vol. 146, No. 1, (2004), 79-84. (<https://doi.org/10.1016/j.synthmet.2004.06.011>).
- Yotkuna, K., Chollakup, R., Imboon, T., Kannan, V. and Thongmee, S., "Effect of aluminum hydroxide on thermal, dynamic mechanical and dielectric properties of hexafluoropropylene-vinylidene fluoride

- elastomeric composites", *Journal of Polymer Research*, Vol. 28, No. 12, (2017), 83-96. (<https://doi.org/10.22606/jan.2017.22001>).
16. Khan, H., Amin, M., Ali, M., Iqbal, M. and Yasin, M., "Effect of micro/nano-SiO₂ on mechanical, thermal, and electrical properties of silicone rubber, epoxy, and EPDM composites for outdoor electrical insulations", *Turkish Journal of Electrical Engineering & Computer Sciences*, Vol. 25, No. 2, (2017), 1426-1435. (<https://doi.org/10.3906/elk-1603-20>).
17. Ullah, I., Akbar, M. and Khan, H.A., "Degradation analysis of RTV-SiR based composites under both polarities DC voltage for insulators coating", *Materials Today Communications*, No. 29, (2021), 102890-102901. (<https://doi.org/10.1016/j.mtcomm.2021.102890>).



Research Note

Investigating the Economic Effects and the Roadmap of Developing Geothermal Systems to Generate Electricity

Mirmahdi Seyedrahimi-Niaraq*, Tohid Nouri

Faculty of Engineering, University of Mohaghegh Ardabili, P. O. Box: 56199-13131, Ardabil, Ardabil, Iran.

PAPER INFO

Paper history:

Received: 01 December 2021
 Revised in revised form: 03 January 2022
 Scientific Accepted: 11 January 2022
 Published: 25 June 2022

Keywords:

Renewable Energy,
 Geothermal Energy,
 Economic Impacts,
 Geothermal Economic Policies,
 Geothermal Energy Roadmap

ABSTRACT

Geothermal energy is a non-carbon renewable source from the earth's internal energy. This energy is considered reliable today and has a high potential to reduce the threat of climate change. The main factor that any investor wants to invest in any natural energy source is the resulting economy. In the case of geothermal energy, factors that increase the risk of investing in this sector include higher investment costs, longer payback times than other renewable power plants, and the uncertainty of the size and quality of the resources before the completion of the well drilling operation. The average payback time in geothermal energy systems is 5.7 years, longer than wind and solar energy. According to these factors, the risk of investing in geothermal technology increases. On the other hand, due to its independence from oil and gas, it increases a country's energy security, helps to create direct, indirect, and induced employment, and affects other economic sectors. Also, unlike renewable wind and solar energies, it is not dependent on climate change; therefore, it has higher reliability than other renewable energies. Also, by combining this energy with other renewable energies, its performance can be optimized. For example, in an optimal geothermal-solar hybrid power plant, solar energy provides 48 % of the total energy. In this case, the Levelized Cost of Energy (LCOE) is reduced from 225 \$ per MWh (only with geothermal source) to 165 \$ per MWh. In this study, while studying the economic effects of geothermal systems, an attempt has been made to address the challenges in this field and present the policies implemented in some countries. It is implied that by providing incentive policies and an appropriate roadmap, it is possible to help attract investment in the operation of geothermal systems.

<https://doi.org/10.30501/jree.2022.317375.1290>

1. INTRODUCTION

To increase human well-being, humans need much more energy. By 2040, population growth and economic expansion will be expected to increase the global energy demand by 37 % compared to the year 2013 [1, 2]. The use of fossil fuel energy leads to threats such as Greenhouse Gas (GHG) emissions, hence global climate change and local climate pollution [3-6]. Renewable energy is one of the key technologies to reduce CO₂ emissions [7,8]. This energy includes wind, solar, and geothermal energies. Meanwhile, geothermal energy is a well-known and reliable energy source with high potential [9-12]. For example, deep geothermal sources are based on hot fluids that are widely used to generate electricity. Figure 1 shows a deep geothermal system. Figure 1a shows the cross-section, and Figure 1b shows the heat source and its interactions with the water cycle [13]. The system has three main components: "magma", which provides heat, "precipitation", which provides geothermal fluid, and "permeable zone", which acts as a fluid transfer medium from

deep to near the surface. In this system, the heat stored in the ground is used for the intended purpose, while the shallow heat pump systems provide heating and ventilation without using the heat stored in the ground.

Geothermal energy is generated by a systematic approach that begins with surface surveys followed by subsurface explorations and experiments to investigate and study the geothermal source or reservoir. This process usually takes between 2 and 3 years. It will take another 3 to 5 years for the well field to be built and installed in the power plant. Meanwhile, high investment risk can slow down geothermal development and sometimes, prevent the project from continuing. However, the growing human need for energy has caused greater investment in renewable energy, especially geothermal energy. By 2040, with population growth and economic expansion, global energy demand is expected to increase by 37 % compared to the year 2013 [1]. This study, while studying the economic effects of geothermal systems, has been made to address the challenges in this field and the policies implemented in some countries. The roadmap of some European and Asian countries in this field has also been reviewed.

2. ECONOMIC ASPECTS

*Corresponding Author's Email: m.seyedrahimi@uma.ac.ir (M. Seyedrahimi-Niaraq)

URL: https://www.jree.ir/article_152426.html



The financial results of exploiting an energy source can be a significant factor in investing in this sector. Factors increasing the investment risk in the field of geothermal energy are given below [14]:

- 1- Higher investment cost than other renewable power plants;
- 2- Longer payback time; and
- 3- Greater uncertainty in the size and quality of resources before completing well drilling operations.

On the other hand, due to its independence from oil and gas, increases a country's energy security, helps create direct, indirect, and induced employment, and affects other economic sectors. Some different economic aspects of geothermal energy are given below:

2.1. Economic sustainability of geothermal power plants

Economic feasibility must be studied for the development of sustainable geothermal systems. There are various methods designed for the economic evaluation of geothermal power plants. One of the most popular methods is the Levelized Cost of Energy (LCOE). This algorithm is used to recover the investment, maintenance, and operation costs of a particular power plant over its lifetime and is defined as the price of electricity. Factors affecting LCOE include investment costs, average power generation rate, power plant life, cost reduction rate, and availability of facilities [15].

A mathematical relation for LCOE is provided by Sheu et al. for hybrid fossil fuel-solar thermal systems [16]:

$$LCOE = \frac{\sum_{t=1}^n \frac{(I_t + M_t + F_t + H_t)}{(1+r)^t}}{\sum_{t=1}^n \frac{E_t}{(1+r)^t}} \quad (1)$$

where

- I_t : Investment expenditures in the year t
- M_t : Operations and maintenance expenditures in the year t
- F_t : Fuel expenditures in the year t
- H_t : Avoided heat production costs in the year t
- E_t : Electricity generation in the year t
- r : Discount rate
- t : Year
- n : An assumed lifetime of the system (integer, in years)

Investment costs represent the main factor in the economic viability of a geothermal power plant. This cost includes surface and subsurface costs. Initial costs and surface exploration, infrastructure design, construction, and operation and site maintenance are part of the surface costs. At the same time, the drilling costs of wells are classified as subsurface costs [17]. Figure 2 analyzes the surface and subsurface costs for the five geothermal power plants installed in Iceland. According to this figure, surface costs are linearly related to the size of the power plant. In addition, the investment costs for unknown fields are higher than the investment costs for known and more informed fields.

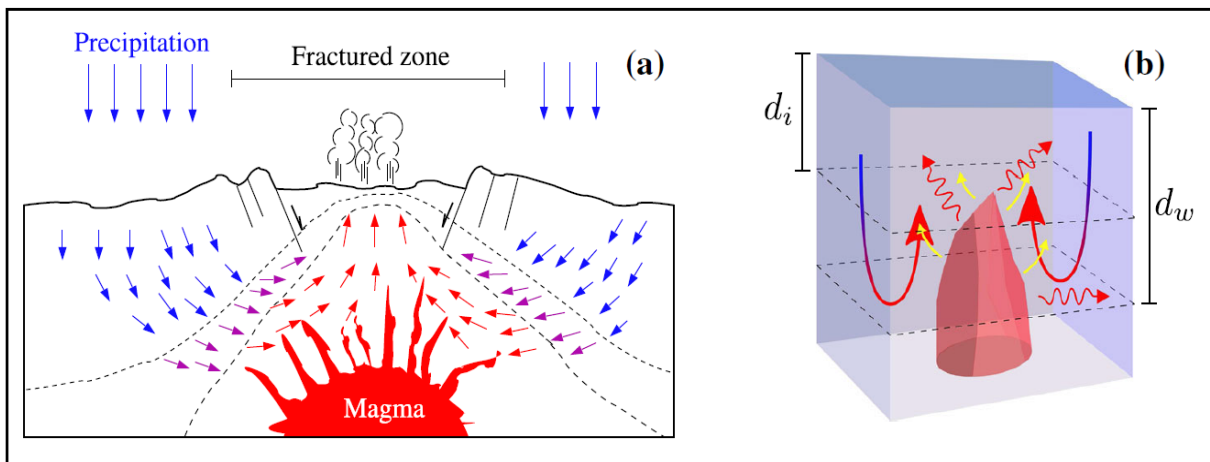


Figure 1. Origin of the geothermal system (a: the components required to form a geothermal system; b: the depth range and heat transfer. d_i (source depth) and d_w (water cycle depth range)) [13]

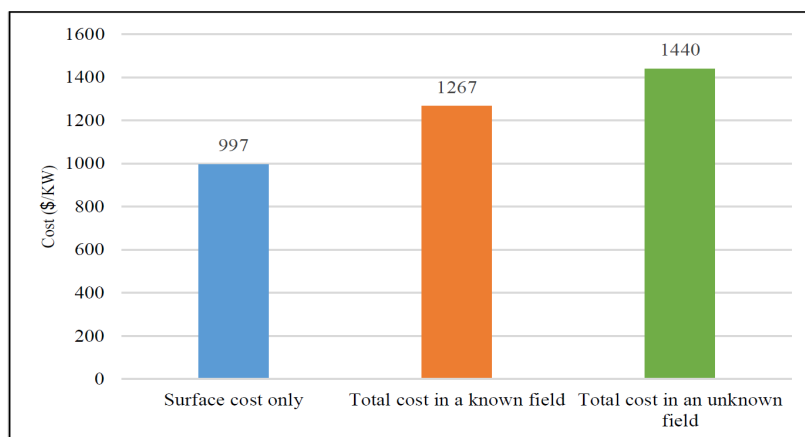


Figure 2. Surface and subsurface costs for five geothermal power plants installed in Iceland [17]

Table 1 also shows the total cost of exploration for the geothermal power plant. This cost varies from one to ten million US dollars.

Table 1. The total cost of exploration for two geothermal power plants with different capacities

Type of cost	Size of power plant (MWs)	Cost	Reference
Total cost	5	1×10^6 €	[18]
	50	9×10^6 \$	[19]

The second phase of building a geothermal power plant is drilling several wells to obtain energy stored underground to generate electricity. At this stage, the geothermal power plant infrastructure must be designed and built; in addition, the reinjection and production system and the power plant installation and connection to the power transmission network must be developed. These cases are the three primary parameters at this phase of development. The cost of the reinjection and production system at this stage is between 2.5 and 50 million US dollars depending on the size of the plant [20]. The temperature and chemistry of geothermal reservoirs are also effective in the cost of designing and building the infrastructure of each geothermal power plant [21]. The geothermal reservoir temperature determines the size and price of the geothermal power plant components. Temperature also determines the type of power plant. For reservoirs with a

temperature of less than 176.6 °C, a binary power plant, and a geothermal reservoir with a temperature higher than the mentioned one, a single flash power plant will be economical. In this regard, it is necessary to install high-quality materials and apply corrosion resistance, which increases the cost of infrastructure [22]. In geothermal power plants, the mass flow rate and the temperature of the reinjected water decrease over time. This reduction affects the performance of the power plant and economic profitability, which should be considered in its better design and more accurate economic analysis. Also, the ambient temperature of the power plant is constantly changing, which affects the performance of the power plant. It is better to take these changes into account in the design of the power plant.

2.2. Comparison of renewable energies

The International Renewable Energy Agency has compared the costs of different power generation technology with installed areas of different colors in Figure 3 [23]. For example, pale blue belongs to the continent of Asia, while dark blue belongs to the continent of Europe. On the horizontal axis, all types of renewable energy given; and on the vertical axis, their prices in 2016 in \$/kWh are provided. As can be seen, the cost of geothermal energy production technology is comparable to those of other renewable energy technologies, and even the equivalent energy cost of South America is lower than those of other renewables.

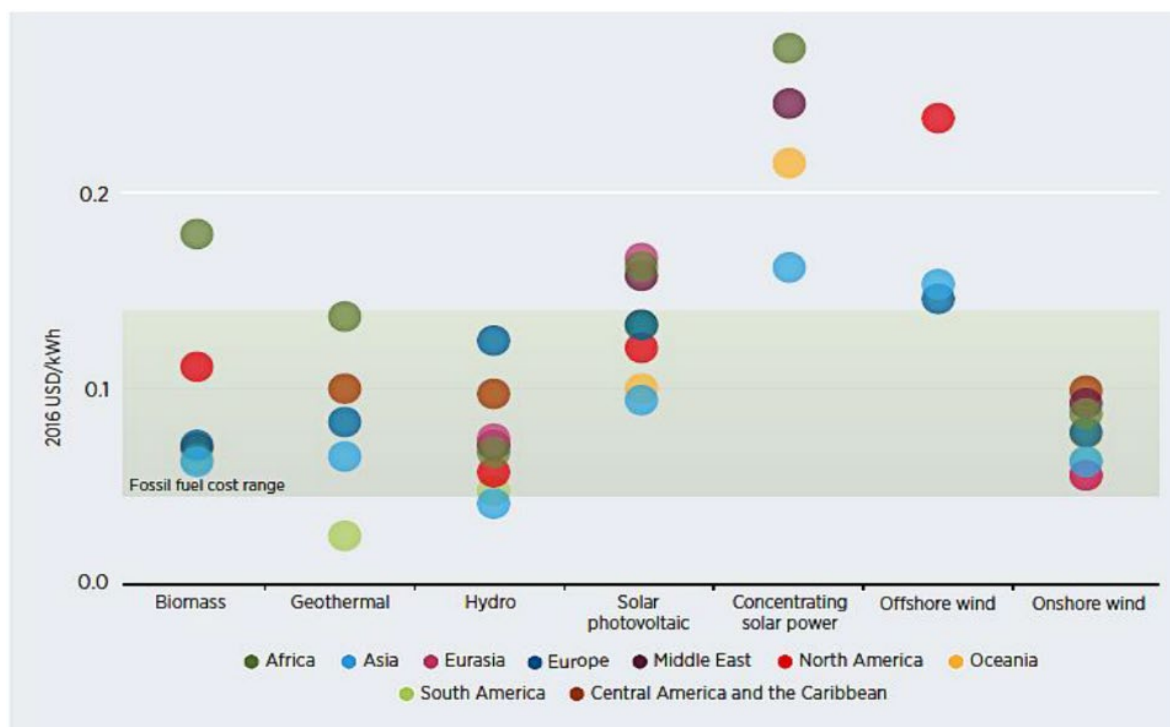


Figure 3. Average levelized costs of different power generation technologies with installed areas [24]

Table 2 shows the payback time and cost of different types of energy [25]. The cost per kilowatt-hour for geothermal energy is very close to the wind, and the costs of the two are higher than water, coal, and gas. However, these costs are significantly lower than photovoltaic (PV) solar power plants.

2.3. Hybrid power plants

Geothermal power plants emit minimal pollution compared to fossil fuels for the same amount of power. Nevertheless, this

energy suffers low extraction efficiency. Other energy sources can be combined with geothermal energy to improve its efficiency. This will help reduce operating and investment costs as well as shorten the payback period, thus shortening geothermal energy installations' payback period and tackling high-peak loads [26]. This can be achieved by creating optimal conditions in the composition for each resource. Geothermal energy is usually combined with solar energy. When solar energy provides 48 % of the total energy, system

performance is optimized to generate electricity. Considering the LCOE value of 225 \$ per MWh only for geothermal sources, this combination is reduced to 165 \$ per MWh [25]. Even though many research projects related to geothermal-hybrid systems focus on combining geothermal and solar technologies, there are also a large number of researches on systems using geothermal technology coupled with biomass, wind, biogas, and other technologies. Toselli et al. [27] combined biogas Waste Heat Recovery (WHR) with a geothermal power plant and designed a new hybrid binary plant. They considered the Oberhaching geothermal reservoir in Germany with a total electric power of 4.3 MWe. One of the main objectives of their research was the techno-economic assessment of this hybrid system compared to the conventional geothermal systems. In addition, financial results were provided for the power-only, and power and heat configurations were combined. The lowest LCOE value was equal to 15.42 €/kWh and was provided by the hybrid power-only model, while the highest LCOE value was equal to 19.13 €/kWh and was found in the geothermal CHP case study [27].

Table 2. Payback period and cost of different types of energy [25]

Type of power plant	Cost (\$/kWh)	Payback period (year)
PV	0.24	1-7.2
Wind	0.07	0.4-1.4
Hydro	0.05	11.8 (small), 0.5 (large)
Geothermal energy	0.07	5.7
Coal	0.04	3.18
Gas	0.05	7

2.4. Investment risk

Figure 4 shows an overview of the different phases of geothermal power plant development, project risk level changes, and the cumulative investment cost [28]. As can be seen, at the early stages of surface surveys and exploratory drilling, there is the most significant risk in a new geothermal project. There is considerable uncertainty in the early stages of power plant development regarding temperature and source flow capacity. After drilling and testing the source, this uncertainty is significantly reduced, which provides financial feasibility of investing at later stages of the development.

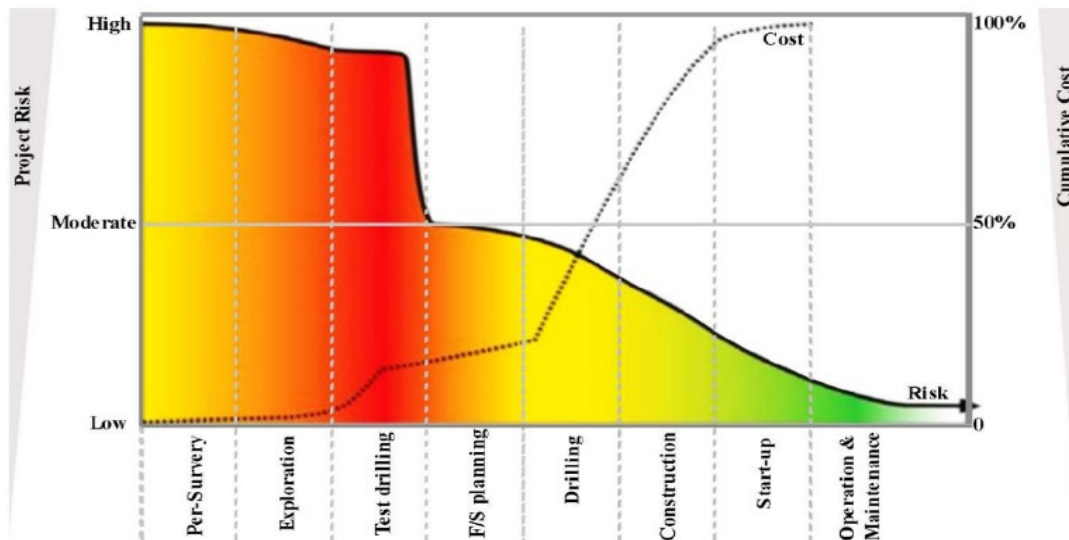


Figure 4. An overview of the different phases of geothermal power plant development and changes in the level of risk and investment cost [28]

3. POLICIES

Geothermal energy enhances a country's energy security, helps create direct, indirect, and induced employment, and affects other sectors of the economy. This energy can improve this security due to its independence from oil and gas, as oil and gas prices are constantly changing. Also, unlike wind and solar energies, it is not dependent on climate change; thus, it has higher reliability than other renewable energies. This reliability will also improve the energy security of countries. Adverse effects of the development of this energy include damage to local lands and grasslands, negative impact on tourist attractions in historical regions and national parks, and the decline of geysers and hot springs. Therefore, it is necessary to consider and manage all cases in implementing and constructing geothermal power plants.

Although geothermal technology has many advantages over other power generation technologies, only about 15 % of the known geothermal resources are currently exploited for electricity production. Two main obstacles that slow down the pace of geothermal development are (1) considerable up-front

capital investment required before earning money through electricity sales; (2) the high resource risk at the early steps of the multi-step geothermal project. A review of global experience shows that government support in this area contributes to the success of geothermal development. This section discusses some of the approaches and economic policies implemented in different countries to support geothermal development.

3.1. Program of loan guarantee

This policy guarantees the loan given by a third party and is referred to as the guarantor. In this case, if the borrower does not repay the loan on time, the guarantor will pledge to pay the debt. One such policy in the United States is the section 1705 loan program, which was initially financed by 6 billion dollars; however, after the reallocation, that amount was reduced to 2.5 billion dollars. In Germany, there is a program called "Risk of Non-Discovery of Deep Geothermal Energy", according to which, in case of exploration failures, a maximum of 100 % of the loan money is given [29].

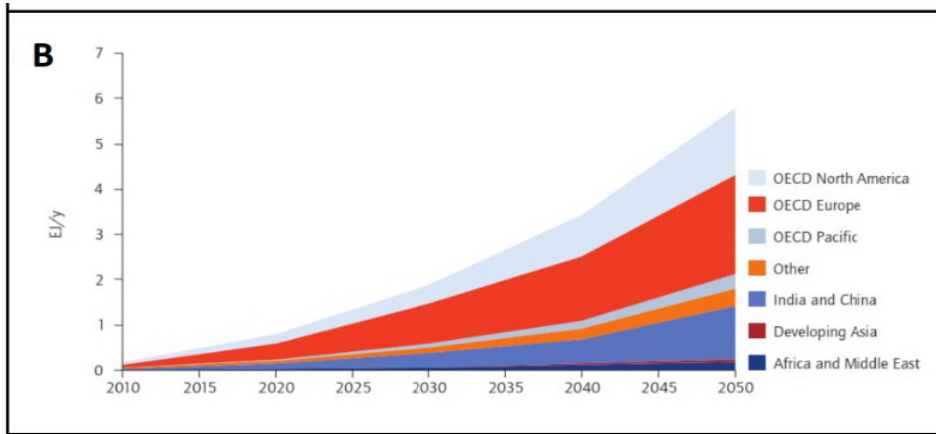


Figure 5. (A) IEA roadmap’s vision for geothermal power production until 2050; (B) Future of direct-use geothermal energy until 2050 [31]

In the following, the geothermal energy roadmap for some countries in continents of Europe and Asia is discussed.

4.1. Europe

A pilot study was concluded in 2010 for long-term scenarios and renewable energy development strategies in Germany (BMU 2010 [32]). One of the achievements of this study for the development of geothermal energy was the definition of a scenario for developing the installed geothermal capacity of nearly 300 megawatts by 2020 and 1 GW in 2030. The estimated geothermal heat will reach 8,000 GWh in 2020 (29 PJ) and will be approximately 25,000 GWh (89 PJ) by 2030 [32]. Figure 6 summarizes research and development efforts directed at exploiting geothermal resources for electricity production over ten years for Switzerland, in other words, a geothermal roadmap. Wide exploitation of geothermal energy

was achieved by solving two questions: (1) How can an efficient heat exchanger underground generate energy for decades? Moreover, (2) At the same time, is it acceptable to maintain the interference and the risks of earthquakes on the surface? While the public agrees with the possibility of controlling underground resources, these goals are endorsed. The answer to these questions as soon as possible creates three initiatives and innovations:

- (A) Advance the ability to model the stimulation process and reservoir operation quantitatively;
- (B) Advance process understanding and validation in underground lab experiments;
- (C) Perform a petrothermal P&D project, supported by a central scientific monitoring and assessment initiative [34].

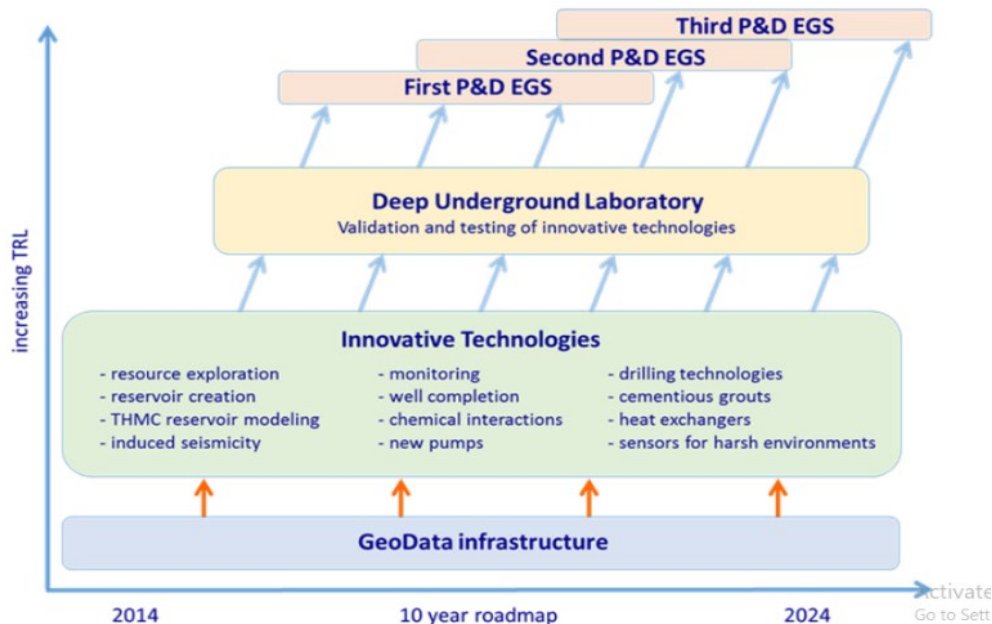


Figure 6. A geothermal roadmap for Switzerland over ten years [34]

A study published by Unione Geotermica Italiana (UGI) in December 2011 concluded that by limiting development to such systems, geothermal electricity of no more than 1,500 MWe and 9 TWh/yr will be obtained in Italy in 2030 (Figure 7); however, if the technology of Unconventional Geothermal Systems (UGS) becomes mature by 2025, it should rise to a maximum of 2000 MW and 12 TWh/yr by 2030 (Figure 8). In

such cases, UGS will contribute to the total geothermal energy of Italy in 2030 by more than 25 % [35, 36].

Recent studies by UGI on the possibility of geothermal energy growth in Italy up to the year 2050 have demonstrated that only by using hydrothermal systems in 1500 km² above high-temperature areas without the help of the UGS, the projected average increase for the future would disappear by

around 2030, after which it would begin to decrease gradually, resulting in a capacity of about 1,200 MW and producing about 7.5 TWh/yr by 2050. On the contrary, the UGS must be technically mature by 2025 and their commercial exploitation begins to generate electricity; they will primarily deal with the reduced production of hydrothermal systems and the production of a combination of hydrothermal systems plus

UGS to by 2050, about 3000 MWe and 18 Wh/yr. Of this total, ~ 1800 MWe and ~ 10.5 TWh/yr belong to UGS only. That is the reason why the long-term increase in geothermal energy in Italy depends mainly on the technical-economic feasibility of exploiting geothermal systems other than traditional hydrothermal systems [35].

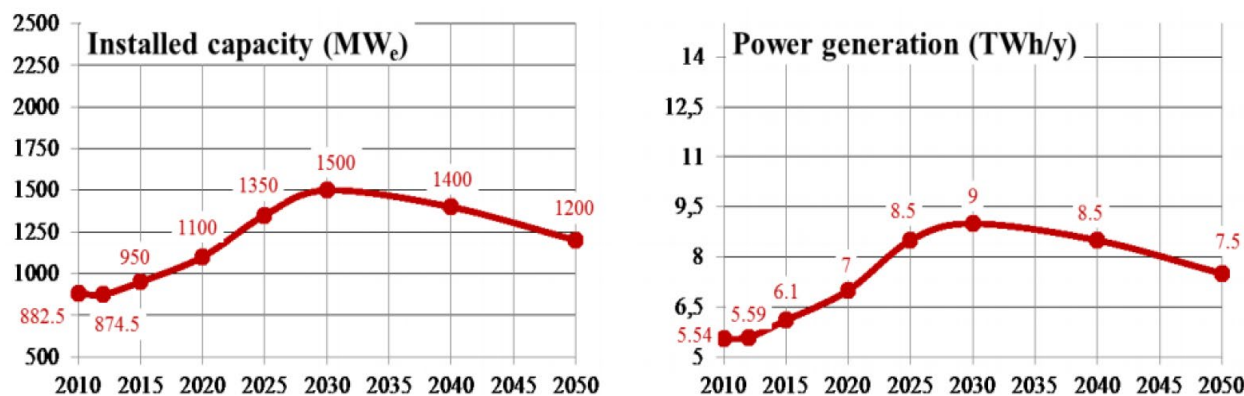


Figure 7. (A), (B). Development of installable capacity and producible energy until 2050 by harnessing hydrothermal systems only according to the best possible growth scenario in Italy [35]

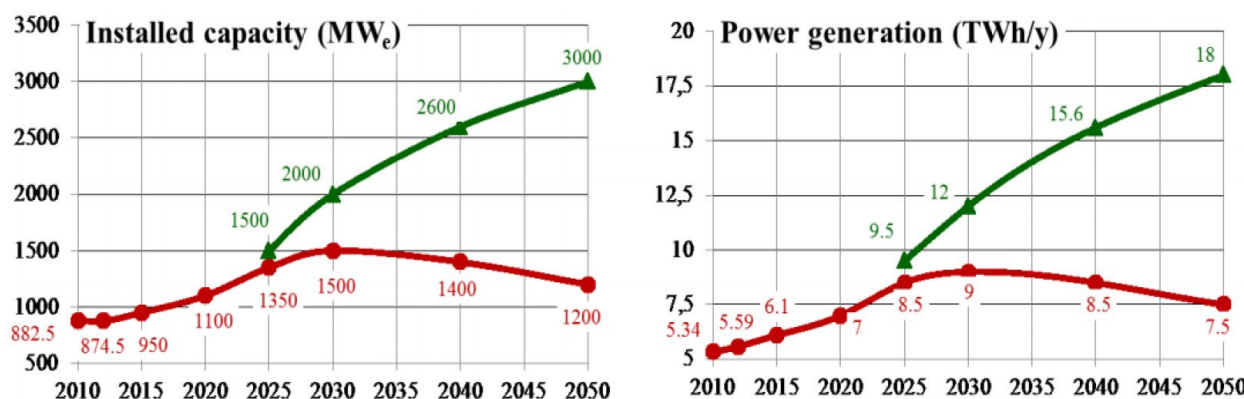


Figure 8. (A), (B). Development of installable capacity and producible energy until 2050 by harnessing hydrothermal systems according to the best possible scenario, jointly with one or more UGS/Unconventional Geothermal systems [35]

The trends in the geothermal market (electricity generation and heating) in 2010-2020 are shown in Table 3 for the European continent. This information is provided by the

Member States at the NREAP. The latest update (data for 2015 and 2014) is provided by European Coal and Steel Community (EGEC) [37].

Table 3. 2010-2020 Trends in geothermal power installed capacity (GPIC) (MWe), geothermal heat production (GHP) (ktoe), and geothermal heat pumps (G-HP) (ktoe) in the EU. Countries not reported in the figure have not reported [38]

Country	Item			Year	Item					
	Year	GPIC	GHP		Year	GPIC	GHP			
France	2010	26.5	2010	98.2	271.1	United Kingdom	2010	N.A.	0.8	21.7
	2017	17.1	2014	125.7	261.6		2014	N.A.	0.8	56.6
	2020	80	2020	500	570		2020	N.A.	0	95.3
Spain	2010	0	2010	16	N.A.	Bulgaria	2010	N.A.	32.7	N.A.
	2017	0	2014	18.8	16.4		2014	N.A.	33.4	N.A.
	2020	50	2020	9.5	40.5		2020	N.A.	9	N.A.
Germany	2010	10	2010	51.7	246.2	Romania	2010	N.A.	21.1	N.A.
	2017	38.19	2014	91	334		2014	N.A.	25.1	N.A.
	2020	298	2020	686	521		2020	N.A.	80	8
Italy	2010	754	2010	139.3	44.2	Poland	2010	N.A.	13.4	3.1
	2017	915.5	2014	129.6	70.18		2014	N.A.	20.2	8.4
	2020	920	2020	300	522		2020	N.A.	178	N.A.

Austria	2010	1	2010	20.5	N.A.	Sweden	2010	N.A.	N.A.	N.A.
	2017	1.2	2014	19.4	N.A.		2014	N.A.	N.A.	8.03.3
	2020	1	2020	40	26		2020	N.A.	N.A.	815
Greece	2010	0	2010	16	N.A.	Finland	2010	N.A.	N.A.	N.A.
	2017	0	2014	11.7	N.A.		2014	N.A.	N.A.	133.8
	2020	120	2020	51	50		2020	N.A.	N.A.	N.A.
Croatia	2010	N.A.	2010	6.8	N.A.	Ireland	2010	0	N.A.	N.A.
	2017	N.A.	2014	10.7	N.A.		2017	0	N.A.	N.A.
	2020	10	2020	15.7	N.A.		2020	5	N.A.	N.A.

4.2. Asia

The distribution of low-temperature geothermal resources in China is more than other sources. Therefore, it is essential that energy be generated at a low cost and on a large scale. In the five-year Chinese geothermal plan, a significant progress has been made in low-temperature geothermal technology. The

next step, which is vital to this five-year program, is improving system performance and expansion. In addition, the cost of construction and operations is reduced [39]. The geothermal energy roadmap for the 15 years in China is depicted in Figure 9.

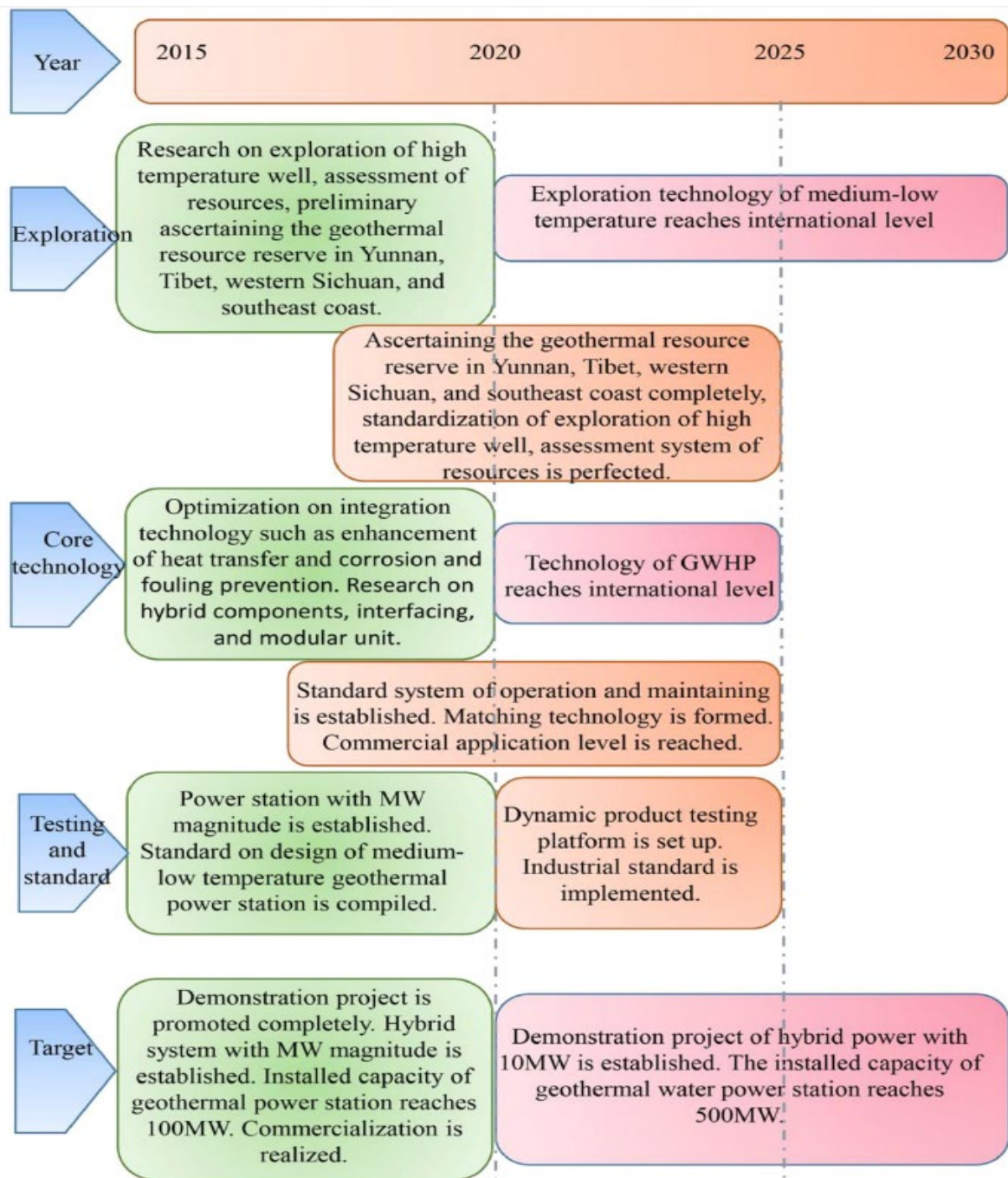


Figure 9. Geothermal power generation roadmap in China [39]

In Iran, since 1995, several promising areas (Figure 10) have been identified by SUNA (Center for Renewable Energy Research and Application) throughout the country [40, 41]. The country's national electricity grid is close to 85 GW, of which about 95 % is due to the burning of fossil fuels. Given this level, it will not be easy to achieve a significant share of

the country's total energy production by geothermal energy. The Iranian government welcomes the development of renewable energy and geothermal resources to offset the solid economic dependence on the export of fossil fuels. Given that geothermal resources can be adjusted and developed, they can play an essential role in the future of Iranian energy.

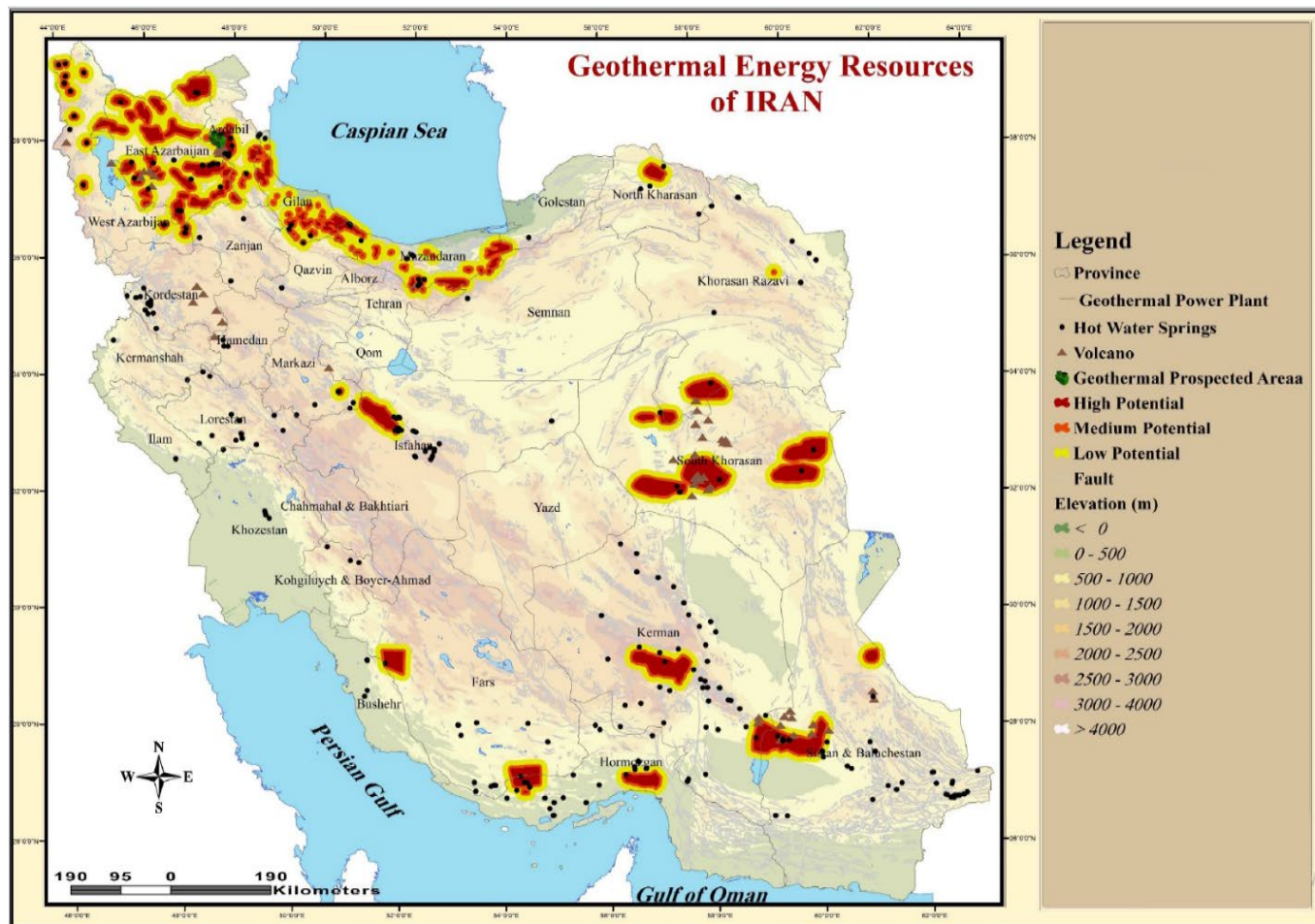


Figure 10. Map of the geothermal prospected area in Iran [55]

According to the above description, due to the geological conditions and the presence of many potentialities of geothermal energy, the lack of high-tech equipment inhibits the growth of this energy source. The association studies in northwestern Iran point to the ability of Meshkinshahr to install a geothermal power plant. The main objective of the project is the discovery and construction of a 55 MW geothermal power plant, which is expected to be operational in the coming years and will produce 410 GW by using high technology [42-50]. The latest information shows that the construction of the first pilot plant is now running with a capacity of 5 MWe, the produced fluid temperature of 86 °C, and a maximum flow rate of 58 l/s (average flow rate: 46 L/s) in the NW Sabalan Site [51-54].

The active subsidy program and special mandatory law in Korea allow geothermal applications and GHP utilization to increase to over 100 megawatts a year in the next few years [56]. Geothermal power generation is expected to increase by EGS over five years. The active participation of industries and commercialization is on the rise. However, it is currently under the influence of the lack of a legal framework to support the production of geothermal power. The regulatory framework of the Renewable Portfolio Standard (RPS) with Renewable Energy Certificates (RECs) monitors geothermal

activities. A technical solution to reducing GHGs in Korea will produce 200 megawatts of geothermal capacity by 2030, one percent of the technical capacity [57]. The result of the EGS project, if successful, is a milestone to building a roadmap which is expected to increase from 5 to 10 MW over the next few years. 2000 MW is the estimated geothermal resource potential of Japan. Currently, the total power generation is 500 MW. Experts have provided a roadmap for various ways to overcome the barriers to geothermal energy development [58]. Technologies expected to reach over 1,000 MW of geothermal power in Japan by 2050 include commercialization of magma power generation and hot dry rock (HDR) power generation. It is necessary to increase the number of researchers for enhancing electricity production. Technical development and road mapping can help secure geothermal energy and prevent accidents (Figure 11) [58].

The MEMR (Ministry of Energy and Mineral Resources, 2012) of Indonesia has established a geothermal development roadmap from 2006 to 2025. Its goal is to develop 9,500 MW in total by 2025. The government has issued EMR No. 21/2013 administrative regulations as an incentive for the development of geothermal energy based on geothermal power plants projects [59].

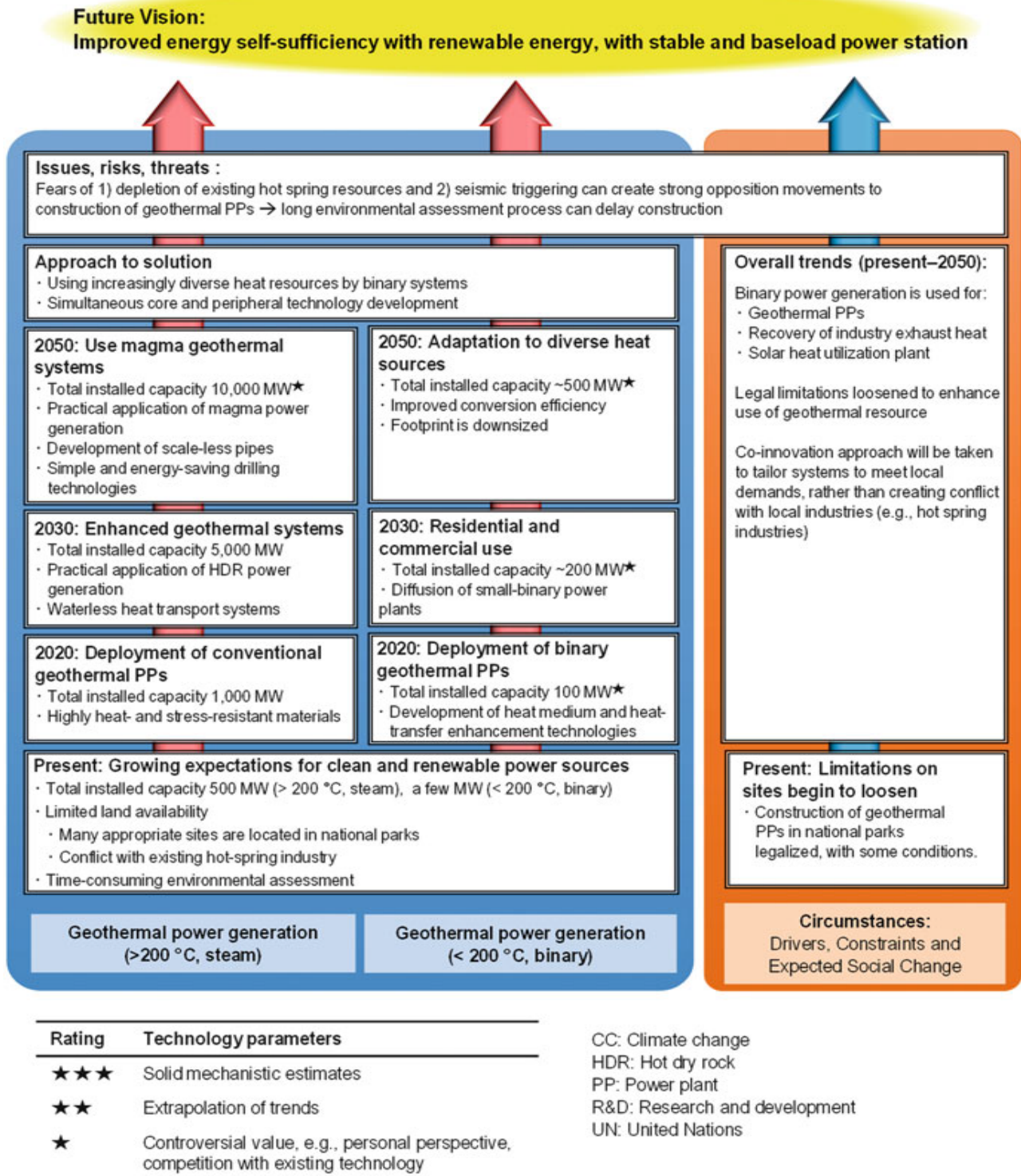


Figure 11. Technical development and road mapping for geothermal energy in Japan [58]

5. CONCLUSIONS AND FUTURE RECOMMENDATION

Various studies related to the economic analysis of geothermal systems were reviewed in this study. Geothermal power plant construction consists of several phases, each with different costs. The highest cost is related to the well drilling operation phase, while the lowest is related to the prospecting and exploration phases. There are two main barriers for slowing the development of the geothermal resources: 1. significant pre-earnings investment; 2. high resource risk at the early stages of a geothermal project. While the environmental damage caused by fossil fuels has not been accounted for, geothermal and other renewables such as bioenergy, onshore

wind, and hydroelectric power are able to compete with fossil fuels. Furthermore, geothermal energy has a more extended payback period than wind, PV, hydro (large), and coal. Geothermal energy projects have positive and negative effects. They can positively affect energy security as well as direct, indirect, and induced employment. They can also have adverse effects by altering local lands used for grazing or hunting, damaging local historical areas or national parks, and destroying natural features such as hot springs and geysers. Considerable up-front capital investment, high drilling costs, and high resource risk are the main obstacles that slow down the pace of geothermal development.

By providing incentive policies to investors and researchers in this field, the development of geothermal resources can be promoted. Some of the most crucial incentive policies that currently exist in some countries and international forums include "Loan Guarantee Program", "Drilling Operations Insurance", "Loan Support Mechanisms", "Grant", and "Exploration under government supervision". It seems that by presenting other encouraging and profound policies in this field, it is possible to help attract investment in the operation of geothermal systems. A roadmap is an essential tool for the development and maintenance of research activities. Also, it is an ideal, integrated, and beneficial mechanism for geothermal resources. The roadmap is usually used by DOE technology agencies to create investment, research, and development strategies. In this study, the roadmaps of several countries from Europe and Asia, including Switzerland, Italy, China, and Japan, were presented schematically, and an overview of the geothermal potentials of several countries from these two continents was presented. Along with proper management, it is necessary to prepare a proper roadmap to illuminate the future of geothermal energy so that appropriate decisions can be made. The roadmap provides a strategy for advancing geothermal systems and sets goals for optimizing energy with the technical advancement required. The development of geothermal energy with current technologies shows that technological advances are associated with improving the economic sector of the geothermal project and reducing risk. Consideration of cost reduction, technical development of geothermal projects, and sustainable production of geothermal reservoirs are all essential to achieving sustainable development in geothermal energy. Exploring geothermal resources, global investment, and feasibility of projects depends on technology development in the next few years. Using the suggestions of other researchers active in this field and investing in Research and Development (R&D) in the next few years can pave the way for the development and progress of geothermal projects. Geothermal energy technology is expected to be economically competitive with other energy sources by 2050.

6. ACKNOWLEDGEMENT

The authors thank the Renewable Energy and Energy Efficiency Organization (SATBA) of Iran for providing up-to-date information on the country's geothermal potential.

REFERENCES

- Wang, H., "International Energy Agency, World Energy Outlook (IEA WEO) Peer review panel global energy & petrochemical investment cost reviews commentaries to the IEA WEO Team in IEA HQ in January 2014", IEA HQ, Paris, France, (2014). (<https://www.iea.org/reports/world-energy-outlook-2021>).
- Haghighi, A., Pakatchian, M.R., Assad, M.E.H., Duy, V.N. and Alhuyi Nazari, M., "A review on geothermal Organic Rankine cycles: Modeling and optimization", *Journal of Thermal Analysis and Calorimetry*, Vol. 144, No. 5, (2021), 1799-1814. (<https://doi.org/10.1007/s10973-020-10357-y>).
- Johansson, T.B. and Goldemberg, J., "Energy for sustainable development: A policy agenda", United Nations Publications, (2002), 219. (http://content-ext.undp.org/aplaws_publications/2101911/Energy%20for%20Sustainable%20Development-PolicyAgenda_2002.pdf).
- Wolf, C., Klein, D., Richter, K. and Weber-Blaschke, G., "Environmental effects of shifts in a regional heating mix through variations in the utilization of solid biofuels", *Journal of Environmental Management*, Vol. 177, (2016), 177-191. (<https://doi.org/10.1016/j.jenvman.2016.04.019>).
- Günther, M. and Hellmann, T., "International environmental agreements for local and global pollution", *Journal of Environmental Economics and Management*, Vol. 81, (2017), 38-58. (<https://doi.org/10.1016/j.jeem.2016.09.001>).
- Soltani, M., Kashkooli, F.M., Dehghani-Saniji, A., Kazemi, A., Bordbar, N., Farshchi, M., Elmi, M., Gharali, K. and Dusseault, M.B., "A comprehensive study of geothermal heating and cooling systems", *Sustainable Cities and Society*, Vol. 44, (2019), 793-818. (<https://doi.org/10.1016/j.scs.2018.09.036>).
- Pan, S.-Y., Gao, M., Shah, K.J., Zheng, J., Pei, S.L. and Chiang, P.C., "Establishment of enhanced geothermal energy utilization plans: Barriers and strategies", *Renewable Energy*, Vol. 132, (2019), 19-32. (<https://doi.org/10.1016/j.renene.2018.07.126>).
- El Haj Assad, M., Aryanfar, Y., Javaherian, A., Khosravi, A., Aghaei, K., Hosseinzadeh, S., Pabon, J. and Mahmoudi, S.M.S., "Energy, exergy, economic and exergoenvironmental analyses of transcritical CO₂ cycle powered by single flash geothermal power plant", *International Journal of Low-Carbon Technologies*, Vol. 16, No. 4, (2021), 1504-1518. (<https://doi.org/10.1093/ijlct/ctab076>).
- Khosravi, A., Syri, S., Zhao, X. and El Haj Assad, M., "An artificial intelligence approach for thermodynamic modeling of geothermal based-organic Rankine cycle equipped with solar system", *Geothermics*, Vol. 80, (2019), 138-154. (<https://doi.org/10.1016/j.geothermics.2019.03.003>).
- El Haj Assad, M., Ahmadi, M.H., Sadeghzadeh, M., Yassin, A. and Issakhov, A., "Renewable hybrid energy systems using geothermal energy: Hybrid solar thermal-geothermal power plant", *International Journal of Low-Carbon Technologies*, Vol. 16, No. 2, (2021), 518-530. (<https://doi.org/10.1093/ijlct/ctaa084>).
- El Haj Assad, M., Aryanfar, Y., Radman, S., Yousef, B. and Pakatchian, M., "Energy and exergy analyses of single flash geothermal power plant at optimum separator temperature", *International Journal of Low Carbon Technology*, (2021). (<https://doi.org/10.1093/ijlct/ctab014>).
- El Haj Assad, M., Sadeghzadeh, M., Ahmadi, M.H., Al-Shabi, M., Albawab, M., Anvari-Moghaddam, A. and Bani Hani, E., "Space cooling using geothermal single-effect water/lithium bromide absorption chiller", *Energy Science & Engineering*, Vol. 9, No. 10, (2021), 1747-1760. (<https://doi.org/10.1002/ese3.946>).
- Gunnarsson, G. and Aradottir, E.S.P., "The deep roots of geothermal systems in volcanic areas: Boundary conditions and heat sources in reservoir modeling", *Journal Transport in Porous Media*, Vol. 108, (2015), 43-59. (<https://doi.org/10.1007/s11242-014-0328-1>).
- Anderson, A. and Rezaie B., "Geothermal technology: Trends and potential role in a sustainable future", *Applied Energy*, Vol. 248, (2019), 18-34. (<https://doi.org/10.1016/j.apenergy.2019.04.102>).
- Dowling, A.W., Zheng, T. and Zavala, V.M., "Economic assessment of concentrated solar power technologies: A review", *Renewable and Sustainable Energy Reviewers*, Vol. 72, No. 10, (2017), 19-32. (<https://doi.org/10.1016/j.rser.2017.01.006>).
- Sheu, E.J., Mitsos, A., Eter, A.A., Mokheimer, E.M.A., Habib, M.A. and Al-Qutub, A., "A review of hybrid solar-fossil fuel power generation systems and performance metrics", *Journal of Solar Energy Engineering*, Vol. 134, No. 4, (2012). (<https://doi.org/10.1115/1.4006973>).
- Stefansson, V., "Investment cost for geothermal power plants", *Geothermics*, Vol. 31, (2002), 263-272. ([https://doi.org/10.1016/S0375-6505\(01\)00018-9](https://doi.org/10.1016/S0375-6505(01)00018-9)).
- Goh, Y.M.F., Kong, H.L. and Wang, C.H., "Simulation of the delivery of doxorubicin to hepatoma", *Pharmaceutical Research*, Vol. 18, (2001), 761-770. (<https://doi.org/10.1023/A:1011076110317>).
- Williamson, J.I., "The future of US geothermal development: Alternative energy or green pipe dream", *Texas Journal of Oil, Gas, and Energy Law*, Vol. 7, No. 1, (2011). (<https://heinonline.org/HOL/LandingPage?handle=hein.journals/texjoge17&div=4&id=&page=>).
- Lukawski, M.Z., Anderson, B.J., Augustine, C., Capuano Jr., L.E., Beckers, K.F., Livesay, B. and Tester, J.W., "Cost analysis of oil, gas, and geothermal well drilling", *Journal of Petroleum Science and Engineering*, Vol. 118, (2014), 1-14. (<https://doi.org/10.1016/j.petrol.2014.03.012>).
- Yost, K., Valentin, A. and Einstein, H.H., "Estimating cost and time of wellbore drilling for Engineered Geothermal Systems (EGS)-Considering uncertainties", *Geothermics*, Vol. 53, (2015), 85-99. (<https://doi.org/10.1016/j.geothermics.2014.04.005>).

22. Hance, C.N., "Factors affecting costs of geothermal power development", Geothermal Energy Association, Department of Energy, USA, (2005). (http://repository.stategeothermaldata.org/metadata/record/98ddf901b9782a25982e01af3b08c9ce/file/cost_of_geothermal_power_and_factors_that_affect_it_-_by_subir_sanyal_sgw_2004.pdf).
23. IRENA | International Renewable Energy Agency, "Renewable power generation costs in 2017", (2017). (<https://www.irena.org/publications/2018/jan/renewable-power-generation-costs-in-2017>).
24. Li, K., Bian, H., Liu, C., Zhang, D. and Yang, Y., "Comparison of geothermal with solar and wind power generation systems", *Renewable and Sustainable Energy Reviews*, Vol. 42, (2015), 1464-1474. (<https://doi.org/10.1016/j.rser.2014.10.049>).
25. Zhou, C., Doroodchi, E. and Moghtaderi, B., "An in-depth assessment of hybrid solar-geothermal power generation", *Energy Conversion and Management*, Vol. 74, (2013), 88-101. (<https://doi.org/10.1016/j.enconman.2013.05.014>).
26. Alaica, A.A. and Dworkin, S.B., "Characterizing the effect of an off-peak ground pre-cool control 1507 strategy on hybrid ground source heat pump systems", *Energy and Buildings*, Vol. 137, (2017), 46-59. (<https://doi.org/10.1016/j.enbuild.2016.12.003>).
27. Toselli, D., Heberle, F. and Brüggemann, D., "Techno-economic analysis of hybrid binary cycles with geothermal energy and biogas waste heat recovery", *Energies*, Vol. 12, (2019), 19-69. (<https://doi.org/10.3390/en12101969>).
28. Gehringer, M. and Loksha, V., "Geothermal handbook: Planning and financing power generation, A pre-launch", (2012). ([https://www.esmap.org/sites/esmap.org/files/Loksha_Gehringer_Geothermal%20Training%20July%202012%20\(Day1\)_0.pdf](https://www.esmap.org/sites/esmap.org/files/Loksha_Gehringer_Geothermal%20Training%20July%202012%20(Day1)_0.pdf)).
29. Speer, B., Economy, R., Lowder, T., Schwabe, P. and Regenthal, S., "Geothermal exploration policy mechanisms: Lessons for the United States from international applications", National Renewable Energy Laboratory (NREL), United States, (2014). (<https://www.osti.gov/biblio/1134132>).
30. Ziagos, J., Phillips, B.R., Boyd, L., Jelacic, A., Stillman, G. and Hass, E., "A technology roadmap for strategic development of enhanced geothermal systems", *Proceedings of the 38th Workshop on Geothermal Reservoir Engineering*, Stanford, CA, Citeseer, (2013), 11-13. (<http://citeseerx.ist.psu.edu/viewdoc/download?doi=10.1.1.296.822&rep=rep1&type=pdf>).
31. Beerepoot, M., "Technology roadmap: Geothermal heat and power", Renewable Energy Division, International Energy Agency, OECD/IEA, Paris, (2011), (https://iea.blob.core.windows.net/assets/f108d75f-302d-42ca-9542-458eea569f5d/Geothermal_Roadmap.pdf).
32. Nitsch, J., Pregger, T., Naegler, T., Heide, D., de Tena, D.L., Trieb, F., Scholz, Y., Nienhaus, K., Gerhardt, N. and Sterner, M., "Langfristszenarien und strategien für den ausbau der erneuerbaren energien in Deutschland bei berücksichtigung der entwicklung in Europa und global", Schlussbericht im Auftragdes BMU, bearbeitet von DLR (Stuttgart), Fraunhofer IWES (Kassel) und IFNE (Teltow), (2012), 345. (<https://elib.dlr.de/76043/>).
33. Agemar, T., Weber, J. and Schulz, R., "Deep geothermal energy production in Germany", *Energies*, Vol. 7, (2014), 4397-4416. (<https://doi.org/10.3390/en7074397>).
34. Evans, K., Wieland, U., Wiemer, S. and Giardini, D., "Deep Geothermal Energy R&D Roadmap for Switzerland, 2014", *Economic Modelling*, Vol. 16, No. 7, (2014). (http://sccer-soe-cms.ethz.ch/export/sites/sccer-soe/aboutus/galleries/dwn_roadmaps/DG_E_Roadmap_2014_Complete.pdf).
35. Cataldi, R., Grassi, W. and Passaleva, G., "Outlook on geothermal Ppower development in Italy by 2050: Up or down?", (2015). (https://scholar.google.com/citations?view_op=view_citation&hl=en&user=W6oIZSIAAAAJ&cstart=100&pagesize=100&sortby=pubdate&citation_for_view=W6oIZSIAAAAJ:YGhAHpnlhDoC).
36. Manzella, A., Donato, A., Gola, G., Santilano, A. and Trumpy, E., "The Italian challenge for geothermal energy", *Perspectives for Geothermal Energy in Europe*, *World Scientific*, (2017), 127-155. (https://doi.org/10.1142/9781786342324_0005).
37. Dumas, P., "Policy and regulatory aspects of geothermal energy: A European perspective", Manzella, A., Allansdottir, A. and Pellizzone, A. (eds.), *Geothermal energy and society, Lecture notes in energy*, Vol 67., Springer, (2019), 19-37. (https://doi.org/10.1007/978-3-319-78286-7_2).
38. Manzella, A., Allansdottir, A. and Pellizzone, A., *Geothermal energy and society, Lecture notes in energy*, Vol 67., Springer, (2019). (<https://link.springer.com/book/10.1007/978-3-319-78286-7?noAccess=true>).
39. Zhu, J., Hu, K., Lu, X., Huang, X., Liu, K. and Wu, X., "A review of geothermal energy resources, development, and applications in China: Current status and prospects", *Energy*, Vol. 93, (2015), 466-483. (<https://doi.org/10.1016/j.energy.2015.08.098>).
40. Nouraliee, J., Satkin, M., Bina, F.A., Ebrahimi, D. and Sheikholeslami, F., "Introducing the second version (2020) of geothermal potential map of Iran", *Proceedings of World Geothermal Congress*, (2020). (https://www.researchgate.net/profile/Javad-Nouraliee/publication/355792601_Introducing_the_Second_Version_2020_of_Geothermal_Potential_Map_of_Iran/links/617e9e4eeef53e1e10ddd61/Introducing-the-Second-Version-2020-of-Geothermal-Potential-Map-of-Iran.pdf).
41. Nouraliee, J., Ebrahimi, D., Dashti, A., Korzani, M.G. and Sangin, S., "Appraising Mahallat geothermal region using thermal surveying data accompanied by the geological, geochemical and gravity analyses", *Scientific Reports*, Vol. 11, No. 1, (2021), 1-14. (<https://doi.org/10.1038/s41598-021-90866-4>).
42. Noorollahi, Y., Shabbir, M.S., Siddiqi, A.F., Ilyashenko, L.K. and Ahmadi, E., "Review of two decade geothermal energy development in Iran, benefits, challenges, and future policy", *Geothermics*, Vol. 77, (2019), 257-266. (<https://doi.org/10.1016/j.geothermics.2018.10.004>).
43. Behnam, S. and Khalajmasoumi, M., "A futuristic review for evaluation of geothermal potentials using fuzzy logic and binary index overlay in GIS environment", *Renewable and Sustainable Energy Reviews*, Vol. 43, (2015), 818-831. (<http://dx.doi.org/10.1016/j.rser.2014.11.079>).
44. Noorollahi, Y., Fotouh, M. and Barnett, P., "Geothermal energy in Iran", *GRC Bulletin*, (2000). (<https://www.geothermal-energy.org/pdf/IGAstandard/WGC/2010/1613.pdf>).
45. Saffarzadeh, A. and Noorollahi, Y., "Geothermal development in Iran: A country update", *Proceedings of World Geothermal Congress*, (2005). (<https://www.geothermal-energy.org/pdf/IGAstandard/WGC/2005/0119.pdf>).
46. Yousefi, H., Ehara, S. and Noorollahi, Y., "Geothermal potential site selection using GIS in Iran", *Proceedings of the 32nd Workshop on Geothermal Reservoir Engineering*, Stanford University, Stanford, California, (2007), 174-182. (<https://pangea.stanford.edu/ERE/pdf/IGAstandard/SGW/2007/yousefi.pdf>).
47. Yousefi, H. and Ehara, S., "Geothermal power plant site selection using GIS in Sabalan area, NW Iran", Department of Earth Resources Engineering, Kyushu University, (2007), 819. (<https://citeseerx.ist.psu.edu/viewdoc/download?doi=10.1.1.507.9937&rep=rep1&type=pdf>).
48. Noorollahi, Y., Yousefi, H., Itoi, R. and Ehara, S., "Geothermal energy resources and development in Iran", *Renewable and Sustainable Energy Reviews*, Vol. 13, (2009), 1127-1132. (<https://doi.org/10.1016/j.rser.2008.05.004>).
49. Najafi, G. and Ghobadian, B., "Geothermal resources in Iran: The sustainable future", *Renewable and Sustainable Energy Reviews*, Vol. 15, (2011), 3946-3951. (<https://doi.org/10.1016/j.rser.2011.07.032>).
50. Tofigh, A.A. and Abedian, M., "Analysis of energy status in Iran for designing sustainable energy roadmap", *Renewable and Sustainable Energy Reviews*, Vol. 57, (2016), 1296-1306. (<https://doi.org/10.1016/j.rser.2015.12.209>).
51. Seyedrahimi-Niaraq, M., Ardejani, F.D., Noorollahi, Y. and Porkhial, S., "Development of an updated geothermal reservoir conceptual model for NW Sabalan geothermal field, Iran", *Geothermal Energy*, Vol. 5, No. 14, (2017), 1-22. (<https://doi.org/10.1186/s40517-017-0073-0>).
52. Seyedrahimi-Niaraq, M., Ardejani, F.D., Noorollahi, Y., Porkhial, S., Itoi, R. and Nasrabadi, S.J., "A three-dimensional numerical model to simulate Iranian NW Sabalan geothermal system", *Geothermics*, Vol. 77, (2019), 42-61. (<https://doi.org/10.1016/j.geothermics.2018.08.009>).
53. Seyedrahimi-Niaraq, M., Ardejani, F.D., Noorollahi, Y., Nasrabadi, S.J. and Hekmatnejad, A., "An unsaturated three-dimensional model of fluid flow and heat transfer in NW Sabalan geothermal reservoir", *Geothermics*, Vol. 77, (2021), 1-19. (<https://doi.org/10.1016/j.geothermics.2020.101966>).
54. Seyedrahimi-Niaraq, M., Bina, S.M. and Itoi, R., "Numerical and thermodynamic modeling for estimating production capacity of NW

- Sabalan geothermal field, Iran", *Geothermics*, Vol. 90, (2021), 1-21. (<https://doi.org/10.1016/j.geothermics.2020.101981>).
55. SATBA | Renewable Energy and Energy Efficiency Organization, Renewable Energy in Iran, (2018), (Retrieved: 15 May 2018). (<http://www.satba.gov.ir/en/home>).
56. Song, Y. and Lee, T.J., "Geothermal development in the Republic of Korea: Country update 2010-2014", *Proceedings of World Geothermal Congress*, (2015), 19-25. (<https://www.semanticscholar.org/paper/Geothermal-Development-in-the-Republic-of-Korea%3A-Song-Lee/8e944daa001d394234765461d4f54df76f0a6696>).
57. KETEP | Korea Institute of Energy Technology Evaluation and Planning, Strategic roadmap for greenhouse gas reduction technology – Geothermal, Ministry of Knowledge Economy, (in Korean), (2017). (<https://www.wikidata.org/wiki/Q30297392>).
58. Kato, Y., Koyama, M., Fukushima, Y. and Nakagaki, T., Energy technology roadmaps of Japan, (2016). (<https://link.springer.com/book/10.1007/978-4-431-55951-1?noAccess=true>).
59. Pambudi, N.A., "Geothermal power generation in Indonesia, a country within the ring of fire: Current status, future development and policy", *Renewable and Sustainable Energy Reviews*, Vol. 81, (2018), 2893-2901. (<https://doi.org/10.1016/j.rser.2017.06.096>).



Research Note

Optimum Orientation of the Multi-Span Greenhouse for Maximum Capture of Solar Energy in Central Region of Iran

Mehran Gheyrati, Asadollah Akram, Hassan Ghasemi-Mobtaker*

Department of Agricultural Machinery Engineering, Faculty of Agricultural Engineering and Technology, University of Tehran, Karaj, Alborz, Iran.

PAPER INFO

Paper history:

Received: 22 September 2021
 Revised in revised form: 16 February 2022
 Scientific Accepted: 16 February 2022
 Published: 02 July 2022

Keywords:

Greenhouse Orientation,
 Mathematical Modeling,
 North Wall,
 Solar Irradiation

ABSTRACT

The orientation of greenhouses is one of the effective factors in terms of radiation they receive. In the present study, a multi-span greenhouse (40 m × 93.5 m with a coverage area of 5457.44 m²) located in the central region of Iran was investigated in three orientations including: North-South (N-S), East-West (E-W), and Northeast-Southwest (NE-SW: the most frequent orientation of the existing greenhouses in the study area). The solar irradiation received on the outside surface of the greenhouse cover and the amount of irradiation captured inside the greenhouse for each orientation during the cold season were calculated using mathematical modeling and the results were compared. According to the results, in the E-W orientation, the main sections of receiving solar irradiation, such as the south and north roofs, have a better angle toward the sun; therefore, the quantity of solar irradiation captured inside the greenhouse with the E-W orientation was on average 361.48 MJ day⁻¹ more than that with the N-S orientation. The north wall of the greenhouse could not receive the beam radiation for all the orientations investigated, and the total irradiation captured by this section was composed of the diffused radiation and the ground-reflected radiation, which is an important result for insulation of some surfaces of greenhouses.

<https://doi.org/10.30501/jree.2022.305780.1259>

1. INTRODUCTION

Achieving food security and reducing environmental pressures require convergence towards healthy and adequate diets. Such a convergence would require increasing the quantity and quality of food supply for many areas [1]. However, 30 % of the world's food is lost due to transportation because of the distance of food production centers from consumers. Controlled Environment Agriculture (CEA), including greenhouse crop production, enables the production of crops outside the climate and their seasons. Prolonging of seasonal crops cultivation periods allows for agricultural crops to be produced beside consumption locations which, in turn, decrease transportation distances [2]. Greenhouse cultivation is one of the main and popular methods to meet the growing need for food universal because compared with field cultivation, it has a so great production [3]. Greenhouse is a structure that provides a suitable environment for plants' production, especially in cold weather.

Due to Iran's locations in arid and semi-arid climates, the development of greenhouses is one of the main programs of the agricultural sector. In recent years, the development of greenhouses in Iran has been seriously pursued and the covered area by the greenhouses has increased from 8,000 ha

to 18,500 ha [4]. Yazd province with more than 1970 greenhouse holdings is one of the most important centers for greenhouse crop production in Iran [5].

The high output requires investment cost, labor, fertilizers, and energy input [6]. The high cost of input energy in greenhouse cultivation is one of the main issues. For greenhouse cultivation in cold weather, the main operating cost after labor is related to energy cost. The major portion of the total energy used in greenhouses (65-85 %) is consumed for heating, and the remainder is used for transportation and electrical equipment [7].

In addition to increasing operating costs, energy supply through fossil fuels also raises environmental issues. About 14 % of the world's net CO₂ emissions come from the agriculture sector [8]. For sustainable energy consumption management, three significant aspects should be considered: energy use, environmental effects, and economic efficiency [9]. Hence, there is a need to use clean energy to reduce environmental impact and operating costs. Solar radiation, as a renewable energy origin, is one of the main sources of clean energy in Iran. In Yazd province, the solar irradiation on the horizontal surface is about 7787 MJ/m² yr [10]. This great amount of solar irradiation can be applied to greenhouse heating and reduction of fossil fuel consumption.

There are some studies carried out on enhancing the greenhouse heating systems and improve use of solar energy

*Corresponding Author's Email: mobtaker@ut.ac.ir (H. Ghasemi-Mobtaker)
 URL: https://www.jree.ir/article_152883.html



inside the greenhouse [11-20]. Yildirim and Bilir [21] modeled a greenhouse in Izmir, Turkey to survey the feasibility of using renewable energy to meet greenhouse energy needs. The greenhouse with an area of 150 m² and three different crops (lettuce, tomato, and cucumber) was investigated. According to the results, with a 21510.4 kWh total electrical energy production of solar cell system, annual coverage ratio values for energy demand of lettuce, tomato, and cucumber are estimated as 104.5 %, 95.7 %, and 86.8 %, respectively. Wei et al. [22] studied two greenhouses types with mobile behind walls to enhance the thermal efficiency of popular single-span greenhouses in China. The mobile behind walls were built of jute fiber boards and were fixed in winter for heat maintenance. The results demonstrated that two types of greenhouses with mobile behind walls could be a better alternative to the popular greenhouse. Also, studies on design principles including the shape and optimal orientation of greenhouses have been conducted for receiving maximum solar radiation. Von Elsner et al. [23] examined the structural requirements of greenhouses in Europe. They reported that compared with N-S orientation, in E-W orientation toward solar radiation passing through greenhouse cover is more in winter and lower in summer. The transmission of solar radiation depends on the sun elevation. Kendirli [24] analyzed greenhouse structures in Turkey. Among the greenhouses studied, 85 % were situated in the E-W orientation and 15 % in the N-S orientation. According to the results, because most of the small family enterprises in the area have single rows, construction of greenhouses in E-W orientation enhances the efficiency of solar energy.

Sethi [25] investigated five popular single-span greenhouses to determine the most appropriate greenhouse shape and orientation. To this end, a mathematical model was developed for computing total transmitted solar radiation through walls, roofs, and inclined surfaces. Greenhouses were investigated for both E-W and N-S orientations. The results showed that uneven-span greenhouse captured the maximum solar energy. In addition, the E-W orientation was the best direction of the greenhouse, because this orientation receives less energy in summer and more energy in winter (except for regions near the equator). Also, for the same greenhouse shape, the amount and pattern of solar radiation availability vary at different latitudes. In another study, the five popular greenhouses were investigated with the aim of optimizing energy consumption in the colder months of the year for a composite climate. To this end, the steady state analysis was developed and numerical calculations were performed for the Delhi climate of India. The greenhouses were single-span shapes and studied in an E-W orientation. According to the results, in the composite climate, the uneven span greenhouse is the best selection and LPG remains the most appropriate fuel for providing additional fuel needs for the given condition [26].

Çakır and Şahin [27] investigated the feasibility of greenhouses use in cold regions. They studied five different shapes of single-span greenhouses and developed a model in MATLAB software for estimating the availability of solar energy. Evaluation comparison was conducted for a greenhouse located in Bayburt, northeastern Anatolia, Turkey. The results indicated that the optimum shape of greenhouse for Bayburt conditions was elliptic. Type shape and of the roof was also the most important parameter affecting the amount of solar radiation received by greenhouses. The greenhouse roof shape and orientation play an important role in using the maximum possible received energy. In another

study in the north tropical region (latitude: 24° to 31.2°) for the single-span greenhouse, the value of solar energy that can be captured by the greenhouse was calculated. According to the results, the ellipse aspect ratio has a great effect on the received solar radiation. In addition, the greenhouse orientation was recommended with respect to south direction because this orientation captured the maximum heat value [28].

The heat demand of the greenhouse depends on its location and shape. Therefore, a local survey is of major significance to modeling the greenhouse loads and supplying portion of the needed energy from renewable energy sources. Accordingly, a study was conducted in Romania (latitude 44.25°N) with the aim of making a comparison between two different orientations of an even-span shape greenhouse. Based on the simulation results, the E-W orientation was advantageous all year along from the energy loads standpoint [29].

In the regions located in the northern hemisphere, the orientation of solar greenhouses has a great effect on the amount of captured solar radiation. Thus, applying Extreme Value Theory, Chen et al. [30] proposed a method to assess the best orientation for Chinese solar greenhouses considering the impact of geographical latitude. They reported that the best orientation depended on the solar greenhouse latitude and for northern China, the solar greenhouse orientation must be from South to West. Ghasemi-Mobtaker et al. [31] compared the solar radiation availability for six different shapes of single-span greenhouses in Tabriz, Iran (latitude 38°N). A dynamic model was used to model all the greenhouse internal temperatures. According to the modeling results, the E-W orientated single-span greenhouse captured the highest amount of solar radiation in winter. In addition, using a northern brick wall can greatly reduce entered radiation loss. Chen et al. [32] established a mathematical model to choose the optimal shape and orientation of the greenhouse in cold season with the aim of receiving the maximum solar energy. The results demonstrated that the greenhouse orientation had a significant effect on the total solar irradiation captured by the greenhouse and that the E-W orientation in southern China was an optimal selection. The latitude also had a significant effect on the greenhouse solar radiation availability, such that upon the increasing latitude, the global solar radiation received in greenhouse decreased gradually in cold season.

Research in different parts of the world indicates that it is not possible to comprehensively make a single recommendation for all latitudes. Thus, for important and developing areas of greenhouse cultivation, the optimal orientation of structures with respect to latitude, climate, and environmental factors specific to the same area should be studied in order to ensure a safe and sustainable investment. Most of the reviewed studies targeted single-span greenhouses, while commercial greenhouses are multi-span and large-scale. Therefore, the findings on solar radiation captured in this group of greenhouses can be important to the agricultural operators. In addition, the study of radiation received for each surface of the structure and the type of radiation is important for researchers and is, also, useful to continue research on the study of energy saving techniques.

In this study, mathematical modeling for the multi-span greenhouse was performed with the aim of determining the optimum orientation in terms of the maximum solar energy captured. Hourly irradiation received on the outer surface of the cover and the irradiation captured inside were calculated for each surface of the structure using total solar radiation

measured on the horizontal surface. For a more detailed study and considering the environmental conditions of the study area, the received solar irradiation was calculated for the dominant orientation of the greenhouses in this region and the results was compared with the two main orientations (E-W and N-S). Moreover, this study investigated the effect of north wall insulation on the amount of energy received inside greenhouses.

2. MATERIALS AND METHODS

2.1. Region of study

This study was conducted in the Hemmatabad region, Yazd province, located at the center of Iran, at a geographical location of 54°8' east longitude and 32°2' north latitude. Hemmatabad region with an area of 75 ha under greenhouse cultivation and an average annual production of 22,500 ton of greenhouse crops is one of the most important areas for the collection of greenhouse units in Yazd province [4]. The experimental site with hyper arid-cold (according to De Martonne climate classification) is 1140 m above the sea level [33]. As shown in Figure 1, the northeast-southwest direction is the dominant orientation of the greenhouses in the Hemmatabad region.

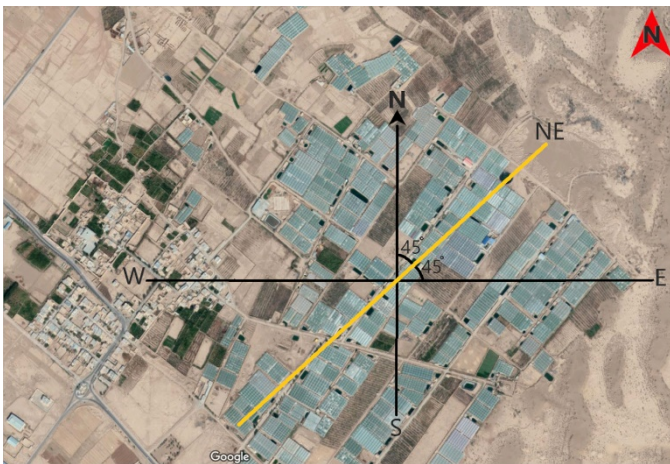


Figure 1. Aerial view of greenhouses in Hemmatabad district

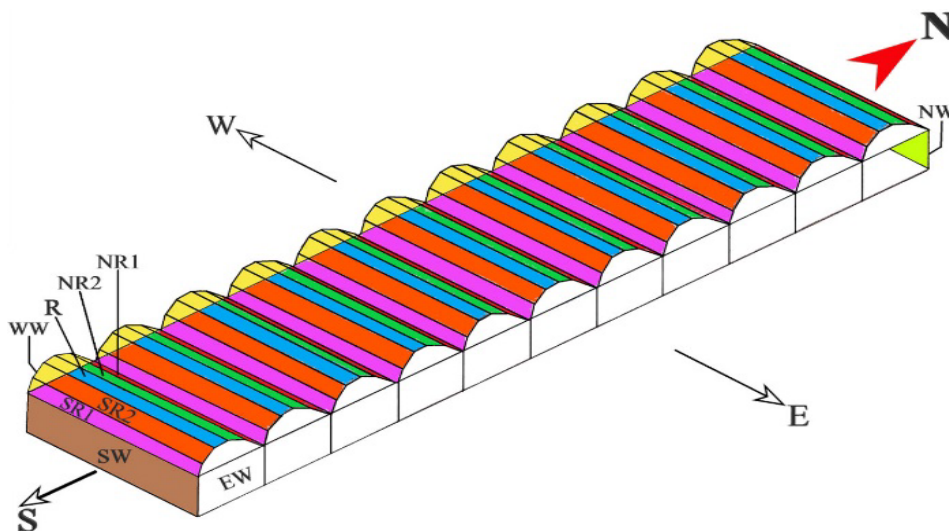
2.2. Greenhouse model

In this study, the effect of orientation on solar irradiation received inside the greenhouses is investigated. For this purpose, a greenhouse with the specifications given in Table 1 was considered in three directions: north-south (N-S), east-west (E-W), and northeast-southwest (NE-SW). In addition, the received radiation was calculated for each orientation and the results were compared with each other. Due to the type and dimensions of most of the existing structures built in the last few years in the study region, a greenhouse with the assumptions of Table 1 was modeled in this study. Considering the latitude of the study region, arch height, and its ratio to the center height ($\frac{2}{7}$) and due to the lack of effective shading of the roofs on each other, it is assumed that the shadow of the roof does not occur.

For computation purposes, the small curved section surfaces (canopy) have been considered as flat surfaces [25]. The conversion of all surfaces of the greenhouse curve into flat plates, along with their naming for one span, is shown in Figure 2 for E-W orientation greenhouse. Moreover, the specifications of each section are given in Table 2. For each of the surfaces introduced in Figure 2, the surface slope angle (B : the angle between the plane of the surface in question and the horizontal) and surface azimuth angle (Y : the deviation of the projection on the horizontal plane of the normal to the surface from the local meridian) for the studied greenhouses are shown in Table 2.

Table 1. Model greenhouse specifications

Parameter	Value
Geometry	Arch / Multi-span
Length	40 m
Arch span	8.5 m
Number of spans	11
Total width	93.5 m
Area	3740 m ²
Column height	4 m
Arch height	1.6 m
Center height	5.6 m
Cover	polyethylene
Total coverage area	5457.44 m ²



SW: south wall, SR: south roof, R: horizontal roof, NW: north wall, NR: north roof, EW: east wall, WW: west wall

Figure 2. Conversion of curved surfaces into flat plates and assigning them for one span of the greenhouse (E-W)

Table 2. Sectional specifications of one span of the greenhouse in the investigated orientations

Sectional specifications in the E-W orientation									
	SW	SR 1	SR 2	R	NW	NR 1	NR 2	EW	WW
Area (m ²)	160	76	76	76	160	76	76	43.52	43.52
β (°)	90	33	16	0	90	33	16	90	90
γ (°)	0	0	0	—	180	180	180	-90	90
Sectional specifications in the N-S orientation									
	EW	ER 1	ER 2	R	WW	WR 1	WR 2	NW	SW
Area (m ²)	160	76	76	76	160	76	76	43.52	43.52
β (°)	90	33	16	0	90	33	16	90	90
γ (°)	-90	-90	-90	—	90	90	90	180	0
Sectional specifications in the NE-SW orientation									
	SE.W*	SE.R 1	SE.R 2	R	NW.W	NW.R 1	NW.R 2	NE.W	SW.W
Area (m ²)	160	76	76	76	160	76	76	43.52	43.52
β (°)	90	33	16	0	90	33	16	90	90
γ (°)	-45	-45	-45	—	135	135	135	-135	45
* SE.W: Southeast wall, SE.R: Southeast roof, R: Horizontal roof, NW.W: Northwest wall, NW.R: Northwest roof, NE.W: Northeast wall, SW.W: Southwest wall									

2.3. Beam and diffuse components of hourly irradiation

The hourly solar irradiation received on the horizontal surface on a day of three colder months of the year (December, January, and February) from 2009 to 2019 was gathered from

$$\frac{I_d}{I} = \begin{cases} 1.0 - 0.09k_t & k_t \leq 0.22 \\ 0.9511 - 0.1604k_t + 4.388k_t^2 - 16.638k_t^3 + 12.366k_t^4 & 0.22 < k_t \leq 0.80 \\ 0.165 & k_t > 0.80 \end{cases} \quad (1)$$

The hourly clearness index (k_t) is the ratio of particular hourly irradiation received on the horizontal surface to the extraterrestrial irradiation for that hour [35].

2.4. Solar radiation on inclined surfaces

The total radiation received on greenhouse roofs and walls was considered to be having 3 components: beam radiation, diffuse radiation, and radiation reflected from the ground. Based on this concept and by applying Eq. (2), the total solar irradiation on any surfaces of greenhouse per square meter were calculated [36]:

$$S_i(t) = I_b R_{b,ave} + I_d R_d + (I_b + I_d) \rho R_r \quad (2)$$

Each of the components of this expression is as follows:

2.4.1. Beam radiation availability on greenhouse cover

The relation between the beam radiation on the horizontal surface and that on the tilted surface (R_b) can be computed as follows [26, 35]:

$$R_b = \frac{\cos \theta_i}{\cos \theta_z} \quad (3)$$

To extend Eq. (3) to an integrated form from an instantaneous equation (limits ω_1 and ω_2 defined in an hour) over a time period of ω_1 to ω_2 , the average R_b is given by [35]:

the Islamic Republic of Iran Meteorological Office data center (IRIMO) in Yazd province.

To calculate the irradiation receiving the inclined surfaces, the contributions of diffuse and beam irradiation of global radiation on the horizontal surface must first be determined, for which purpose Eq. (1) was used [34, 35]:

$$R_{b,ave} = \frac{\int_{\omega_1}^{\omega_2} \cos \theta_i d\omega}{\int_{\omega_1}^{\omega_2} \cos \theta_z d\omega} \quad (4)$$

where

$$\int_{\omega_1}^{\omega_2} \cos \theta_i d\omega = (\sin \delta \sin \Phi \cos \beta - \sin \delta \cos \Phi \sin \beta \cos \gamma) \frac{1}{180} (\omega_2 - \omega_1) \pi + (\cos \delta \cos \Phi \cos \beta + \cos \delta \sin \Phi \sin \beta \cos \gamma) (\sin \omega_2 - \sin \omega_1) - (\cos \delta \sin \beta \sin \gamma) (\cos \omega_2 - \cos \omega_1) \quad (5)$$

and:

$$\int_{\omega_1}^{\omega_2} \cos \theta_z d\omega = (\cos \Phi \cos \delta) (\sin \omega_2 - \sin \omega_1) + (\sin \Phi \sin \delta) \frac{1}{180} (\omega_2 - \omega_1) \pi \quad (6)$$

2.4.2. Diffuse radiation and radiation reflected from the earth's ground

Some parts of the solar radiation reach the earth's surface after scattering in the atmosphere. The current study assumes that

the solar diffuse radiation in the atmosphere is isotropic (the diffuse radiation from the whole sky is of the same strength approximately). Thus, to determine the diffuse radiation received by a face tilted from the horizontal at slope β , first, the view factor of surface to the sky was calculated [26, 35]:

$$R_d = \frac{1 + \cos \beta}{2} \quad (7)$$

To calculate the solar radiation diffusely reflected from the earth's surface and received by a surface with a slope β relative to the horizontal, the view factor for the earth's surface was calculated:

$$R_r = \frac{1 - \cos \beta}{2} \quad (8)$$

Each type of ground reflects radiation differently; thus, the ground reflection factor (ρ) is used. ρ is the so-called albedo value (ALB) and its value for heath surfaces is 0.10 to 0.25 [37]. In the present case, in terms of the land type and vegetation of the investigated region, the value of 0.25 has been applied.

2.5. Solar radiation received on greenhouse cover

Total solar radiation falling on the outer surface of greenhouse cover is thus calculated as follows [31]:

$$S_t = \sum S_i(t)A_i \quad (9)$$

In the case of the multi-span greenhouse under investigation, there are several roofs and walls whose factors mentioned in Table 2 (depending on the orientation) are the same for some of their surfaces. Therefore, calculations are performed for one of these surfaces and the result is multiplied by their number. As shown in Figure 2, the flat plates that receive equal radiation are shown in the same color.

2.6. Solar radiation transmission from greenhouse cover

The entire radiation on the outer surface of the greenhouse cover does not reach the environment; instead, some of it is reflected by the greenhouse cover, some is absorbed by the cover while the remainder is transferred to the inside environment of the greenhouse. The initially transmitted solar radiation (regardless of the absorption factor of cover) dependent on parallel component ($r_{||}$) and perpendicular component (r_{\perp}) [19] is given below:

$$\tau_r = \frac{1}{2} \left[\frac{1 - r_{||}}{1 + r_{||}} + \frac{1 - r_{\perp}}{1 + r_{\perp}} \right] \quad (10)$$

where:

$$r_{||} = \frac{\tan^2(\theta_r - \theta_i)}{\tan^2(\theta_r + \theta_i)} \quad (11)$$

$$r_{\perp} = \frac{\sin^2(\theta_r - \theta_i)}{\sin^2(\theta_r + \theta_i)} \quad (12)$$

θ_i is the incidence angle of the unpolarized radiation and considered equal to the average value at the one-hour interval. θ_r is the refraction angle. These angles are dependent on the refraction indices in the cover medium as follows:

$$\frac{n_i}{n_r} = \frac{\sin \theta_r}{\sin \theta_i} \quad (13)$$

The values of refractive indices of air (n_i) and polyethylene (n_r) are taken as 1 and 1.37, respectively [25]. The absorption of solar radiation in a semi-transparent medium can be calculated based on Bouguer's law. For this reason, the following function was used [35]:

$$\tau_a = \frac{I_{\text{transmitted}}}{I_{\text{incident}}} = \exp\left(-\frac{KL}{\cos \theta_r}\right) \quad (14)$$

where K is the extinction coefficient (assumed to be a fixed in the solar spectrum) and its value was considered to be 400 m^{-1} for the polyethylene sheet [38]. The cover thickness (L) of 0.2 mm was used for polyethylene case [25]. Finally, the transmittance coefficient of a single cover is calculated as follows:

$$\tau = \tau_r \tau_a \quad (15)$$

Equations (10)-(15) can be applied only to the solar beam radiation because its incidence angle (θ_i) is calculated. However, for diffuse and reflected radiation, this angle is unknown. The results presentation can be facilitated by determining an equivalent angle for solar beam radiation. Thus, for incident isotropic radiation, it is assumed that a cover has equal transmittance for reflected and diffuse radiation as it does for beam radiation event at an angle of 60° [35].

3. RESULTS AND DISCUSSION

Based on the meteorological data (from 2009 to 2019), the average of solar energy on the average day of each month was calculated for Yazd province. The average daily irradiation of solar energy for this province was about 25 MJ m^{-2} .

3.1. The portion of beam and diffuse irradiation

The portion of beam and diffuse components of hourly irradiation for the mean of the average days of the investigated months is illustrated in Figure 3. At Hour 12 (noon, local meridian), the maximum beam radiation occurs due to the position of the sun perpendicular to the earth and traversing of the shortest distance in the atmosphere by the sun's rays.

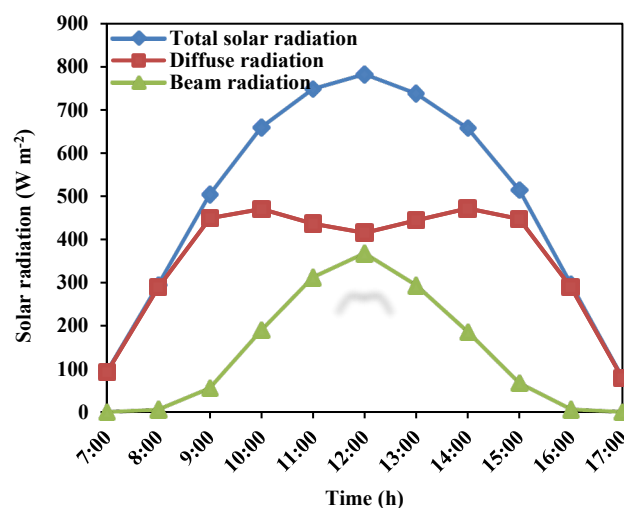


Figure 3. Share of beam and diffuse radiation of global solar radiation

3.2. Irradiation received on the outer surface of the cover

The most important factors in the solar irradiation captured by the greenhouse are the position of the plates relative to the sun and their view factor to the sky. The average of solar irradiation captured by the greenhouse for each orientation is illustrated in Figure 4.

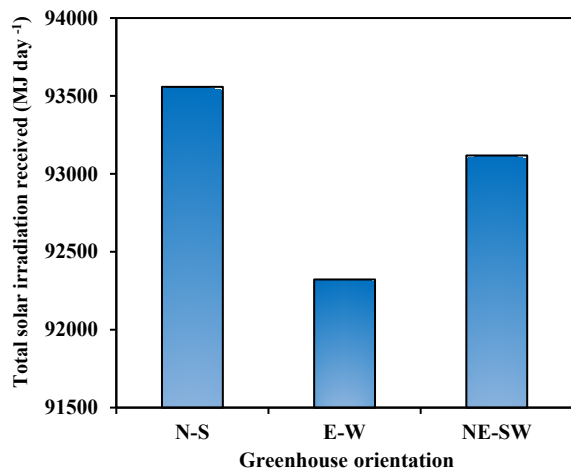


Figure 4. Total solar irradiation captured by the greenhouse for each orientation

The N-S orientation received more irradiation on the outer surface of the cover, compared to other two orientations. However, not all of this irradiation is incorporated into the inside environment of the greenhouse and the changes occur as a result of the cover transmittance.

3.3. Total irradiation captured inside the greenhouse

In this study, hourly transmissivity (τ) for each greenhouse surface on the average day (for each month) was computed. Table 3 shows this coefficient for surfaces of the greenhouse in E-W orientation on the average day of January.

According to Table 3, the West Wall (WW) in the morning and the East Wall (EW) in the afternoon did not receive beam radiation due to the sun location. Figure 5 shows the total solar radiation that the greenhouse received in each orientation.

The greenhouse captured the maximum solar irradiation in E-W orientation. Kendirli [24] reported that the east-west orientation for greenhouses in Turkey increased the solar energy efficiency. According to Table 4, the greenhouse located in the E-W orientation on 10 December captured 424.8 MJ more radiation than N-S orientation. The energy value of the natural gas is 49.5 MJ m⁻³ [39]. Thus, in December, the E-W orientation captured more energy equivalent to 257.4 m³ of natural gas than the N-S orientation.

Table 3. Transmittance coefficient for surfaces of east-west greenhouse on 17 January

Time \ Section	Beam radiation											Diffuse radiation and ground-reflected
	7:00	8:00	9:00	10:00	11:00	12:00	13:00	14:00	15:00	16:00	17:00	---
SW	0.33	0.40	0.45	0.48	0.50	0.50	0.48	0.45	0.40	0.33	0.00	0.80
SR1	0.25	0.38	0.47	0.53	0.56	0.56	0.53	0.47	0.38	0.25	0.00	0.80
SR2	0.17	0.30	0.40	0.46	0.49	0.49	0.46	0.40	0.30	0.17	0.00	0.80
R	0.08	0.20	0.30	0.36	0.39	0.39	0.36	0.30	0.20	0.08	0.00	0.80
NW	0.00	0.00	0.00	0.00	0.00	0.00	0.00	0.00	0.00	0.00	0.00	0.80
NR1	0.00	0.00	0.00	0.03	0.05	0.05	0.03	0.00	0.00	0.00	0.00	0.80
NR2	0.00	0.08	0.16	0.22	0.24	0.24	0.22	0.16	0.08	0.00	0.00	0.80
EW	0.53	0.47	0.38	0.25	0.09	0.00	0.00	0.00	0.00	0.00	0.00	0.80
WW	0.00	0.00	0.00	0.00	0.00	0.09	0.25	0.38	0.47	0.53	0.55	0.80

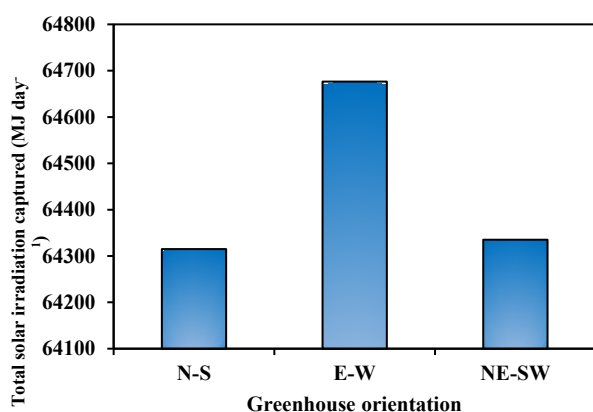


Figure 5. Total solar irradiation captured inside the greenhouse for each orientation

Table 4. Total irradiation captured in the greenhouse on average days in each orientation (MJ)

	N-S	E-W	NE-SW
10 December	59941.2	60366.0	60032.5
17 January	64985.4	65517.2	65063.0
16 February	68018.3	68146.2	67910.0
Mean of the average days	64315.0	64676.5	64335.2

Sethi [25] and Chen et al. [32] reported that the E-W orientation captured maximum solar irradiation in winter. In another study conducted at 44°N latitude, for the E-W orientation, energy saving was reported at about 125 kWh day⁻¹ in June and 87 kWh day⁻¹ in January [29].

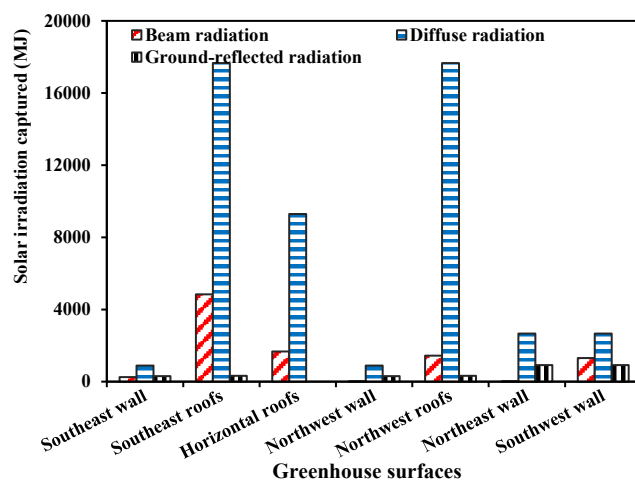
3.3.1. The types of irradiation received inside the greenhouse

Each type of irradiation captured inside the greenhouse is shown for each orientation and surface of the structure in Figure 6.

The west and east roofs in the N-S orientation captured greater irradiation than other parts of the greenhouse due to their good position relative to the sun during the day and the large area of these surfaces (1672 m² for each group of roofs in the total of structure). In Argentina, for an even span greenhouse with N-S orientation, the east roof received the highest solar irradiation in winter [13].

Figure 6 (b) shows that in the E-W orientation, the north roofs (red and green surfaces in Figure 2) and south roofs (purple and orange surfaces in Figure 2) received greater irradiation. This was due to the large area of these surfaces and their wide view factor to the sky. The horizontal roofs also received a lot of diffuse irradiation due to their maximum view factor to the sky ($R_d=1$). The beam radiation was not captured by north wall of the greenhouse. Table 3 shows that the transmissivity coefficient (τ) of beam radiation from the north wall (for E-W orientation) was zero during the day and the total irradiation received by this section consisted of diffuse and reflected irradiation. In the NE-SW orientation, the phenomenon of non-capturing of beam radiation by the north wall occurred for both northeast and northwest walls.

The reason for the high amount of diffuse radiation, as shown in Figure 6, is that the study was conducted for the cold season. According to Figure 3, in this season, the diffuse irradiation received on the ground's surface was much more than beam radiation.



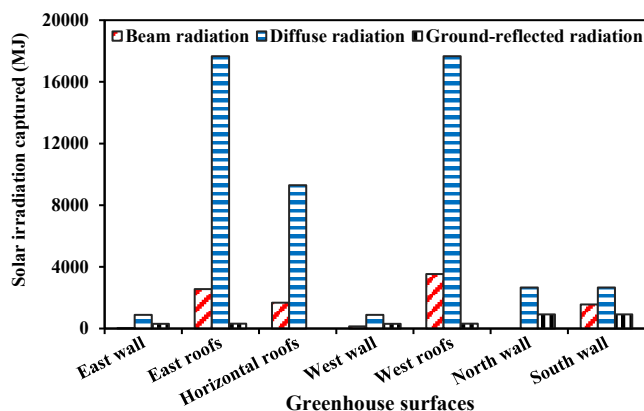
(c)

Figure 6. Components of total irradiation received inside the three orientations (a: N-S; b: E-W; c: NE-SW) for each surface of the greenhouse

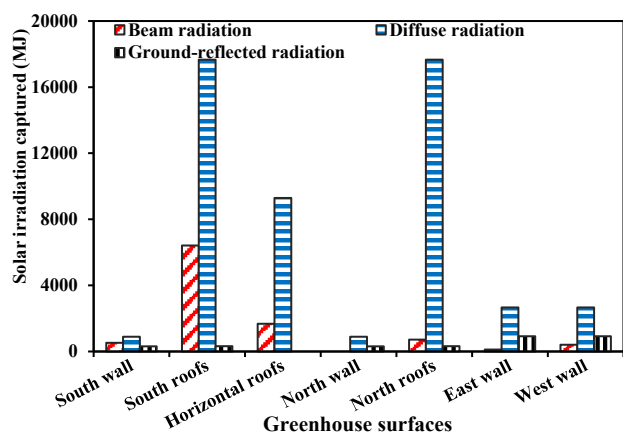
3.4. Hourly analysis of irradiation captured for each surface

The hourly variations of irradiation captured by each section (walls and roofs) of the greenhouse for N-S orientation are shown in Figure 7.

As can be seen from Figure 7, according to the direction of the east and west roofs and the path of the sun, the irradiation captured by the eastern roofs is reduced during the day and added to the irradiation received by the western roofs. Thus, it can be concluded that the sun is inclined toward these surfaces during the day. Due to this angle of inclination (solar incidence angle), not all of the irradiation received on the outer surface of the cover is added to the greenhouse and the large amount of it is wasted. Therefore, the greenhouse with N-S orientation in the cold season, despite having greater irradiation received (on the outer surface of the cover) than the E-W orientation, captured less irradiation inside the greenhouse.



(a)



(b)

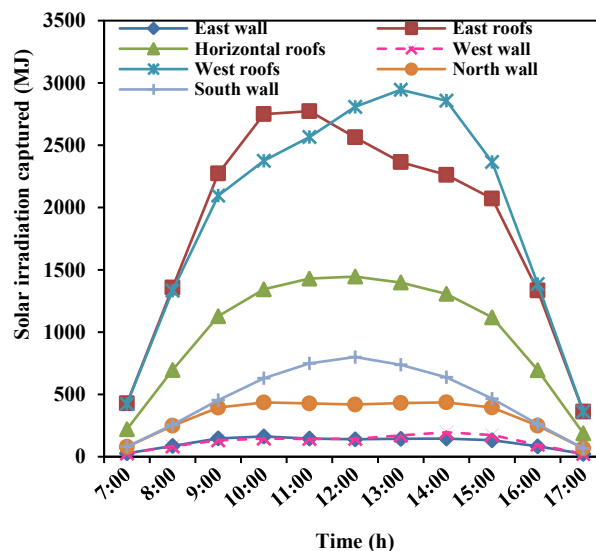


Figure 7. Hourly variations of irradiation received on each section of the greenhouse for the N-S orientation

Figure 8 shows that in the E-W orientation, the movement of the sun from east to west had a significant effect on the

irradiation captured by the southern roofs, and this section of the greenhouse received irradiation on a horizontal surface. Therefore, the large amount of irradiation received on the outer surface of the southern roofs was transferred from the cover and captured inside the greenhouse. In other words, the main section of the irradiation receiver in the greenhouse with E-W orientation was perpendicular to the sun; thus, greater irradiation spread into the environment, compared to the N-S orientation. Finally, it can be concluded that the solar transmittance of cover was affected by incidence angle and sun elevation. Von Elsner et al. [23] reported that for greenhouses in European Union countries, the transmittance through multi-span pitched-roof structures was lower in winter for the N-S than that for the E-W orientation.

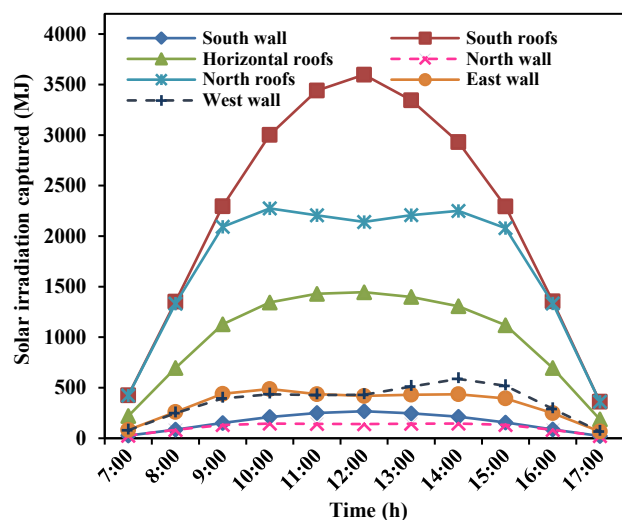


Figure 8. Hourly variations of irradiation captured by each surface of the greenhouse for the E-W orientation

Figure 9 shows that in the NE-SW orientation, the southeast and northwest roofs received greater irradiation. In general, it can be said that the greenhouse conditions with this orientation were in the middle of the E-W and N-S orientation. Therefore, in order to correctly understand the pattern and amount of radiation received for a greenhouse with the NE-SW orientation, calculations should be done for the whole year to evaluate its suitability than other two orientations.

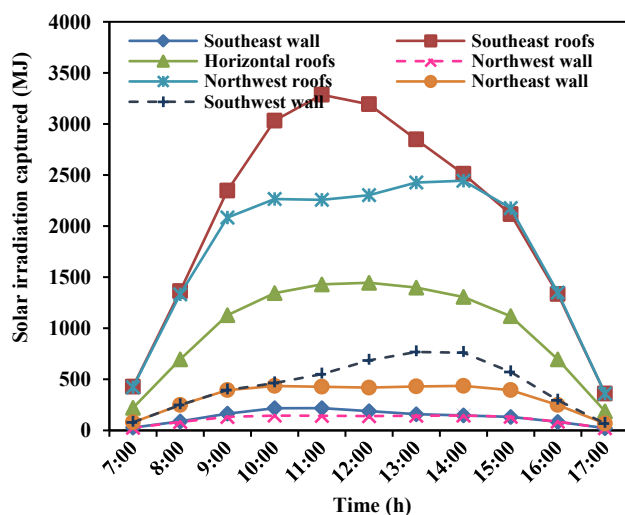


Figure 9. Hourly variations of irradiation captured by each surface of the greenhouse for the NE-SW orientation

In the NE-SW orientation, if the northeast wall was insulated despite the large area of this wall (478.72 m^2), only 5.6 % of the total irradiation captured during the day would be reduced. Ignoring this amount of captured irradiation can be justified in comparison with energy savings caused by the insulation of this surface of the greenhouse. In general, due to the non-capturing of the beam irradiation by the north wall for the three orientations, its insulation can be effective in saving energy consumption. Gupta and Chandra [12] reported that insulation of north wall in E-W oriented greenhouse could reduce 30 % of the structure's heating requirements. Also, another study demonstrated that the use of brick wall on the northern side of greenhouse with E-W orientation could reduce 31.7 % of heating demand in winter [19].

3.5. Importance of time of receiving maximum irradiation

According to Figure 8, the maximum solar irradiation received inside the E-W oriented greenhouse was at noon. Although this amount of energy is greater than what the greenhouse needs at noon, a large portion of it must be removed from the greenhouse by ventilation system [19]. Therefore, use of energy storage methods can be useful. Berroug et al. [40] reported that on winter nights, the application of phase change material placed in the north wall of the E-W oriented greenhouse could increase the temperature of plants and the air inside by 6–12 °C. On the other hand, Figure 7 shows that the maximum solar energy received inside the greenhouse for the N-S orientation was at 10:00 AM by the eastern roofs and at 13:00 to 14:00 by the western roofs. Thus, compared to the E-W orientation, there is better concordance between the time of receiving maximum radiation and heating needs of the greenhouse. At solar noon, the intensity of the total radiation and possible surplus energy were reduced.

4. CONCLUSIONS

This study managed to determine the optimum orientation of the greenhouses for Hemmatabad region located in the central part of Iran. For this purpose, a comparison was made between the irradiation received on the outer surface of the greenhouse cover and the irradiation captured inside the multi-span greenhouse with three different orientations (N-S, E-W and NE-SW). The main findings of this research are given below.

1. The greenhouse in the N-S orientation received greater irradiation on the outer surface of the cover in winter. However, the irradiation captured inside the greenhouse for the E-W orientation was more than that in other orientations, pointing to the significance of the solar incidence angle in the rate of radiation transmission through the cover and their penetration into the greenhouse.
2. The E-W orientation was the best selection for greenhouses in the study area because in the cold season, it captured an average of $361.48 \text{ MJ day}^{-1}$ more energy than that in the N-S orientation and $341.29 \text{ MJ day}^{-1}$ more energy than that in the NE-SW orientation. In addition, energy saving methods such as insulating some greenhouse surfaces and storing surplus solar energy can also be useful in this regard.

- The north wall could not receive the beam radiation for all the orientations investigated, and the total irradiation captured by this section was the diffuse radiation and the ground-reflected radiation.
- In the N-S orientation, compared to the E-W orientation, there was better concordance between the time of receiving maximum radiation and heating needs of the greenhouse.

The method used in the current study can be used to model and study different shapes of greenhouses at all latitudes and other seasons of the year.

5. ACKNOWLEDGEMENT

The financial support provided by Department of Agricultural Machinery Engineering, University of Tehran, Iran, is dully acknowledged.

NOMENCLATURE

A_i	Area of walls and roofs (m^2)
I	Total radiation on a horizontal surface (Wm^{-2})
I_b	Beam radiation (Wm^{-2})
I_d	Diffuse radiation (Wm^{-2})
R_d	View factor of tilted surface to the sky
R_r	View factor of tilted surface to the ground
$S_i(t)$	Total solar radiation on various walls and roofs (Wm^{-2})
S_t	Total solar radiation falling on the greenhouse cover (W)

Greek letters

β	Slope of the surface with horizontal ($^\circ$)
γ	Surface azimuth angle ($^\circ$)
δ	Declination angle of the sun ($^\circ$)
θ_i	Angle of incidence ($^\circ$)
θ_z	Zenith angle ($^\circ$)
ρ	Reflectivity of the ground
τ	Transmissivity of the greenhouse cover
ω	Hour angle ($^\circ$)
Φ	Latitude angle of a place ($^\circ$)

REFERENCES

- Duro, J.A., Lauk, C., Kastner, T., Erb, K.-H. and Haberl, H., "Global inequalities in food consumption, cropland demand and land-use efficiency: A decomposition analysis", *Global Environmental Change*, Vol. 64, (2020), 102124. (<https://doi.org/10.1016/j.gloenvcha.2020.102124>).
- Iddio, E., Wang, L., Thomas, Y., McMorrow, G. and Denzer, A., "Energy efficient operation and modeling for greenhouses: A literature review", *Renewable & Sustainable Energy Reviews*, Vol. 117, (2020), 109480. (<https://doi.org/10.1016/j.rser.2019.109480>).
- Taki, M., Rohani, A. and Rahmati-Joneidabad, M., "Solar thermal simulation and applications in greenhouse", *Information Processing in Agriculture*, Vol. 5, (2018), 83-113. (<https://doi.org/10.1016/j.inpa.2017.10.003>).
- Anonymous, Annual agricultural statistics, Organization agriculture, (2019). (<https://yazd.maj.ir>), (Accessed: 7 May 2019).
- FAO, Iranian National Census of Agriculture, Food and Agriculture Organization, (2014). (<http://www.fao.org>), (Accessed: 24 July 2020).
- Mohammadi, B., Ranjbar, S.F. and Ajabshirchi, Y., "Application of dynamic model to predict some inside environment variables in a semi-solar greenhouse", *Information Processing in Agriculture*, Vol. 5, (2018), 279-288. (<https://doi.org/10.1016/j.inpa.2018.01.001>).
- Shamim Ahamed, M., Guo, H. and Tanino, K., "Energy saving techniques for reducing the heating cost of conventional greenhouses", *Biosystems Engineering*, Vol. 178, (2019), 9-33. (<https://doi.org/10.1016/j.biosystemseng.2018.10.017>).
- Pishgar-Komleh, S.H., Omid, M. and Heidari, M.D., "On the study of energy use and GHG (greenhouse gas) emissions in greenhouse cucumber production in Yazd province", *Energy*, Vol. 59, (2013), 63-71. (<https://doi.org/10.1016/j.energy.2013.07.037>).
- Vadiee, A. and Martin, V., "Energy management in horticultural applications through the closed greenhouse concept, state of the art", *Renewable & Sustainable Energy Reviews*, Vol. 16, (2012), 5087-5100. (<https://doi.org/10.1016/j.rser.2012.04.022>).
- Zarezade, M. and Mostafaeipour, A., "Identifying the effective factors implementing the solar dryers for Yazd province, Iran", *Renewable & Sustainable Energy Reviews*, Vol. 57, (2016), 765-775. (<https://doi.org/10.1016/j.rser.2015.12.060>).
- Tiwari, G.N., Din, M., Srivastava, N.S.L., Jain, D. and Sodha, M.S., "Evaluation of solar fraction (Fn) for the north wall of a controlled environment greenhouse: An experimental validation", *International Journal of Energy Research*, Vol. 26, (2002), 203-215. (<https://doi.org/10.1002/er.776>).
- Gupta, M.J. and Chandra, P., "Effect of greenhouse design parameters on conservation of energy for greenhouse environmental control", *Energy*, Vol. 27, (2002), 777-794. ([https://doi.org/10.1016/S0360-5442\(02\)00030-0](https://doi.org/10.1016/S0360-5442(02)00030-0)).
- Ghosal, M.K. and Tiwari, G.N., "Mathematical modeling for greenhouse heating by using thermal curtain and geothermal energy", *Solar Energy*, Vol. 76, (2004), 603-613. (<https://doi.org/10.1016/j.solener.2003.12.004>).
- Gupta, R. and Tiwari, G.N., "Modeling of energy distribution inside greenhouse using concept of solar fraction with and without reflecting surface on north wall", *Building and Environment*, Vol. 40, (2005), 63-71. (<https://doi.org/10.1016/j.buildenv.2004.03.014>).
- Gupta, R., Tiwari, G.N., Kumar, A. and Gupta, A., "Calculation of total solar fraction for different orientation of greenhouse using 3D-shadow analysis in Auto-CAD", *Energy and Building*, Vol. 47, (2012), 27-34. (<https://doi.org/10.1016/j.enbuild.2011.11.010>).
- Attar, I., Naili, N., Khalifa, N., Hazami, M. and Farhat, A., "Parametric and numerical study of a solar system for heating a greenhouse equipped with a buried exchanger", *Energy Conversion and Management*, Vol. 70, (2013), 163-173. (<https://doi.org/10.1016/j.enconman.2013.02.017>).
- Bouadila, S., Kooli, S., Skouri, S., Lazaar, M. and Farhat, A., "Improvement of the greenhouse climate using a solar air heater with latent storage energy", *Energy*, Vol. 64, (2014), 663-672. (<https://doi.org/10.1016/j.energy.2013.10.066>).
- Zhang, L., Xu, P., Mao, J., Tang, X., Li, Z. and Shi, J., "A low cost seasonal solar soil heat storage system for greenhouse heating: Design and pilot study", *Applied Energy*, Vol. 156, (2015), 213-222. (<https://doi.org/10.1016/j.apenergy.2015.07.036>).
- Ghasemi-Mobtaker, H., Ajabshirchi, Y., Ranjbar, S.F. and Matloobi, M., "Solar energy conservation in greenhouse: Thermal analysis and experimental validation", *Renewable Energy*, Vol. 96, (2016), 509-519. (<https://doi.org/10.1016/j.renene.2016.04.079>).
- Shamim Ahamed, M., Guo, H. and Tanino, K., "A quasi-steady state model for predicting the heating requirements of conventional greenhouses in cold regions", *Information Processing in Agriculture*, Vol. 5, (2018), 33-46. (<https://doi.org/10.1016/j.inpa.2017.12.003>).
- Yildirim, N. and Bilir, L., "Evaluation of a hybrid system for a nearly zero energy greenhouse", *Energy Conversion and Management*, Vol. 148, (2017), 1278-1290. (<https://doi.org/10.1016/j.enconman.2017.06.068>).
- Wei, B., Guo, S., Wang, J., Li, J., Wang, J., Zhang, J., Qian, C. and Sun, J., "Thermal performance of single span greenhouses with removable back walls", *Biosystems Engineering*, Vol. 141, (2016), 48-57. (<https://doi.org/10.1016/j.biosystemseng.2015.11.008>).
- Von Elsner, B., Briassoulis, D., Waaijenberg, D., Mistriotis, A., von Zabeltitz, C., Grattraud, J., Russo, G. and Suay-Cortes, R., "Review of structural and functional characteristics of greenhouses in European union countries: Part I, Design requirements", *Journal of Agricultural Engineering Research*, Vol. 75, (2000), 1-16. (<https://doi.org/10.1006/jaer.1999.0502>).
- Kendirli, B., "Structural analysis of greenhouses: A case study in Turkey", *Building and Environment*, Vol. 41, (2006), 864-871. (<https://doi.org/10.1016/j.buildenv.2005.04.013>).
- Sethi, V.P., "On the selection of shape and orientation of a greenhouse: Thermal modeling and experimental validation", *Solar Energy*, Vol. 83, (2009), 21-38. (<https://doi.org/10.1016/j.solener.2008.05.018>).
- Singh, R.D. and Tiwari, G.N., "Energy conservation in the greenhouse system: A steady state analysis", *Energy*, Vol. 35, (2010), 2367-2373. (<https://doi.org/10.1016/j.energy.2010.02.003>).

27. Çakır, U. and Şahin, E., "Using solar greenhouses in cold climates and evaluating optimum type according to sizing, position and location: A case study", *Computers and Electronics in Agriculture*, Vol. 117, (2015), 245-257. (<https://doi.org/10.1016/j.compag.2015.08.005>).
28. El-Maghlany, W.M., Teamah, M.A. and Tanaka, H., "Optimum design and orientation of the greenhouses for maximum capture of solar energy in North tropical region", *Energy Conversion and Management*, Vol. 105, (2015), 1096-1104. (<https://doi.org/10.1016/j.enconman.2015.08.066>).
29. Stanciu, C., Stanciu, D. and Dobrovicescu, A., "Effect of greenhouse orientation with respect to E-W axis on its required heating and cooling loads", *Energy Procedia*, Vol. 85, (2016), 498-504. (<https://doi.org/10.1016/j.egypro.2015.12.234>).
30. Chen, C., Li, Y., Li, N., Wei, S., Yang, F., Ling, H., Yu, N. and Han, F., "A computational model to determine the optimal orientation for solar greenhouses located at different latitudes in China", *Solar Energy*, Vol. 165, (2018), 19-26. (<https://doi.org/10.1016/j.solener.2018.02.022>).
31. Ghasemi-Mobtaker, H., Ajabshirchi, Y., Ranjbar, S.F. and Matloobi, M., "Simulation of thermal performance of solar greenhouse in north-west of Iran: An experimental validation", *Renewable Energy*, Vol. 135, (2019), 88-97. (<https://doi.org/10.1016/j.renene.2018.10.003>).
32. Chen, J., Ma, Y. and Pang, Z., "A mathematical model of global solar radiation to select the optimal shape and orientation of the greenhouses in southern China", *Solar Energy*, Vol. 205, (2020) 380-389. (<https://doi.org/10.1016/j.solener.2020.05.055>).
33. Baghestani Maybodi, N., Baghestani Maybodi, M.A. and Soufizadeh, S., "Pruning height and its effect on quantitative and qualitative seed production in old saxual (*Haloxylon aphyllum*) forests of Yazd, Iran", *Desert*, Vol. 11, (2006), 27-33. (<https://doi.org/10.22059/jdesert.2006.31864>).
34. Erbs, D.G., Klein, S.A. and Duffie, J.A., "Estimation of the diffuse radiation fraction for hourly, daily and monthly-average global radiation", *Solar Energy*, Vol. 28, (1982), 293-302. ([https://doi.org/10.1016/0038-092X\(82\)90302-4](https://doi.org/10.1016/0038-092X(82)90302-4)).
35. Duffie, J.A. and Beckman, W.A., *Solar engineering of thermal processes*, Fourth Ed., John Wiley & Son, New Jersey, (2013). (<https://doi.org/10.1002/9781118671603>).
36. Sethi, V.P. and Sharma, S.K., "Thermal modeling of a greenhouse integrated to an aquifer coupled cavity flow heat exchanger system", *Solar Energy*, Vol. 81, (2007), 723-741. (<https://doi.org/10.1016/j.solener.2006.10.00-2>).
37. Mertens, K., *Photovoltaics: Fundamentals, technology and practice*, First Ed., John Wiley & Sons, Chichester, UK, (2014). (<https://www.google.com/books/edition/Photovoltaics/AMNcDwAAQBAJ?hl=en&gbpv=1&dq=Mertens,+K.,+Photovoltaics:+fundamentals,+technology+and+practice+first+edition&pg=PR14&printsec=frontcover>).
38. Godbey, L.C., Bond, T. and Zornig, E.H.F., "Transmission of solar and long-wavelength energy by materials used as covers for solar collectors and greenhouses", *Transactions of the ASAE*, Vol. 22, (1979), 1137-1144. (<https://doi.org/10.13031/2013.35169>).
39. Kitani, O. and Jungbluth, T., *CIGR handbook of agricultural engineering*, ASAE Publications, St. Joseph, Michigan, (1999). (<https://doi.org/10.13031/2013.36337>).
40. Berroug, F., Lakhel, E.K., El Omari, M., Faraji, M. and El Qarnia, H., "Thermal performance of a greenhouse with a phase change material north wall", *Energy and Building*, Vol. 43, (2011), 3027-3035. (<https://doi.org/10.1016/j.enbuild.2011.07.020>).



Research Article

Energy Analysis of Utilizing Biomass Gasification to Partially Substitution Fossil Fuels in an IBG-GT-ST-Kalina Cycle

Mohammad Hosseinpour ^a, Hassan Ali Ozgoli ^{b*}, Seyed Alireza Haji Seyed Mirza Hosseini ^a, Amir Hooman Hemmasi ^a, Ramin Mehdipour ^c

^a Faculty of Natural Resources and Environment, Science and Research Branch, Islamic Azad University, Tehran, Tehran, Iran.

^b Department of Mechanical Engineering, Iranian Research Organization for Science and Technology (IROST), Tehran, Tehran, Iran.

^c Department of Mechanical Engineering, Tafresh University, Tafresh, Markazi, Iran.

PAPER INFO

Paper history:

Received: 27 December 2021

Revised in revised form: 16 February 2022

Scientific Accepted: 09 March 2022

Published: 02 July 2022

Keywords:

Biomass Gasification,
Fluidized Bed,
Kalina Cycle,
Combined Cycle,
Energy Efficiency

ABSTRACT

In this study, the partial alteration of fuel consumption of combined cycle power plants was investigated and analyzed using an innovative model. This system is applicable using the fuel derived from the biomass gasification process. For this purpose, energy modeling of an advanced gasification system to supply a share of the gas fuel was fulfilled. The results demonstrated that by considering the reasonable capacities for the design, up to 10 % of natural gas fuel could be replaced with syngas. In addition, heat recovery of the plant stack in the Kalina low-temperature cycle enhanced the total efficiency by up to 1.7 %. Therefore, the competitive advantage of the proposed cycle was enhanced compared to conventional power generation systems. A parametric study of the components affecting the integrated cycle performance including alternative biomass fuels, moisture content of biomass fuel, steam-to-biomass ratio, and equivalence ratio of the gasifier was performed, and the permissible values of each factor were obtained. Thus, by utilizing the proposed approach, it is possible to gradually substitute the consumed fossil fuels of power plants with renewable resources to achieve the objectives of sustainable energy development.

<https://doi.org/10.30501/jree.2022.321835.1307>

1. INTRODUCTION

Gasification, considered a significantly high-efficiency technology for thermo-chemical conversion of biomass, has been converted into a promising approach to generating energy from solid waste [1-3]. Gasification is implemented using a gasifying agent (oxygen, air, or steam) to convert biomass into combustible synthesis gas through the reduction process at high temperatures (around 800-1000 °C) [1, 4]. Syngas includes methane, hydrogen, carbon monoxide, carbon dioxide, water steam, and unfortunate by-products. Each component concentration pertains to oxidant (i.e., gasifying agent), conditions of the process such as temperature and pressure, use or non-use of catalysts or sorbents like CO₂ capturing process, design of the gasifier, residence time of components, and feedstock composition [1, 5-9]. Furthermore, several types of gasifiers are used depending on the operating conditions and the type of biomass fuel. For instance, Rahman et al. [10] designed and implemented a low-tar downdraft biomass gasifier connected to a power generation system. The optimum equivalence ratio lies between 0.29 and 0.41 for the best performance of the mentioned gasifier. Using mass and

energy balances, the average gasifier capacity and cold gas efficiency are about 23.1 kW and 82.7 % for wood chips, whereas they are 33.1 kW and 60.5 % for wood pellets. Sorbents in the shape of CaO might cause a shift to the thermodynamic equilibrium and increase the H₂ content up to 90 %. Therefore, different efforts have been made through simulation models such as mathematical programming to achieve a significant progress in performance prediction. An accurate presentation of the chemical and physical attributes of various gasifier types facilitates an evaluation of syngas composition or formation of an optimized biomass gasifier plant for green power supply prospects [11-13].

Figure 1 shows how to technically design and implement the concept of Fast Internal Circulated Fluidized Bed (FICFB) gasifier. Biomass is first gasified in the gasification reactor and the ungasified char is combusted in the FB combustion reactor. Therefore, biomass is burned to heat the substrate material. Particles of hotbed material are separated from the flue gas in the cyclone separator. Hot particles are transported to the gasifier through a sealed tube. The sealing of this area is to prevent gas leakage between the gasification and the combustion zone and to provide a desirable solid exit of the system.

*Corresponding Author's Email: a.ozgoli@irost.org (H.A. Ozgoli)

URL: https://www.jree.ir/article_152884.html

Please cite this article as: Hosseinpour, M., Ozgoli, H.A., Haji Seyed Mirza Hosseini, S.A.R., Hemmasi, A.H. and Mehdipour, R., "Energy analysis of utilizing biomass gasification to partially substitution fossil fuels in an IBG-GT-ST-Kalina cycle", *Journal of Renewable Energy and Environment (JREE)*, Vol. 9, No. 3, (2022), 75-86. (<https://doi.org/10.30501/jree.2022.321835.1307>).



The input biomass is transferred directly to a bubble fluidized bed gasification reactor by screw conveyors. In this chamber, several processes are performed in parallel. These processes include drying, volatilization, heat decomposition, and somewhat heterogeneous gasification. The bed temperature is set at 850 to 900 °C. The remaining char from the gasifier and the bed material is removed from the combustion zone in this system through a sloping channel [14-16].

According to the study results (as shown in Table 1), the electricity generation potential of municipal waste, solid biomass (wood), and agricultural residues were calculated for Iran until 2050. Its results indicate that the full potential will be around 23.7 TWh y^{-1} , equivalent to 3390 MW of power plants [17]. Moreover, Azizaddini et al. [18] demonstrated that the potential of available biomass resources in Iran was about 51 TWh, which is applicable to about 1400 MW of rural gasification power plants to 2300 MW of advanced gasification power plants.

In addition, low-temperature cycles that operate with different working fluids are conveniently suitable for recovering heat from steam turbines at small and medium power plants in the capacity range of hundreds of kilowatts. In fact, instead of water, organic chemicals with desirable thermodynamic properties are used in these cycles so that the enthalpy drop is much lower. Therefore, the flow can be expanded in several stages in the turbine [19, 20].

Rentizelas et al. [21] compared two types of power generation systems including biomass-fueled boiler-ORC and biomass gasifier-stirling engine. Their results indicate that the generated electricity in the gasification cycle is more than three times that of the boiler cycle. Moreover, they indicate that the application of gasification instead of a biomass combustion system would lead to many economic advantages.

In another study, Kalina [22] examined three arrangements for a small-scale power generation cycle including the downdraft biomass gasifier, gas engine, and organic Rankine cycle. The results indicated that the lowest energy efficiency of 23.6 % was obtained for the simple cycle, while the highest efficiency of 28.3 % was calculated for the dual ORC configuration.

Puig-Arnabat et al. [23] presented and compared five different arrangements for trigeneration cycles including electricity generation, heating, and cooling applying biomass gasification. The capacity of the studied cycles in the range of 250 kW to 2 MW was considered. The highest equivalent energy efficiency of 42.7 % was obtained for an arrangement that used the generated steam by the heat recovery system in a double-effect absorption chiller.

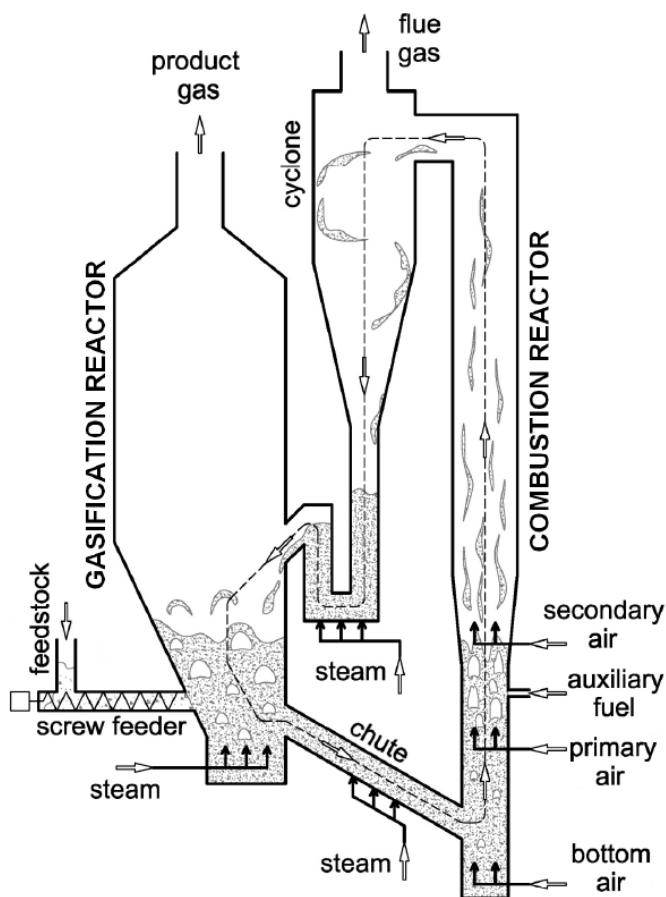


Figure 1. Fast Internal Circulating Fluidized Bed (FICFB) steam gasifier [14]

Table 1. The biomass electricity potential from agricultural waste (mainly bagasse), wood, and municipal waste in Iran until 2050

Year	Municipal wastes						Wood wastes	Agricultural wastes	Total
	2000	2010	2020	2030	2040	2050	2050	2050	2050
Biomass electricity potential (TWh y^{-1})	7.44	9.33	11.46	13.03	14.69	15.94	7.3	0.46	23.7

Fortunato et al. [24] proposed some schemes of the integrated power plant using biomass gasification as an alternative fuel. The presented solutions were based on two different regeneration scenarios and their results were compared. The results demonstrated the ineffectiveness of the extra combustor for regeneration. This study suffers from the simplicity of the mathematical model to solve complex thermodynamic cycles and the failure to consider essential components in the parametric analysis of gasifier, providing the entire system capacity with biomass fuel (in some months of the year), the feasibility of more efficient heat recovery, and use of low-temperature cycles for the cogeneration system.

As can be deduced from the findings mentioned above, it is not possible to replace biomass fuels with fossil fuels at

conventional power plants at once. Therefore, the present study investigates the use of biomass fuels (with a reasonable and practical share) in the case of conventional power generation systems, especially for regions like Iran that benefit from natural gas. Previous studies have failed to comprehensively address this issue in countries with enormous oil and natural gas resources. Thus, gradual elimination of fossil fuels and development of renewable resources, as the objectives of sustainable energy development, can be considered two of the innovative research achievements.

In addition, this study investigated the increase in the power of the proposed power plant using a low-temperature Kalina cycle. This point is essential because upon increasing the power and output efficiency of power generation systems

composition and calorific value of the produced synthesis gas. Many researchers believe that stoichiometric and non-stoichiometric methods are equivalent in modeling value.

In this research, the non-stoichiometric method is used and in a thermodynamic model, the following are assumed:

1. The circulating fluidized bed reactor is assumed to be dimensionless and it does not need to be designed.

2. Heat loss in the reactor is negligible.

3. Temperature distribution is uniform and complete mixing of materials occurs.

4. Sufficient residence time is considered to reach equilibrium.

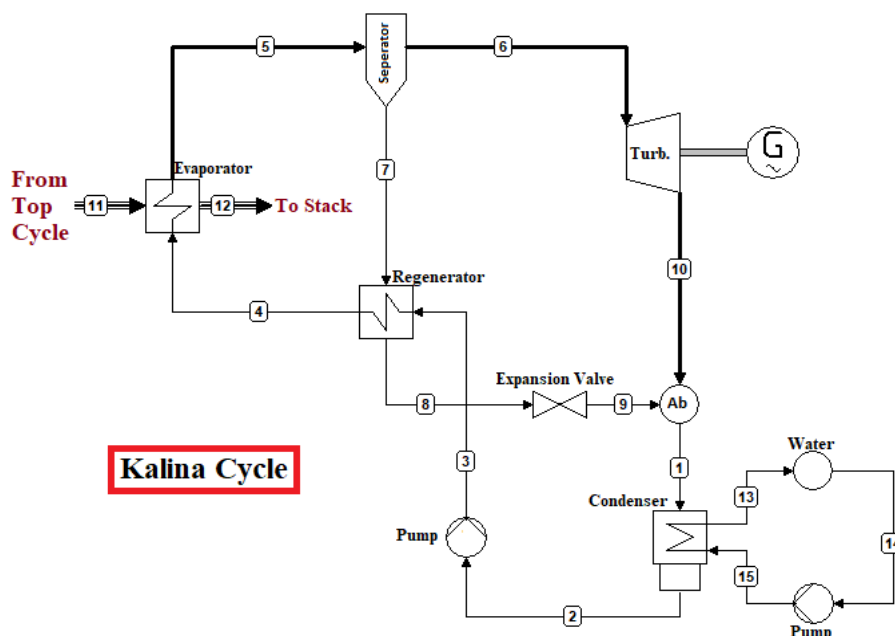


Figure 3. Schematic of the modeled Kalina cycle

A Siemens twin-shaft industrial gas turbine SGT-400 and a Siemens steam turbine SST-110 have been considered in this study with the nominal power generation capacities of 12.9 MWe and 7 MWe, respectively [28, 29].

The following assumptions are defined to implement the energy model:

1. All the proposed cycles operate in a steady-state condition;
2. Pressure drops in all heat exchangers and pipes are ignored.
3. The isentropic efficiencies of pumps and turbines are constant.
4. Changes in potential and kinetic energies are ignored.

The produced gas's Lower Heating Value (LHV) is estimated from the standard low calorific values (MJ kg^{-1}) of the syngas characteristics. For instance, 120 MJ kg^{-1} , 10 MJ kg^{-1} , and 50 MJ kg^{-1} for H_2 , CO , and CH_4 are mainly considered based on their mass concentrations in the whole produced gas.

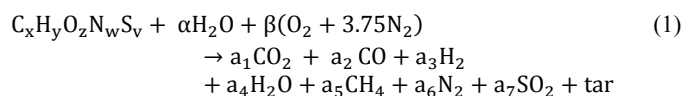
The gasifier model operation conditions are presented in Table 3.

Table 3. Input parameters of the proposed biomass gasifier

Parameter	Value	Unit
Biomass moisture content	14	[wt %]
Steam-to-biomass ratio	0.5	-
The temperature of biomass fuel at feedstock	298	[K]
Biomass inlet flowrate	0.1	[kg s^{-1}]

The considered reactions in the proposed simulation are shown in Table 4. The gasifying agent is steam in this study. Steam gasification is usually implemented via a fluidized bed gasifier that can provide material recirculation to prepare the required heat of gasification reactions. Afterward, the design of the gasifier reactor might be a regular cylinder. Other descriptions could be found in the research executed by Di Carlo et al. [30].

The governing equations of a gasifier with air or steam agent are presented. The ratios of biomass chemical components can be expressed as $\text{C}_x\text{H}_y\text{O}_z\text{N}_w\text{S}_v$, where v , w , z , y are the molar ratios of hydrogen to carbon, oxygen to carbon, and nitrogen to carbon, and sulfur to carbon in the biomass, respectively [32].



a_i represents the number of moles of gaseous components leaving the gas generator, β is the amount of air per kilomole of biomass feed, and α the kilogram of moisture per kilomole of biomass feed. Tar production calculations are neglected in the present study.

The coefficients of the products of production ($a_1, a_2, a_3, \dots, a_7$) are unknown, and to obtain them, the Gibbs function of the products must reach the minimum possible value. On the other hand, the following equations are accepted according to the mass balance.

$$x = a_1 + a_2 + a_5 \quad \text{Carbon balance} \quad (2)$$

$$y + 2\alpha = 2a_3 + 2a_4 + 4a_5 \quad \text{Hydrogen balance} \quad (3)$$

$$z + \alpha + 2\beta = 2a_1 + a_2 + a_4 + 2a_7 \quad \text{Oxygen balance} \quad (4)$$

$$w + 7.5\beta = 2a_6 \quad \text{Nitrogen balance} \quad (5)$$

$$v = a_7 \quad \text{Sulfur balance} \quad (6)$$

$$x = 1 \quad (7)$$

$$a_8 = a_1 + a_2 + a_3 + a_4 + a_5 + a_6 \quad (8)$$

There are a total of 7 equations and ten unknowns. Therefore, the function must be minimized for several dependent variables, which can be three of ($a_1, a_2, a_3, \dots, a_7$).

The Gibbs function for $\text{SO}_2, \text{H}_2\text{O}, \text{H}_2, \text{CO}_2, \text{CO}$ is obtained and finally, the relation is calculated through the following equation.

$$\text{Gibbs}_{\text{fun}} = a_1 g_{\text{CO}_2} + a_2 g_{\text{CO}} + a_3 g_{\text{H}_2} + a_4 g_{\text{H}_2\text{O}} + a_5 g_{\text{CH}_4} + a_6 g_{\text{N}_2} + a_7 g_{\text{SO}_2} \quad (9)$$

This general function must be minimized for the three independent variables a_1, a_2, a_3 .

It should be noted that minimizing the Gibbs function can be used only when the temperature of the products is known.

$$\frac{\Delta G}{RT} = -\ln(K) \quad (10)$$

Table 4. Gasification reactions [31]

Reaction	Reaction name	Heat of reaction	Reaction number
Combustion reactions			
$\text{C} + 0.5 \text{O}_2 \rightarrow \text{CO}$	Char partial combustion	-111 MJ kmol ⁻¹	R1
$\text{CO} + 0.5 \text{O}_2 \rightarrow \text{CO}_2$	CO partial combustion	-283 MJ kmol ⁻¹	R2
$\text{H}_2 + 0.5 \text{O}_2 \rightarrow \text{H}_2\text{O}$	H ₂ partial combustion	-283 MJ kmol ⁻¹	R3
Heterogeneous reactions			
$\text{C} + \text{H}_2\text{O} \leftrightarrow \text{CO} + \text{H}_2$	Water-gas	+131 MJ kmol ⁻¹	R4
$\text{C} + \text{CO}_2 \leftrightarrow 2\text{CO}$	Boudouard	+172 MJ kmol ⁻¹	R5
$\text{C} + 2\text{H}_2 \leftrightarrow \text{CH}_4$	Methanation	-75 MJ kmol ⁻¹	R6
Homogeneous reactions			
$\text{CO} + \text{H}_2\text{O} \leftrightarrow \text{CO}_2 + \text{H}_2$	Water gas-shift	-41 MJ kmol ⁻¹	R7
$\text{CH}_4 + \text{H}_2\text{O} \rightarrow \text{CO} + 3\text{H}_2$	Steam-methane reforming	+206 MJ kmol ⁻¹	R8

In this case, another indeterminate variable, temperature, is added to the equations and the dimension ΔG is written for the significant gas equations including the Boudouard reaction equation, the water-gas reaction, and the methane reactions. This method assigns a value to the Gibbs function in standard conditions (pressure and temperature). The enthalpy value is also obtained using this method. Finally, the energy balance is obtained by solving the following equation.

$$h_r = h_{f_{\text{Biomass}}} + \alpha h_{\text{H}_2\text{O}} + \beta h_{\text{O}_2} + \beta(3.76h_{\text{N}_2}) \quad (11)$$

$$h_p = a_1 h_{\text{CO}_2} + a_2 h_{\text{CO}} + a_3 h_{\text{H}_2} + a_4 h_{\text{H}_2\text{O}} + a_5 h_{\text{CH}_4} + a_6 h_{\text{N}_2} + a_7 h_{\text{SO}_2} \quad (12)$$

$$h_r = h_p \quad (13)$$

h_r is the enthalpy of the reactants and h_p is the enthalpy of the products.

The two thermodynamic parameters commonly used to investigate gasification operations are the calorific value of the synthesis gas and the cold gas efficiency, obtained from the following equations.

$$h_{f_{\text{Biomass}}} = \text{LHV}_{\text{dry}} + \left(\frac{1}{M_{\text{bio}}}\right) (a_1 h_{\text{CO}} + a_2 h_{\text{CO}_2} + a_3 h_{\text{H}_2} + a_4 h_{\text{H}_2\text{O}} + a_5 h_{\text{CH}_4} + a_6 h_{\text{N}_2} + a_7 h_{\text{SO}_2}) \quad (14)$$

$$\text{LHV}_{\text{gas}} = \left(\left(\frac{a_1}{M_{\text{bio}}}\right) \text{LHV}_{\text{CO}} + \left(\frac{a_3}{M_{\text{bio}}}\right) \text{LHV}_{\text{H}_2} + \left(\frac{a_5}{M_{\text{bio}}}\right) \text{LHV}_{\text{CH}_4}\right) \quad (15)$$

$$\text{CGE} = \frac{a_3 \text{RT}_0 \text{LHV}_{\text{gas}}}{M_{\text{bio}} \text{LHV}_{\text{bio}}} (\%) \quad (16)$$

Hydrogen is the desired product in this process and the efficiency of hydrogen production can be described as system efficiency in general or Equation 17:

$$\eta_{\text{H}_2} = \frac{\dot{m}_{\text{H}_2} \text{LHV}_{\text{H}_2}}{M_{\text{bio}} \text{LHV}_{\text{bio}}} (\%) \quad (17)$$

Equivalence Ratio (ER) indicates air-to-biomass ratio and plays an essential role in biomass gasification. When the ER value is reduced, the share of H₂ and CO in the synthesized gas increases [33].

Higher ER leads to less H₂ and CO and more CO₂, which increases the amount of heat in the synthesized gas due to increased oxygen reactions. ER is also affected by moisture and raw biomass volatiles. If biomass water is higher than 15 %, it increases the ER and the amount of gas. More volatiles in biomass increase tar production.

Steam to biomass ratio (S/B) is an essential parameter in gasification because it affects the volume of synthesized gas and its calorific value. Increasing the vapor ratio increases H₂ and increases the calorific value of the synthesized gas. It also reduces bitumen production due to water-gas change reactions, but the value of S/B can be increased to some extent because this increase causes excess steam vapor in the synthesized gas. Reducing the enthalpy in the production of this excess steam reduces the efficiency of this process; thus, this ratio should be optimal.

The modeling process for solving the gasification equations is presented in Figure 4.

The electrical efficiency of the integrated cycle is obtained by Equation 18:

$$\eta_{\text{Electrical,IC}} = \frac{\dot{W}_{\text{GC}} + \dot{W}_{\text{SC}} + \dot{W}_{\text{BC}}}{\dot{Q}_{\text{in}}} \quad (18)$$

where $\eta_{\text{Electrical,IC}}$ presents the electrical efficiency of the integrated cycle, \dot{W}_{GC} , \dot{W}_{SC} , and \dot{W}_{BC} are the gas cycle, steam

cycle, and bottoming cycle delivered power, and \dot{Q}_{in} is the supplied heat by fuels (biomass and natural gas).

Some of the critical equations of gas cycle calculations are presented in Table 5 [34].

The main equations of steam cycle calculations are given in Table 6 [35]. Table 7 shows the initial values for base combined cycle modeling.

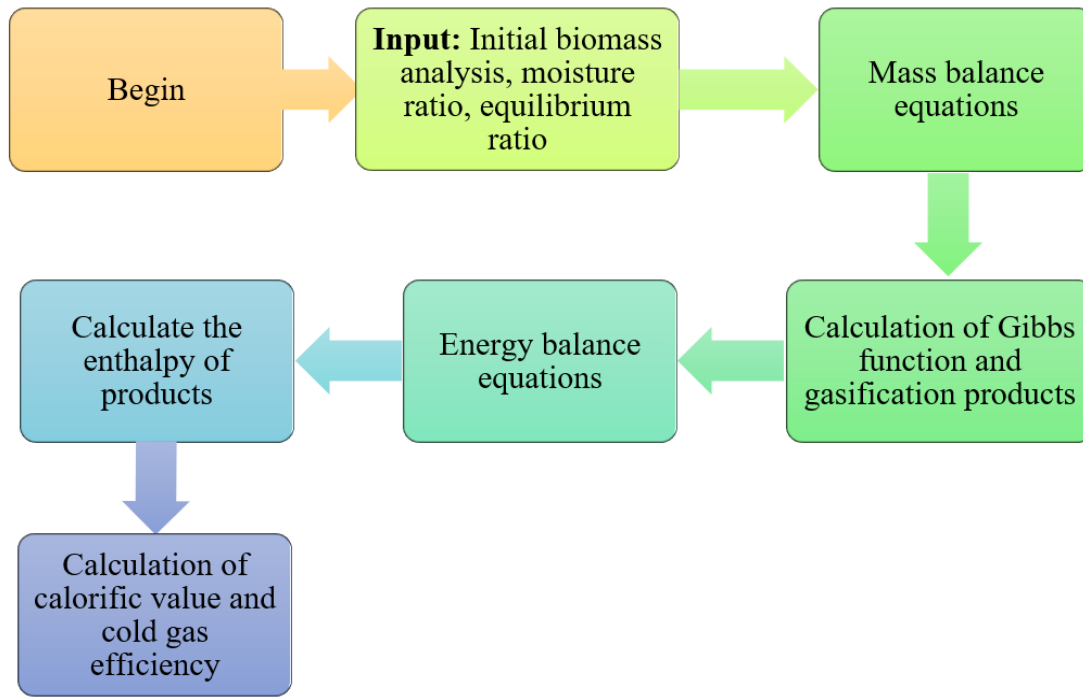


Figure 4. The modeling process of the gasification equations in the present study

Table 5. The main equations of the gas cycle

Parameter	Equation	Description	No.
Heat rate	$\text{Heat rate} = \frac{3412(\text{Btu/kWh})}{\eta_{\text{Prime}}}$	η_{Prime} is the GC thermal efficiency defined by manufacture	(19)
Actual air flow rate	$\dot{m}_{\text{actual}} = \dot{m}_{\text{theoretical}} \times \text{Excess Air}$	Excess air is defined as input data	(20)
GC net delivered power	$\dot{W}_{\text{GC,net}} = \dot{W}_{\text{turbine}} - \dot{W}_{\text{compressor}}$	-	(21)
GC net efficiency	$\eta_{\text{GC,net}} = \frac{\dot{W}_{\text{GC,net}}}{\dot{Q}_{\text{in}}}$	\dot{Q}_{in} is the supplied heat by fuel	(22)

Table 6. The main equations of the steam cycle

Parameter	Equation	Description	No.
Flue gas enthalpy	$\dot{m}_{\text{Flue gas}} \cdot h_{\text{Flue gas}} = (\dot{m}_{\text{GT,out}} \cdot h_{\text{GT,out}}) + (\dot{m}_{\text{gasifier combustor,out}} \cdot h_{\text{gasifier combustor,out}})$	Gasifier combustor components are H ₂ O, CO ₂ , N ₂ , SO ₂	(23)
Duct burner outlet flow rate	$\dot{m}_{\text{Duct burner,out}} = (\dot{m}_{\text{Flue gas}} + \dot{m}_{\text{Fresh air}} + \dot{m}_{\text{Auxiliary fuel}})$	The duct burner is activated if the flue gas enthalpy is not enough.	(24)
SC net delivered power	$\dot{W}_{\text{SC,net}} = \dot{W}_{\text{turbine}} - \dot{W}_{\text{pump}}$	-	(25)
SC net efficiency	$\eta_{\text{SC,net}} = \frac{\dot{W}_{\text{SC,net}}}{\dot{Q}_{\text{in}}}$	\dot{Q}_{in} is the supplied heat by flue gas	(26)

Table 7. Initial values of the base combined cycle

Parameter	Value	Unit
Specific heat capacity of flue gas in GC [36]	1.185	[kJ (kg K) ⁻¹]
Reference temperature when the enthalpy and entropy are assumed zero	273	[K]
Reference pressure when the enthalpy and entropy are assumed zero	1.013	[bar]
Specific heat capacity of air	1.005	[kJ (kg K) ⁻¹]
Specific heat capacity of fuel	1.148	[kJ (kg K) ⁻¹]
Air heat capacity ratio	1.4	-
Natural gas heat capacity ratio	1.333	-
Universal gas constant	8314	[J (kmol K) ⁻¹]
The pressure of inlet water into the cycle	101.3	[kPa]
The temperature of inlet water into the cycle	20	[°C]
The outlet temperature of the steam turbine	54	[°C]

To calculate natural gas fuel conservation by biomass consumption in the combined cycle, the equivalence biomass flow rate has been considered in Equation 27. Therefore, fossil fuel conservation could be obtained.

$$\dot{m}_{eq,biomass} = \frac{(\dot{m}_{syngas} \times LHV_{syngas})}{LHV_{fuel,GC}} \quad (27)$$

$$\dot{m}_{fuel,conservation} = \frac{(\dot{m}_{eq,biomass})}{LHV_{fuel,GC}} \quad (28)$$

Then, by placing the integrated cycle flow rate in Equation 30, the combined cycle efficiency is calculated.

$$\dot{m}_{IC} = (\dot{m}_{fuel,GC} - \dot{m}_{eq,biomass}) \quad (29)$$

$$\eta_{IC} = \frac{(\dot{W}_{net,CC})}{(LHV_{biomass} \times \dot{m}_{biomass} \times 1000) + (\dot{m}_{IC} \times LHV_{fuel,GC})} \quad (30)$$

The mass balance of the Kalina cycle working fluid is represented by Equation 31:

$$\sum (\dot{m}_{in} \cdot x) = \sum (\dot{m}_{out} \cdot x) \quad (31)$$

In this equation, x represents the amount of ammonia concentration in the ammonia-water mixture.

The absorbed heat in the evaporator is obtained by Equation 32:

$$q_{Evaporator} = h_{Evaporator,out} - h_{Evaporator,in} \quad (32)$$

Also, dissipated heat in the condenser is presented by the following equation:

$$q_{Condenser} = h_{Condenser,out} - h_{Condenser,in} \quad (33)$$

The net Kalina delivered power can be evaluated by Equation 34:

$$\dot{W}_{Kalina,net} = \dot{W}_{Turbine} - \dot{W}_{Pumps} \quad (34)$$

Furthermore, the energy efficiency of the Kalina cycle is shown in Equation 35 [22]:

$$\eta_{Kalina} = \frac{\dot{W}_{net,Kalina}}{\dot{Q}_{Evaporator}} \quad (35)$$

4. RESULTS AND DISCUSSION

4.1. Biomass gasifier

Syngas composition is compared in Table 8 with the generated results of the previous studies according to the literature data including findings of Fercher et al. and Hofbauer et al. [37-39] at an S/B of 0.5. It should be noted that all components of the produced gas have been considered in modeling pertaining to the written values in this Table.

Table 8. Comparison of syngas characteristics with experimental and mathematical studies

S/B = 0.5 (kg _{steam} /kg _{biomass})	Literature Data [37, 38]	Literature Data [40]	Current Study
H ₂ (% dry mole fraction)	30-40	42.2	41.9
CO (% dry mole fraction)	20-30	22.9	23.3
CO ₂ (% dry mole fraction)	15-25	21.8	21.7
CH ₄ (% dry mole fraction)	8-12	13.1	7.3
LHV (MJ kg ⁻¹)	14.1-15.2	14.2	15.8

According to the comparison made in Table 8, it is discussed that due to the use of catalysts in the experimental study of References 37 and 38, the water-gas shift reactions and steam methane reforming are presented in relations, R7 and R8, producing less carbon monoxide and carbon dioxide. However, the results obtained from this study and Reference 40 have been adjusted based on the equilibrium conditions of gasification and the correction coefficients of the FICFB

biomass gasifier system, causing a slight difference between the results. Thus, it is clear that the model proposed in the present study has acceptable validity.

Of note, fluidized bed gasifiers operate in unstable temperature conditions due to their turbulent conditions, and simple models cannot achieve high-precision responses. Therefore, the reasonable accuracy of the model presented in this study is confirmed.

4.2. Combined cycle

The results of the main parameters of the base cycle are presented in Table 9. The total delivered power of the cycle is 17.94 kW. The results indicate acceptable conformity to the details published by the manufacturer of gas and steam turbines [28, 29].

Table 9. Results of the base proposed combined cycle

Parameter [Unit]	Value
Gas cycle	
Heat rate [Btu kWh ⁻¹]	9805
Inlet GC fuel flowrate [kg s ⁻¹]	0.8147
Inlet GC air flowrate [kg s ⁻¹]	37.14
Compressor outlet temperature [K]	661.3
Flue gas mass flow rate [kg s ⁻¹]	38.08
Steam cycle	
Inlet feed water pump flowrate [kg s ⁻¹]	5.1
HP steam demand [kg s ⁻¹]	5
HP steam produced [kg s ⁻¹]	6.122
Temperature in A [K]	837
Temperature in C [K]	538.5
Power and Efficiencies	
Gas cycle net delivered power [kW]	12,850
Steam cycle net delivered power [kW]	5090
Gas cycle efficiency [%]	34.67
Steam cycle efficiency [%]	13.74

4.3. Kalina cycle

The proposed integrated power system results based on the Kalina cycle are presented in Table 10. Also, the thermodynamic values for all nodes of the Kalina cycle are shown in Table 11.

According to the modeling results given in Table 10, the utilization of the Kalina cycle leads to the improvement of the total cycle power by approximately 1.7 %.

Table 10. The results of the IBG-CC-Kalina modeling

Parameter	Value	Unit
Integrated cycle efficiency	52.58	[%]
Kalina cycle efficiency	19.82	[%]
Integrated cycle net delivered power	18,535	[kW]
Kalina expander delivered power	620	[kW]
Kalina cycle net delivered power	592	[kW]

Table 11. The thermodynamic values of each node of the Kalina cycle in the proposed integrated cycle

State	T (K)	P (bar)	x (%)	m (kg s ⁻¹)
1	315.3	10.74	95	2.5
2	302	10.74	95	2.5
3	303.8	80	95	2.5
4	309.8	80	95	2.5
5	426.2	80	95	2.5
6	426.2	80	96.54	2.38
7	426.2	80	64.31	0.1195
8	307.8	80	64.31	0.1195
9	308.9	10.74	64.31	0.1195
10	314.2	10.74	96.54	2.38
11	433.5	1	-	38.08
12	423.5	1	-	38.08

4.4. Parametric study

4.4.1. Steam to biomass ratio

Figure 5 shows the outcome of parametric analysis for the proposed model by changing the S/B ratio from 0.1 to 0.9 and the gasifier temperature is 820 °C.

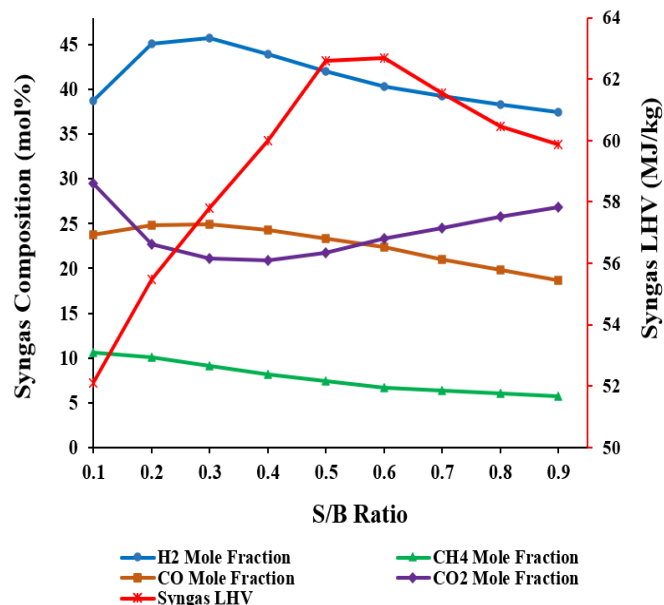


Figure 5. Syngas composition and LHV changes relative to steam-to-biomass ratio variation in the proposed combined cycle

Given the formula observed for calculating LHV (Equation (15)) [41], the coefficient corresponding to the molar fraction of CO is higher than that of H₂. Therefore, the LHV decreases as SB increases, as shown in Figure 5, in a wide range of SB ratios. It can be seen that increase in H₂ is always followed by a decrease in CO and an increase in CO₂. Hence, the value of the SB ratio should not be too large, especially at high gasification temperatures.

4.4.2. Alternative fuels

To conduct a technical feasibility study and compare the effectiveness of alternative biomass fuels, three agricultural and horticultural biomass fuels were considered as the input of the proposed gasifier system in this study. These fuels include two types of gardens pruning wastes and sugarcane bagasse. The specifications of alternative fuels and the results obtained for the base cycle are given in Table 12 [42].

Table 12. Mole fraction of the selected alternative biomass fuels

Component	Garden Prunings #1	Garden Prunings #2	Bagasse
C (% dry mole fraction)	51.02	50.38	46.96
H (% dry mole fraction)	6.41	6.2	5.72
O (% dry mole fraction)	35.63	35.38	44.05
N (% dry mole fraction)	0.64	0.86	0.27
S (% dry mole fraction)	0.0	0.0	0.02
Cl (% dry mole fraction)	0.0	0.0	0.04
Ash (% dry mole fraction)	6.3	7.18	2.94
Moisture Content (%)	10	10	10
HHV (MJ kg ⁻¹)	19.48	19.26	18.5

The results obtained from modeling the base cycle for the primary and alternative fuels are shown in Table 13. The use of wood chip fuel in the gasifier exhibits better results than other alternative fuels due to its higher calorific value.

However, the results of this study prove that the application of biomass fuels will save more than 8 % in natural gas consumption at the proposed power plant.

Table 13. Results of the base proposed combined cycle for the selected biomass fuels

Parameter [Unit]	Wood Chips	Garden Prunings #1	Garden Prunings #2	Bagasse
Natural Gas fuel conservation by using biomass [kg s^{-1}]	0.08288	0.07754	0.07447	0.07011
Natural Gas fuel conservation rate [%]	10.17	8.51	8.14	8.60
Duct burner fuel flowrate [kg s^{-1}]	-0.0428	-0.0424	-0.0429	-0.0428
Duct burner input air flowrate [kg s^{-1}]	-0.5397	-0.5416	-0.5418	-0.5401
High heating value of biomass [MJ kg^{-1}]	20.96	20.14	19.72	17.27
Low heating value of cold gas [kJ kg^{-1}]	15,867	13,117	15,733	16,203
Low heating value of syngas ($\text{CO}+\text{CH}_4+\text{H}_2$) [kJ kg^{-1}]	52,352	49,524	49,522	48,434
Biomass molar weight [kg kmol^{-1}]	23.57	22.06	22.13	24.81
Produced gas molar weight [kg kmol^{-1}]	8.873	8.409	8.282	8.12
Syngas mass flowrate ($\text{CO}+\text{CH}_4+\text{H}_2$) [kg s^{-1}]	0.07908	0.07124	0.06842	0.06587
Gasification temperature [$^{\circ}\text{C}$]	821	714	696	797
Gasifier cold-gas efficiency [%]	79.75	75.46	74.85	78.22
Hydrogen production energy efficiency [%]	20.67	10.46	8.99	18.91
Combined cycle efficiency [%]	50.90	48.47	48.33	49.40

4.4.3. Fuel conservation

Figure 6 shows the rate of changes in natural gas consumption savings relative to the evolution of steam-to-biomass ratio in the studied combined cycle using the proposed biomass gasification system. Increasing the amount of hydrogen produced by Reactions R4, R7, and R8 will increase the calorific value of the syngas and make it possible to reduce the share of natural gas.

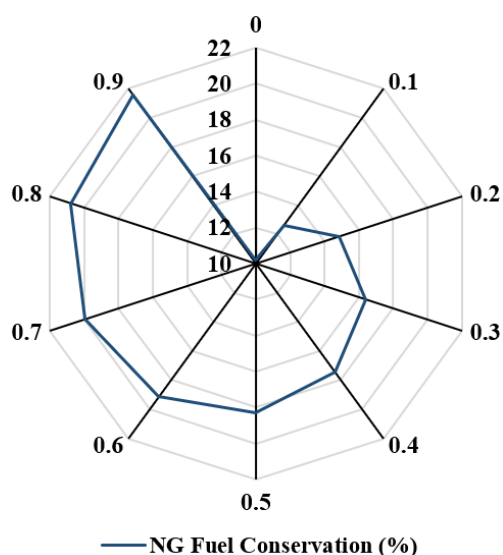


Figure 6. Natural gas fuel conservation relative to steam-to-biomass ratio changes in the proposed combined cycle

Changes in the molar percentage of each component of the synthesized gas due to the variation of the biomass fuel water content entering the system are given in Figure 7. Moisture content increase has a positive effect on the water gasification process, and gas shift reaction in the gasifier and hydrogen content increase is expectable. As can be seen, despite the rise

in the amount of moisture in the fuel, the amount of hydrogen in the syngas composition increases; it is not desirable due to the increased production of carbon dioxide. The temperature in the gasifier reactor decreases with fuel moisture content growth. There is some critical point when the temperature at the reactor is too low and the intensity of hydrogen production is down. Therefore, the amount of 10 % humidity can be the acceptable level of biomass bulb content for consumption in this cycle and it will cause, unfavorably, more production of environmental pollutants.

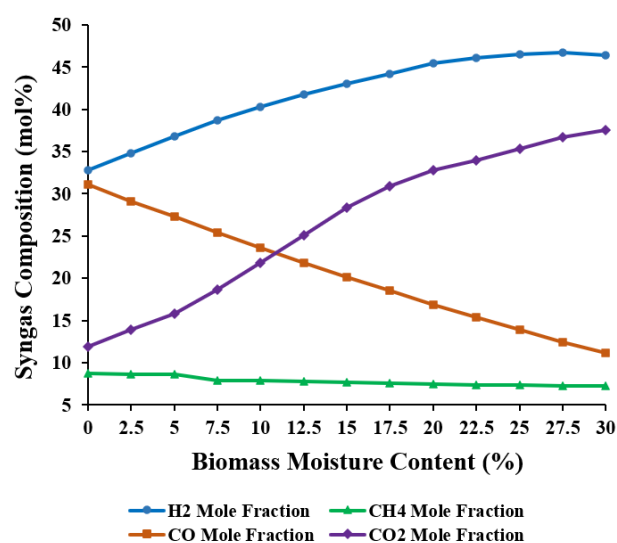


Figure 7. Syngas composition changes relative to biomass moisture variation in the proposed combined cycle

The curve of changes in the syngas components relative to the changes in the equilibrium rate is presented in Figure 8. Based on the results, the equilibrium rate in the range of 0.15 to 0.35 can be acceptable. In this range, the concentrations of major combustible gases, including H_2 , CH_4 , and CO , are

reduced because of oxidation reactions (R1-R3). Higher values lead to a decrease in the share of hydrogen and consequently, reduction of the calorific value of the gas produced. Thus, it is understood that the value considered in this research is a suitable and permissible value according to other parameters affecting the gasification process.

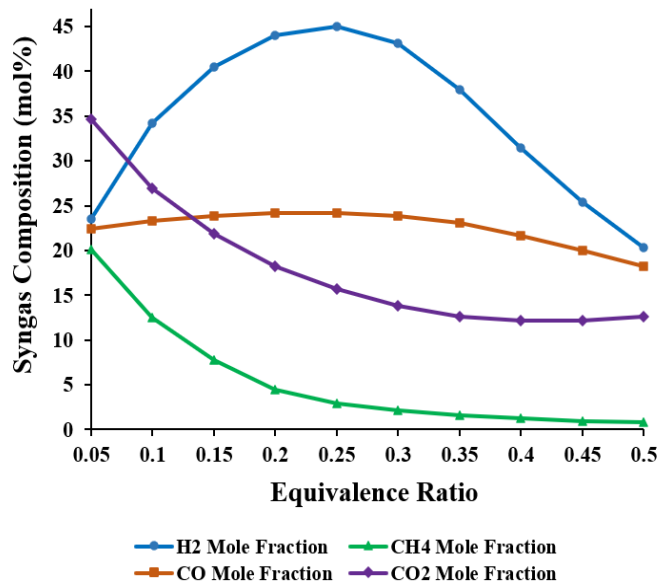


Figure 8. Syngas composition changes relative to equivalence ratio variation in the proposed combined cycle

The effect of the equivalence ratio on lower heating value and cold gas efficiency is presented in Figure 9. As can be seen in the curves of this figure, by increasing the equivalence ratio by more than 0.3, the amount of cold gas efficiency of the gasifier decreases significantly, which is not desirable. Based on what was stated in Section 3, an excessive increase in the amount of air compared to the biomass fuel entering the system will have a negative effect on the production of valuable syngas.

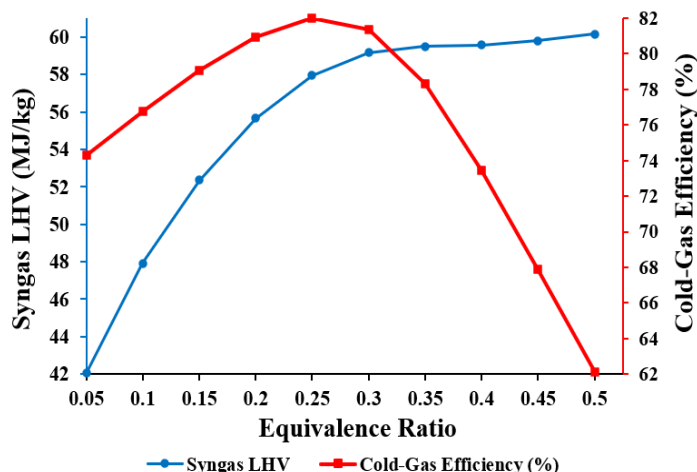


Figure 9. Syngas LHV and gasifier cold gas efficiency changes relative to equivalence ratio variation in the proposed combined cycle

The reduction of the natural gas consumption rate due to the replacement of the syngas in the proposed cycle, compared to the equivalence ratio changes greater than 0.35, is shown in Figure 10. Reducing the amount of syngas production in the gasifier will increase the system's share of natural gas consumption. Therefore, adjusting the cycle fuel system in the

declared range for the equivalence ratio is necessary to achieve the goals mentioned in this cycle.

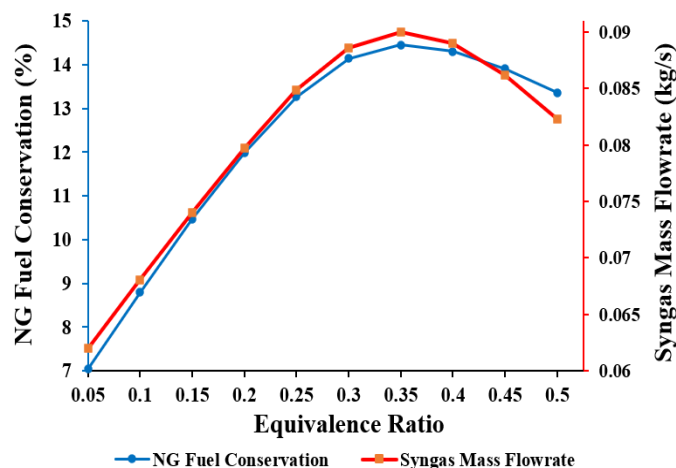


Figure 10. Natural gas consumption and syngas production change relative to equivalence ratio variation in the proposed combined cycle

5. CONCLUSIONS

The present study investigated and analyzed the application of FICFB as an advanced biomass gasification system in a small-scale combined cycle power plant to generate the required fuel fraction. For this purpose, first, thermodynamic study of a combined cycle power plant consisting of two accessible types of gas and steam turbines with nominal capacities of 12.9 and 7 MW was performed. Then, based on the amount of biomass fuel available in Iran, calculations related to the mass and energy balance of the biomass gasifier were fulfilled. The energy modeling results in the proposed power plant indicate that syngas produced by the gasifier could supply about 10 % of the share of fuel consumed.

To increase the competitiveness of the studied cycle, the utilization of a low-temperature cycle to recover the stack heat of the topping combined cycle was proposed. The results demonstrate that the application of the Kalina cycle increased the total efficiency by about 1.7 %.

A parametric study on four biomass fuels of the agricultural type illustrated that wood chips were more desirable in producing syngas with a higher calorific value. Also, parametric analyses were performed on the influential factors of the studied biomass gasifier, and the maximum permissible equivalence ratio was 0.35. In addition, the need to dry the biomass fuel before gasifier feeding and having a maximum of 10 % moisture content were other achievements of this study.

Based on the present study results, gradual elimination of fossil fuels is possible in a step-by-step fashion with renewable energy technologies. Therefore, more steps can be taken for sustainable energy development by adopting a policy of sequential replacement of fossil fuels in regions with adequate biomass fuel capacities.

6. ACKNOWLEDGEMENT

We thank our colleagues who provided insight and expertise that greatly assisted the research.

NOMENCLATURE

C_p	Specific heat capacity ($J kg^{-1} K^{-1}$)
ER	Equivalence ratio

LHV	Lower heating value (kJ kg ⁻¹)
HHV	Higher heating value (kJ kg ⁻¹)
m	Mass (kg)
P	Pressure (bar)
Q̇	Heat (W)
S/T	Steam to biomass ratio
T	Temperature (K)
Ẇ	Power (W)

Abbreviations

BC	Bottoming Cycle
CHP	Combined Heat and Power
CGE	Cold Gas Efficiency
FB	Fluidized Bed
FICFB	Fast Internal Circulating Fluidized Bed
GC	Gas Cycle
GT	Gas Turbine
HRSG	Heat Recovery Steam Generator
IBG	Integrated Biomass Gasification
IC	Integrated Cycle
ORC	Organic Rankine Cycle
ST	Steam Turbine

Greek letters

η	Efficiency
---	------------

REFERENCES

- Bocci, E., Sisinni, M., Moneti, M., Vecchione, L., Di Carlo, A. and Villarini, M., "State of art of small scale biomass gasification power systems: A review of the different typologies", *Energy Procedia*, Vol. 45, (2014), 247-256. (<https://doi.org/10.1016/j.egypro.2014.01.027>).
- Arnavat, M.P., Bruno, J.C. and Coronas, A., "Review and analysis of biomass gasification models", *Renewable and Sustainable Energy Reviews*, Vol. 14, (2010), 2841-2851. (<https://doi.org/10.1016/j.rser.2010.07.030>).
- Ozgoli, H.A., Ghadamian, H. and Pazouki, M., "Economic analysis of biomass gasification-solid oxide fuel cell-gas turbine hybrid cycle", *International Journal of Renewable Energy Research (IJRER)*, Vol. 3, (2017), 1007-1018. (<https://doi.org/10.20508/ijrer.v7i3.5814.g7131>).
- Ramzan, N., Ashraf, A., Naveed, S. and Malik, A., "Simulation of hybrid biomass gasification using Aspen plus: A comparative performance analysis for food, municipal solid and poultry waste", *Biomass and Bioenergy*, Vol. 35, (2011), 3962-3969. (<https://doi.org/10.1016/j.biombioe.2011.06.005>).
- Villarini, M., Marcantonio, V., Colantoni, A., Bocci, E., Villarini, M., Marcantonio, V., Colantoni, A. and Bocci, E., "Sensitivity analysis of different parameters on the performance of a CHP internal combustion engine system fed by a biomass waste gasifier", *Energies*, Vol. 12, (2019), 688. (<https://doi.org/10.3390/en12040688>).
- Bocci, E., Di Carlo, A., McPhail, S.J., Gallucci, K., Foscolo, P.U., Moneti, M., Villarini, M. and Carlini, M., "Biomass to fuel cells state of the art: A review of the most innovative technology solutions", *International Journal of Hydrogen Energy*, Vol. 39, (2014), 21876-21895. (<https://doi.org/10.1016/j.ijhydene.2014.09.022>).
- Dascomb, J., Krothapalli, A. and Fakhrai, R., "Thermal conversion efficiency of producing hydrogen enriched syngas from biomass steam gasification", *International Journal of Hydrogen Energy*, Vol. 38, (2013), 11790-11798. (<https://doi.org/10.1016/j.ijhydene.2013.07.022>).
- Kumar, A., Jones, D.D., and Hanna, M.A., "Thermochemical biomass gasification: A review of the current status of the technology", *Energies*, Vol. 2, (2009), 556-581. (<https://doi.org/10.3390/en20300556>).
- Marcantonio, V., Bocci, E., Ouweltjes, J.P., Del Zotto, L. and Monarca, D., "Evaluation of sorbents for high temperature removal of tars, hydrogen sulphide, hydrogen chloride and ammonia from biomass-derived syngas by using Aspen Plus", *International Journal of Hydrogen Energy*, Vol. 45, (2020), 6651-6662. (<https://doi.org/10.1016/j.ijhydene.2019.12.142>).
- Rahman, M.D.M., Henriksen, U.B., Ahrenfeldt, J. and Arnavat, M.P., "Design, construction and operation of a low-tar biomass (LTB) gasifier for rural applications", *Energy*, Vol. 204, (2020), 117914. (<https://doi.org/10.1016/j.energy.2020.117944>).
- Ahmed, T.Y., Ahmad, M.M., Yusup, S., Inayat, A. and Khan, Z., "Mathematical and computational approaches for design of biomass gasification for hydrogen production: A review", *Renewable and Sustainable Energy Reviews*, Vol. 16, (2012), 2304-2315. (<https://doi.org/10.1016/j.rser.2012.01.035>).
- Ozgoli, H.A., "Simulation of integrated biomass gasification-gas turbine-air bottoming cycle as an energy-efficient system", *International Journal of Renewable Energy Research*, Vol. 7, (2017), 275-284. (<https://doi.org/10.20508/ijrer.v7i1.5428.g6986>).
- Ozgoli, H.A., Safari, S. and Sharifi, M.H., "Integration of a biomass-fueled proton exchange membrane fuel cell system and a vanadium redox battery as a power generation and storage system", *Sustainable Energy Technologies and Assessments*, Vol. 42, (2020), 100896. (<https://doi.org/10.1016/j.seta.2020.100896>).
- Pfeifer, C., Schmid, J.C., Pröll, T. and Hofbauer, H., "Next generation biomass gasifier", *Proceedings of 19th European Biomass Conference and Exhibition*, Berlin, Germany, (2011), 1-7. (<https://doi.org/10.5071/19THEUBCE2011-VP2.3.24>).
- Hosseinpour, S., HajiSeyed Mirzahassemi, A., Mehdipour, R., Hemmasi, A. H. and Ozgoli, H.A., "Energy modeling and techno-economic analysis of a biomass gasification-CHAT-ST power cycle for sustainable approaches in modern electricity grids", *Journal of Renewable Energy and Environment (JREE)*, Vol. 7, (2020), 43-51. (<https://doi.org/10.30501/JREE.2020.106780>).
- Safari, S., Ghasedi, A.H. and Ozgoli, H.A., "Integration of solar dryer with a hybrid system of gasifier-solid oxide fuel cell/micro gas turbine: Energy, economy and environmental analysis", *Environmental Progress & Sustainable Energy*, Vol. 40, (2020), e13569. (<https://doi.org/10.1002/ep.13569>).
- Trieb, F., "Concentrating solar power for the mediterranean region", Final report by German aerospace center (DLR), Institute of technical Thermodynamics, Section systems analysis and technology assessment, (2005). (https://www.dlr.de/tt/Portaldata/41/Resources/dokumente/institut/systeme/projects/MED-CSP_Full_report_final.pdf), (Accessed: 16 April 2005).
- Azizaddini, S.N., Haghparast, A., Adl, M. and Hadjifari, P., "Assessment of gasification potential of agricultural and woody biomass resources in Iran", *International Journal of Environment and Bioenergy*, Vol. 3, (2012), 75-87. (<http://www.modernscientificpress.com/Journals/ViewArticle.aspx?gkN1Z6Pb60HNQPymfPQZA6c3PoRIUU8KyuL+AntiXnOzSTP1K6wFq+XYVRbDQeD>).
- Javanshir, N., Seyed Mahmoudi, S.M., Kordlar, M.A. and Rosen, M.A., "Energy and cost analysis and optimization of a geothermal-based cogeneration cycle using an ammonia-water solution: Thermodynamic and thermoeconomic viewpoints", *Sustainability*, Vol. 12, (2020), 484. (<https://doi.org/10.3390/su12020484>).
- Sun, L., Han, W., Jing, X., Zheng, D. and Jin, H., "A power and cooling cogeneration system using mid/low-temperature heat source", *Applied Energy*, Vol. 112, (2013), 886-897. (<https://doi.org/10.1016/j.apenergy.2013.03.049>).
- Rentizelas, A., Karellas, S., Kakaras, E. and Tatsiopoulos, I., "Comparative techno-economic analysis of ORC and gasification for bioenergy applications", *Energy Conversion and Management*, Vol. 50, (2009), 674-681. (<https://doi.org/10.1016/j.enconman.2008.10.008>).
- Kalina, J., "Integrated biomass gasification combined cycle distributed generation plant with reciprocating gas engine and ORC", *Applied Thermal Engineering*, Vol. 31, (2011), 2829-2840. (<https://doi.org/10.1016/j.applthermaleng.2011.05.008>).
- Puig-Arnavat, M., Bruno, J.C. and Coronas, A., "Modeling of trigeneration configurations based on biomass gasification and comparison of performance", *Applied Energy*, Vol. 114, (2014), 845-856. (<https://doi.org/10.1016/j.apenergy.2013.09.013>).
- Fortunato, B., Camporeale, S.M. and Torresi, M., "A gas-steam combined cycle powered by syngas derived from biomass", *Procedia Computer Science*, Vol. 19, (2013), 736-745. (<https://doi.org/10.1016/j.procs.2013.06.097>).
- Pallozzi, V., Di Carlo, A., Bocci, E., Villarini, M., Foscolo, P. and Carlini, M., "Performance evaluation at different process parameters of an innovative prototype of biomass gasification system aimed to hydrogen production", *Energy Conversion and Management*, Vol. 130, (2016), 34-43. (<https://doi.org/10.1016/j.enconman.2016.10.039>).
- Toonssen, R., "Sustainable power from biomass: Comparison of technologies for centralized or de-centralized fuel cell systems", Ph. D. Thesis, TU Delft, (2010). (<https://repository.tudelft.nl/islandora/object/uuid:57068674-c6fa-4d5c->

- [a7ca-a3e68c2d8324/datastream/OBJ/download](#)), (Accessed: 8 July 2010).
27. Jayah, T.H., Aye, L., Fuller, R.J. and Stewart, D.F., "Computer simulation of a downdraft wood gasifier for tea drying", *Biomass and Bioenergy*, Vol. 25, (2003), 459-469. ([https://doi.org/10.1016/S0961-9534\(03\)00037-0](https://doi.org/10.1016/S0961-9534(03)00037-0)).
 28. Siemens gas turbine portfolio, SGT-400 Industrial gas turbine, (2022). (<https://www.siemens-energy.com/global/en/offers/power-generation/gas-turbines/sgt-400.html>), (Accessed: 12 February 2022).
 29. Reliable steam turbines, Siemens steam turbine SST-110, (2022). (<https://www.siemens-energy.com/global/en/offers/power-generation/steam-turbines.html>), (Accessed: 12 February 2022).
 30. Di Carlo, A., Borello, D. and Bocci, E., "Process simulation of a hybrid SOFC/mGT and enriched air/steam fluidized bed gasifier power plant", *International Journal of Hydrogen Energy*, Vol. 38, (2013), 5857-5874. (<https://doi.org/10.1016/j.ijhydene.2013.03.005>).
 31. Marcantonio, V., Bocci, E. and Monarca, D., "Development of a chemical quasi-equilibrium model of biomass waste gasification in a fluidized-bed reactor by using Aspen Plus", *Energies*, Vol. 13, (2019), 53. (<https://doi.org/10.3390/en13010053>).
 32. Barrio, M., Göbel, B., Risnes, H., Henriksen, U., Hustad, J. and Sørensen, L., "Steam gasification of wood char and the effect of hydrogen inhibition on the chemical kinetics. Progress in thermochemical biomass conversion", Vol. 1, (2001), 32-46. (<https://doi.org/10.1002/9780470694954.ch2>).
 33. DeLasa, H., Ali, S.A.M. and Hossain, M.M., "Biological CO₂ fixation with production of microalgae in wastewater—a review", *Renewable and Sustainable Energy Reviews*, Vol. 76, (2017), 379-390. (<https://doi.org/10.1016/j.rser.2017.02.038>).
 34. Razak, A.M.Y., Industrial gas turbines, performance and operability, Woodhead Publishing Limited, UK, (2007). (<https://www.sciencedirect.com/book/9781845692056/industrial-gas-turbines>).
 35. Boyce, M.P., Handbook for cogeneration and combined cycle power plants, Second Edition, ASME Press, The USA, (2010). (<https://asmedigitalcollection.asme.org/ebooks/book/198/Handbook-for-Cogeneration-and-Combined-Cycle-Power>).
 36. Dahlquist, A., Genrup, M., Sjoedin, M. and Jonshagen, K., "Optimization of an oxyfuel combined cycle regarding performance and complexity level", *Proceedings of the ASME Turbo Expo 2013: Power for Land, Sea and Air*, Turbine Technical Conference and Exposition. Volume 2: Aircraft engine; Coal, Biomass and Alternative Fuels; Cycle Innovations, San Antonio, Texas, USA, (2013). (<https://doi.org/10.1115/GT2013-94755>).
 37. Hofbauer, H., Fercher, E., Fleck, T., Rauch, R. and Veronik, G., "Two years experience with the FICFB-gasification process", *Proceedings of the 10th European Conference and Technology Exhibition*, Wurzburg, Germany, (1998), 3-6. (<https://pivotalirm.com/files/tech/016.pdf>).
 38. Hofbauer, H., Rauch, R., Loeffler, G., Kaiser, S., Fercher, E. and Tremmel, H., "Six years experience with the FICFB-gasification process", *Proceedings of the 12th European Conference and Technology Exhibition on Biomass for Energy, Industry and Climate Protection*, Amsterdam, The Netherlands, (2002), 982-985. (https://www.researchgate.net/publication/228797225_Six_Years_Experience_with_the_FICFB-Gasification_Process), (Accessed: 21 June 2002).
 39. Pfeifer, C., Rauch, A.R. and Hofbauer, H., "In-bed catalytic tar reduction in a dual fluidized bed biomass steam gasifier", *Industrial & Engineering Chemistry Research*, Vol. 43, (2004), 1634–1640. (<https://doi.org/10.1021/ie030742b>).
 40. Marcantonio, V., Ferrario, A.M., Di Carlo, A., Del Zotto, L., Monarca, D. and Bocci, E., "Biomass steam gasification: A comparison of syngas composition between a 1-D MATLAB kinetic model and a 0-D Aspen Plus quasi-equilibrium model", *Computation*, Vol. 8, (2020), 86. (<https://doi.org/10.3390/computation8040086>).
 41. Eri, Q., Wu, W. and Zhao, X., "Numerical investigation of the air-steam biomass gasification process based on thermodynamic equilibrium model", *Energies*, Vol. 10, (2017), 2163. (<https://doi.org/10.3390/en10122163>).
 42. Nilsson, S., Gómez-Barea, A., Pardo-Arias, I., Suárez-Almeida, M. and de Almeida, V.F., "Comparison of six different biomass residues in a pilot-scale fluidized bed gasifier", *Energy & Fuels*, Vol. 33, (2019), 10978-10988. (<https://doi.org/10.1021/acs.energyfuels.9b01513>).



Research Article

The Influence of Research and Development Activities and NanoFab Centers on Product Development in Nanotechnology: Focusing on Solar Thermal Energy and Photovoltaic Technology

Amrollah Dehghani Sanij^a, Taghi Torabi^{b*}, Abbas Khamseh^c, Alireza Boshehri^d

^a Department of Technology Management, Sciences and Research Branch, Islamic Azad University, Tehran, Tehran, Iran.

^b Department of Economics, Sciences and Research Branch, Islamic Azad University, Tehran, Tehran, Iran.

^c Department of Industrial Management, Karaj Branch, Islamic Azad University, Karaj, Alborz, Iran.

^d School of Management and Soft Technologies, Malek Ashtar University of Technology, Tehran, Tehran, Iran.

PAPER INFO

Paper history:

Received: 09 July 2021

Revised in revised form: 12 October 2021

Scientific Accepted: 27 December 2021

Published: 05 July 2022

Keywords:

NanoFab,
Nanotechnology,
Research and Development,
Structural Equations,
Fuzzy Inference,
Renewable Energy

A B S T R A C T

This research aims to determine the influence of fundamental, applied, developmental research and Nanofabrication (NanoFab) centers on the final outcomes achieved by research and development activities, implying product development and value creation in nanotechnology. Data were collected through library studies and field studies in this study and research factors were also identified. To confirm the collected factors, structural equation technique and Smart PLS software were used and after confirming the research factors, the collected data were analyzed using fuzzy inference method and MATLAB software. The achieved results indicated that this field had the most performance despite the minimal influence of fundamental research on the final results of research and development activities and developmental research, while NanoFabs had the poorest performance with the highest influence on the final results of research activities. It is possible to conclude according to the research results that research and development activities at the fundamental and applied levels cannot easily be connected to the end ring, i.e., industry without NanoFab centers, and provide the final product and create value. Furthermore, providing NanoFab or NanoFabs with emphasis on the development of nanomaterial can significantly affect the development of renewable energies.

<https://doi.org/10.30501/jree.2022.292097.1222>

1. INTRODUCTION

Fossil fuel-based energy sources such as gas, coal, and diesel are the main energy resources of traditional generators in the power system and, fossil fuel energy production leads to air pollution by increasing the load demands. Thus, development of a Renewable Energy Sources (RES) based system is essential to ensure a reliable, low-pollution and inexpensive energy production [1]. Of course, the high penetration of Renewable Energy Resources (RERs) increases the fault current level of Direct Current (DC) microgrids, and it may cause miscoordination between protection devices [2]. In this regard, nanotechnology as a new wave of technology has a high capacity to transform industries. Many experts call nanotechnology the next industrial revolution that will influence all sciences [3]. Developing and applying nanotechnology is a comparatively new but quickly growing development in the field of renewable energy. Achieved advancements indicate that nanotechnology plays a significant role in all fields of renewable energy. In fact, it is possible to

state that nanotechnology can play a crucial role in achieving higher and more efficient energy storage and supply [4].

A special headquarter to develop nanotechnology was established in 2003 in Iran because of the significance and application of this technology and the necessity to help develop it. According to the strategic document on nanotechnology development, Iran should have ranked 15th in the three indices of science, technology, and market production during a period of ten years and by the end of 2013. Realizing the fourth rank in science production in 2013 indicates that this plan had been considered highly successful in the science index; however, the other two indices, despite all efforts, had no good global ranking. Iran has 44th rank in the Technology Development Index in the same year with a share of 0.03 % of the global market share. Failing to achieve the objectives determined in technology and market indices as well as the slow speed of innovation in this field, despite the high rate of scientific production, represent a complex issue that required greater investigation [5]. In fact, the companies active in the field of nanotechnology and their market share have not grown in accordance with the growth of fundamental research in this field. It is possible to conclude that the

*Corresponding Author's Email: tttorabi@gmail.com (T. Torabi)

URL: https://www.jree.ir/article_153080.html

Please cite this article as: Dehghani Sanij, A., Torabi, T., Khamseh, A. and Boshehri, A.R., "The influence of research and development activities and NanoFab centers on product development in nanotechnology: Focusing on solar thermal energy and photovoltaic technology", *Journal of Renewable Energy and Environment (JREE)*, Vol. 9, No. 3, (2022), 87-100. (<https://doi.org/10.30501/jree.2022.292097.1222>).



improvements made in fundamental research that have taken place frequently at universities have failed to facilitate development of the technology, to present a product and create wealth, and to ensure effective coherence and relationship among fundamental, applied, and developmental researches. Accordingly, this research aims to investigate the strengths and weaknesses of fundamental, applied, and developmental researches in the field of nanotechnology in Iran and to calculate the influence rate of each factor on the final results of research and development activities. Also, this research aims to examine the type of the requirements to create a connection among fundamental, applied, and developmental researches in the field of nanotechnology so that fundamental research conducted at universities yield developmental research in the industrial sector.

Accordingly, Therefore, two questions can be asked for this research:

1 -Why do the industrial sector fail to apply the results of academic research to develop products and create value in the field of nanotechnology?

2- What are the strengths and weaknesses of research and development activities in nanotechnology?

2. LITERATURE REVIEW

Global experience confirms that the countries that have dedicated the greatest costs to conduct different kinds of research are those that enjoy advanced technology and industry [6]. Table 1 shows the top 15 countries in terms of research and development expenditure in 2019. In this table, the United States, China, and Japan are ranked first to third. Another important indicator of R&D is the percentage of R&D expenditures of the Gross Domestic Product (GDP). As shown in this table, South Korea ranks 5th in terms of R&D after Germany. 4.6 % of its GDP is dedicated to research and development, which is the highest value among the 15 countries evaluated [7].

Table 1. Top 15 countries in terms of research and development expenditures

Rank	Country	Expenditures on R&D (billions of US\$, PPP)	% of GDP PPP
1	United States	612.714	3.1
2	China	514.798	2.2
3	Japan	172.614	3.2
4	Germany	131.932	3.2
5	South Korea	100.055	4.6
6	France	63.658	2.2
7	United Kingdom	51.702	1.8
8	Taiwan	42.945	3.5
9	Russia	38.549	1.0
10	Italy	33.840	1.4
11	Canada	26.636	1.5
12	Turkey	24.827	1.1
13	Spain	22.468	1.3
14	Netherlands	20.167	2.2
15	Sweden	17.722	3.4

The remarkable thing about emerging technologies, such as nanotechnology, is that these technologies have often been initially developed out of intense research by government research institutes and have gradually encouraged commercial companies to conduct applied and developmental research. In this respect, it is possible to distinguish between the roles of universities, government research institutes, and private companies in the field of developing these technologies [8], but the essential point is that research and development is a dynamic and continuous process of fundamental, applied, and developmental researches. Therefore, it is required that the scientific results related to each stage be used as valuable reserves as input to the next stage [9]. Accordingly, Research & Technology Organizations (RTOs) are the links between scientific research findings on the one hand and technical application on the other, and they are the link that connects universities to industry [10]. NanoFabs centers are the link between academic and industrial researches in nanotechnology and play the role of research and technology organizations in this field. NanoFabs are national, educational, and service centers with free access that have centered on academic and industrial applications to produce nanotechnology products [11].

2.1. Types of research and development activities

It is possible to classify the research and development activities into three main classes: fundamental research, applied research, and development. Therefore, it is required that nearly every activity be performed in particular environments and centers. Also, one should expect specific outputs from each of these centers. In fact, the direct path of research results in universities to end-users has not been defined [12]. Burns & Rajcan [13] stated the most outstanding output of the university in published articles. Ivančević & Luković [14] introduced factors including the number of articles, number of references, professors, and graduates as the main criteria to evaluate at the academic centers. Also, Zarei et al. [15] stated that universities, research institutes, and the industrial sector were responsible for conducting research and development activities. This study stated the results of research and development activities in universities as the number of articles as well as the indices of research organizations as the costs spent on conducting the research and development, product development, and process or technology development. Furthermore, the output of research and development in the industry has been considered to be patent registration and market development. Maghferti et al. [16] considered the evaluation indices of the research and development department of industrial units as product development, new process and technology, reduction of the production costs, patenting and optimization of the current products, and market development.

Unfortunately, the government has not been significantly successful in promoting commercialization activities in universities after spending large amounts in Malaysia. The Ministry of Higher Education reported in 2008 that only 58 products were successfully commercialized (i.e., 18 %) among 313 projects recognized with commercial potential. This amount was decreased to 6 % in the report published in 2010 [17]. Ali & Sinha [18] expressed the improvement of performance, reduced production costs of commercialized products, and also explained that by presenting new products as an achievement of nanotechnology, the gap between

fundamental research and applying the nanotechnology in the industry is one of the current difficulties. Shamsi and Noor Mohammadi [19] considered factors such as the number of patents and the costs spent on conducting the research and development among the evaluation indices of the industrial sector. Chen et al. [20] also mentioned the number of articles and patents as the output of these activities at the national level. Shapira et al. [21] conducted a study on research and development activities in various countries from the stages of exploration to commercialization and considered the articles and patents as research and development indices in universities and industrial centers, respectively, and also considered the number of nanotechnology companies as an index to develop the nanotechnology. Wang & Guan [22] introduced patents as output indices of universities, research institutes, and industry in nanotechnology and concluded that the share of industry in patents was higher than the other two sectors in industrialized countries. Iran Nanotechnology Innovation Council (INIC) [23] has presented indices such as the number of articles, related references, the number of companies, and nanotechnology products separately in various industrial fields. Additionally, Stat Nano [24] statistics and information database produced indices such as the amount of investment, the number of companies, and Nano products in different countries in order to evaluate the final output of research and development activities.

2.2. The role of research and technology organizations in research and development

Research and technology organizations have an intermediary role between industry and university, particularly in developing countries. These organizations form a significant part of the infrastructure to develop science, technology, and innovation and play an intermediary role between research and production sections [25]. In general, research and development organizations are the ones that provide research and development, technology, and innovation services to the government, industry, markets, and other customers. These organizations are mission-oriented which make it possible to increase economic competitiveness and support innovation and small- and large-sized companies in all fields of the economy in order to assist the government [26].

Aleman et al [27] believed that research and technology organizations had a significant intermediate role in innovation systems and concentrated on applied research. Furthermore, the Research Center of the Islamic Consultative Assembly [28] introduced these organizations as mission-oriented groups that try to solve real-world problems and despite the diversity of their activities, emphasize particularly applied research. Figure 1 shows the functions of research and technology organizations in developing and developed countries.

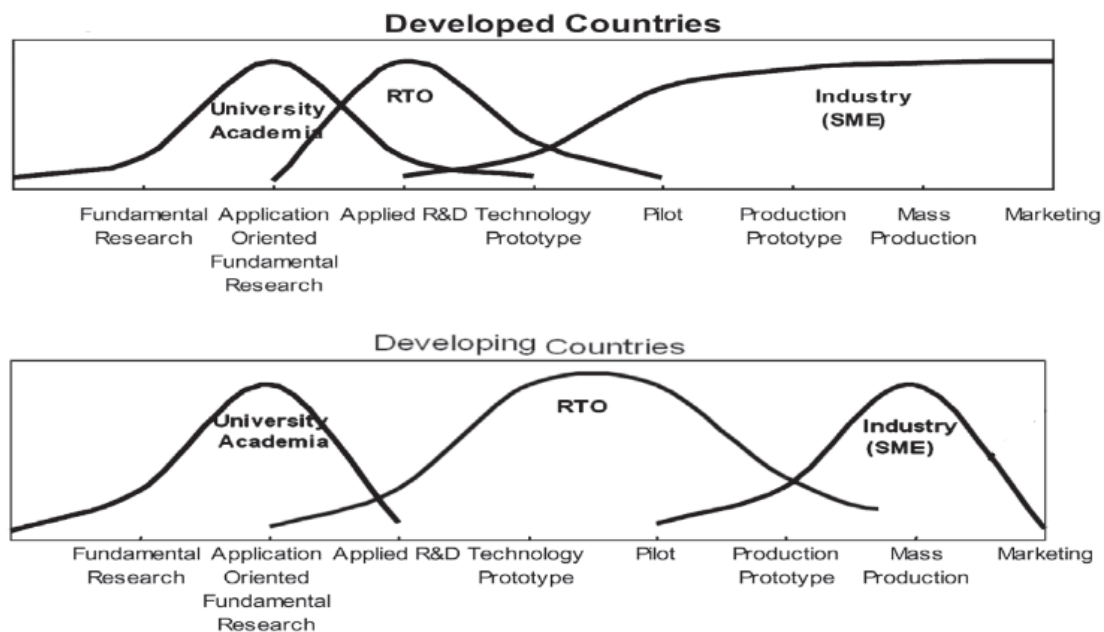


Figure 1. Function of research and technology organizations in developing and developed countries [22]

2.3. NanoFabs or research and technology organizations in the field of nanotechnology

NanoFabs play the role of research and technology organizations in nanotechnology, and various countries have created research and development centers in the field of nanotechnology in order to develop nanotechnology. Nanotechnology can create significant outcomes for industry and economics, but it still is an emerging technology at the university level [29]. NanoFabs are required to transfer technical knowledge and industrial research results to companies that are able to use nanotechnology. NanoFabs cooperated with the universities and the private sector to perform the research activities in nanotechnology and present

a diverse range of high-tech services to satisfy the requirements of companies [30]. Chung et al. [31] established one of the strategies for developing nanotechnology in South Korea and there were also two NanoFab centers called the National NanoFab Center (NNFC) and the Korea Advanced NanoFab Center. The National Research Council (NRC) [32] has evaluated the Center for Nano Science and Nanotechnology (CNSNT) in a report as one of the main NanoFabs in the United States. This evaluation introduces this NanoFab as unique organization to provide services to users in all industrial, academic, and government sections and recommends: it is required to increase its focus on the industry as its main customer. The Center for Nano science and Nanotechnology [33] in the United States also declares that

this NanoFab is responsible for supporting companies active in nanotechnology in different stages of research and development to manufacturing the product.

2.4. Application of nanotechnology in renewable energies

The materials with nanostructure provide potential advantages for a wide range of renewable energy applications that rely principally on connectors to separate the loads such as photovoltaic, thermoelectric, and electrochemical energy storage. Applying nanostructures enables scientists and engineers to increase the chemical active level for any determined volume in electrochemical systems and increases energy and power density [34]. Also, nanomaterial includes a wide range of materials including Nano crystals, Nano composites, carbon nanotube (CNT), and metal-based nanomaterial that are possible for use to improve renewable energy sources; for example, it is possible that wind energy efficiency be improved using lighter nanomaterial with greater resistance in the rotor blades. Nano-coatings can be used to prevent corrosion in tidal energy equipment, and it is possible to use Nano composites in order to provide higher resistance to drilling machine wear in geothermal energy. Nano crystals have a significant role in increasing the efficiency of solar cells [35]. It appears in this field that nanotechnology is mostly applied in the field of efficient use of solar energy applying photovoltaic (PV) cells. The PV system has a high potential to win energy supply challenges in developing

countries. Also, batteries and capacitors are the most significant energy storage systems in energy storage. Carbon nanotube (CNT) is presently applied to replace regular batteries with graphite electrodes [36]. The National Nanotechnology Initiative (NNI) was established in 2001 in the United States to coordinate research and development activities at three levels: science, technology, and nanotechnology. NNI has created national infrastructure using advanced equipment that is required to conduct research, but all groups or institutions cannot afford its cost to purchase it. NNI has also produced NanoFabs in which each one has special features and expertise that can be used to solve complex problems if required [37]. NNI defined the Solar Nanotechnology Project in 2010 in order to understand the phenomena of energy conversion and storage on the Nano scale and improve the properties and features of nanomaterial for solar technology. The following three axes were identified to concentrate on research and development in this project:

1. Improving the production of photovoltaic solar power with nanotechnology;
2. Improving the production of solar thermal energy and its conversion with nanotechnology; and
3. Improving the conversion of solar energy into fuel with nanotechnology [38].

Table 2 presents the summary of factors and indices identified in Section 2.

Table 2. Indices that define the research factors

Factor(variable)	Index
Basic research	Number of articles published in international journals
	H-index of published articles
	Number of professors in the field of nanotechnology
	Number of nanotechnology majors in universities
	Number of nanotechnology graduates
	Laboratories and university equipment
Applied research	Defining the academic theses based on industry requirements
	Producing Prototype
	Number of patents by research centers
	Simulation of a system, product, or process
Developmentl research	Presence of R&D unit in the industry sector
	R&D costs in the industrial sector
	Number of patents by industrial centers
	Reducing the costs for production
	Pilot production (industrial product sample)
NanoFab	Producing the prototypes for a new product according to the requirements related to the industry
	Establishing the specialized laboratories for the final product
	Providing standards and achieving domestic and international approvals
	Granting R&D facilities for startups and knowledge-based companies
	Access to measuring equipment
	Production equipment and methods for production
	Number of researchers
Developing the product and creating value	Increasing the market share
	Number of commercialized products
	Producing nanomaterial
	Producing intermediate nanomaterial
	Number of companies active in producing the nano products
	Longer life of products
	Improving the performance of available products

3. METHODOLOGY

First of all, this study emphasizes the main factors affecting the value creation from research and development activities in the nanotechnology field and also, extracts the characteristics of these factors by the study of research literature, theoretical basis, and exploratory interviews and the related indices have been confirmed from the viewpoint of experts. Thereafter, on the basis of the confirmed factors and indices, the questionnaire of the inquiry was compiled and the validity and stability of it were tested using the Confirmatory Factorial Analysis method and the employment of the Smart PLS3 software. Afterwards, the conceptual method of the research was prepared on the basis of the literature of the subject and confirmed factors. In the final phase, the extracted model was validated under the employment of the fuzzy interference

method and the MATLAB software. Also, in terms of purpose, considering the viability of the results and the special nanotechnology development, staff and companies are active and the nanotechnology field this research is of a practical type. Since the purpose of the study is to obtain a model for accomplishing research and development activities. By considering the unanimity of a group of professors and experts in the field of nanotechnology, the proposed methodology is a development methodology and our research is indeed of survey research type.

3.1. Administrative model of the study

Considering what was mentioned in the previous section, the administrative model of the inquiry can be described in Figure 2.

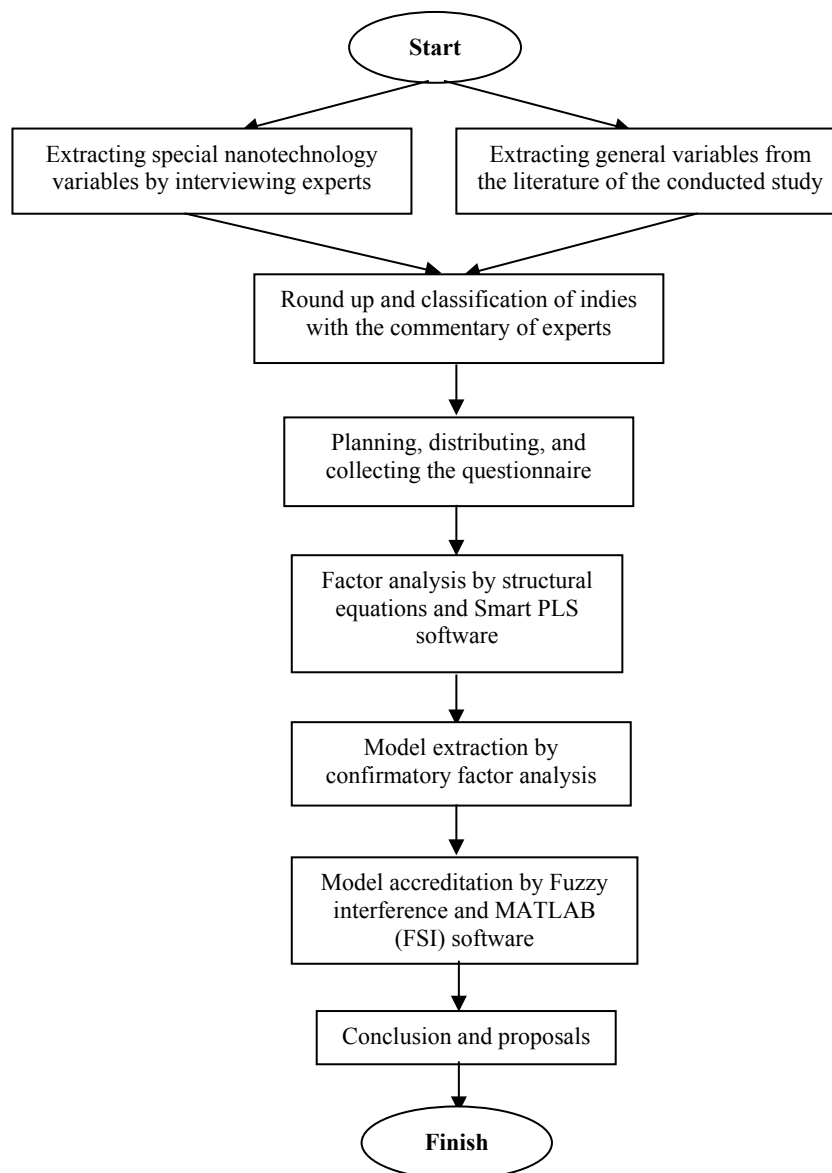


Figure 2. Executive model

3.2. Methods and tools of data collection

In order to collect data in this study besides library studies, interview with experts, field investigations, and collection of information using a questionnaire were conducted. The most important methods of data collection are given below:

Library studies: In this section, librarian sources, Farsi and English articles as well as books that are relevant to the subject of inquiry and some related websites were employed in order to collect information in the field of theoretical basis and the literature of the subject of inquiry.

Field researches: Considering that the purpose of this research is to study the effect of research and development activities and NanoFab centers on the development of the product in nanotechnology, a narrow rationalist viewpoint cannot be the loan basis of research. Hence, the compound quantitative and qualitative approach was added to the work formula. First of all, in this research, the viewpoint of experts that was obtained by interviews in terms of factors and indices related to the subject of research, which was extracted by librarian studies, was improved and confirmed. At the next stage, a questionnaire was employed to collect information.

Questionnaire: The type and nature of this study were added to the questionnaires or conducted as explained below. Data collection was achieved through the use of mansion questionnaires. The first questionnaire computed the effect level of each index related to research factor and the second questionnaire determined the function level of each of the mentioned indices in the field of nanotechnology. According to these two questionnaires, 22 indices were distributed in the form of five factors within the intended sample and the respondents assessed the indices.

3.3. Statistical population and determination of research sample size

In this study, limitation of access to experts and the low possibility of their response determine the statistical population; in this state, judgment sampling can be used to determine the sample size.

Judgment sampling is the choosing of test subjects that are highly qualified to provide necessary information and it is used when a limited category of individuals has the intended information within grasp. The statistical population of this

research is composed of special staff managers of nanotechnology development, president and managers of Nano companies who possessed experience and research and development activities and product development. Thus, employing the judgment sampling method and number of 32 individuals were selected as sample size with the two following characteristics:

1. Experts and managers of nanotechnology development staff holding Master’s or higher degrees in education with over 5 years of occupational proceedings and being familiar with nano companies’ research and development activities.
2. Managers of nano companies with an age rank higher than 5 years possessing experience and research and development activities and product development.

Table 3 shows the information on the indices of population description of sample size.

Table 3. Population properties of the respondents

Education	Master’s degree 62 %	Doctorates 38 %
Sex	Male 75 %	Female 25 %
Occupation	Nano staff managers 21 %	Nano company managers 79 %
Occupational precedence	Over 5 years	

3.4. Conceptual model of the study

Figure 3 shows the conceptual model, which is the outcome of literature review and variable effects of the study on each other.

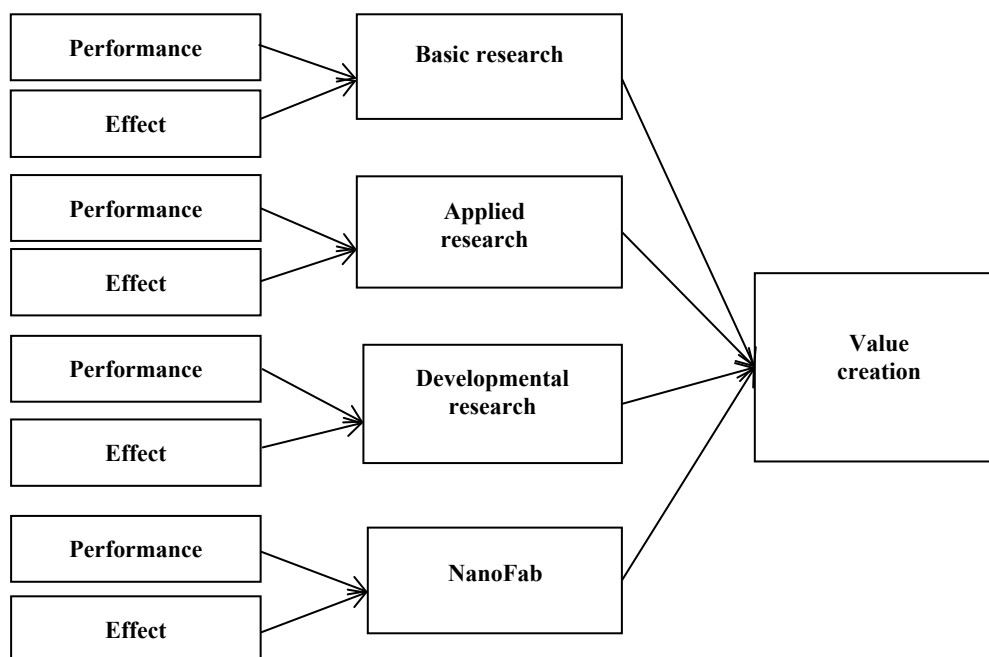


Figure 3. Conceptual model of research

3.5. Methods and tools of data analysis

In this inquiry, the results obtained from the questionnaire are classified and rounded up. Necessary diagrams are drawn based on descriptive statistics. To this end, task Exel and

SPSS software were put to use. Moreover, to assess the stability of the questionnaire, Cronbach's alpha coefficient in the SPSS software was used. In the following, to obtain the final model of the research and its fitting, the smart PLS 3 software was employed to perform confirmatory factor

analysis with the purpose of confirming the construct of research factors, and the integrity of the buoys used in the questionnaire should be ensured to measure the relevant variable. Finally, MATLAB was employed in conjunction with the fuzzy interference technique for fitting the conceptual model of the research and measuring the degree of the effects of independent variables on dependent variables.

4. FINDINGS

4.1. Standard coefficient estimation test

Figure 4 shows the number of factor loads of the research variables and also the measures related to each factor that also shows the estimation of factor loads with standard coefficients.

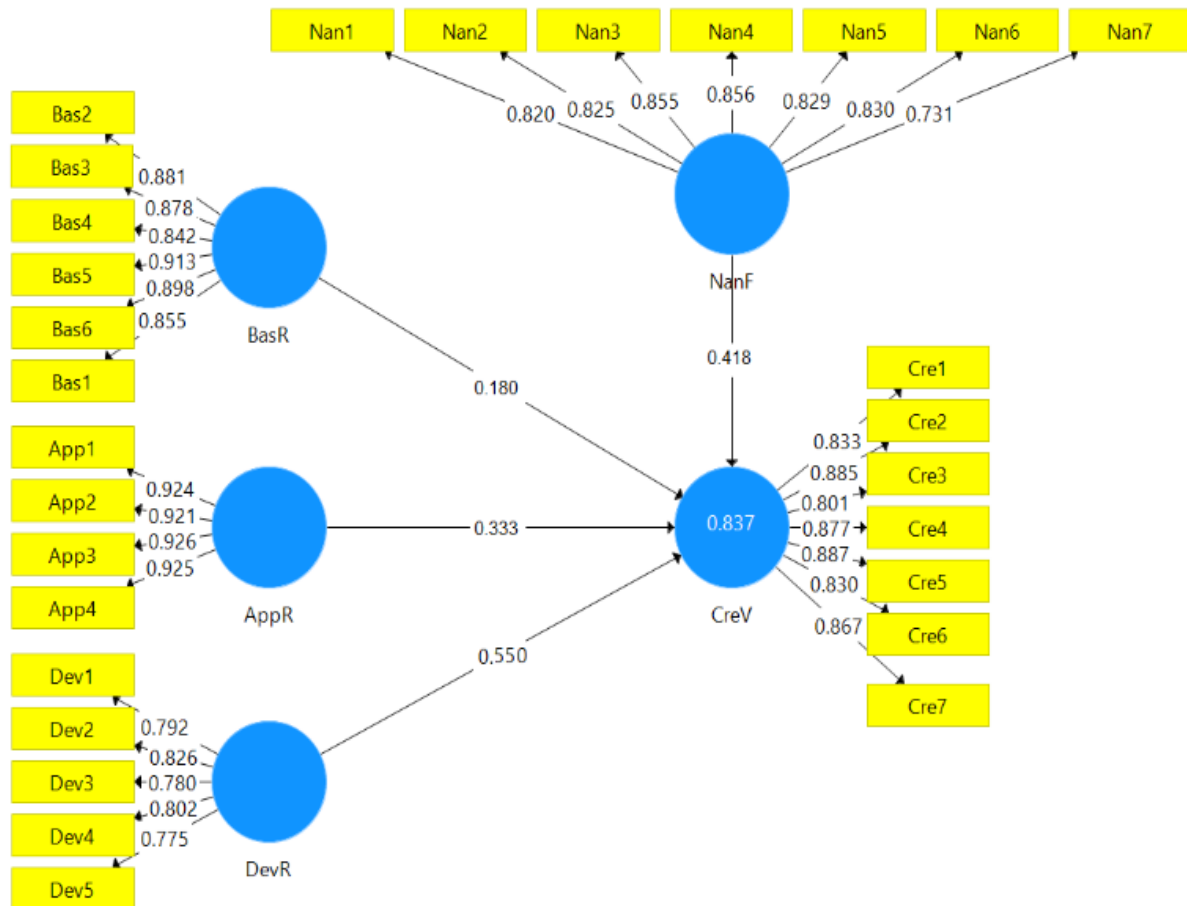


Figure 4. Measurement model in the standard coefficient estimation state (factor load)

4.2. Structural model analysis

Path analysis is a statistical method that uses standard multivariate regression coefficients in structural models and aims to gain quantitative estimates of the causal relationships between a set of variables. Table 4 presents the influence rate of each research factor on value creation.

4.3. Design of a fuzzy inference system

Fuzzy logic presents a method that is possible to use a broad variety of information, objective data, quantitative information, opinions, and subjective judgments to describe phenomena [39]. Fuzzy inference system is one of the most effective tools used in situations where we use the knowledge of experts. In a fuzzy inference system, researchers can identify and predict the relationships between variables based on fuzzy logic and the available basic and limited information on a phenomenon [40]. In fuzzy inference systems, experts are consulted to receive their expert opinions on model variables in the form of a set of fuzzy if-then rules. This set operates as an inference engine and combines the inputs of this system based on this inference engine, leading to the mapping of the input space to the output space.

Table 4. Path coefficients of research factors in factor analysis

Factors affecting product development and value creation from R&D activities in nanotechnology	Path coefficient
Basic research	0.18
Applied research	0.333
Developmental research	0.55
NanoFabs	0.418

4.3.1. Fuzzy sets

Fuzzy sets represent a mathematical method to express linguistic variables. Fuzzy set theory can express many concepts and expressions in mathematical language and provide the basis for reasoning, inference, control, and decision-making in conditions of uncertainty. According to fuzzy logic, definition words including low, medium, high or bad, good, excellent, etc. are interpreted to certain defined numbers.

4.3.2. Defining the membership functions for the input and output variables

A set of membership degrees of the members of a fuzzy set such as A is called the membership function of the set A. The membership function is a mapping of the members of the set A in the range of [0,1] so that $A: y \rightarrow [1,0]$. In general, this type of mapping can be considered as a membership function of fuzzy collection and fuzzy systems; triangular, trapezium, Gaussian, belle shirt, ring-shaped, and left and right membership functions are a few to mention. Triangular and trapezium membership functions are very versatile because of the simplicity of their theorem and optimality of conclusions. These membership functions are linear, but the other mentioned membership functions are described as nonlinear membership functions. In this study, the triangular membership function is used.

Figure 5 shows the triangular fuzzy number. The parameters m , l , and u indicate the lowest possible value, the highest expected value, and the largest possible value in order to describe a fuzzy number, respectively.

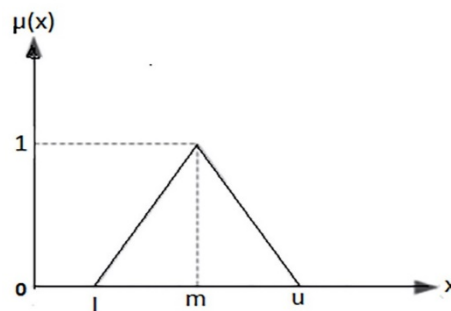


Figure 5. Fuzzy triangular number

4.3.3. Designing the system input component (Sub-FIS)

The independent variables are influenced by two inputs: the influence rate and the performance rate. Hence, they create the sub-FIS of the system. Figure 6 presents four system inputs.

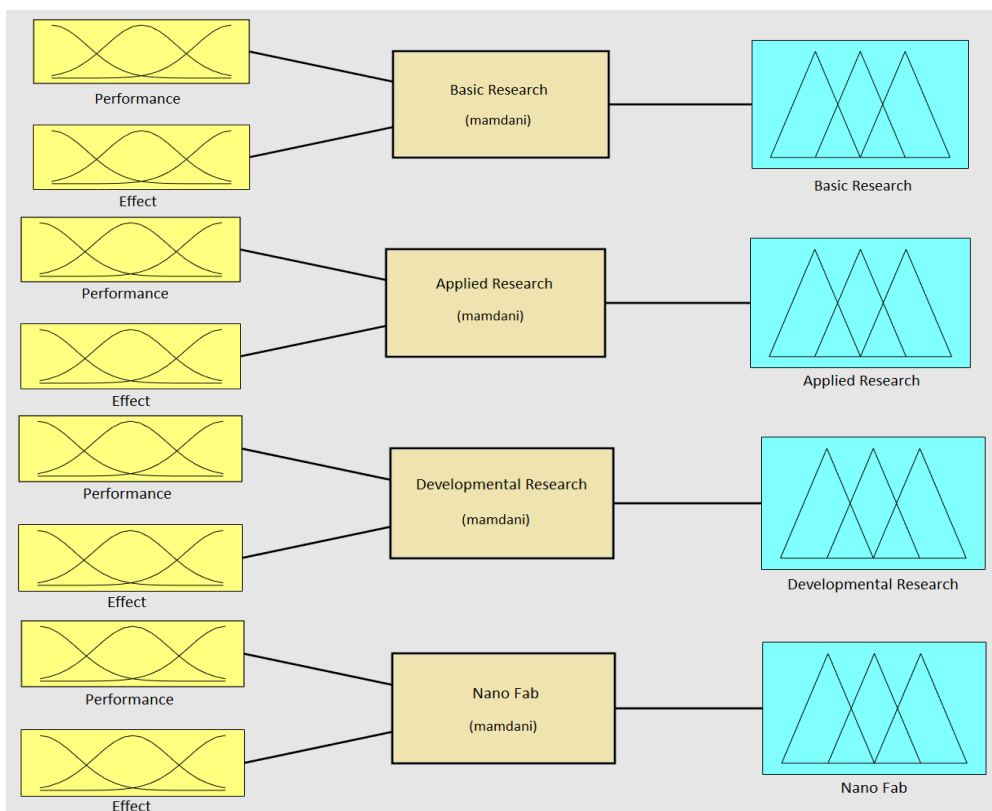


Figure 6. System input components

4.3.4. Fuzzy value of variables for Sub-FISs

Language variables including the influence and performance of each independent variable on the dependent variables have

been predicted based on the questionnaire. Accordingly, it is required to determine the mathematical fuzzy value equivalent to the language variables. Table 5 shows this equivalence.

Table 5. Fuzzy value of language variables

Linguistic variables of performance (input)	Linguistic variables of effect (input)	Linguistic variables of factors (output)	Definition interval (Mathematical fuzzy value)
Very weak	Very low	Attenuation	(1,4)
Weak	Low	Shortage	(2.5,5.5)
Medium	Medium	Balance	(4,7)
Well	High	Adequate	(5.5,8.5)
Very well	Very high	Affluence	(7,10)

It is possible to draw the membership functions for the Sub-FISs according to the mathematical fuzzy value defined

in Table 5. Figure 7 presents the drawing of membership functions for Sub-FIS.

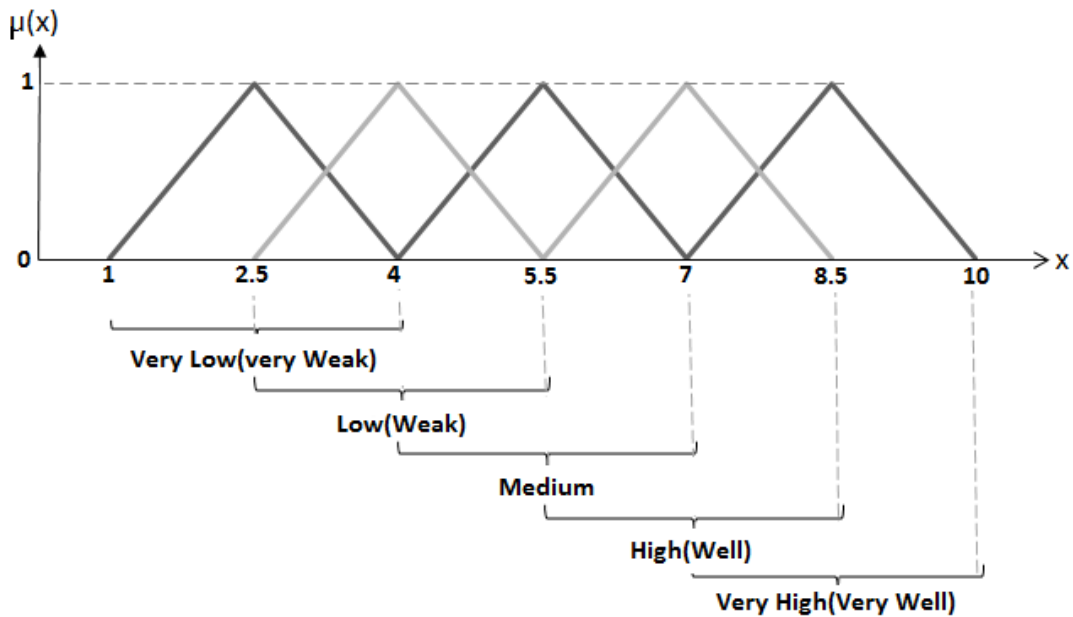


Figure 7. Sub-FIS membership functions

4.3.5. Structuring fuzzy inference rules

The most significant part of a fuzzy system is its rule base. This database is a set of logical if-then rules that result in mapping input variables to output variables. In the present study, inferential rules were designed based on experts' knowledge and interviews in the field of nanotechnology. Each factor in this study including basic, applied, developmental research, and NanoFabs was evaluated in terms of effect rate and performance rate and then, the inference rules of output were expressed with different input

combinations. Table 6 summarizes the fuzzy inference rules for Sub-FISs.

4.4. Designing the key components of value creation of R&D results

In fact, the output of the models of the previous stages (Sub-FISs) is the input of this stage in the main FIS. Figure 8 shows the overall designed fuzzy system related to the value creation of R&D results.

Table 6. Rules of fuzzy inference research

Effect	High and Very high	Attenuation ¹	Shortage ²	Balance ³
	Medium	Shortage	Balance	Adequate ⁴
	Low and Very low	Balance	Adequate	Affluence ⁵
		Weak and Very weak	Medium	Well and Very well
Performance				
1- It should have special support to correct the input-output in the "attenuated" state. 2- It must be amplified in the "shortage" state for the input-output modifying. 3- The input does not need to be modified in the "balance" mode. 4- The input should not be amplified in the case of "adequate". 5- The input should not be completely amplified in the case of "affluence".				

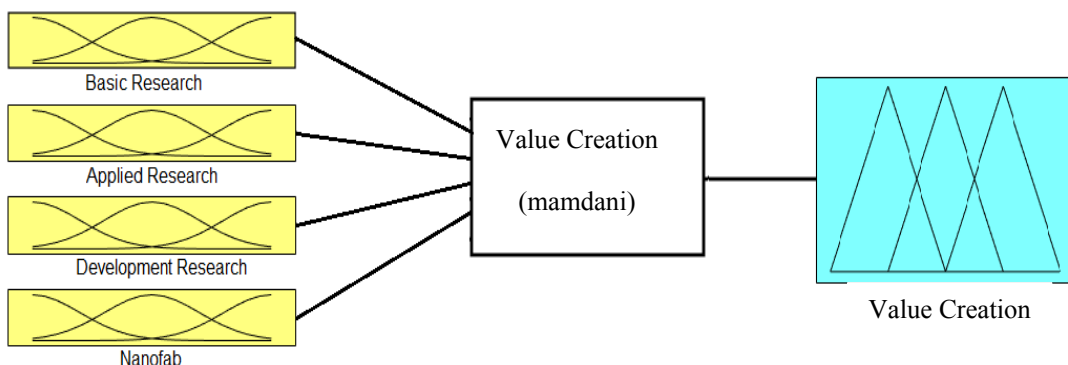


Figure 8. Key factors in creating value from R&D results

4.4.1. Fuzzy value of the main FIS variables

Table 7 shows the fuzzy values of the linguistic variables for the main inference system with triangular membership functions.

Table 7. Fuzzy values of Linguistic variables for the original FIS

Linguistic variables of factors (input)	Value creation linguistic variable (output)	Definition interval (Mathematical fuzzy value)
undesirable	undesirable	(1,6)
desirable	desirable	(4,8)
excellent	excellent	(6,8)

4.5. Implementing the fuzzy inference mathematical model

Table 8 presents the results of implementing the mathematical model in the Sub-FISs.

Table 8. Results of implementing the mathematical model for Sub-FISs

	Basic research	Applied research	Developmental research	NanoFabs centers
Performance	7.1	3.4	3.3	2.1
Effect	3.2	5.2	7.2	6.8
Result	7.43	4.4	3.23	1.38

The output of these Sub-FISs is applied as the main FIS input to evaluate the value creation of R&D activities after implementing Sub-FISs. Table 9 indicates the values of these inputs and outputs in the main model. In addition, Figure 9 shows these results including an image of the original FIS rules database. A fuzzy inference system generates the output by receiving input using rule-based inference motors and other parts of fuzzy systems such as fuzz makers and non-fuzzmakers. Fuzzy rules are the phrases with a fuzzy if-then construct in which each of these compounds affecting the rules of indices is determined. Using the graphic section of fuzzy logic in MATLAB software, Figure 9 shows the schematic presentation of a fuzzy inference with a triangular membership function for the four inputs of

fundamental research with a value of 7.43, functional research with a value of 4.4, developmental research with a value of 3.23, and NanoFab centers with a value of 1.38. The output of the system (value creation) is an equivalent of 3.71.

Obviously, value creation performance of R&D activities was estimated at 3.71, being in the undesirable range. Figures 10-A to 10-C show three curves of factors effective in the value creation of R&D activities. The inputs were compared with each other in pairs in each of these curves and their influence on the level of value creation performance of R&D activities was shown.

Figure 11 shows the results of implementing the mathematical model in the fuzzy inference system.

Table 9. FIS input and output values related to value creation performance of R&D activities

Basic research	Applied rresearch	Developmental research	Centers of NanoFabs	Value creation
7.43	4.4	3.23	1.38	3.71

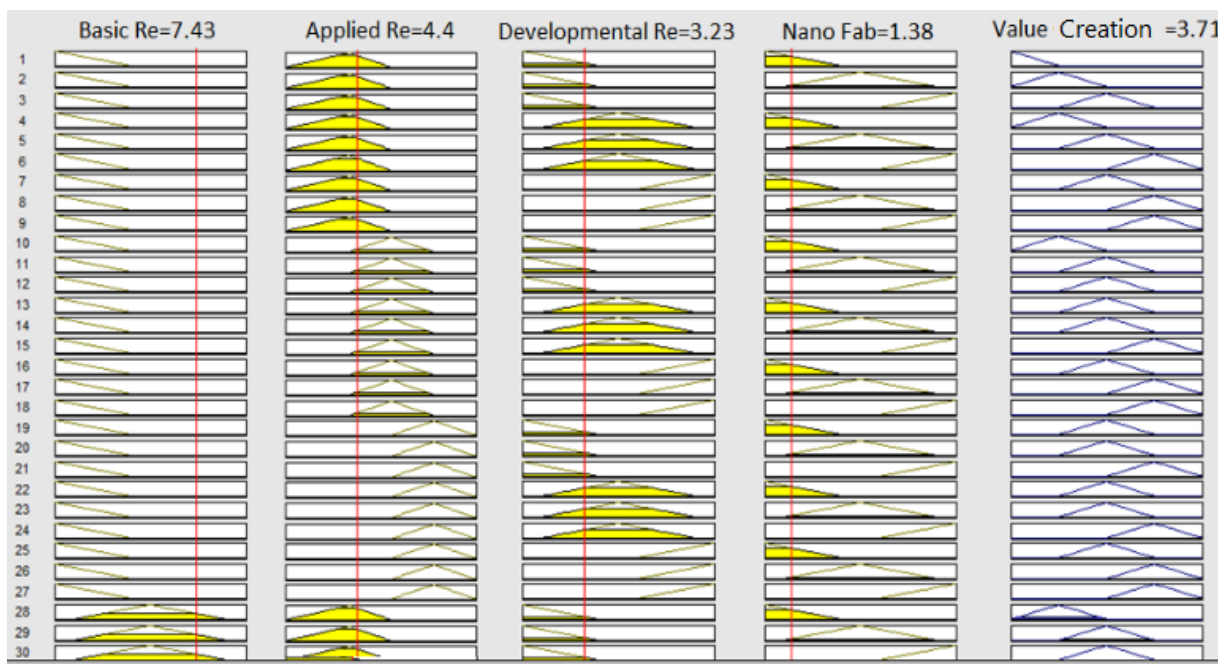


Figure 9. Value creation rules database of R&D activities

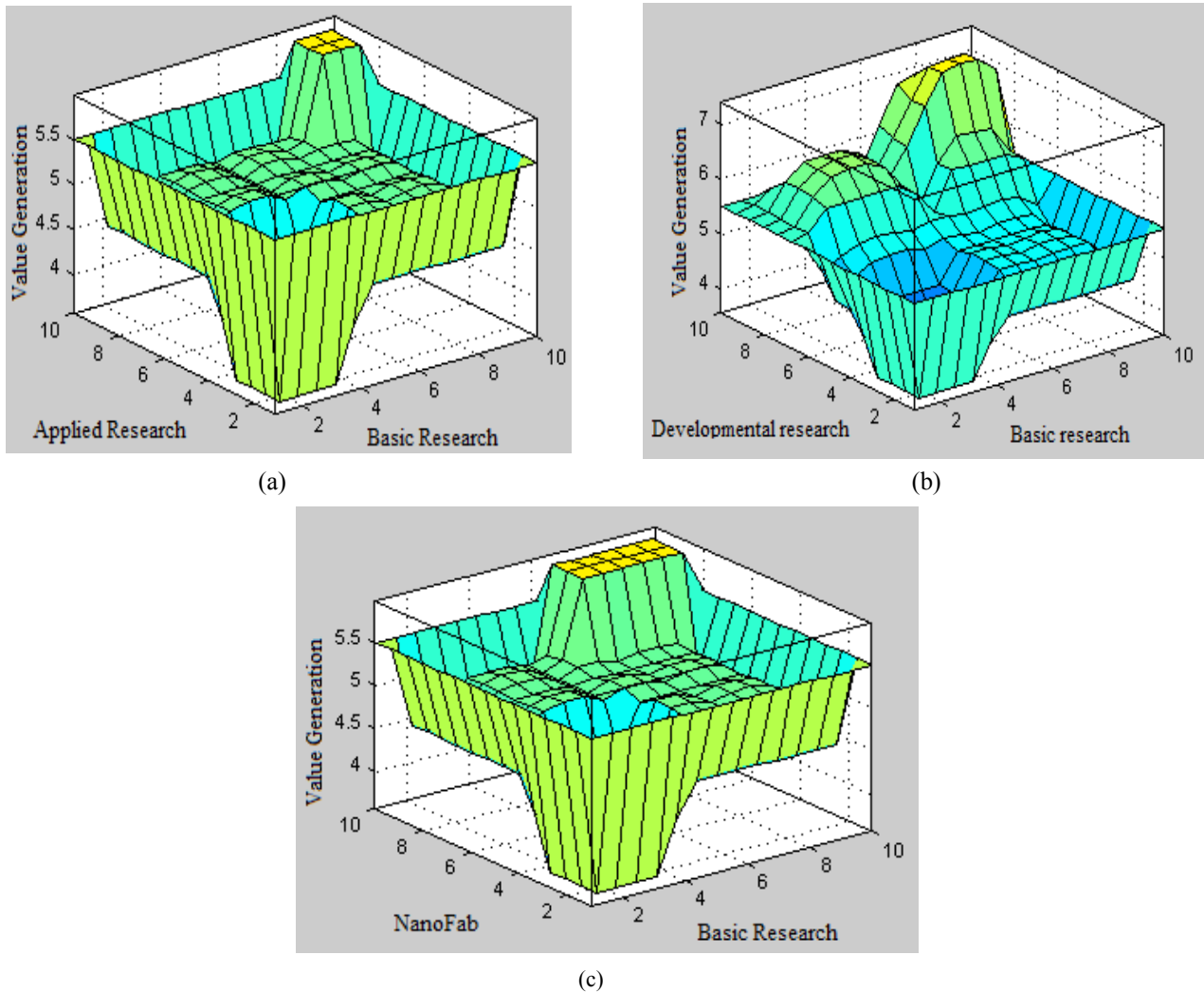


Figure 10. a) Influence curve of applied and basic research on output, b) Influence curve of developmental and basic research on output, c) Influence curve of NanoFab and basic research on output

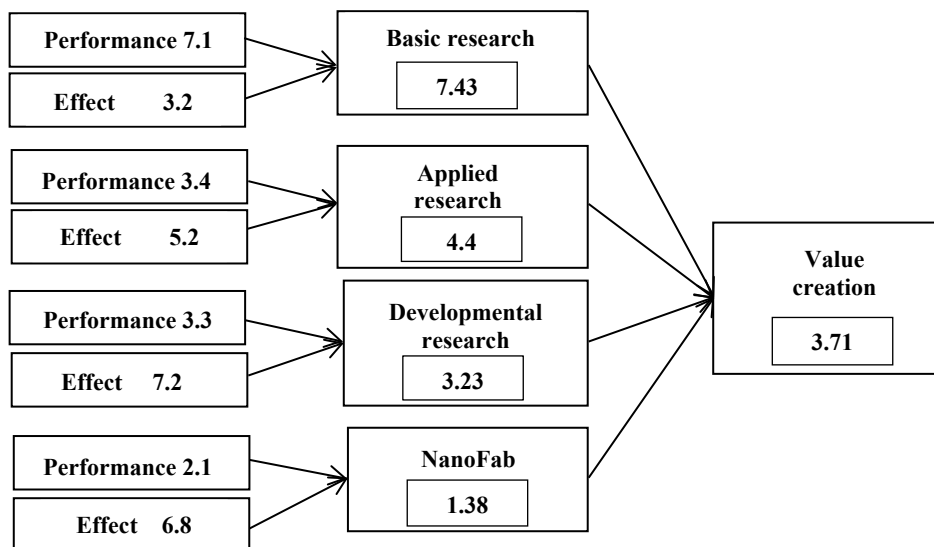


Figure 11. Implementation results of the mathematical model

5. DISCUSSION AND CONCLUSIONS

It is required to determine the position of each of the system inputs to analyze the results, according to Table 6, which is actually a fuzzy map of the rules expressed for the system. Based on the results, Table 10 shows the position of the

inputs. As observed earlier, none of the inputs are in the balance state.

In the following, the status of each of the inputs is examined according to their position in Table 10 as well as the extent of their impact and performance on the output.

Table 10. State of system inputs according to performance and its influence rate on output

Effect	High and Very high	Attenuation (Development Research) (NanoFab)	Shortage	Balance
	Medium	Shortage (Applied Research)	Balance	Adequate
	Low and Very low	Balance	Adequate	Affluence (Fundamental Research)
		Weak and Very weak	Medium	Well and Very well
Performance				

Fundamental research: Fundamental research is in affluence position, indicating that input should not be reinforced. Fundamental research with the score 3.2 is in the fourth rank in terms of the impact on the output, and it affects the output insignificantly among the various inputs of the system while it has the highest performance and has the score 7.1. It is possible to attribute this issue to Iran's high ranking in publishing scientific articles in nanotechnology.

Applied research: Applied research is in a shortage state, indicating that the input should be amplified to modify the output. Applied research with a score of 5.2 is in the medium state and the third place in terms of influence on the output; however, it is in the weak zone with the score 3.4 in terms of performance.

Developmental research: Developmental research is in the weakened position, indicating that input should be supported to modify the output. Developmental research with the score of 7.2 is in the high state and ranks first in terms of influence

on output, but it is in the weak zone with the score of 3.3 in terms of performance.

NanoFab: NanoFab is in a weakened state indicating that the input needs particular support in order to modify the output. NanoFab with the score of 6.8 is in the second place in terms of influence on the output, but it is in a very weak area in terms of performance with score of 2.1.

Examination of these results and Figure 11 helps understand that fundamental research is one of the strengths of nanotechnology research and development activities; however, the applied development research and activities related to NanoFab centers are the weaknesses of research and development activities in nanotechnology. Of course, these strengths and weaknesses are not the same in all of these sections. Table 11 indicates the performance of each of the research factors based on Figure 11.

Table 11. The performance rate of research factors

Factors affecting the value creation of R&D activities in nanotechnology	Performance rate	Linguistic variables
Basic research	7.1	Well
Applied research	3.4	Weak
Developmental research	3.3	Weak
NanoFabs	2.1	Very weak

6. RESULTS AND FINDINGS ACHIEVED BY RESEARCH QUESTIONS

1-Why do the industrial sector fail to use the results of academic research in order to develop products and create value in the field of nanotechnology?

In this study, four factors are identified as influential and causal factors in creating value from R&D results in nanotechnology, which are fundamental (academic), applied, developmental research and intermediate research centers, or NanoFabs. Academic research has the least influence on R&D results among these factors; therefore, it is possible to expect that value creation indices such as new product production or product quality are to be improved and in fact, the industry can use academic research because of the good scientific position in the field of nanotechnology and good performance in this factor. However, the weakness in the performance of the two factors of development research and NanoFabs as the two factors that have the highest influence on the value creation of R&D activities in nanotechnology is the most significant issue. Although establishing the NanoFab centers has a more limited influence on output than development research and is in the second place among these two factors, as an intermediate research center, it is a bridge between fundamental research in the university and development research in industry; consequently, it is possible to state that

the industry sector does not use academic research which is due to the lack of NanoFab research centers. It can be concluded that in the field of renewable energy, according to the role of nanomaterial in improving the efficiency of renewable energy systems, creating NanoFab or NanoFabs focusing on the development of nanomaterial can significantly affect the development of renewable energy.

In fact, the main reason as to why the industry section is unable to use university researches for the product development is that the mentioned researchers are mostly engaged with basic scientific development. However, what is needed in the industry for product development is the knowledge of engineering and programming the way to exploit different types of science in actual environments, not a type of knowledge that is developed in scientific and laboratorial environments. In addition, what can make university researches applicable to the industry is filled researches which are done through NanoFabs in nanotechnology. In fact, the NanoFabs are the intermediate circle between university researches and developmental researches in the industry, and the industrial section is unable to utilize university resources for product development until NanoFabs are made.

2-What are the strengths and weaknesses of research and development activities in nanotechnology?

Figure 9 shows the status of the inputs of the fuzzy inference system (research factors) considering their performance and influence on the output, helping recognize that fundamental research is one of the strengths of research and development activities in nanotechnology. However, applied, development research, and also activities related to NanoFab centers are the weaknesses of research and development activities in nanotechnology. Of course, all these sectors do not have the same strength and weaknesses. In fact, analysis of the performance of the factors influencing the value creation of R&D activities in nanotechnology allows recognizing that the factors with the greatest influence on output, such as developmental research and NanoFab centers, have the lowest performance, while fundamental research has the highest performance with the least influence on the output. Accordingly, it is possible to consider this imbalance between the influence of a factor and the performance of that factor as the main weakness in the system of R&D activities in nanotechnology.

Considering the conclusions made within by this study, it can be acknowledged that due to the gap between basic research conducted in universities and development research conducted in industry. The industry sector can not use the research done in universities to develop the product. But the results of applied research in NanoFabs that lead to the production of prototypes can be used to develop a product in the industry. Therefore, to create a bridge between the university and industry, there is no other way but to create an intermediate research center called NanoFab. NanoFab acts as a link between academic research and developmental research.

7. ACKNOWLEDGEMENT

The authors would like to thank the Iran Nanotechnology Innovation Council (INIC) for providing the required data.

NOMENCLATURE

RERs	Renewable Energy Resources
RES	Renewable Energy Sources
NanoFab	Nanofabrication
RTO	Research & Technology Organization
NNFC	National NanoFab Center
CNSNT	Center for Nano Science and Nanotechnology
CNT	Carbon Nanotube
PV	Photovoltaic
NNI	National Nanotechnology Initiative
INIC	Iran Nanotechnology Innovation Council

REFERENCES

1. Aghaee, F., Mahdian Dehkordi, N., Bayati, N. and Hajizadeh, A., "Distributed control methods and impact of communication failure in AC microgrids: A comparative review", *Electronics*, Vol. 8, No. 11, (2019), 231-254. (<https://doi.org/10.3390/electronics8111265>).
2. Bayati, N., Baghaee, H.R., Hajizadeh, A. and Soltani, M., "A fuse saving scheme for DC microgrids with high penetration of renewable energy resources", *IEEE Access*, Vol. 8, (2020), 137407-137417. (<https://doi.org/10.1109/ACCESS.2020.3012195>).
3. Miller, G. and Senjen, R., "Out of the laboratory and on to our plates: Nanotechnology in food & agriculture", (2014). (<http://emergingtech.foe.org.au/resources/out-of-the-laboratory-and-on-to-our-plates-nanotechnology-in-food-and-agriculture/>), (Accessed: 25 July 2014).
4. StatNano | Roadmap; nanotechnology and Dutch opportunities, (2013). (<https://statnano.com/policydocument/79/Roadmap-Nanotechnology-and-Dutch-Opportunities#ixzz6u4aBw5bu>), (Accessed: 7 May 2013).
5. Mahmoodzadeh, M., Alborzi, M. and Khalili Shorini, S., "Analysis of the structure of Iran's nano-innovation network in the field of health", *Quarterly of Scientific-Research of Science-Technology Policy*, Vol. 6, No. 3, (2014), 29-53. (In Farsi). (http://jstp.nrisp.ac.ir/article_12908.html).
6. Keshavarz, M., Rahimi, M. and Salimi, M., "The Role of research and development centers (R&D) in innovation system", *Industry and University*, Vol. 3, No. 7, (2020), 13-29. (In Farsi). (<http://jiu.ir/fa/Article/6620>).
7. OECD | Gross domestic spending on R&D, (2019). (<https://data.oecd.org/rd/gross-domestic-spending-on-r-d.htm>), (Accessed: 20 June 2019).
8. Miyazaki, K. and Islam, N., "Nanotechnology systems of innovation-An analysis of industry and academia research activities", *Technovation*, Vol. 27, No. 11, (2007), 661-675. (<https://doi.org/10.1016/j.technovation.2007.05.009>).
9. OECD | Frascati manual, guide lines for collecting and reporting data on research and experimental development, (2015). (<https://www.oecd.org/publications/frascati-manual-2015-9789264239012-en.htm>), (Accessed: 10 August 2015).
10. Azarpajhoh, E. and Hamedzadeh, T., "A study of research and development systems in developed and developing countries", *Proceedings of the National Conference of Industrial Research and Development Centers of the Country*, Tehran, IR Iran, (2000), 474-489. (In Farsi). (<https://civilica.com/doc/21662/>).
11. ALBERTA | NanoFab, fabrication & characterization centre, (2019). (<https://www.nanofab.ualberta.ca>), (Accessed: 14 October 2019).
12. Novickis, L., Mitasiunasb, A. and Ponomarenkoa, V., "Information technology transfer model as a bridge between science and business sector", *Procedia Computer Science*, Vol. 104, (2017), 120-126. (<https://doi.org/10.1016/j.procs.2017.01.083>).
13. Burns, E. and Rajcan, A., "Research productivity of sociology PhD candidates at interdisciplinary schools of social science at elite Australian universities, 2013-17: A gender perspective", *Journal of Sociology*, Vol. 57, No. 3, (2021), 501-521. (<https://doi.org/10.1177%2F1440783320927094>).
14. Ivančević, V. and Luković, I., "National university rankings based on open data: A case study from Serbia", *Procedia Computer Science*, Vol. 126, (2018), 1516-1525. (<https://doi.org/10.1016/j.procs.2018.08.124>).
15. Zarei Mahmoodabadi, M., Tahari Mehrjerdi, M.H. and Mahdavian, A.R., "Evaluation of R&D activities in Iran: An approach to data envelopment analysis", *Industrial Management. University of Tehran*, Vol. 6, No. 1, (2015), 47-55. (In Farsi). (https://imj.ut.ac.ir/article_52235.html).
16. Pourghafarmaghferati, A., Pishgar, F. and Gharakhani, D., "Presenting a conceptual model for evaluating the performance of R&D units of manufacturing companies with DEA / AHP approach, Case study: Guilan province", *Industrial Management*, Vol. 9, (2014), 25-40. (In Farsi). (<https://www.sid.ir/fa/journal/ViewPaper.aspx?id=230681>).
17. Abd Latif, N.S., Abdullah, A. and Mohd Jan, N., "A pilot study of entrepreneurial orientation towards commercialization of university research products", *Procedia Economics and Finance*, Vol. 37, (2016), 93-99. (<https://www.sciencedirect.com/science/article/pii/S2212567116300983>).
18. Ali, A. and Sinha, K., "Exploring the opportunities and challenges in nanotechnology innovation in India", *Journal of Social Science for Policy Implications*, Vol. 2, No. 2, (2014), 227-251. (<http://jsspi.com/vol-2-no-2-june-2014-abstract-12-jsspi>).
19. Shamsi, M. and Nourmohammadi, H.A., "Identification of the most important models and indicators in the evaluation of science and technology in Iranian knowledge-based companies", *Journal of Scientometrics*, Vol. 4, No. 2, (2018), 1-16. (http://rsci.shahed.ac.ir/article_536.html).
20. Chen, K., Kou, M. and Fu, X., "Evaluation of multi-period regional R&D efficiency: An application of dynamic DEA to China's regional R&D systems", *Omega*, Vol. 74, (2018), 103-114. (<https://doi.org/10.1016/j.omega.2017.01.010>).
21. Shapira, P., Youtie, J. and Kay, L., "National innovation systems and the globalization of nanotechnology innovation", *Technology Transfer*, Vol. 36, No. 6, (2011), 587-604. (<https://doi.org/10.1007/s10961-011-9212-0>).
22. Wang, G. and Guan, J., "Value chain of nanotechnology: A comparative study of some major players", *Journal of Nanoparticle Research*, Vol. 14, No. 2, (2012), 1-14. (<https://doi.org/10.1007/s11051-011-0702-7>).

23. INIC | Performance report of the document on the development of nanotechnology in Iran, (2015). (<https://nano.ir/page/1/5009#rep2>), (Accessed: 18 April 2015).
24. StatNano | Status of nano-science, technology and innovation, (2017). (<https://statnano.com/publications/4144/StatNano-2016-Status-of-Nano-science-Technology-and-Innovation>), (Accessed: 25 July 2017).
25. Ansari, R. and Tayebi, H.R., "Study and explanation of research and technology organizations in Iran's national innovation , Case study: University Jihad", *Technology Growth*, Vol. 10, No. 37, (2012), 13-21. (In Farsi). (<https://www.sid.ir/fa/journal/ViewPaper.aspx?id=217026>).
26. EARTO | Position on the next generation of European union research and innovation programmers, (2011). (https://www.earto.eu/wp-content/uploads/EARTO_Response_Innovation_Union_Final_01.pdf), (Accessed: 25 July 2011).
27. Thuriaux-Alemán, B., Eagar, R., Webster, P. and Ku, B., "Research & technology institutes-meeting the challenges of the post-recession world", (2010). (https://www.adlittle.com/sites/default/files/viewpoints/ADL_Research_Technology_Institutes.pdf), (Accessed: 27 July 2010).
28. Alizadeh, P., "Promotion policies of R&D and innovation (2): Research and technology Oorganizations", (2012). (<https://rc.majlis.ir/fa/report/show/804856>). (In Farsi). (Accessed: 27 January 2012)
29. Sá, C.M., "Redefining university roles in regional economies: A case study of university–industry relations and academic organization in nanotechnology", *Springer Science*, Vol. 61, (2011), 193-208. (<https://link.springer.com/article/10.1007%2Fs10734-010-9332-8>).
30. Franco, R., "NanoFab: Making nanotechnology work for industry Veneto", (2010). (https://ec.europa.eu/regional_policy/en/projects/best-practices/italy/1367), (Accessed: 10 July 2010).
31. Chung, B.H., Park, H.K. and Jung, Y., "Nanobiotechnology R&D strategy in the Republic of Korea", *Asia-Pacific Biotech News*, Vol. 10, No. 17, (2006), 978-987. (<https://doi.org/10.1142/S0219030306001510>).
32. NIST | An assessment of the national institute of standards and technology center for nanoscale science and technology fisical year 2016, (2017). (https://www.nist.gov/system/files/documents/2017/01/03/cnst_nas_assessment_fy_2016_final_report.pdf), (Accessed: 27 April 2017).
33. NIST | The NIST center for nanoscale science and technology: Ssupporting US innovation in nanotechnology, (2010). (<https://www.nist.gov/publications/nist-center-nanoscale-science-and-technology-supporting-us-innovation-nanotechnology>), (Accessed: 15 July 2011).
34. NIST | Theory and modeling of materials for renewable energy, (2020). (<https://www.nist.gov/programs-projects/theory-and-modeling-materials-renewable-energy>), (Accessed: 18 August 2020).
35. Kadhim Hussein, A., "Applications of nanotechnology in renewable energies. A comprehensive overview and understanding", *Renewable and Sustainable Energy Reviews*, Vol. 42, (2015), 460-476. (<https://doi.org/10.1016/j.rser.2014.10.027>).
36. Amagu Echiegu, E., "Nanotechnology as a tool for enhanced renewable energy application in developing countries", *Journal of Fundamentals of Renewable Energy and Applications*, Vol. 6, No. 6, (2016). (<https://doi.org/10.4172/2090-4541.1000e113>).
37. Moon, R.J., Frihart, C.R. and Wegner, T., "Nanotechnology applications in the forest products industry", *Forest Products Journal*, Vol. 56, No. 5, (2006), 4-10. (<https://www.fs.usda.gov/treesearch/pubs/24445>).
38. NNI | A progress review of the nanotechnology for solar energy collection and conversion (Solar) NSI, (2015). (https://www.nano.gov/sites/default/files/pub_resource/nsi_status_report_solar_12_2015.pdf), (Accessed: December 2015).
39. Faramarzi, V. and Sofyanian, A.R., "Evaluation of environmental effects using fuzzy logic inference model", *Environmental Science*, Vol. 40, No. 4, (2014), 973-988. (In Farsi). (<https://dx.doi.org/10.22059/jes.2014.53013>).
40. Nematizadeh, S., Bidar, A. and Alizadeh, N., "Evaluation of the use of DMA electronic trading system in increasing the volume of transactions on the Tehran Stock Exchange using the fuzzy inference model", *Quarterly of Scientific-Research of Financial Knowledge of Securities Analysis*, Vol. 5, No. 15, (2012), 131-150. (In Farsi). (https://jfkasr.srbiau.ac.ir/article_3154.html).



Research Note

Multi-Criteria Analysis of Biogas Feed Fuel Cell-Based Electricity Generation: Economic and Environmental Factors

Shafini Mohd Shafie^{a*}, Zakirah Othman^a, A. Harits Nu'man^b, Nik Nurul Anis Nik Yusuf^c

^a Technology and Supply Chain Excellent Institute (TeSCE), School of Technology Management and Logistics, College of Business, Universiti Utara Malaysia, 06010 UUM Sintok, Kedah Darul Aman, Malaysia.

^b Universitas Islam Bandung, Jalan Tamansari No. 20, 40116 Bandung, West Java, Indonesia.

^c Department of Energy, Minerals and Materials Technology, Universiti Malaysia Kelantan, 17600 Jeli, Kelantan, Malaysia.

PAPER INFO

Paper history:

Received: 05 December 2021

Revised in revised form: 18 January 2022

Scientific Accepted: 29 January 2022

Published: 17 July 2022

Keywords:

Biogas,
Solid Oxide Fuel Cell,
Multi-Criteria Analysis,
Analytic Hierarchy Process,
Sustainable Energy

ABSTRACT

Penetration of renewable energy in the energy generation mix must be viewed from different angles. This issue shall not only cover the technological part, but also economic, environmental, and social criteria. The fuel cell provides huge potential with less reliance on fossil fuel-based electricity generation. This paper aims to model the optimum design of fuel cell-based electricity generation in Malaysia. Economic and environmental aspects are indicators that contribute to designing an optimum model. Both Multi-Criteria Analysis and Analytic Hierarchy Process were employed in order to decide on the optimum site for the system. Truck transportation, biogas storage, and fuel cell system are among the most important criteria that provide final weighted criteria. Considering both criteria for the economic and environment concerns, the best optimum location is in Sarawak State. The findings of this study influence the decision-making and help researchers and decision-makers develop proper strategies in the renewable energy roadmap.

<https://doi.org/10.30501/jree.2022.317755.1292>

1. INTRODUCTION

Currently, sustainable energy becomes the main concern in power production. Climate change issues, energy security, social awareness, and fossil fuel dominance are the factors that contribute to renewable energy development. Fuel cell consumption in electricity production is one technique feed gas as input and gets the electricity and water as the output. The most applicable fuel cell is the Solid Oxide Fuel Cell (SOFC) due to its great efficiency, minimal emissions, low level of noise, and fuel flexibility [1]. Malaysia, as a tropical country, provides huge potential for producing biogas, especially from oil palm residue [2]. A combination of biogas and solid oxide fuel cell systems has been identified as a very smart energy resolution for a distributed generation [3]. To increase the percentage of renewable energy consumption, economic, social, and environmental perspectives need to be considered. Integration of all perspectives into one tool helps decision-makers analyze using Multi-Criteria Decision Analysis (MCDA). These techniques offer more robust results than other decision support systems based on cost-based or environmental-based perspective, because several criteria are combined in decision-making practice to finally influence a valid and steady-state balance which would be great assistance

to all decision-makers [4]. The most widely applied method to MCDM is Analytic Hierarchy Process (AHP). AHP method has been used to determine the weights of the multiple criteria (techno-economic and environmental) as a more suitable tool to solve site selection problems [5]. Several studies have employed AHP to explore renewable energy using the pairwise comparison between the criteria [6]. Therefore, this study aims to (1) determine the criteria weights based on the relative importance of each one and (2) evaluate the multiple criteria for optimum site selection.

2. METHOD

2.1. Methodology

Data collection for each process in developing the optimum model considers the palm oil mills located in Kedah, northern region of Malaysia. About 6 mills registered under Malaysia Palm Oil Board are used as a case study in this study [7]. Figure 1 shows the location of each mill and its output capacity. Biogas production was calculated using Equation (1) in previous publication [2]. The data derived from economic and environmental criteria are obtained based on these mills as a case study, which were reported in the previous publication. Table 1 lists the main resources considered in this study [8]. The data from this analysis were used in this study to select the optimized site location.

*Corresponding Author's Email: shafini@uum.edu.my (S.M. Shafie)

URL: https://www.jree.ir/article_153561.html

Please cite this article as: Shafie, S.M., Othman, Z., Harits Nu'man, A. and Nik Yusuf, N.N.A., "Multi-criteria analysis of biogas feed fuel cell-based electricity generation: Economic and environmental factors", *Journal of Renewable Energy and Environment (JREE)*, Vol. 9, No. 3, (2022), 101-104. (<https://doi.org/10.30501/jree.2022.317755.1292>).



Table 1. Main resources data used in this study

Parameter	Resources	Ref.
Environmental	Biogas Fed-Fuel Cell Based Electricity Generation: A Life Cycle Assessment Approach	[8]
Economic	Life Cycle Cost of Biogas Feeding into Fuel Cell: Case of Malaysia	[13]

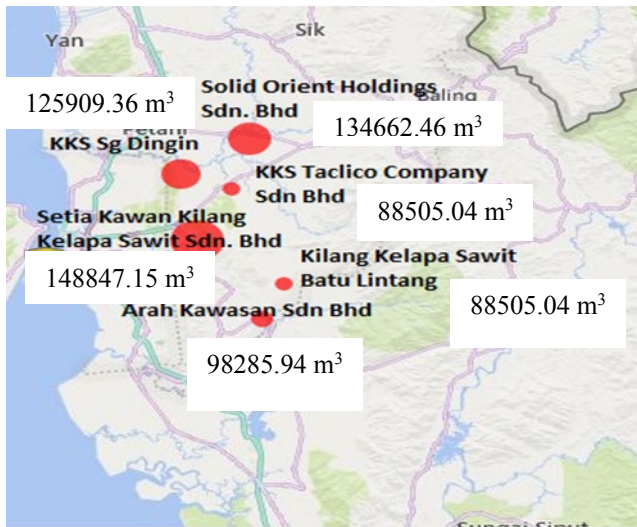


Figure 1. Kedah palm oil mill location and capacity output

Initially, the aim of the AHP process is set, as shown in Figure 2. Both economic and environmental aspects consider the following criteria or process mentioned in Figure 2: biogas production_BP, pipeline_P, biogas storage_BS, truck transportation_T, and fuel cell system_FC). The pairwise comparison is estimated on a 1-to-9 scale for each process, as developed by [9].

Then, build a pairwise comparison matrix M (n X n), where n is the number of process or criteria. Table 2 and Table 3 show the comparison matrix for economic and environmental aspects, respectively.

Table 2. Pairwise comparison matrix for the economic process

Process	BP	P	BS	FC	T
BP	1	9	0.14	0.14	7
P	0.11	1	0.11	0.11	0.33
BS	7	9	1	3	5
FC	7	9	0.33	1	5
T	0.14	3	0.2	0.2	1
Total	15.25	31	1.79	4.45	18.33

Table 3. Pairwise comparison matrix for the environmental process

Process	BP	P	BS	FC	T
BP	1	0.33	3	3	0.11
P	3	1	7	0.33	0.2
BS	0.33	0.14	1	0.2	0.11
FC	0.33	3	5	1	0.11
T	9	5	9	9	1
Total	13.67	9.48	25	13.53	1.53

From the comparison matrix table, the normalized comparison matrix (\bar{a}_{jk}) is obtained. Equation (1) is used to calculate each cell for matrix, as presented in Table 4 and Table 5.

$$\bar{a}_{jk} = a_{jk} / \sum_1^n a_{1k} \tag{1}$$

Table 4. Normalized economic pairwise comparison matrix

Process	BP	P	BS	FC	T	Normalized priority	Weight %
BP	0.07	0.29	0.08	0.03	0.38	0.17	16.99
P	0.01	0.03	0.06	0.02	0.02	0.03	2.90
BS	0.46	0.29	0.56	0.67	0.27	0.45	45.10
FC	0.46	0.29	0.19	0.22	0.27	0.29	28.66
T	0.01	0.10	0.11	0.04	0.05	0.06	6.35

Table 5. Normalized economic pairwise comparison matrix

Process	BP	P	BS	FC	T	Normalized priority	Weight %
BP	0.07	0.04	0.12	0.22	0.07	0.10	11.08
P	0.22	0.11	0.28	0.02	0.13	0.15	13.85
BS	0.02	0.02	0.04	0.01	0.07	0.03	3.51
FC	0.02	0.32	0.20	0.07	0.07	0.14	16.01
T	0.66	0.53	0.36	0.67	0.65	0.57	55.55

The overall weight vector is computed using Equation (2). Finally, the consistency of the comparison matrix is checked. The value of the random consistency index, RI, was pursued

Step in AHP.

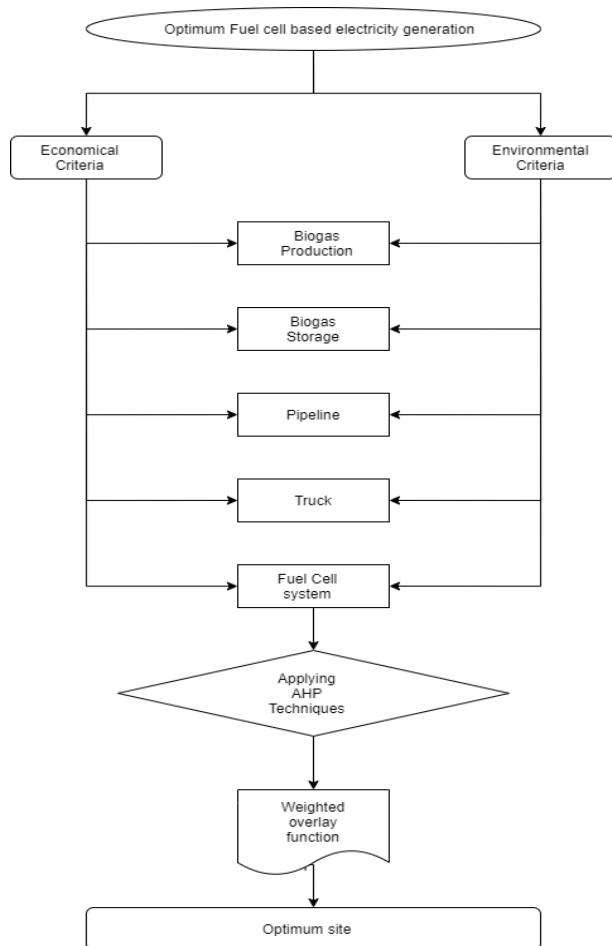


Figure 2. Approach to formation of the optimum model

in [9]. **Equation 3** is used to calculate the consistency ratio, CR. The obtained value of CR determines the acceptable ratio of the study with < 10 %; if CR > 10 %, it requires to revise the analysis and decision made [9].

$$W_j = \sum_{i=1}^n a_{ji} / m \tag{2}$$

$$CR = CI/RI \tag{3}$$

Then, the final weight is used in **Equation 4** for determining the optimum site location for Malaysia. The optimum site location index is estimated using Equation (4) [10]. The obtained results are applied to estimate the optimum site for Malaysia based on the availability of palm oil mills for the whole country [7].

$$SI = \sum_{i=1}^n W_i \mu_i \tag{4}$$

where n denotes the total number of preference process; i is the final weight of preference process for both economic and environmental aspects; W stands for the weight reflecting the relative importance of preference process; μ is the spatial percentage of preference process for the state.

3. RESULTS AND DISCUSSION

The obtained result is discussed in this section. Table 6 shows the final weights of the sub-criteria obtained using the AHP method. In the case of economic criterion, the greatest contribution came from biogas storage (22.55 %), while for the environmental perspective, truck transportation made the greatest contribution with 27.78 %. The significance of biogas storage is for later on-site consumption and storage before or after transportation to the next process of fuel cell systems. Location of palm oil mill proportionally affects the sub-criteria associated with truck transportation, mainly due to diesel usage.

Table 6. The final weights of the sub-criteria by AHP method

Goal	Criteria	Weight %	Sub criteria	CR %	Weight %	Final weight%
Selecting optimum site	Economical	50 %	Biogas production	2.5	16.99	8.5
			Pipeline		2.9	1.45
			Biogas storage		45.10	22.55
			Fuel cell system		28.66	14.33
			Truck transportation		6.35	3.18
	Environment	50 %	Biogas production	2.7	11.08	5.54
			Pipeline		13.85	6.93
			Biogas storage		3.51	1.76
			Fuel cell system		16.01	8.01
			Truck transportation		55.55	27.78

According to Table 6, truck transportation made the highest percentage of contribution to the system (30.96 %), followed by biogas storage (24.31 %), fuel cell system (22.34 %), biogas production (14.04 %), and pipeline (8.34 %). Transportation also becomes the preferred factor in modeling biogas plant in Turkey [10]. The pairwise comparisons of economic and environmental aspects are acceptable and consistent since CR 2.5 % and 2.7 %. As a result, the AHP technique is an excellent method for measuring the different weights of multiple criteria. These can avoid the conflict between the varieties of layer application.

Biogas storage is also a relatively simple construction in the form of a large metal canister with a large piston inside, ensuring proper pressure through gravity [11].

Figure 3 shows the optimum model for both economic and environment perspectives. Sarawak is the optimum state from both economic and environmental perspectives. This means that developing the model in Sarawak will provide both advantages with minimum economic and environmental impacts. With strong support from the government, it is possible to introduce this new type of energy resource in Sarawak. Moreover, this state is also the initial state in Malaysia starting with a feasibility study on hydrogen and fuel cell applications there [12]. Meanwhile, in Peninsular Malaysia, Johor is the best selection for modeling power generation. However, this system design is generalized to the whole state. To increase the efficiency of the system design, more specific details of the on-site location need to be investigated for future research.

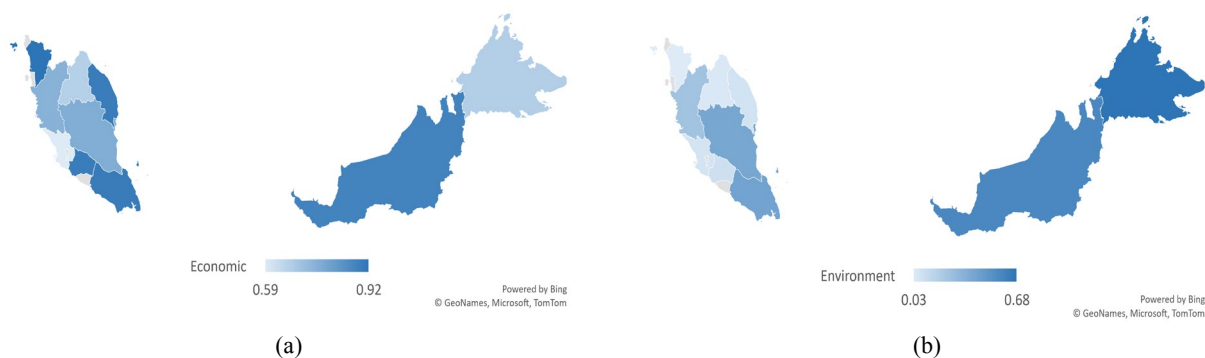


Figure 3. The model based on (a) Economic and (b) Environmental perspectives

4. CONCLUSIONS

The most important criterion or process in AHP final weight is the truck transportation system (30.96 %), followed by biogas storage (24.31 %) and fuel cell system (22.34 %). Thus, these processes are the key to increase the suitability index for the selected site in this study. The most optimum design from both economic and environmental criteria was Sarawak State. Modeling this system in that state obtain minimum economic and environmental impacts compared to other states in Malaysia.

5. ACKNOWLEDGEMENT

This research was supported by Ministry of Higher Education (MoHE) of Malaysia through Fundamental Research Grant Scheme (FRGS/1/2018/TK07/UUM/02/3). The authors would like to thank the reviewers and associate editor for their comments that have improved this manuscript.

REFERENCES

- Peng, J., Huang, J., Wu, X.L., Xu, Y.W., Chen, H. and Li, X., "Solid oxide fuel cell (SOFC) performance evaluation, fault diagnosis and health control: A review", *Journal of Power Sources*, Vol. 505, (2021), 230058. (<https://doi.org/10.1016/j.jpowsour.2021.230058>).
- Shafie, S.M., Othman, Z., Hami, N. and Omar, S., "The potential of using biogas feeding for fuel cells in Malaysia", *International Journal of Energy Economics and Policy*, Vol. 10, No. 1, (2020), 109-113. (<https://doi.org/10.32479/ijeeep.8373>).
- Leone, P., Lanzini, A., Santarelli, M., Cali, M., Sagnelli, F., Boulanger, A., Scaletta, A. and Zitella, P., "Methane-free biogas for direct feeding of solid oxide fuel cells", *Journal of Power Sources*, Vol. 195, No. 1, (2010), 239-248. (<https://doi.org/10.1016/j.jpowsour.2009.06.108>).
- Soltani, A., Hewage, K., Reza, B. and Sadiq, R., "Multiple stakeholders in multi-criteria decision-making in the context of Municipal Solid Waste Management: A review", *Waste Management*, Vol. 35, (2015), 318-328. (<https://doi.org/10.1016/j.wasman.2014.09.010>).
- Habib, S.M., Suliman, A.E.E., Nahry, A.H.A. and Rahman, E.N.A., "Spatial modeling for the optimum site selection of solar photovoltaics power plant in the northwest coast of Egypt", *Remote Sensing Applications: Society and Environment*, Vol. 18, (2020), 100313. (<https://doi.org/10.1016/j.rsase.2020.100313>).
- Ibhar, E., Cebi, S. and Kahraman, C., "A state-of-the-art review on multi-attribute renewable energy decision making", *Energy Strategies Reviews*, Vol. 25, (2019), 18-33. (<https://doi.org/10.1016/j.esr.2019.04.014>).
- Malaysian Palm Oil Board (MPOB), "Directory of Malaysian palm oil processing sectors", Ministry of Primary Industries, Kuala Lumpur, Malaysia (2019), 100. (https://econ.mpo.gov.my/economy/publications/EID_publication.htm).
- Shafie, S.M., Othman, Z., Hami, N., Nu'man, A.H., Yusuf, N.N.A.N. and Shah, A., "Biogas fed-fuel cell based electricity generation: A life cycle assessment approach", *International Journal of Energy Economics and Policy*, Vol. 10, No. 5, (2020), 498-505. (<https://doi.org/10.32479/ijeeep.9957>).
- Saaty, R.W., "The analytic hierarchy process—What it is and how it is used", *Mathematical Modelling*, Vol. 9, No. 3-5, (1987), 161-176. ([https://doi.org/10.1016/0270-0255\(87\)90473-8](https://doi.org/10.1016/0270-0255(87)90473-8)).
- Yalcinkaya, S., "A spatial modeling approach for siting, sizing and economic assessment of centralized biogas plants in organic waste management", *Journal of Cleaner Production*, Vol. 255, (2020), 1-13. (<https://doi.org/10.1016/j.jclepro.2020.120040>).
- Østergaard, P.A., "Comparing electricity, heat and biogas storages' impacts on renewable energy integration", *Energy*, Vol. 37, No. 1, (2012), 255-262. (<https://doi.org/10.1016/j.energy.2011.11.039>).
- The Borneo Post Online, "Green energy gets a boost from 'Hydrogen' technology", (2019). (https://sarawak.gov.my/web/home/news_view/223/13364/), [Cited 1 June 2021].
- Shafie, S.M., Othman, Z., Nu'man, A.H. and Yusuf, N.N.A.N., "Life cycle cost of biogas feeding into fuel cell: Case of Malaysia", (2021). (Unpublished manuscript). (<https://drive.google.com/file/d/1GomYA2pE9cNyu1APkihp6MHV14WyWBRS/view?usp=sharing>).

ABSTRACTS

Improved Droop Control Method for Reactive Power Sharing in Autonomous Microgrids

Babak Keyvani^a, Bahador Fani^{b,c}, Hamed Karimi^{b,c}, Majid Moazzami^{b,c}, Ghazanfar Shahgholian^{b,c*}

^a Department of Electrical Engineering, Boroujen Branch, Islamic Azad University, Boroujen, Iran.

^b Smart Microgrid Research Center, Najafabad Branch, Islamic Azad University, Najafabad, Iran.

^c Department of Electrical Engineering, Najafabad Branch, Islamic Azad University, Najafabad, Iran.

PAPER INFO

Paper history:

Received: 01 September 2021

Revised in revised form: 18 December 2021

Scientific Accepted: 07 December 2021

Published: 23 February 2022

Keywords:

Autonomous Microgrids,
Droop Control,
Power Sharing,
Stability,
Control System

ABSTRACT

Conventional droop control method has been widely adopted for power sharing between Distributed Generators (DGs) in microgrids. However, the mismatched feeder impedance of the Voltage-Sourced Inverters (VSI) may generate reactive power sharing error during islanding operation of a microgrid. In this paper, an improved droop control method is suggested to improve the reactive power sharing accuracy. In the proposed method, the slope correction of the droop characteristics is performed in such a way that the reactive power sharing error is reduced. In this method, the errors of reactive power sharing are detected by applying a clear signal to the microgrids and, then, by adding a new term to the $P-\omega$ and correcting the slope of $Q-E$, the reactive power sharing is done. In this way, the proposed method can successfully improve the reactive power sharing accuracy even at different X/R ratios. Another feature of this method is its high operation speed compared to the other methods of droop feature correction. The simulation results for a prototype microgrid point to the efficiency and flexibility of the proposed method.

<https://doi.org/10.30501/jree.2021.298138.1235>

2423-7469/© 2022 The Author(s). Published by MERC. This is an open access article under the CC BY license (<https://creativecommons.org/licenses/by/4.0/>).



چکیده

روش معمول برای تقسیم توان راکتیو بین ژنراتورها در میکروگرید، کنترل افتی متداول است. با این حال، روش‌های افتی معمول برای کنترل ریزش‌بکه‌ها به دلیل عدم تطابق در امپدانس خط، معمولاً توانایی تقسیم دقیق توان راکتیو را ندارند. در این مقاله، یک روش کنترل افتی بهبودیافته برای تقسیم توان راکتیو در ریزش‌بکه‌های خودگردان پیشنهاد شده است. در روش پیشنهادی، اصلاح شیب مشخصه‌های افتی به گونه‌ای انجام می‌شود که خطای تقسیم توان راکتیو کاهش می‌یابد. در این روش، خطاهای تقسیم توان راکتیو با اعمال یک سیگنال مشخص به ریزش‌بکه‌ها تشخیص داده می‌شود و سپس با افزودن یک عبارت جدید به $P-\omega$ و اصلاح شیب مشخصه $Q-E$ ، تقسیم توان راکتیو انجام می‌شود. یکی از ویژگی‌های این روش، سرعت بالای عملکرد آن در مقایسه با سایر روش‌های اصلاح ویژگی افتی است. نتایج شبیه‌سازی بر روی یک ریزش‌بکه نمونه، کارایی و انعطاف‌پذیری روش پیشنهادی را نشان می‌دهد.

Application of Artificial Neural Network to Solar Potential Estimation in Hilly Region of India

Rahul Dogra^a, Sanjay Kumar^b, Nikita Gupta^{b*}

^a School of Computing and Electrical Engineering (SCEE), Indian Institute of Technology Mandi (IIT Mandi), Mandi, India.

^b Department of Electrical Engineering, University Institute of Technology, Himachal Pradesh University (HPU), Shimla, India.

PAPER INFO

Paper history:

Received: 22 October 2021

Revised in revised form: 29 December 2021

Scientific Accepted: 05 January 2022

Published: 10 May 2022

Keywords:

Artificial Neural Networks (ANN),

Global Sun Radiation,

Solar,

Mean Absolute Percentage Error (MAPE)

ABSTRACT

The use of these conventional resources causes continuous depletion of fossil fuels and increased greenhouse effect. Solar power is the major renewable resource used for power generation across the globe. Solar energy activities depend on the available potential of any geographical location. Therefore, prior to the installation of solar technologies for these activities, estimation of solar potential is very important due to costly technologies. Data of solar potential is not present at every location in Himachal Pradesh (H. P.) due to the high cost of measurement instruments. The objective of this study includes the solar potential estimation for 12 cities of the H. P. The present study could be divided into two parts. Initially, Artificial Neural Networks (ANNs) are utilized to estimate global sun radiation utilizing meteorological and geographical data from 23 places. The ANN model with seven input parameters including latitude, longitude, altitude, air temperature, humidity, pressure, and wind speed were used to estimate the solar irradiation. Statistical indicators including Mean Absolute Percentage Error (MAPE) were used for the performance evaluation of these ANNs. The minimum MAPE value was obtained to be 2.39 % with Multi-Layer Perception (MLP) architecture 7-11-1. For the 12 districts of the H. P., the acquired network 7-11-1 was utilized to estimate Global Solar Radiation (GSR). The output of ANN model was implemented in Geographic Information System (GIS) environment to obtain the solar potential map for each month. The available map of the present study may be helpful for solar application in each district.

<https://doi.org/10.30501/jree.2022.307064.1267>

2423-7469/© 2022 The Author(s). Published by MERC. This is an open access article under the CC BY license (<https://creativecommons.org/licenses/by/4.0/>).



چکیده

استفاده از منابع مرسوم باعث کاهش مداوم سوخت‌های فسیلی و افزایش اثر گلخانه‌ای می‌شود. انرژی خورشیدی منبع اصلی تجدیدپذیر بوده که برای تولید برق در سراسر جهان استفاده می‌شود. کیفیت راندمان انرژی خورشیدی به پتانسیل موجود در هر موقعیت جغرافیایی بستگی دارد. بنابراین قبل از نصب فناوری‌های خورشیدی برای این فعالیت‌ها، برآورد پتانسیل خورشیدی به دلیل فناوری‌های پرهزینه بسیار حائز اهمیت است. داده‌های پتانسیل خورشیدی در هیمچال پرادش (نام محلی در هند) به دلیل هزینه بالای ابزار اندازه‌گیری وجود ندارد. هدف از این مطالعه شامل برآورد پتانسیل خورشیدی برای ۱۲ شهر هیمچال پرادش است. مطالعه حاضر را می‌توان به دو بخش تقسیم کرد. در ابتدا، از شبکه‌های عصبی مصنوعی (ANN) برای تخمین تابش خورشید با استفاده از داده‌های هواشناسی و جغرافیایی از ۲۳ مکان استفاده شده است. از مدل ANN با هفت پارامتر ورودی شامل عرض جغرافیایی، طول جغرافیایی، ارتفاع، دمای هوا، رطوبت، فشار و سرعت باد برای تخمین تابش خورشیدی استفاده شده است. برای ارزیابی عملکرد شبکه‌های عصبی مصنوعی از شاخص‌های آماری شامل میانگین درصد مطلق خطا (MAPE) استفاده شد. حداقل مقدار میانگین درصد مطلق خطا ۲/۳۹ درصد با معماری درک چند لایه (MLP) ۷-۱۱-۱ به دست آمد. برای ۱۲ ناحیه از هیمچال پرادش، شبکه به دست آمده ۷-۱۱-۱ برای تخمین تابش خورشید (GSR) مورد استفاده قرار گرفت. خروجی مدل ANN در محیط سیستم اطلاعات جغرافیایی برای بدست آوردن نقشه پتانسیل خورشید برای هر ماه پیاده‌سازی شد. نقشه مطالعه حاضر ممکن است برای کاربرد خورشیدی در هر منطقه مفید باشد.

Modified Concrete for Impeding Chloride Diffusion from Sea Water in the Marine Environment

Davar Rezakhani ^a, Abdol Hamid Jafari ^{a*}, Mohammad Ali Hajabassi ^b

^a Department of Electrical Engineering, Shahed University, P. O. Box: 18155-159, Tehran, Tehran, Iran.

^b Space Transportation Research Institute, Iranian Space Research Center, P. O. Box 13445-754, Tehran, Tehran, Iran.

PAPER INFO

Paper history:

Received: 11 July 2021

Revised in revised form: 17 January 2022

Scientific Accepted: 25 September 2021

Published: 11 May 2022

Keywords:

Chloride,
Diffusion,
Graphene Oxide,
Marine Environment,
Ground Granulated Blast Furnace Slag

ABSTRACT

The application of nanomaterials to concrete is an innovative approach to enhance mechanical properties and durability performances. In this work, the addition of a combination of Graphene Oxide Nano-Platelets (GONP) and Ground Granulated Blast Furnace Slag (GGBFS) was studied as admixture in concrete. Tests on mechanical and chloride permeation properties were conducted. The results showed that the mix with 0.05 % GONP and the mix with 30 % GGBFS obtained better mechanical strength than the rest of the mixes. The highest electrical resistivity was achieved for the 90-day cured sample with 50 % GGBFS in GONP-free concrete and the 0.01 % GONP in GGBFS-free concrete, which was found to be the most effective in increasing concrete resistance to chloride permeation. The mix with 0.1 w % GONP and 50 w % GGBFS exhibited considerable performance even with other mechanical and durability performances. The addition of 0.1 % graphene oxide and 50 % granular slag increased the compressive strength of the concrete sample by 19.9 % during 28 days and 17.6 % during 90 days compared to the conventional concrete sample. Concrete with a combination of 0.1 % graphene oxide and 50 % granular slag experienced an increase in flexural strength by 15 % during 28 days and 13.6 % during 90 days. A significant reduction in electrical conductivity from 4012C to 1200C was observed for 90-day cured samples containing 0.1 wt % GO and 50 wt % GGBFS compared to the conventional sample. Response Surface Method (RSM) applied to the test data presented an optimized concrete mix containing 0.08 w % GONP and 50 w % GGBFS, the outcome of which was in close agreement with the experimental results.

<https://doi.org/10.30501/jree.2022.293613.1227>

2423-7469/© 2022 The Author(s). Published by MERC. This is an open access article under the CC BY license (<https://creativecommons.org/licenses/by/4.0/>).



چکیده

کاربرد نانومواد در بتن یک رویکرد ابتکاری برای افزایش خواص مکانیکی و دوام ارائه می‌دهد. در این کار، افزودن ترکیب نانوپلاکت‌های اکسید گرافن (GONP) و سرباره کوره بلند دانه‌ای (GGBFS) به عنوان افزودنی در بتن مورد مطالعه قرار گرفت. آزمایشات بر روی خواص مکانیکی و نفوذ کلرید انجام شد. نتایج نشان داد که طرح اختلاط با ۰/۰۵٪ از GONP و طرح اختلاط با ۳۰٪ از GGBFS، مقاومت مکانیکی بهتری نسبت به بقیه اختلاط‌ها به دست آوردند. بیشترین مقاومت الکتریکی برای نمونه پخت شده ۹۰ روزه با ۵۰٪ از GGBFS در بتن بدون GONP و ۰/۰۱٪ از GONP در بتن بدون GGBFS بدست آمد تا در افزایش مقاومت بتن در برابر نفوذ کلرید مؤثر باشد. ترکیب با ۰/۱٪ از GONP و ۵۰٪ از GGBFS عملکرد قابل توجهی را همراه با سایر عملکردهای مکانیکی و دوام نشان داد. افزودن ۰/۱٪ اکسید گرافن و ۵۰٪ سرباره دانه‌ای مقاومت فشاری نمونه بتن را در طول ۲۸ روز ۱۹/۹٪ و در طول ۹۰ روز ۱۷/۶٪ در مقایسه با نمونه بتنی معمولی افزایش داد. بتن با ترکیب ۰/۱٪ اکسید گرافن و ۵۰٪ سرباره گرانوله، مقاومت خمشی را ۱۵٪ طی ۲۸ روز و ۱۳/۶٪ در طول ۹۰ روز افزایش داد. کاهش زیاد هدایت الکتریکی از ۴۰۱۲ C به ۱۲۰۰ C برای نمونه‌های ۹۰ روزه حاوی ۰/۱٪ GO و ۵۰٪ GGBFS در مقایسه با نمونه معمولی مشاهده شد. روش سطح پاسخ (RSM) که به داده‌های آزمایش اعمال گردید، مخلوط بتنی بهینه شده حاوی ۰/۰۸٪ GONP و ۵۰٪ GGBFS را در توافق نزدیک با نتایج تجربی ارائه داد.

DC Microgrid Voltage Stability through Inertia Enhancement Using a Bidirectional DC-DC Converter

Shokoofeh Bagheri^a, Hassan Moradi CheshmehBeigi^{a,b*}

^a Department of Electrical Engineering, Faculty of Engineering, Razi University, P. O. Box: 67144-14971, Kermanshah, Iran.

^b Industrial Intelligent Systems Research Center (IISRC), Razi University, Kermanshah, Iran.

PAPER INFO

Paper history:

Received: 01 October 2021

Revised in revised form: 27 December 2021

Scientific Accepted: 12 December 2021

Published: 28 May 2022

Keywords:

Renewable Energy Source (RES),
DC Microgrid (DCMG),
Cascaded Buck-Boost Converter
(CBBC),
Virtual Inertia,
Virtual DC Machine (VDCM),
DC Bus

ABSTRACT

Today, the presence of energy storage systems along with the alternative nature of renewable energy sources has become undeniable and one of these types of systems is battery energy storage systems. The most important factor in studying the stability of DC microgrids (DCMGs) is the stabilization of the DC bus voltage when an error occurs on its reference value. Therefore, batteries along with power electronic converters play an important role in maintaining DCMG stability. In this paper, the use of Cascaded Buck-Boost Converter (CBBC) can be considered as a suitable alternative to bidirectional buck-boost converter due to such advantages as high power density, 98 % efficiency, and higher operating temperature in battery. The control strategy is applied in the microgrid implemented in the converter system set with storage, and Virtual DC Machine (VDCM) is based on charging and discharging battery through CBBC. In the studied control method, the theoretical properties of the DC machine, which is responsible for amplifying the virtual inertia in the system, are directed to the CBBC for correct switching. VDCM can be changed from motoring to generating mode or vice versa, regardless of mechanical machinery. Therefore, the proposed control system is simulated in an islanded DCMG in Matlab/Simulink and the stability of the studied system is analyzed according to the small-signal model of the proposed control and converter units. According to the simulation results and small-signal model analysis, the stability of the proposed idea under different scenarios is confirmed.

<https://doi.org/10.30501/jree.2021.298032.1233>

2423-7469/© 2022 The Author(s). Published by MERC. This is an open access article under the CC BY license (<https://creativecommons.org/licenses/by/4.0/>).



چکیده

امروزه حضور سیستم‌های ذخیره انرژی در کنار ماهیت متناوب منابع انرژی تجدیدپذیر به امری انکارناپذیر تبدیل شده است که یکی از انواع این سیستم‌ها، سیستم‌های ذخیره انرژی باتری هستند. مهم‌ترین فاکتور مورد مطالعه در بررسی پایداری میکروشبکه‌های DC (DCMGs)، تثبیت ولتاژ باس DC در هنگام بروز خطا بر روی مقدار مرجع آن است. بنابراین، باتری‌ها به همراه مبدل‌های الکترونیک قدرت نقش مهمی در حفظ پایداری DCMG دارند. در این مقاله استفاده از مبدل باک-بوست آبشاری (CBBC) به دلیل مزایایی مانند چگالی توان بالا، راندمان ۹۸٪ و دمای عملیاتی بالاتر در باتری، می‌تواند به عنوان گزینه‌ی جایگزین مناسب برای مبدل دو طرفه باک-بوست در نظر گرفته شود. استراتژی کنترل اعمال شده در میکروشبکه پیاده‌سازی شده در مجموعه سیستم مبدل به همراه ذخیره‌ساز، ماشین DC مجازی (VDCM) مبتنی بر شارژ و دشارژ باتری از طریق CBBC می‌باشد. در روش کنترلی مورد مطالعه، خصوصیات تئوری ماشین DC که وظیفه تقویت اینرسی مجازی در سیستم را دارد، برای کلیدزنی مناسب به CBBC هدایت می‌شود. VDCM را می‌توان بدون در نظر گرفتن ماشین آلات مکانیکی، از حالت موتوری به حالت ژنراتوری و یا برعکس تغییر داد. از این رو سیستم کنترل کننده پیشنهاد شده در یک DCMG جزیره‌ای در Matlab/Simulink شبیه سازی شده است و پایداری سیستم مورد مطالعه با توجه به مدل سیگنال کوچک واحدهای کنترل و مبدل پیشنهادی تحلیل شده است. با توجه به نتایج شبیه سازی و تحلیل مدل سیگنال کوچک، پایداری ایده پیشنهادی تحت سناریوهای مختلف تأیید می‌شود.

A New Approach Based on RTV/SiO₂ Nano Coating for Tackling Environmental Pollution on Electrical Energy Transmission and Distributions

Ashkan Zolriasatein ^{a*}, Zahra RajabiMashhadi ^a, Majid Rezaei Abadchi ^a, Nastaran Riahi Noori ^a, Siamak Abyazi ^b

^a Department of Non-Metallic Materials Research, Niroo Research Institute (NRI), P. O. Box: 14665517, Tehran, Tehran, Iran.

^b Department of High Voltage Studies Research, Niroo Research Institute (NRI), P. O. Box: 14665517, Tehran, Tehran, Iran.

PAPER INFO

Paper history:

Received: 14 August 2021

Revised in revised form: 05 January 2022

Scientific Accepted: 18 January 2022

Published: 29 May 2022

Keywords:

Silicon Rubber Nanocomposite,

Salt Fog Test,

Hydrophobicity,

Leakage Current,

Breakdown Voltage

ABSTRACT

The crisis of contamination that leads to the accumulation of dust particles on insulation equipment and electrical insulators has disrupted the electricity grid. Electric discharge on infected insulators in wet conditions is a serious threat to the reliability of the grid, which can lead to grid failure and blackout. In this regard, the importance of hydrophobic and dustproof coatings in the electricity industry has increased in recent years. In this paper, silica nanoparticles in the silicon rubber matrix were used to coat ceramic insulators to decrease the environmental impact of dust and moisture on the insulator's coatings. One of the essential properties of these coatings is their hydrophobicity to prevent possible problems in power transmission. With this regard, nanocomposites were applied to 70 kN insulators and the tests were designed according to the available standards. The performance of these nanocoatings was evaluated by the implementation of electrical, salt fog, and hydrophobicity tests. Finally, the nanocomposite sample containing 3 wt % silica was recognized as the best one.

<https://doi.org/10.30501/jree.2022.299858.1244>

2423-7469/© 2022 The Author(s). Published by MERC. This is an open access article under the CC BY license (<https://creativecommons.org/licenses/by/4.0/>).



چکیده

بحران اخیر هجوم ریزگردها منجر به نشست ذرات گرد و غبار بر روی تجهیزات عایقی، مقره‌های الکتریکی و اختلال در عملکرد شبکه برق‌رسانی کشور گشته است. در همین راستا، اهمیت پوشش‌های آب‌گریز و ضد گرد و غبار در صنعت برق، در سال‌های پیشین افزایش یافته است. در این مقاله با هدف بهبود خواص و عملکرد این پوشش‌ها از نانوذرات سیلیکا در زمینه سیلیکون رابر (نانوکامپوزیت) برای پوشش‌دهی مقره‌های سرامیکی و جهت کاهش اثرات زیست‌محیطی گرد و غبار و رطوبت بر آنها استفاده شد. یکی از اساسی‌ترین خواص این پوشش‌ها، آب‌گریزی آنها برای جلوگیری از بروز مشکلات احتمالی در انتقال نیرو است. برای بهبود این خاصیت، پوشش‌های تهیه شده روی مقره‌های ۷۰ کیلو نیوتونی اعمال شده و همچنین آزمایش‌های مورد نظر با توجه به مراجع و استانداردهای موجود، طراحی گردید. با ساخت نمونه‌های آزمایشی بر اساس طراحی آزمایش‌های انجام شده و بهینه‌سازی پارامترهای ساخت آنها، عملکرد این نانوپوشش‌ها از نظر خواص الکتریکی، تست مه نمکی و آب‌گریزی مورد بررسی قرار گرفت. در نهایت نمونه کامپوزیتی با ۳ درصد وزنی سیلیکا به عنوان بهترین نمونه شناخته شد.

Investigating the Economic Effects and the Roadmap of Developing Geothermal Systems to Generate Electricity

Mirmahdi Seyedrahimi-Niaraq*, Tohid Nouri

Faculty of Engineering, University of Mohaghegh Ardabili, P. O. Box: 56199-13131, Ardabil, Ardabil, Iran.

PAPER INFO

Paper history:

Received: 01 December 2021

Revised in revised form: 03 January 2022

Scientific Accepted: 11 January 2022

Published: 25 June 2022

Keywords:

Renewable Energy,
Geothermal Energy,
Economic Impacts,
Geothermal Economic Policies,
Geothermal Energy Roadmap

ABSTRACT

Geothermal energy is a non-carbon renewable source from the earth's internal energy. This energy is considered reliable today and has a high potential to reduce the threat of climate change. The main factor that any investor wants to invest in any natural energy source is the resulting economy. In the case of geothermal energy, factors that increase the risk of investing in this sector include higher investment costs, longer payback times than other renewable power plants, and the uncertainty of the size and quality of the resources before the completion of the well drilling operation. The average payback time in geothermal energy systems is 5.7 years, longer than wind and solar energy. According to these factors, the risk of investing in geothermal technology increases. On the other hand, due to its independence from oil and gas, it increases a country's energy security, helps to create direct, indirect, and induced employment, and affects other economic sectors. Also, unlike renewable wind and solar energies, it is not dependent on climate change; therefore, it has higher reliability than other renewable energies. Also, by combining this energy with other renewable energies, its performance can be optimized. For example, in an optimal geothermal-solar hybrid power plant, solar energy provides 48 % of the total energy. In this case, the Levelized Cost of Energy (LCOE) is reduced from 225 \$ per MWh (only with geothermal source) to 165 \$ per MWh. In this study, while studying the economic effects of geothermal systems, an attempt has been made to address the challenges in this field and present the policies implemented in some countries. It is implied that by providing incentive policies and an appropriate roadmap, it is possible to help attract investment in the operation of geothermal systems.

<https://doi.org/10.30501/jree.2022.317375.1290>

2423-7469/© 2022 The Author(s). Published by MERC. This is an open access article under the CC BY license (<https://creativecommons.org/licenses/by/4.0/>).



چکیده

انرژی زمین گرمایی به عنوان یک منبع تجدیدپذیر غیرکربنی است که از انرژی درونی زمین نشأت می گیرد. در انرژی زمین گرمایی، از عواملی که باعث افزایش ریسک سرمایه گذاری در این بخش می شود، می توان به مواردی چون هزینه سرمایه گذاری بالاتر، زمان بازگشت سرمایه طولانی تر نسبت به سایر نیروگاه های تجدیدپذیر و همچنین مشخص نبودن اندازه و کیفیت منابع قبل از اتمام عملیات حفاری چاه اشاره نمود. زمان بازگشت سرمایه در بهره برداری از سیستم های انرژی زمین گرمایی به طور متوسط ۵/۷ سال است. مطابق این عوامل، خطر سرمایه گذاری روی فناوری زمین گرمایی افزایش خواهد یافت. ولی در مقابل، این انرژی به دلیل عدم وابستگی به نفت و گاز، امنیت انرژی یک کشور را بالا برده و به ایجاد اشتغال مستقیم، غیرمستقیم و القایی کمک کرده و سایر بخش های اقتصادی را تحت تأثیر قرار می دهد. همچنین با ترکیب این انرژی با سایر انرژی های تجدیدپذیر می توان عملکرد آن را بهینه کرد. برای مثال، در یک نیروگاه هیبریدی زمین گرمایی-خورشیدی بهینه، انرژی خورشیدی ۴۸ درصد کل انرژی را فراهم می کند. در این حالت، هزینه تراز شده انرژی (LCOE) از ۲۲۵ دلار بر مگاوات ساعت (تنها با منبع زمین گرمایی) به ۱۶۵ دلار بر مگاوات ساعت کاهش می یابد. در این پژوهش، ضمن بررسی اثرات اقتصادی سیستم های زمین گرمایی، سعی شده است به چالش های موجود در این بخش پرداخته شده و سیاست های پیاده شده در کشورهای دیگر در این زمینه، ارائه شود. به نظر می رسد با ارائه سیاست های تشویق کننده و نقشه راه مناسب، می توان به جذب سرمایه گذاری در زمینه بهره برداری از سیستم های زمین گرمایی کمک کرد.

Optimum Orientation of the Multi-Span Greenhouse for Maximum Capture of Solar Energy in Central Region of Iran

Mehran Gheyрати, Asadollah Akram, Hassan Ghasemi-Mobtaker *

Department of Agricultural Machinery Engineering, Faculty of Agricultural Engineering and Technology, University of Tehran, Karaj, Alborz, Iran.

PAPER INFO

Paper history:

Received: 22 September 2021
Revised in revised form: 16 February 2022
Scientific Accepted: 16 February 2022
Published: 02 July 2022

Keywords:

Greenhouse Orientation,
Mathematical Modeling,
North Wall,
Solar Irradiation

ABSTRACT

The orientation of greenhouses is one of the effective factors in terms of radiation they receive. In the present study, a multi-span greenhouse (40 m × 93.5 m with a coverage area of 5457.44 m²) located in the central region of Iran was investigated in three orientations including: North-South (N-S), East-West (E-W), and Northeast-Southwest (NE-SW: the most frequent orientation of the existing greenhouses in the study area). The solar irradiation received on the outside surface of the greenhouse cover and the amount of irradiation captured inside the greenhouse for each orientation during the cold season were calculated using mathematical modeling and the results were compared. According to the results, in the E-W orientation, the main sections of receiving solar irradiation, such as the south and north roofs, have a better angle toward the sun; therefore, the quantity of solar irradiation captured inside the greenhouse with the E-W orientation was on average 361.48 MJ day⁻¹ more than that with the N-S orientation. The north wall of the greenhouse could not receive the beam radiation for all the orientations investigated, and the total irradiation captured by this section was composed of the diffused radiation and the ground-reflected radiation, which is an important result for insulation of some surfaces of greenhouses.

<https://doi.org/10.30501/jree.2022.305780.1259>

2423-7469/© 2022 The Author(s). Published by MERC. This is an open access article under the CC BY license (<https://creativecommons.org/licenses/by/4.0/>).



چکیده

جهت‌گیری گلخانه‌ها یکی از عوامل مؤثر در میزان تابش دریافتی آنها می‌باشد. در مطالعه حاضر یک گلخانه تجاری چنددهانه (۴۰ متر در ۹۳/۵ متر با سطح پوشش ۵۴۵۷/۴۴ متر مربع) در منطقه مرکزی ایران در سه جهت شمالی-جنوبی، شرقی-غربی و شمال شرقی-جنوب غربی (جهت غالب گلخانه‌ها در منطقه مورد مطالعه) از نظر میزان تابش دریافتی مورد بررسی قرار گرفت. با استفاده از مدل ریاضی، میزان تابش دریافتی در سطح بیرونی پوشش و داخل گلخانه در هر سه جهت مذکور در طول ماه‌های سرد سال محاسبه و نتایج با هم مقایسه شد. با توجه به نتایج، در گلخانه شرقی-غربی، سقف‌های جنوبی و شمالی که بیشترین نقش را در دریافت تابش خورشید دارند، زاویه مناسب‌تری نسبت به خورشید داشتند، بنابراین مقدار تابش خورشیدی که به داخل گلخانه شرقی-غربی می‌رسد، به‌طور متوسط ۳۶۱/۴۸ MJ day⁻¹ بیشتر از جهت شمالی-جنوبی محاسبه شد. نتایج همچنین نشان داد دیوار شمالی گلخانه در تمام جهت‌های مورد بررسی تابش مستقیم دریافت نمی‌کند و کل تابش جذب شده توسط این بخش شامل تابش پخش و تابش بازتابی از سطح زمین است. بنابراین توصیه می‌شود دیوار شمالی گلخانه عایق شود.

Energy Analysis of Utilizing Biomass Gasification to Partially Substitution Fossil Fuels in an IBG-GT-ST-Kalina Cycle

Mohammad Hosseinpour^a, Hassan Ali Ozgoli^{b*}, Seyed Alireza Haji Seyed Mirza Hosseini^a, Amir Hooman Hemmasi^a, Ramin Mehdipour^c

^a Faculty of Natural Resources and Environment, Science and Research Branch, Islamic Azad University, Tehran, Tehran, Iran.

^b Department of Mechanical Engineering, Iranian Research Organization for Science and Technology (IROST), Tehran, Tehran, Iran.

^c Department of Mechanical Engineering, Tafresh University, Tafresh, Markazi, Iran.

PAPER INFO

Paper history:

Received: 27 December 2021

Revised in revised form: 16 February 2022

Scientific Accepted: 09 March 2022

Published: 02 July 2022

Keywords:

Biomass Gasification,
Fluidized Bed,
Kalina Cycle,
Combined Cycle,
Energy Efficiency

ABSTRACT

In this study, the partial alteration of fuel consumption of combined cycle power plants was investigated and analyzed using an innovative model. This system is applicable using the fuel derived from the biomass gasification process. For this purpose, energy modeling of an advanced gasification system to supply a share of the gas fuel was fulfilled. The results demonstrated that by considering the reasonable capacities for the design, up to 10 % of natural gas fuel could be replaced with syngas. In addition, heat recovery of the plant stack in the Kalina low-temperature cycle enhanced the total efficiency by up to 1.7 %. Therefore, the competitive advantage of the proposed cycle was enhanced compared to conventional power generation systems. A parametric study of the components affecting the integrated cycle performance including alternative biomass fuels, moisture content of biomass fuel, steam-to-biomass ratio, and equivalence ratio of the gasifier was performed, and the permissible values of each factor were obtained. Thus, by utilizing the proposed approach, it is possible to gradually substitute the consumed fossil fuels of power plants with renewable resources to achieve the objectives of sustainable energy development.

<https://doi.org/10.30501/jree.2022.321835.1307>

2423-7469/© 2022 The Author(s). Published by MERC. This is an open access article under the CC BY license (<https://creativecommons.org/licenses/by/4.0/>).



چکیده

در این مطالعه، جایگزینی جزئی مصرف سوخت نیروگاه‌های سیکل ترکیبی با ارائه یک مدل ابتکاری مورد بررسی و تحلیل قرار گرفته است. این سیستم با استفاده از سوخت حاصل از فرآیند گازسازی زیست‌توده قابل اجرا می‌باشد. برای این منظور مدل‌سازی انرژی یک سیستم گازسازی پیشرفته برای تأمین سهمی از سوخت گاز انجام شده است. نتایج نشان داد که با در نظر گرفتن ظرفیت‌های مناسب برای طراحی، می‌توان تا ۱۰٪ سوخت گاز طبیعی را با گاز سنتز جایگزین کرد. علاوه بر این، بازیابی گرمای دودکش نیروگاه در سیکل دمایی پایین کالینا، بازده کل را تا ۱.۷٪ بهبود می‌بخشد. بنابراین، مزیت رقابتی چرخه پیشنهادی در مقایسه با سیستم‌های تولید توان معمولی بهبود می‌یابد. مطالعه پارامتریک اجزای مؤثر بر عملکرد سیکل یکپارچه مانند سوخت‌های زیست‌توده جایگزین، رطوبت سوخت زیست‌توده، نسبت بخار به زیست‌توده و نسبت هم‌ارزی گازسازی انجام شد و مقادیر مجاز هر یک از فاکتورها به دست آمد. بنابراین، با استفاده از رویکرد پیشنهادی، امکان جایگزینی تدریجی سوخت‌های فسیلی مصرفی نیروگاه‌ها با منابع تجدیدپذیر برای دستیابی به اهداف توسعه انرژی پایدار فراهم می‌شود.

The Influence of Research and Development Activities and NanoFab Centers on Product Development in Nanotechnology: Focusing on Solar Thermal Energy and Photovoltaic Technology

Amrollah Dehghani Sanij^a, Taghi Torabi^{b*}, Abbas Khamseh^c, Alireza Boshehri^d

^a Department of Technology Management, Sciences and Research Branch, Islamic Azad University, Tehran, Tehran, Iran.

^b Department of Economics, Sciences and Research Branch, Islamic Azad University, Tehran, Tehran, Iran.

^c Department of Industrial Management, Karaj Branch, Islamic Azad University, Karaj, Alborz, Iran.

^d School of Management and Soft Technologies, Malek Ashtar University of Technology, Tehran, Tehran, Iran.

PAPER INFO

Paper history:

Received: 09 July 2021

Revised in revised form: 12 October 2021

Scientific Accepted: 27 December 2021

Published: 05 July 2022

Keywords:

NanoFab,
Nanotechnology,
Research and Development,
Structural Equations,
Fuzzy Inference,
Renewable Energy

ABSTRACT

This research aims to determine the influence of fundamental, applied, developmental research and Nanofabrication (NanoFab) centers on the final outcomes achieved by research and development activities, implying product development and value creation in nanotechnology. Data were collected through library studies and field studies in this study and research factors were also identified. To confirm the collected factors, structural equation technique and Smart PLS software were used and after confirming the research factors, the collected data were analyzed using fuzzy inference method and MATLAB software. The achieved results indicated that this field had the most performance despite the minimal influence of fundamental research on the final results of research and development activities and developmental research, while NanoFabs had the poorest performance with the highest influence on the final results of research activities. It is possible to conclude according to the research results that research and development activities at the fundamental and applied levels cannot easily be connected to the end ring, i.e., industry without NanoFab centers, and provide the final product and create value. Furthermore, providing NanoFab or NanoFabs with emphasis on the development of nanomaterial can significantly affect the development of renewable energies.

<https://doi.org/10.30501/jree.2022.292097.1222>

2423-7469/© 2022 The Author(s). Published by MERC. This is an open access article under the CC BY license (<https://creativecommons.org/licenses/by/4.0/>).



چکیده

هدف از این پژوهش، تعیین میزان تأثیر تحقیقات بنیادی، کاربردی، توسعه‌ای و مراکز نانوفاب¹ بر نتایج نهایی فعالیت‌های تحقیق و توسعه یعنی توسعه محصول و خلق ارزش در حوزه فناوری نانو است. در این تحقیق گردآوری داده‌ها از روش مطالعات کتابخانه‌ای و مطالعات میدانی صورت گرفته است که طی آن عوامل تحقیق مشخص گردید. برای تأیید عوامل احصاء شده، از تکنیک معادلات ساختاری و نرم افزار Smart PLS استفاده شد و بعد از تأیید عوامل تحقیق، داده‌های جمع آوری شده با استفاده از روش استنتاج فازی و نرم افزار MATLAB تحلیل گردید. نتایج، نشانگر آن است که علیرغم کمترین تأثیر تحقیقات بنیادی بر روی نتایج نهایی فعالیت‌های تحقیق و توسعه، بیشترین عملکرد در این بخش وجود داشته و تحقیقات توسعه‌ای و نانوفاب‌ها با بیشترین تأثیر بر روی نتایج نهایی فعالیت‌های تحقیق و توسعه، کمترین عملکرد را داشته‌اند. از این پژوهش می‌توان نتیجه گرفت که بدون وجود مراکز نانوفاب، فعالیت‌های تحقیق و توسعه در سطوح بنیادی و کاربردی نمی‌توانند به راحتی به حلقه انتهایی یعنی صنعت متصل شوند و منجر به محصول نهایی و خلق ارزش شوند. همچنین ایجاد نانوفاب یا نانوفاب‌هایی با تمرکز بر توسعه نانومواد می‌تواند تأثیر بسزایی بر توسعه انرژی‌های تجدیدپذیر داشته باشد.

¹ Nanofabrication (NanoFab)

Multi-Criteria Analysis of Biogas Feed Fuel Cell-Based Electricity Generation: Economic and Environmental Factors

Shafini Mohd Shafie^{a*}, Zakirah Othman^a, A. Harits Nu'man^b, Nik Nurul Anis Nik Yusuf^c

^a *Technology and Supply Chain Excellent Institute (TeSCE), School of Technology Management and Logistics, College of Business, Universiti Utara Malaysia, 06010 UUM Sintok, Kedah Darul Aman, Malaysia.*

^b *Universitas Islam Bandung, Jalan Tamansari No. 20, 40116 Bandung, West Java, Indonesia.*

^c *Department of Energy, Minerals and Materials Technology, Universiti Malaysia Kelantan, 17600 Jeli, Kelantan, Malaysia.*

PAPER INFO

Paper history:

Received: 05 December 2021

Revised in revised form: 18 January 2022

Scientific Accepted: 29 January 2022

Published: 17 July 2022

Keywords:

Biogas,
Solid Oxide Fuel Cell,
Multi-Criteria Analysis,
Analytic Hierarchy Process,
Sustainable Energy

ABSTRACT

Penetration of renewable energy in the energy generation mix must be viewed from different angles. This issue shall not only cover the technological part, but also economic, environmental, and social criteria. The fuel cell provides huge potential with less reliance on fossil fuel-based electricity generation. This paper aims to model the optimum design of fuel cell-based electricity generation in Malaysia. Economic and environmental aspects are indicators that contribute to designing an optimum model. Both Multi-Criteria Analysis and Analytic Hierarchy Process were employed in order to decide on the optimum site for the system. Truck transportation, biogas storage, and fuel cell system are among the most important criteria that provide final weighted criteria. Considering both criteria for the economic and environment concerns, the best optimum location is in Sarawak State. The findings of this study influence the decision-making and help researchers and decision-makers develop proper strategies in the renewable energy roadmap.

<https://doi.org/10.30501/jree.2022.317755.1292>

2423-7469/© 2022 The Author(s). Published by MERC. This is an open access article under the CC BY license (<https://creativecommons.org/licenses/by/4.0/>).



چکیده

نفوذ انرژی‌های تجدیدپذیر در ترکیب تولید انرژی را باید از زوایای مختلف نگریست. این موضوع نه تنها بخش فناوریانه، بلکه معیارهای اقتصادی، زیست‌محیطی و اجتماعی را نیز پوشش می‌دهد. پیل سوختی، پتانسیل عظیمی را با اتکای کمتر به تولید برق مبتنی بر سوخت فسیلی فراهم می‌کند. هدف از این مقاله، مدل‌سازی طراحی بهینه تولید برق مبتنی بر پیل سوختی در مالزی است. جنبه‌های اقتصادی و زیست‌محیطی، شاخص‌هایی هستند که به طراحی یک مدل بهینه کمک می‌کنند. تجزیه و تحلیل چند معیاره و فرآیند تحلیل سلسله مراتب به منظور تصمیم‌گیری در مورد سایت بهینه برای سیستم مورد استفاده قرار گرفتند. حمل و نقل کامیون، ذخیره بیوگاز و سیستم پیل سوختی از مهمترین معیارهایی هستند که معیارهای وزنی نهایی را ارائه می‌کنند. با در نظر گرفتن هر دو معیار برای نگرانی‌های اقتصادی و زیست‌محیطی، بهترین مکان در ایالت ساراواک است. یافته‌های این مطالعه بر تصمیم‌گیری تأثیر می‌گذارد و به محققان و تصمیم‌گیرندگان کمک می‌کند تا استراتژی‌های مناسبی را در نقشه راه انرژی‌های تجدیدپذیر توسعه دهند.

CONTENTS

<p>Babak Keyvani Bahador Fani Hamed Karimi Majid Moazzami Ghazanfar Shahgholian</p>	<p>Improved Droop Control Method for Reactive Power Sharing in Autonomous Microgrids</p>	<p>1-9</p>
<p>Rahul Dogra Sanjay Kumar Nikita Gupta</p>	<p>Application of Artificial Neural Network to Solar Potential Estimation in Hilly Region of India</p>	<p>10-16</p>
<p>Davar Rezakhani Abdol Hamid Jafari Mohammad Ali Hajabassi</p>	<p>Modified Concrete for Impeding Chloride Diffusion from Sea Water in the Marine Environment</p>	<p>17-31</p>
<p>Shokoofeh Bagheri Hassan Moradi CheshmehBeigi</p>	<p>DC Microgrid Voltage Stability through Inertia Enhancement Using a Bidirectional DC-DC Converter</p>	<p>32-44</p>
<p>Ashkan Zolriasatein Zahra RajabiMashhadi Majid Rezaei Abadehi Nastaran Riahi Noori Siamak Abyazi</p>	<p>A New Approach Based on RTV/SiO₂ Nano Coating for Tackling Environmental Pollution on Electrical Energy Transmission and Distributions</p>	<p>45-51</p>
<p>Mirmahdi Seyedrahimi-Niaraq Tohid Nouri</p>	<p>Investigating the Economic Effects and the Roadmap of Developing Geothermal Systems to Generate Electricity</p>	<p>52-64</p>
<p>Mehran Gheyrati Asadollah Akram Hassan Ghasemi-Mohtaker</p>	<p>Optimum Orientation of the Multi-Span Greenhouse for Maximum Capture of Solar Energy in Central Region of Iran</p>	<p>65-74</p>
<p>Mohammad Hosseinpour Hassan Ali Ozgoli Seyed Alireza Haji Seyed Mirza Hosseini Amir Hooman Hemmasi Ramin Mehdipour</p>	<p>Energy Analysis of Utilizing Biomass Gasification to Partially Substitution Fossil Fuels in an IBG-GT-ST-Kalina Cycle</p>	<p>75-86</p>
<p>Amrollah Dehghani Sanij Taghi Torabi Abbas Khamseh Alireza Boshehri</p>	<p>The Influence of Research and Development Activities and NanoFab Centers on Product Development in Nanotechnology: Focusing on Solar Thermal Energy and Photovoltaic Technology</p>	<p>87-100</p>
<p>Shafiqi Mohd Shafie Zakirah Othman A. Harits Nu'man Nik Nurul Anis Nik Yusuf</p>	<p>Multi-Criteria Analysis of Biogas Feed Fuel Cell-Based Electricity Generation: Economic and Environmental Factors</p>	<p>101-104</p>

